Author:
Mistry, Krishna

Title:
Transition Metal Complexes in Cooperative Lewis Pairs for Small Molecule Activation

Transition Metal Complexes in Cooperative Lewis Pairs for Small Molecule Activation

Krishna Mistry

A dissertation submitted to the University of Bristol in accordance with the requirements for award of the degree of Doctor of Philosophy in the Faculty of Science.

School of Chemistry

September 2018

Bristol Chemical Synthesis
Centre for Doctoral Training

Abstract

The development of transition metal complexes as a component of Lewis acid/base pairs for use in small molecule activation is presented. This concept stems from the nascent field of frustrated Lewis pair (FLP) chemistry.

A Pt(0)-diphosphine monocarbonyl complex, [Pt(CO)(**L**)] was shown to act as the Lewis base component of a cooperative Lewis pair with tris(pentafluorophenyl)borane ($B(C_6F_5)_3$). The synthesis of [Pt(CO)(**L**)] with the two diphosphine ligands, 1,2-bis(di-*tert*-butylphosphino)xylene (**L1**) and 1,2-bis(di-*tert*-butylphosphinooxy)benzene (**L2**), was achieved with **L2** being a stronger π-acceptor than **L1**. The cooperative Lewis pair system [Pt(CO)(**L**)]/$B(C_6F_5)_3$ successfully activated H_2, ethene, phenylacetylene, THF, H_2O and CO_2. The difference in the electronics of the two systems and the use of isotopically labelled [Pt(^{13}CO)(**L**)] led to a proposed pathway of activation for the small molecules tested. NMR spectroscopy was used to observe the binuclear Pt(I) cation, part of the ion pair $[Pt_2(\mu\text{-}H)(\mu\text{-}CO)(\mathbf{L})_2][HC(O\text{-}B(C_6F_5)_3)B(C_6F_5)_2]$, as a key intermediate in the pathway of dihydrogen activation of the system.

Preliminary investigations into the modification of the Pt(0)/B Lewis pair system were made through variation of the ligand diphosphine backbone and it was found that a sufficiently bulky phosphine substituent was necessary to stabilise a Pt(0)-monocarbonyl complex. A range of Lewis acids were substituted for $B(C_6F_5)_3$ and were tested for dihydrogen activation. Primarily in these cases, oxidative addition of H_2 to [Pt(CO)(**L**)] was observed followed by cooperative action of the Lewis acid to form cation $[Pt_2(\mu\text{-}H)_3(\mathbf{L})_2]^+$, observable by NMR spectroscopy.

A new series of pendant amine diphosphine ligands (R'PCH$_2$N(R)PR' ($P^{R'}N^RP^{R'}$), R'P = *s*-PhobP (9-phosphabicyclononane) or CgP (1,3,5,7-tetramethyl-2,4,8-trioxa-6-phosha-adamantane cage), R = Me, ^{i}Pr, Bn) and the corresponding manganese complexes $[Mn(CO)_3(PNP)][BAr^F{}_4]$ were synthesised as an intramolecular cooperative Lewis pair system. H_2 activation was only successful when using $P^{Cg}N^RP^{Cg}$ with slower rates observed for larger N-substituents. Initial results for their use in the electrocatalytic oxidation of H_2 is also presented.

Acknowledgments

This will unquestionably be the most difficult part of my thesis to write but I will give it a go. Firstly, I would like to thank my parents and brother for being supportive in all aspects of my life throughout my whole time in education…I promise this is it now! I wouldn't have been able to get as far as I have without you.

Next, I want to thank my supervisors. Duncan, thank you for all of your support and guidance through my PhD and making sure I didn't give up when I just couldn't see the end! Paul, your passion for what we do as research students kept me going. I couldn't be more grateful for the advice and support you've given me over the course of this project, 2 pm on Tuesdays won't be the same! Morris, thank you very much for having me as part of your research group, albeit a short trip! It was truly an unforgettable experience. Special thanks go to Rich, it's been a pleasure being your lab neighbour and I blame you for making me enjoy my rotation in the group and giving me my first taste of inorganic chemistry, which resulted in this thesis! Geoffrey, thank you so much for all you taught me on my trip to the PNNL and the endless trips to excellent local food establishments.

Katy, words cannot describe how grateful I am to have you by my side throughout all of this, whether it was giving advice, just letting me rant about chemistry or being my gin partner! Jess, your friendship was worth doing all of this, I am so proud of how far we've come, and I can't wait to see where life takes us. Tom, how you dealt with me is beyond me, but I am grateful for all the chats and yummy food outings! Stephie, Jo and Ness, my Fittini ladies, thank you for keeping me smiling through spin every morning, I will truly miss our morning workouts. Shay, you have been my best friend and supported the decisions I have made and even tried to understand my babbling about chemistry! Thank you for being there through the ups and downs, you helped make this possible.

Thank you to all of the members of the Wass and Pringle groups, past and present: Anna, Giulio, Patryk, Steph, Owen, Hope, Hugh, Alex, Ashley, Josephine, Taha, Jamie, Sophia Louise, Tim, Charly, Adam, Hubert, Lexy, Ailis, Callum, Dan, Sarah, Rachel and the endless list of students who came through the groups during my time. I wish I could acknowledge you all individually but that would make this longer than my thesis itself. Thanks for all of the support through the good and the bad, you've made my time in Bristol an unforgettable four years. Of course, I can't forget my wonderful CDT cohort, who provided great entertainment throughout the whole of my PhD.

All the work in this thesis wouldn't have been able to happen without the excellent staff within the Chemistry department. I'd like to thank Tony, Chris, Paul E., Mark, Richard, Jim, Vince, Ian, Bryony, Paul G., Paul L, Duncan, everyone in the mechanical and electronics workshops, Hazel and Natalie for dealing with my bizarre requests. It's been a pleasure to meet you all and your kindness really made a difference to my time here. I still cannot believe it's over. Thank you to everyone I've had the pleasure of crossing paths with. It'll be fours years I'll never forget.

Declaration

I declare that the work in this dissertation was carried out in accordance with the requirements of the University's *Regulations and Code of Practice for Research Degree Programmes* and that it has not been submitted for any other academic award. Except where indicated by specific reference in the text, the work is the candidate's own work. Work done in collaboration with, or with the assistance of, others, is indicated as such. Any views expressed in the dissertation are those of the author.

SIGNED: ..... DATE:.....

Table of Contents

List of Figures

List of Schemes

List of Tables

Abbreviations

Ar	Aryl
Ar^F	3,5-Bis(trifluoromethyl)phenyl
BAr^F_4	Tetrakis[3,5-bis(trifluoromethyl)phenyl]borate
BCF	Tris(pentaflurorophenyl)borane
Bn	Benzyl
bppm	Bis(bis(3,5-bis(trifluoromethyl)phenyl)phosphino)methane)
CgP	1,3,5,7-Tetramethyl-2,4,8-trioxa-6-phosha-adamantane cage
COD	1,5-Cyclooctadiene
COSY	Correslation Spectroscopy
Cp	Cyclopentadienyl
Cp*	Pentamethylcyclopentadienyl
CV	Cyclic voltammetry
Cy	Cyclohexyl
DCM	Dichloromethane
dcpob	Dicyclohexylphosphinooxybenzene
dcpp	1,3-Bis(dicyclohexylphosphino)propane
dcpx	Dicyclohexylphosphinoxylene
DFT	Density functional theory
dppe	1,2-Bis(diphenylphosphino)ethane
dppm	1,2-Bis(diphenylphosphino)methane
dppx	1,2-Bis(diphenylphosphino)xylene
dtbpob	1,2-Bis(di-*tert*-butylphosphinooxy)benzene
dtbpx	1,2-Bis(di-*tert*-butylphosphino)xylene
ESI	Electrospray ionisation
Et	Ethyl
FLP	Frustrated Lewis pair
h	Hour
HBPin	4,4,5,5-Tetramethyl-1,3,2-dioxaborolane
HMQC	Heteronuclear Multiple Quantum Coherence

HOMO	Highest occupied molecular orbital
Hz	Hertz
^{i}Pr	Isopropyl
IR	Infra-red
LA	Lewis acid
LB	Lewis base
LUMO	Lowest occupied molecular orbital
Me	Methyl
Mes	Mesityl
min	Minute
MS	Mass spectrometry
nbe	Norbornene
NMR	Nuclear Magnetic Resonance Spectroscopy
NOSEY	Nuclear Overhauser Effect Spectroscopy
o-tol	*ortho*-Tolyl
Ph	Phenyl
PhCl	Chlorobenzene
PhF	Fluorobenzene
ppm	Parts per million
s-PhobP	9-Phosphabicyclononane
syn gas	Synthesis gas
^{t}Bu	*tertiary*-Butyl
TCE	1,1,2,2-Tetrachloroethane
THF	Tetrahydrofuran
$w_{1/2}$	Line width at half height

Chapter 1

Introduction

1.1 Lewis Acids and Bases

The Brønsted-Lowry theory of acids and bases defines acids and bases by their proton donor and acceptor abilities respectively.[1,2] In 1923, Lewis introduced a new classification of acids and bases to more broadly identify them as electron pair acceptors and donors respectively.[3] The lowest unoccupied molecular orbital (LUMO) of a Lewis acid interacts with a lone pair of electrons in the highest occupied molecular orbital (HOMO) of a Lewis base. The combination of a Lewis acid and a Lewis base leads to a Lewis adduct being formed (Figure 1.1A). A classic example of a Lewis adduct is ammonia-borane (Figure 1.1B); the lone pair on the nitrogen of ammonia donates into the vacant orbital on the boron of borane.[4]

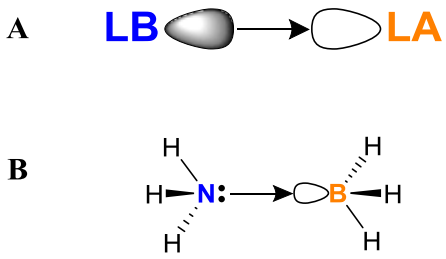

Figure 1.1: A) A schematic representation of a Lewis acid-base adduct; B) one of the simplest Lewis adducts ammonia-borane.

Moving on from the original definition in 1923, systems have been reported which deviate from Lewis's classification. In 1942, Brown *et al*. observed that 2,6-lutidine was capable of forming a stable Lewis adduct with boron trifluoride (Scheme 1.1A).[5,6] However, no interaction was observed upon mixing 2,6-lutidine with trimethylboron. It was noted that this was most likely a consequence of adverse steric interactions between the *ortho*-methyl groups of 2,6-lutidine and the methyl groups of trimethylborane. Almost two decades later, Wittig *et al.* reported the reaction of triphenylphosphine and triphenylborane with *in situ* generated benzyne to form phosphonium borate **1.1** (Scheme 1.1B).[7] During studies of organic ate-complexes, Tochtermann observed the formation

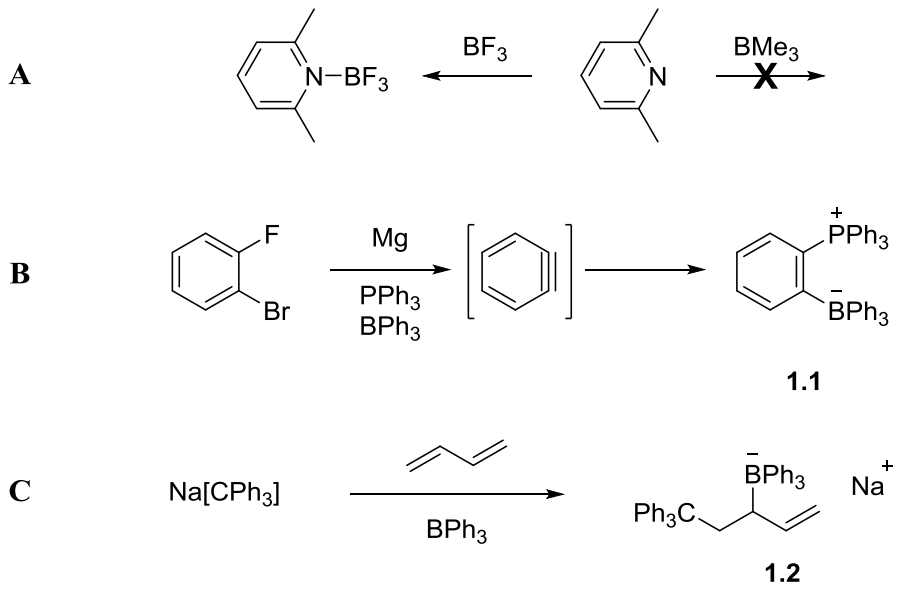

Scheme 1.1: A) Reaction of 2,6-lutidine with boranes reported by Brown *et al*.; B) Reaction of *in situ* generated benzyne with a phosphine and borane reported by Wittig; C) Formation of trapping product **1.2** by Tochtermann.

of trapping product **1.2** instead of the formation of polybutadiene.[8] The lack of formation of classical Lewis adducts was realised and it was this work which led Tochtermann to describe such a compound using the German term ‘‘antagonistiches paar’’. The subsequent reactivity of these systems was not explored further by the authors at the time.

1.2 Frustrated Lewis Pairs

Whilst investigating phosphine-borane interactions in 2006, Stephan *et al*. reported the serendipitous synthesis of zwitterion **1.3** which resulted from *para*-nucleophilic aromatic substitution of $B(C_6F_5)_3$ with the sterically demanding phosphine Mes_2PH (Mes = 2,4,6-trimethylphenyl) (Scheme 1.2);[9] a similar observation was made by Erker *et al*. on a related phosphine-borane system.[10] Treatment of **1.3** with Me_2SiHCl formed zwitterion **1.4** which contains both hydridic and protic fragments. Simply heating **1.4** led to a dramatic colour change of the solution from colourless to orange-red and the elimination of H_2 was observed to form species **1.5**. Most importantly, this reaction was reversible and reaction of H_2 with **1.5** at room temperature regenerated **1.4**. This was the first known example of reversible dihydrogen activation by a system solely synthesised from main group elements.

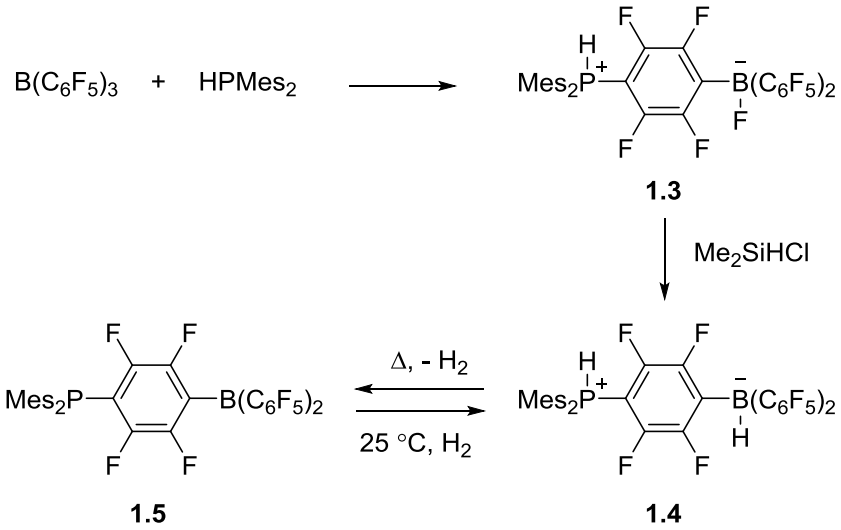

Scheme 1.2: Synthesis of zwitterion **1.5** and the reversible reaction with H_2.

Phosphine-borane **1.5** was proven to be monomeric in solution and the lack of aggregation was reasoned to be due to the steric congestion surrounding the boron and phosphorus centres.[9] This was later defined as the first example of a 'frustrated Lewis pair' (FLP), a term defined in 2007 by Stephan when investigating the reactivity of related intermolecular phosphine-borane systems with olefins.[11]

Returning to Lewis's definition, the combination of a Lewis acid and a Lewis base should result in the formation of a Lewis adduct where there is a dative bond between the two components (Figure 1.2). A frustrated Lewis pair is defined as a Lewis pair which cannot form the classical donor-acceptor interactions due to the steric demands around the Lewis acidic and basic centres. This results in latent, unquenched reactivity of the Lewis pair which has evidently been used for a variety of transformations.[12,13]

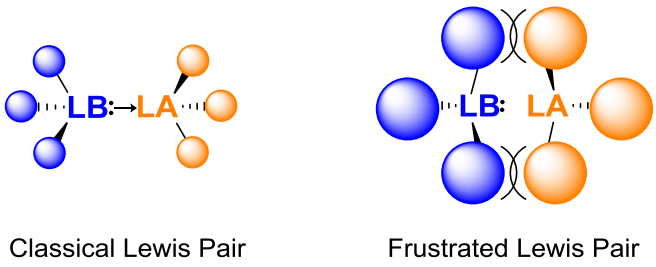

Figure 1.2: Schematic representation of a classical Lewis pair (left) and a frustrated Lewis pair (right).

1.3 Main Group FLPs and Small Molecule Activation

Initially, work surrounding small molecule activation by FLPs focused on systems comprising of sterically hindered, electron rich phosphines (P^tBu_3 and $PMes_3$) partnered

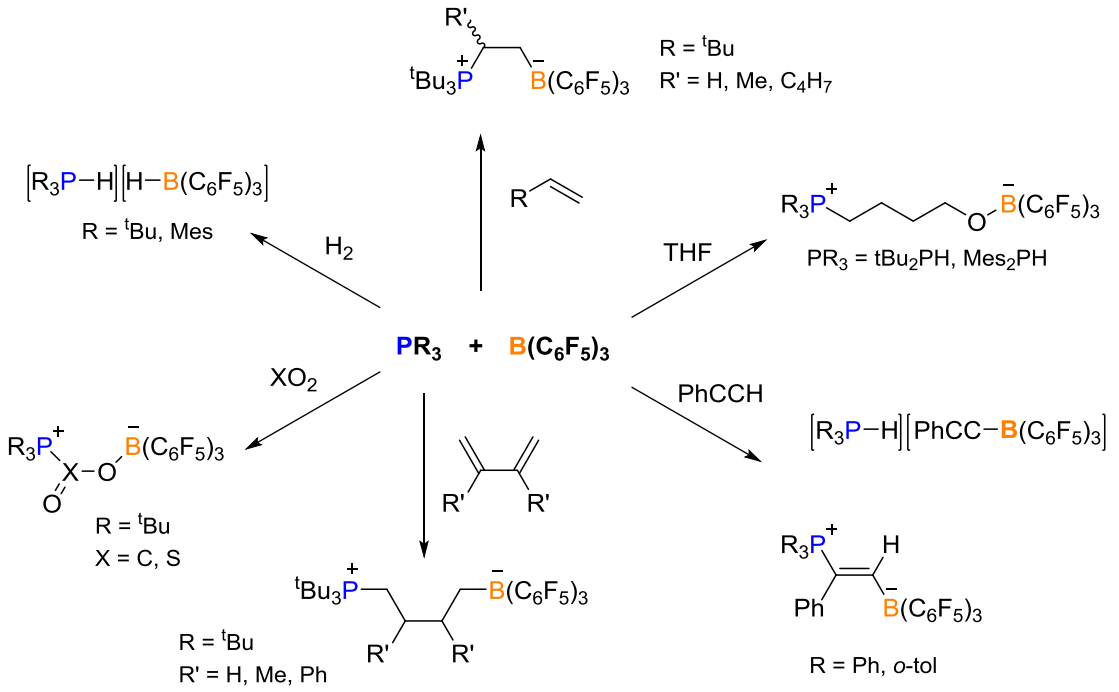

Scheme 1.3: Summary of small molecules activations by intermolecular FLP $PR_3/B(C_6F_5)_3$.

with a highly Lewis acidic fragment, predominantly $B(C_6F_5)_3$. These systems have shown to activate a variety of small molecules under relatively mild conditions (Scheme 1.3).

After the initial discovery of reversible dihydrogen activation with phosphino-borane **1.5**, investigations focused on a simpler intermolecular system $PR_3/B(C_6F_5)_3$. No evidence of Lewis adduct formation was observed for $PR_3/B(C_6F_5)_3$ (R = ^{t}Bu, Mes) but facile activation of H_2 was achieved at room temperature.[14] Unfortunately, this activation was found to be irreversible. Several other combinations of less Lewis acidic and basic phosphines and boranes were attempted with little success in dihydrogen activation. Some dihydrogen activation was observed with P^tBu_3/BPh_3 but only gave 33% yield of the H_2 heterolytic cleavage product and required much longer reaction times than $PR_3/B(C_6F_5)_3$ (R = ^{t}Bu, Mes). Even from this early study it was apparent that the correct combination of sterics and electronics were necessary to achieve the desired reactivity.

The $PR_3/B(C_6F_5)_3$ system also showed high reactivity to alkenes giving 1,2-addition products across simple terminal alkenes[11] and 1,4-addition products across 1,3-dienes (Scheme 1.3).[15] Interestingly, activation of an intermolecular alkene was shown by combination of $CH_2=(CH_2)_3PR_2$ (R = ^{t}Bu, Mes) and $B(C_6F_5)_3$.[11] Reaction of $PR_3/B(C_6F_5)_3$ with alkynes were slight more complex where two competing pathways of activation of PhCCH observed.[16] When using P^tBu_3, deprotonation of the terminal alkyne

was observed but when PPh_3 and P(*o*-tol)$_3$ were used the 1,2-addition product forms. This was reasoned to be due to the relative high basicity of P^{t}Bu$_3$ promoting deprotonation over 1,2-addition. The same reactivity was also observed when using $Al(C_6F_5)_3$ in place of $B(C_6F_5)_3$.

Secondary phosphines ^{t}Bu$_2$PH and Mes_2PH were shown to ring open THF by attack at the activated α-carbon of the cyclic ether after initial coordination to $B(C_6F_5)_3$ (Scheme 1.3).[17] The $PR_3/B(C_6F_5)_3$ system was also shown to be able to sequester CO_2 with heating to 80 °C necessary (R = ^{t}Bu) to liberate CO_2.[18] $PR_3/B(C_6F_5)_3$ reacted rapidly with SO_2 to form a product reminiscent of the CO_2 activation product.[19] However, the molecular structure revealed distorted trigonal pyramidal geometry at the sulfur indicating S-centred chirality.

The ethylene linked intramolecular FLP $Mes_2P(CH_2)_2B(C_6F_5)_3$ contains Lewis acidic and Lewis basic centres similar to the intermolecular system shown in Scheme 1.3. The synthesis and reactivity of this linked P/B FLP has been explored extensively by Erker *et al* (Scheme 1.4). The FLP exists in solution as a quenched four-membered cyclic intramolecular phosphine-borane.[20] This exists in equilibrium with its 'open' state which is then capable of further reactivity with small molecules.

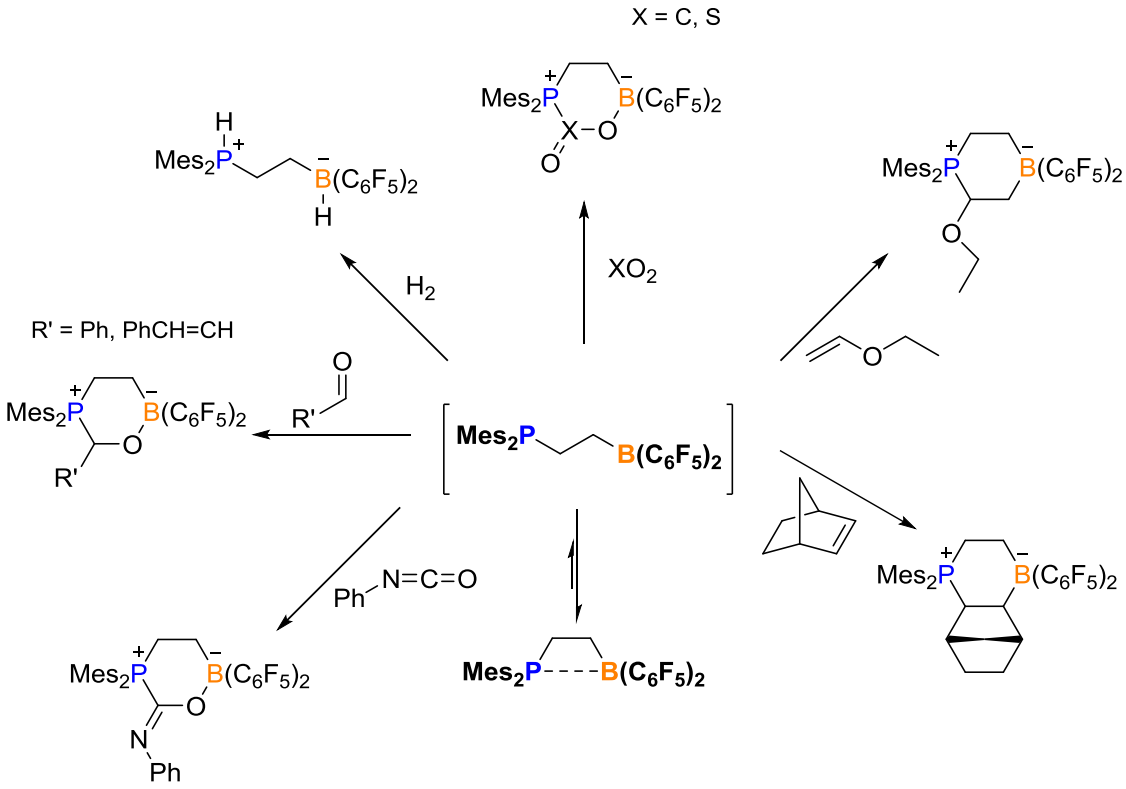

Scheme 1.4: Summary of small molecule activations by intramolecular FLP $Mes_2P(CH_2)_2B(C_6F_5)_2$.

This intramolecular FLP reacts with H_2 at room temperature irreversibly but it was shown that the subsequent reduction of benzaldehyde by the zwitterionic cleavage product could be achieved (Scheme 1.4).[20] The activation of CO_2 was found to be extremely reversible with the product being relatively stable as a solid but in solution CO_2 rapidly dissociates above −20 °C.[18] The analogous reaction with SO_2 at −78 °C again led to a chiral product as with the intermolecular FLP system.[19] The system reacted with alkenes[21] and carbonyl compounds[22] where the regiochemistry followed the tendency of forming new P-C and B-O bonds in the products. The most interesting observation was the activation of the carbonyl group in *trans*-cinnamic aldehyde over the alkene bond.

The design of frustrated Lewis pairs containing phosphorus as the Lewis base and boron as the Lewis acid in either intra- or intermolecular systems has rapidly expanded since the term FLP was coined in 2007. Figure 1.3 shows a range of intra- and intermolecular FLP systems.[23–29] Many of these systems have shown reactivity towards small molecules although these systems do not exhibit reactivity with such an extensive range of substrates compared to the systems shown in Scheme 1.3 and 1.4. It is of interest to note that some of the examples show the use of relatively electron-withdrawing phosphines and relatively electron-donating boranes contrary to initial requirements thought to be

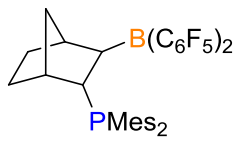

Erker *et al.* 2013
H_2, NO, CO_2, SO_2, PhCHO

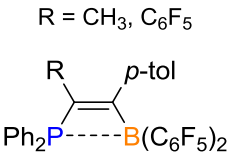

Erker *et al.* 2013
tBuCN

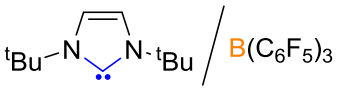

Tamm *et al.* 2008
H_2, THF

Stephan *et al.* 2008
H_2, HNR_2

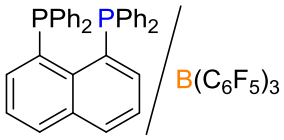

Erker *et al.* 2008
H_2

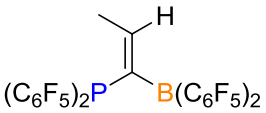

Erker *et al.* 2011
RCCH, ArNCO, R'CHO

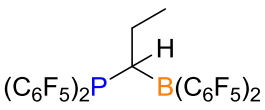

Erker *et al.* 2011
PrCCH, *p*-tolNCO, C_2H_4, N_3Mes

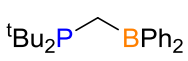

Slootweg and Lammerstma *et al.* 2011
H_2, CO_2, ^{t}BuNCO

Figure 1.3: Selected examples of intra- and intermolecular P/B FLP systems which display a range of small molecule activation.

necessary for FLP reactivity. This demonstrates that it may not be necessary to use highly Lewis acidic/basic components to enable small molecule activation.

The alkyne activation shown in Scheme 1.3 by an intermolecular FLP also proceeded with the use of $Al(C_6F_5)_3$ instead of $B(C_6F_5)_3$.[16] This was one of the first examples of using an element other than boron for the Lewis acidic centre in an FLP. Since then a variety of intra- and intermolecular P/Al FLPs have been developed (Scheme 1.5).[30–34]

The geminal P/Al system **1.6** was developed by Lammertsma and Uhl *et al*. in 2011 by the hydroalumination of alkynylphosphines (Scheme 1.5A).[30] Reaction with phenylacetylene initially gave a 3:1 deprotonation/1,2-addition product (**1.7**/**1.8**) respectively. Heating the reaction mixture to 70 °C for 1 h resulted in the full conversion to **1.8**. P/Al FLP **1.6** was also shown to activate CO_2 and H_2. More recently, Uhl *et al*. have shown an analogue to activate α,β-unsaturated carbonyl compounds, aldehydes, azides, isocyanates and carbodiimides.[31,33]

In 2011, Stephan *et al.* reported the use of simple aluminium halides as the Lewis acidic components of an intermolecular FLP (Scheme 1.5B).[34] It was shown that activation of CO_2 occurs with a 2:1 stoichiometry of AlX_3 (X = Cl, Br, I) to $PMes_3$ and further reaction of **1.10** led to the stoichiometric reduction of CO_2 to CO. Harder *et al*. has recently shown the use of a highly Lewis acidic cationic aluminium complex with the simple Lewis base

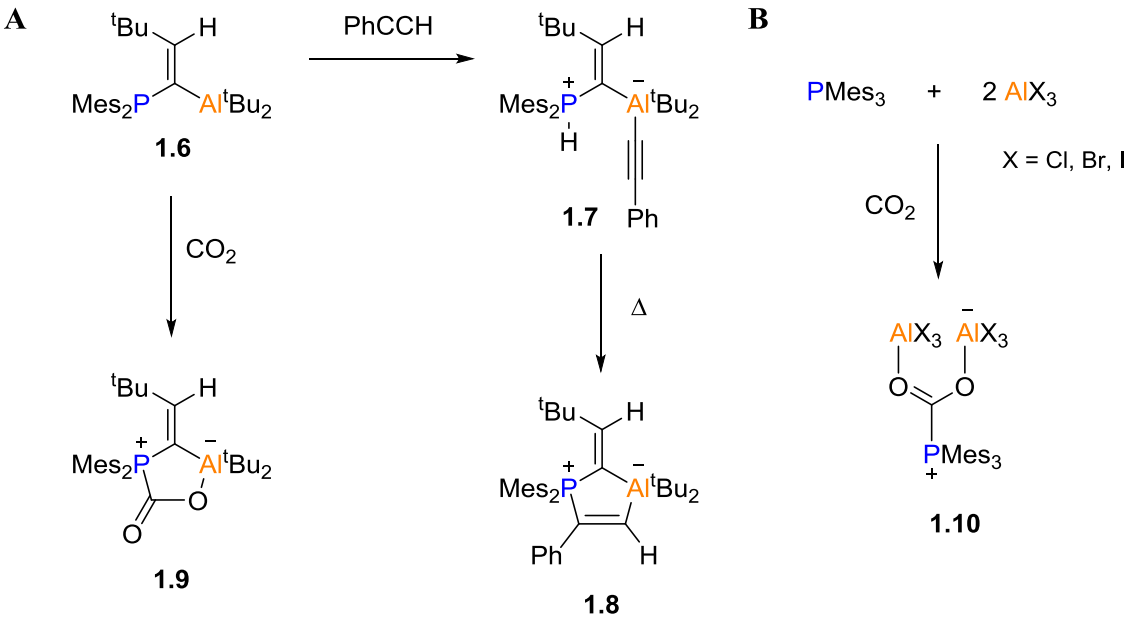

Scheme 1.5: A) Geminal P/Al FLP capable of activating phenylacetylene and CO_2; B) Intermolecular P/Al FLP capable of stoichiometrically reducing CO_2 to CO.

PPh_3 in the activation of terminal alkynes and alkenes, carbon dioxide, epoxides and alkyl chlorides.[32]

Stephan *et al*. have exploited the use of highly acidic phosphorus(V) Lewis acids in FLP chemistry.[35–38] 1,2-Diphosphonium dication **1.11** acts as a P(V) Lewis acid in combination with a P(III) Lewis base in the FLP activation of B-H, Si-H, C-H and H-H bonds (Figure 1.4A).[37] Amidophosphorane **1.12** was found to sequester CO_2 under mild conditions despite there being a formal, albeit weak, bond between the P and N centres (Figure 1.4B).[35] It was thought that the reactivity occurred from the resonance form **1.13** which contains a charge-separated P-N bond that is reminiscent of 'classical' FLPs.

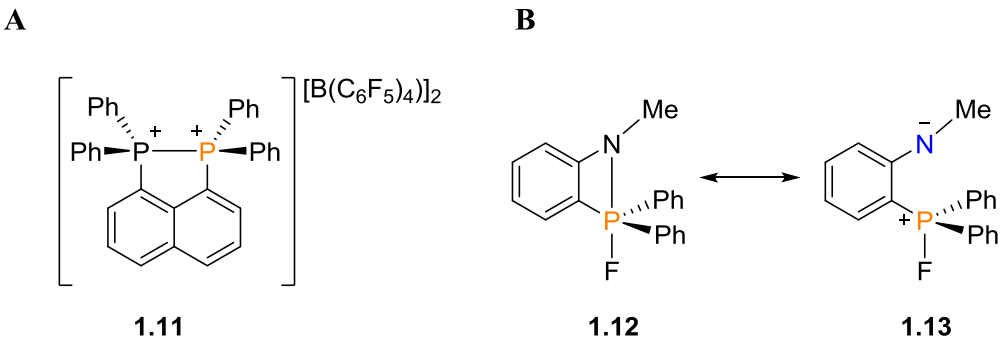

Figure 1.4: Phosphorus(V) Lewis acids used for small molecule activation

Following on from this, the use of amines as a Lewis base in FLPs has been thoroughly explored.[39–47] Scheme 1.6 shows some examples of N/B FLPs which successfully activated small molecules. A simple N/B FLP $^{i}PrNH_2/B(C_6F_5)_3$ activated H_2 after 1 h at 110 °C to form the heterolytic cleavage product **1.14** (Scheme 1.6A).[39] 2,6-Dimethylpiperidine in combination with $B(C_6F_5)_3$ heterolytically cleaved H_2 at room temperature with $B(C_6F_5)_3$ (Scheme 1.6B). Several substituted piperidine and lutidine components were successfully tested for H_2 activation with $B(C_6F_5)_3$.[41] Most notably, 2,6-lutidine/$B(C_6F_5)_3$ was capable of H_2 heterolytic cleavage with 2,6-lutidine being one of the components of the early examples of FLP chemistry before the name was coined in 2007. In 2012, Stephan and Erker *et al*. reported the use of several different amine/$B(C_6F_5)_3$ combinations and showed the extent to which small molecule activation possible with this intermolecular system.[48] This included activation of dihydrogen, alkenes, alkynes, carbon dioxide, and diynes.

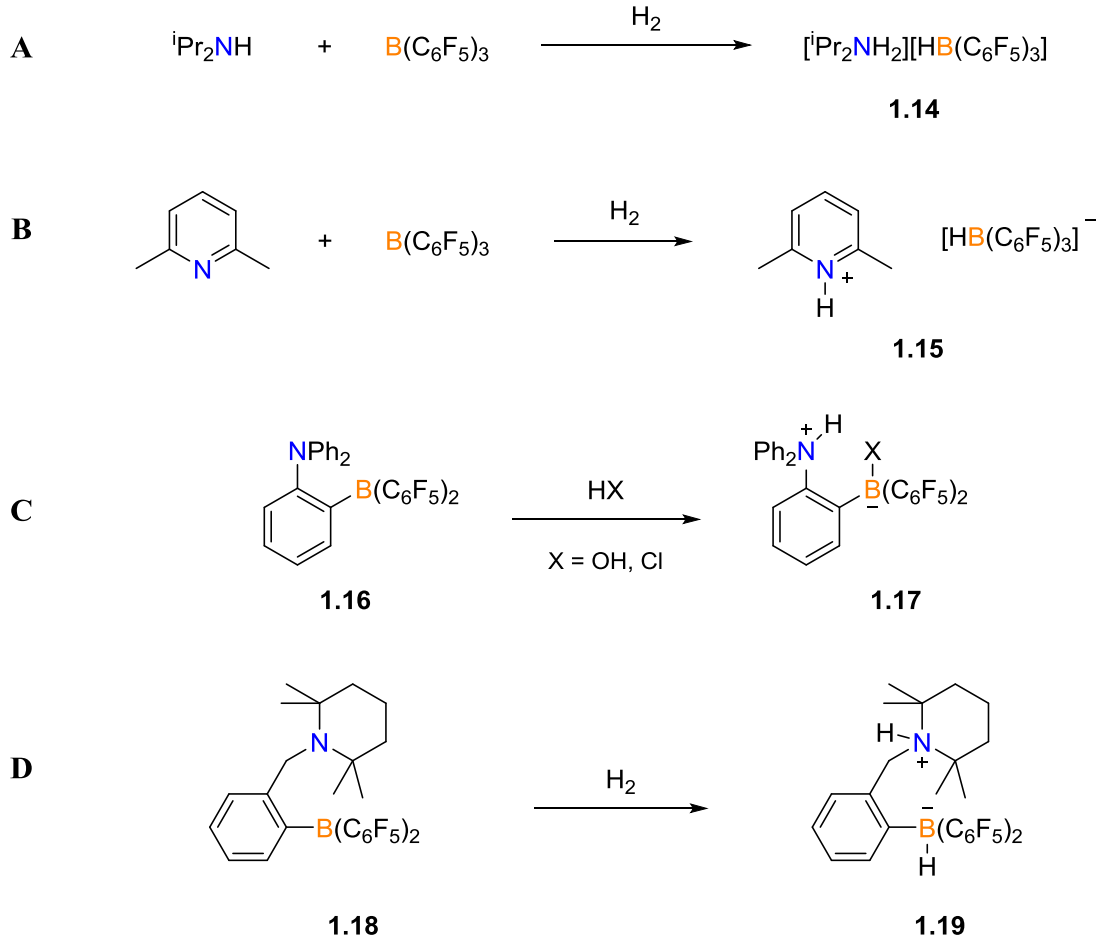

Scheme 1.6: Examples of activation by inter- and intramolecular N/B FLPs.

Intramolecular systems have also been developed with the first notable example reported by Piers *et al*. in 2003, before the FLP paradigm was discovered.[49] Amino-borane **1.16** was shown to trap H_2O and HCl but did not show reactivity towards H_2 (Scheme 1.6C). Attempts to chemically synthesise the H_2 cleavage product simply led to the expulsion of dihydrogen which was rationalised to be due to the low Lewis basicity of the nitrogen component, which is now known to have a significant effect on small molecule activation. Several other examples have been report by the groups of Erker[50] and Repo.[43] The *ansa*-aminoboranes were described as 'molecular tweezers' as the amine and borane were orientated towards each other but in a noncoordinating mode (**1.18**, Scheme 1.6D).[40]

1.3.1 Catalysis with Main Group FLPs

A wide range of main group FLPs has been developed and their use in stoichiometric small molecule activation is well documented. A principal focus has been to utilise these main group systems for catalytic transformations.[51] A notable progression in the field of FLPs has been the development of transition metal free systems for hydrogenation

catalysis. In 2007, Stephan *et al.* reported the use of the 'first' FLP **1.5** as a hydrogenation catalyst for imines, nitriles and aziridines.[52] It was noted here that the steric hinderance around the nitrogen centre on the amine product played an important role in preventing catalyst deactivation by formation of a strong Lewis adduct. The dissociation of the resultant amine-borane adduct can be encouraged by the use of bulky substituents, which appears to be the limitation of the substrate scope of imine hydrogenation by FLPs.[53]

Following on from the reactivity of **1.5** as a hydrogenation catalyst, in 2008, Stephan *et al*. reported the use of $B(C_6F_5)_3$ as a Lewis acid hydrogenation catalyst where the initial hydrogenation activation occurs between the starting imine and $B(C_6F_5)_3$ in an FLP-type manner (Scheme 1.7).[54] This generated an activated iminium cation which underwent reduction to form the borane adduct of the product amine. If the stereoelectronic properties of this adduct are suitable then $B(C_6F_5)_3$ catalyst and amine product are released generating a catalytic system.

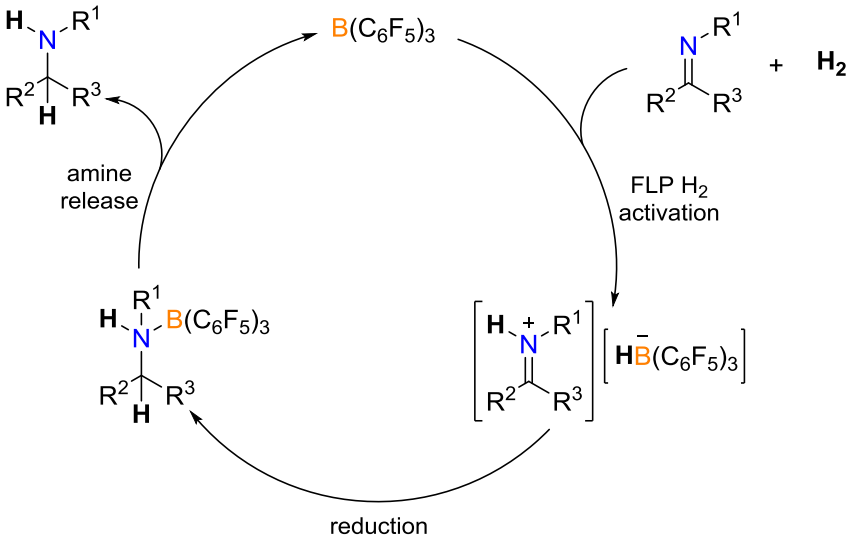

Scheme 1.7: Mechanism of $B(C_6F_5)_3$ catalysed-imine hydrogenation with FLP activation of H_2.

The substrate scope of hydrogenation by FLP catalysts has been extended to enamines,[55] silyl enol ethers,[56] oxime ethers,[57] and have even been used successfully in transfer hydrogenation of imines and cyclohexa-1,4-dienes.[58,59] This chemistry has also extended to the hydrogenation of non-polar bonds including alkenes[60,61] and alkynes.[62]

The hydrogenation of carbonyl compounds by FLPs was problematic initially due to the formation of boronic esters due to the high oxophilicity of boron.[63] In 2014, the groups of Stephan and Ashley concomitantly reported the use of ethers (Et_2O, THF) to

successfully hydrogenate carbonyl compounds.[64,65] The oxygen of the ether solvent acts as the Lewis base with Lewis acidic $B(C_6F_5)_3$ to initiate the catalysis by dihydrogen activation to form [(Ether)-OH][H-$B(C_6F_5)_3$)] from which transfer of the hydride and the proton to the carbonyl compound is facile.[66]

When employing an asymmetric FLP, the chirality has been successfully induced to the product for enantioseletive hydrogenations.[67–72] Figure 1.5 shows some examples of chiral boranes which, with varying success (*ee* ranging from 13 to 99%), have hydrogenated prochiral imines and ketimines enantioselectively.

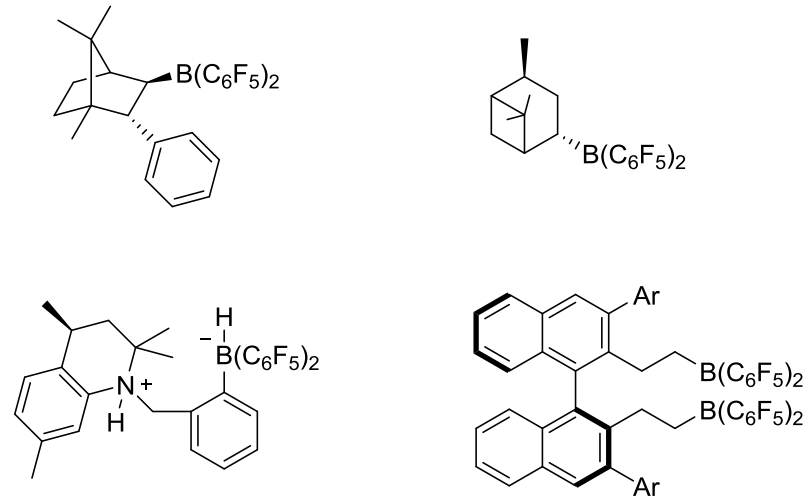

Figure 1.5: A selection of chiral boranes capable of enantioselective hydrogenations.

Research has also evolved to investigate the catalytic reduction of CO_2.[73–76] In 2009, Ashley and O'Hare *et al*. reported the use of 2,2,6,6-tetramethylpiperidine and $B(C_6F_5)_3$ with H_2 to reduce CO_2 to MeOH after simple work-up.[73] However, this process was not catalytic as the borane was destroyed in the work-up. Fontaine *et al*. was the first to report the catalytic reduction of CO_2 to MeOH using a P/B FLP in the presence of a sacrificial hydroborane.[74]

In 2013, Stephan *et al*. also showed the hydroamination of terminal alkynes catalysed by $B(C_6F_5)_3$ to form **1.20** (Scheme 1.8).[77] The initial addition product can undergo a 1,3-proton transfer to release the enamine **1.21** and regenerate $B(C_6F_5)_3$. It has also been shown that a one-pot hydroamination/hydrogenation is possible to form the corresponding amine **1.22**.

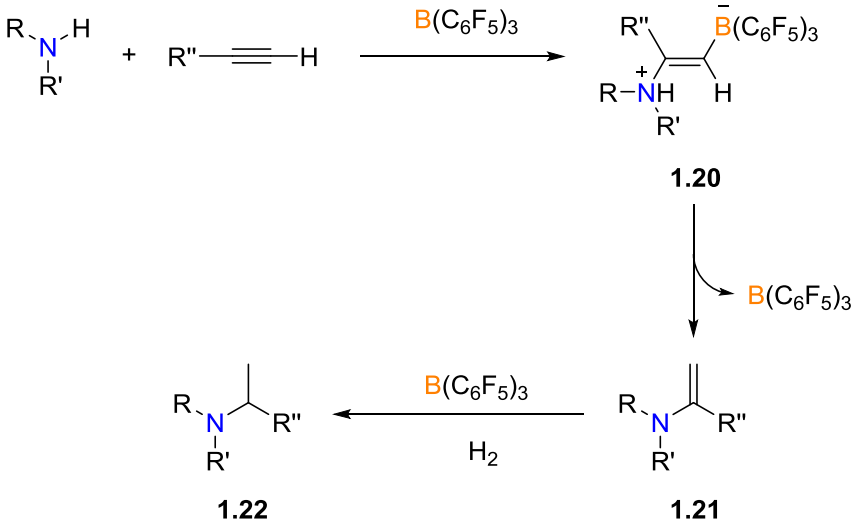

Scheme 1.8: Tandem catalytic hydroamination/hydrogenation of terminal alkynes by $B(C_6F_5)_3$.

1.4 Transition Metal FLPs and Small Molecule Activation

Further developments in the field of frustrated Lewis pair chemistry has seen the replacement of main group elements for transition metals as either the Lewis acidic or Lewis basic component. An appeal of using transition metals in FLP systems is the ease with which the properties of the metal system can be changed by simple synthetic modification of the ligand. This is in comparison to the challenging methods needed to modify the fluorinated boranes used in main group FLP chemistry. The reactivity of traditional transition metal complexes is instrumental in homogeneous catalysis and includes reactivity such as oxidative addition, reductive elimination and migratory insertion. It was envisaged that the right combination of this transition metal reactivity in combination with FLP systems could lead to the design of novel activation catalysts.[78]

Transition metal complexes comprised of titanium and zirconium centres have been used widely in homogenous catalysis as a Lewis acid for a variety of synthetic transformations.[79,80] In 2011, whilst investigating Lewis acid exchange reactions, Stephan *et al*. reported the synthesis of a Lewis acidic zirconocene complex, $[Zr(Cp^*)_2(OMe)][B(C_6F_5)_4]$ (Cp^* = pentamethylcyclopentadienyl) and, in combination with the Lewis base P^tBu_3, was capable of N_2O activation.[81] No further small molecule activation was investigated in this study.

In 2011, the Wass research group reported the synthesis and application of a series of intramolecular Zr^+/P FLP systems.[82] These systems were based on a zirconocene alkoxide complex with a tethered Lewis basic phosphine group with variation with the Cp (Cp = cyclopentadienyl) rings or the phosphine substituents (**1.23**, Scheme 1.9). No Zr-P interaction was observed in solution or the solid state with the complex isolated as a labile chlorobenzene solvate. This system was shown to undergo a variety of small molecule activations, both reactions ubiquitous in FLP chemistry (such as H_2, CO_2 and ethene) as well as more exotic activations such as alkyl halide bonds (Scheme 1.9).

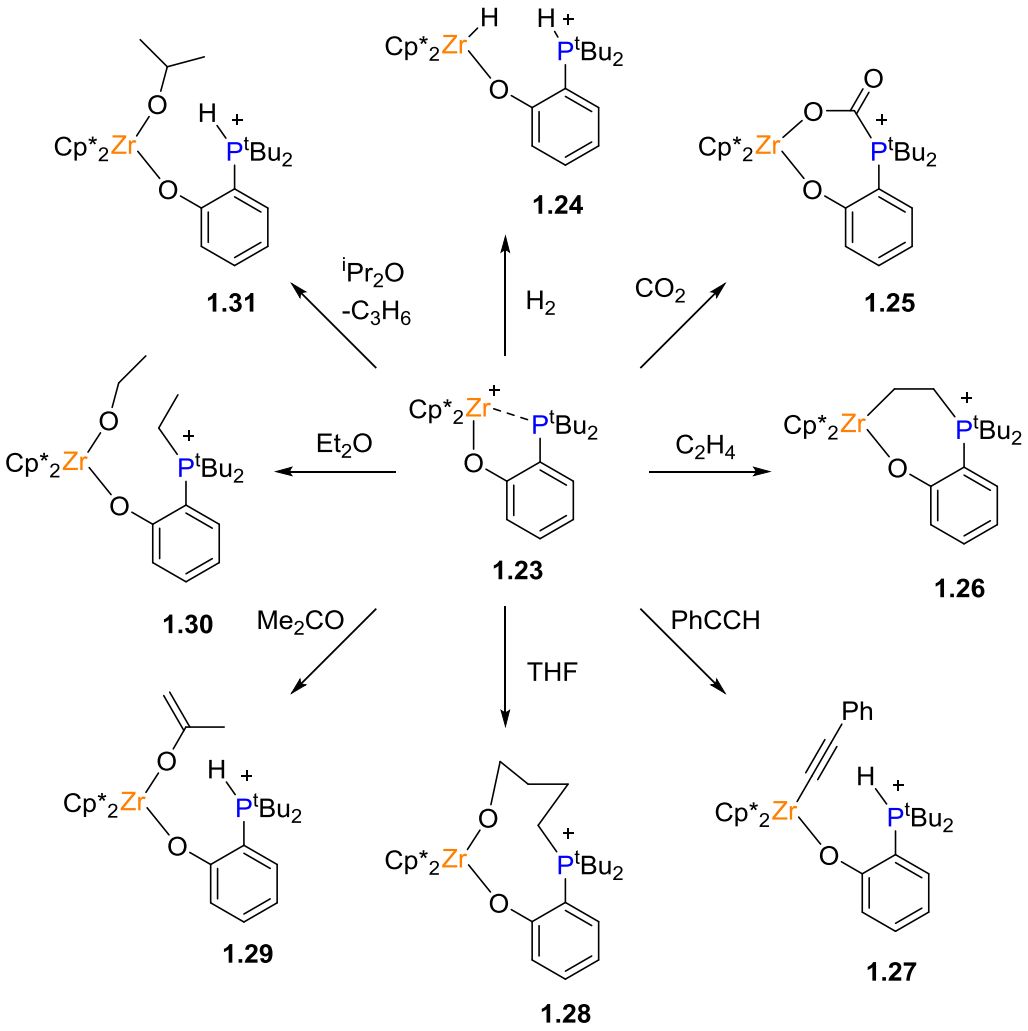

Scheme 1.9: Small molecule activations by intramolecular Zr^+/P Lewis pair **1.23**. $[B(C_6F_5)_4]^-$ omitted for clarity.

An interesting observation was made for the activation of H_2. FLP **1.23** underwent facile but irreversible H_2 activation whereas the Cp analogue did not react at all. It was proposed that it was necessary to use more electron rich ligands to increase the electron density at

the Zr centre, as this enabled the initial binding of H_2 as a necessary but transient mechanistic intermediate. Using the mixed Cp/Cp* analogue of **1.23** led to reversible heterolytic cleavage of H_2.

These Zr^+/P FLPs systems were also shown to be active in the catalytic dehydrogenation of various amine-boranes.[82] The Ti analogue of **1.23** was also synthesised and reacted with H_2, resulting in the reduction of Ti^{IV} to Ti^{III}, and was also shown to catalyse the dehydrogenation of $Me_2HN.BH_3$.[83] The chemistry was extended by the ring opening of THF by the La analogue of **1.23**.[84]

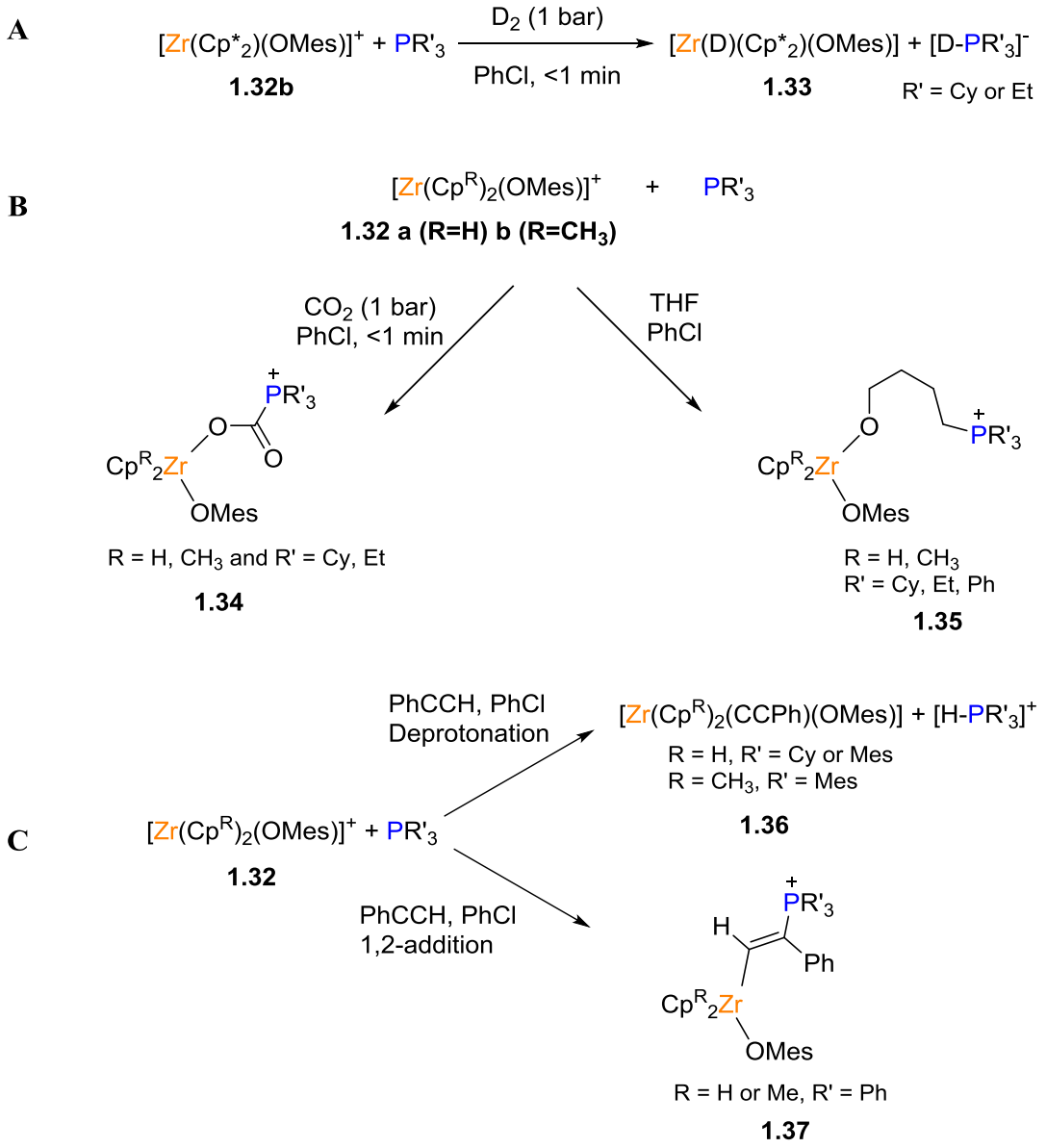

Scheme 1.10: Small molecule activation by intermolecular Zr^+/P Lewis pairs. $[B(C_6F_5)_4]^-$ omitted for clarity.

More recently, the Wass group demonstrated the modification of their original zirconocene system to an intermolecular equivalent, eliminating the synthetic challenge of incorporating an internal Lewis base.[85] Lewis acidic fragments $[Zr(Cp)_2(OMes)]^+$ and $[Zr(Cp^*)_2(OMes)]^+$ (both with $[B(C_6F_5)_4]^-$ counterion) were able to be combined with a variety of phosphines (PR_3, R = Cy, Et, Ph, Mes and C_6F_5) and tested for small molecule activation (Scheme 1.10). Only the Cp* variant with PCy_3 and PEt_3 reacted with D_2 which is thought to be due to the necessity of an electron rich ligand to help facilitate the initial binding of D_2. Both **1.32a** and **1.32b** in combination with selected phosphines activated CO_2 and THF in a typical FLP fashion. Upon reaction with phenylacetylene, depending on the combination of cyclopentadienyl ring and phosphine, either deprotonation or 1,2-addition of the alkyne was observed.

Following on from this, the synthesis of related zirconocene Lewis acidic fragments and their application in imine hydrogenation was reported by the Wass group.[86] They proposed the mechanism to go via FLP-type cleavage of H_2 between the zirconium centre and the substrate imine nitrogen followed by subsequent imine reduction in the same manner as $B(C_6F_5)_3$ (Scheme 1.7, Section 1.3.1). The only caveat of the studies was that a bulky group (^{t}Bu) on the imine nitrogen was required for hydrogenation activity.

Erker *et al*. have also researched a variety of intramolecular zirconocene FLP systems with a variety of backbone linkers. These include both unsaturated and saturated backbones with either phosphine or amine Lewis bases (Figure 1.6).[87–94] These systems showed a range of stoichiometric reactivity with a diverse library of small molecules typically used in FLP chemistry, for example, CO_2, isocyanates, benzaldehyde and

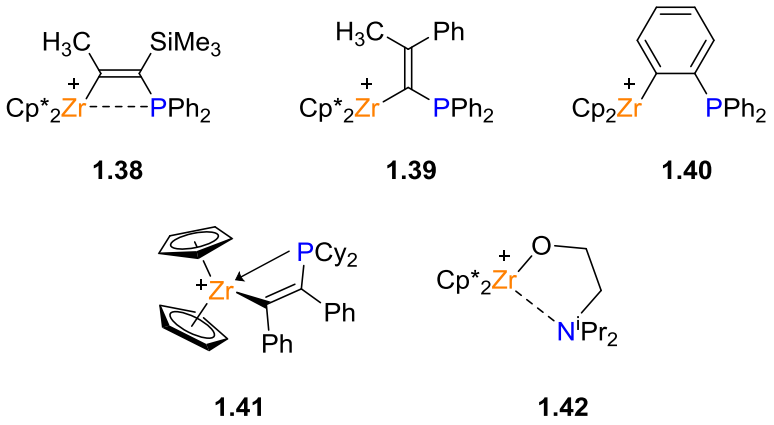

Figure 1.6: Intramolecular zirconocene based FLPs developed by Erker *et al*. $[B(C_6F_5)_4]^-$ counterion omitted for clarity.

alkenes. Zr^{+}/N FLP **1.42** also displayed catalytic activity for the hydrogenation of a variety of alkenes and alkynes.[90]

In 2017, Erker *et al*. showed the ability of zirconocene hydride [Zr(H)(Cp*)$_2$(OMes)] with Pier's borane ([HB(C_6F_5)$_2$]) to reduce CO to form formylhydridoborate complex **1.43** (Scheme 1.11).[95,96] This complex was then found to react as an oxygen/boron frustrated Lewis pair where the zirconium is a spectator to small molecule activation. **1.43** reacted with H_2 to form **1.45** with the release of methane. The initial step is thought to follow traditional FLP chemistry and heterolytically cleave H_2. which was followed by carbon-oxygen bond cleavage in an S_{Ni} process to yield [Zr(Cp*)$_2$(OMes)(OH)] and [H_3C-B(C_6F_5)$_2$]. Similar subsequent steps are presumed to follow to form the final product **1.45**. The O/B FLP **1.43** was also shown to react with CO, CO_2 and PhNSO by traditional FLP mechanisms but then further reactivity of these intermediates led to the final products **1.44**, **1.46** and **1.47** respectively.[95]

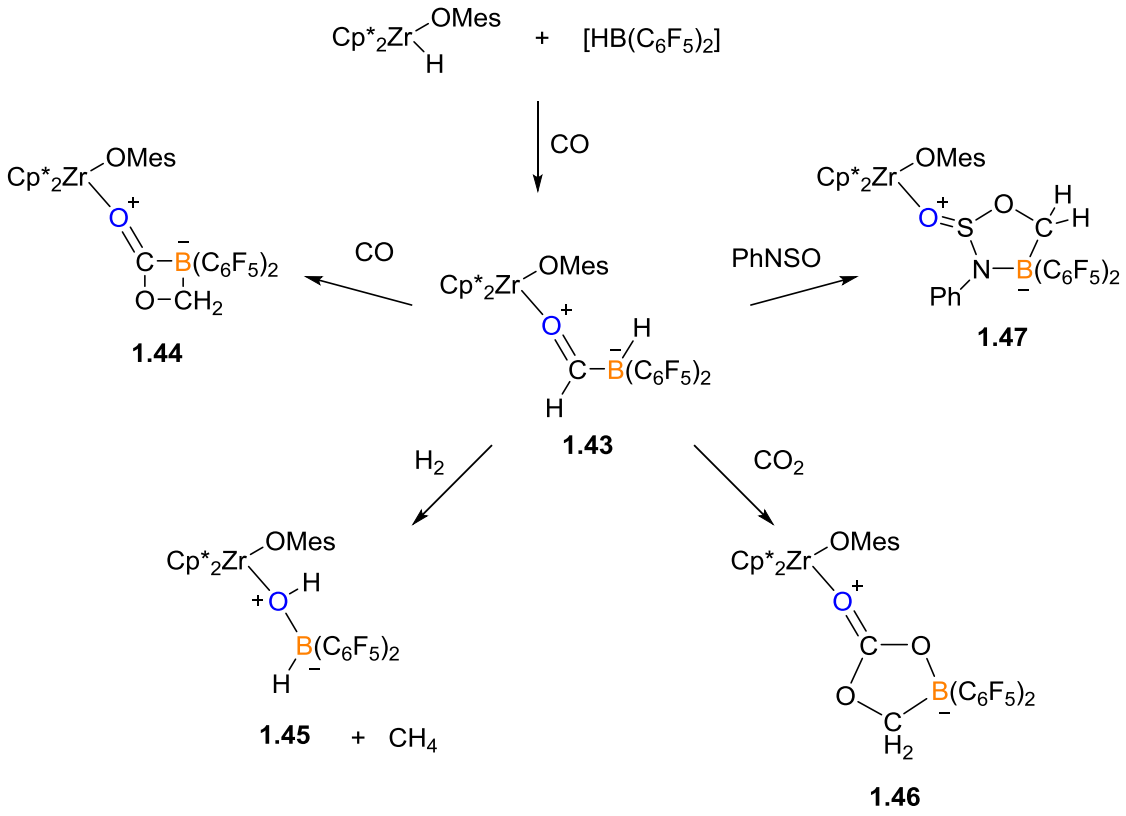

Scheme 1.11: Reactivity of O/B FLP **1.43**.

Group 3 systems displaying FLP-type behaviour have been reported by the groups of Piers[97,9] and Xu.[99,100] In 2012, Piers *et al*. recorded the use of a dimethylscandocinium complex-hydridoborate ion pair **1.48** to activate CO (Scheme 1.12A).[97] It was also shown

to activate CO_2 forming an ion pair **1.49** and, when in the presence of $B(C_6F_5)_3$ as a co-catalyst and triethylsilane, is able to induce deoxygenative hydrosilation of CO_2 to CH_4.[98] Unfortunately, this system did not show any reactivity towards D_2 or propene.

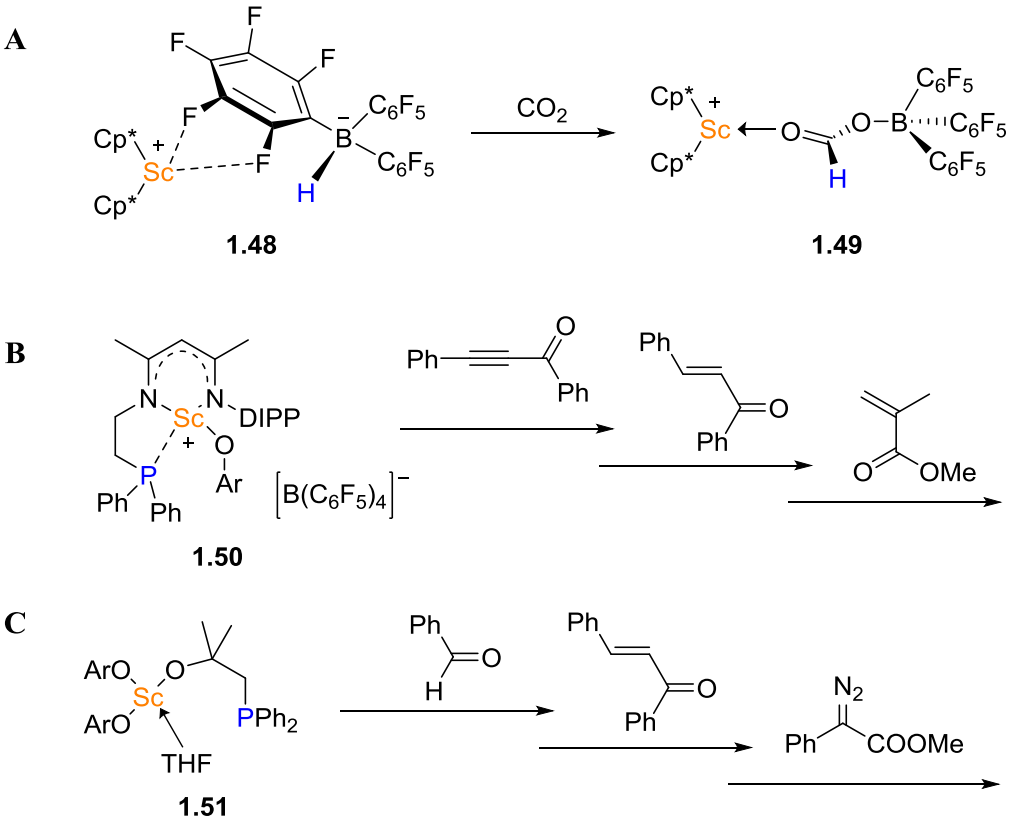

Scheme 1.12: Scandium FLPs and some examples of their reactivity.

More recently, Xu *et al*. have reported the synthesis of scandium complexes **1.50** and **1.51** which both act as intramolecular FLPs with their respective tethered phosphine moiety. Despite the persistent Sc-P interaction, **1.50** displayed stoichiometric 1,4-addition to conjugated carbonyl substrates such as enones, ynones and acrylic substrates and were also shown to be active catalysts for polymerisation of polar conjugated alkenes[99]. Xu *et al*. also reported the neutral scandium complex **1.51** which displays no Sc-P interaction due to the Sc centre being stabilised by coordination of a molecule of THF.[100] This system was shown to react stoichiometrically with benzaldehyde, benzylideneacetophenone and methyl diazophenylacetate to form FLP activation products. The yttrium and lutetium analogues were also synthesised, but the only reactivity observed was with 1,3-di-phenyl-2-propyn-1-one for the lutetium analogue, with no reactivity observed for the yttrium complex.

In 2013, Stephan *et al.* reported activation of CO_2 by a Hf complex **1.52** containing sulfur-phosphidoamine ligands (Scheme 1.13).[101] With phenyl substituents on the phosphorus, multiple products were observed upon reaction with CO_2. Initially the formation of twofold symmetric bimetallic **1.53** was observed in the solid state. Upon dissolution in THF, monomer **1.54** was formed and further reaction with CO_2 yielded double CO_2 activated product **1.55**. Starting with ^{i}Pr on the phosphorus atom only the double CO_2 product **1.55** was observed. This product was stable in the absence of CO_2 and was isolated in a 77% yield. This is thought to be due to the greater basicity of the phosphorus centre.

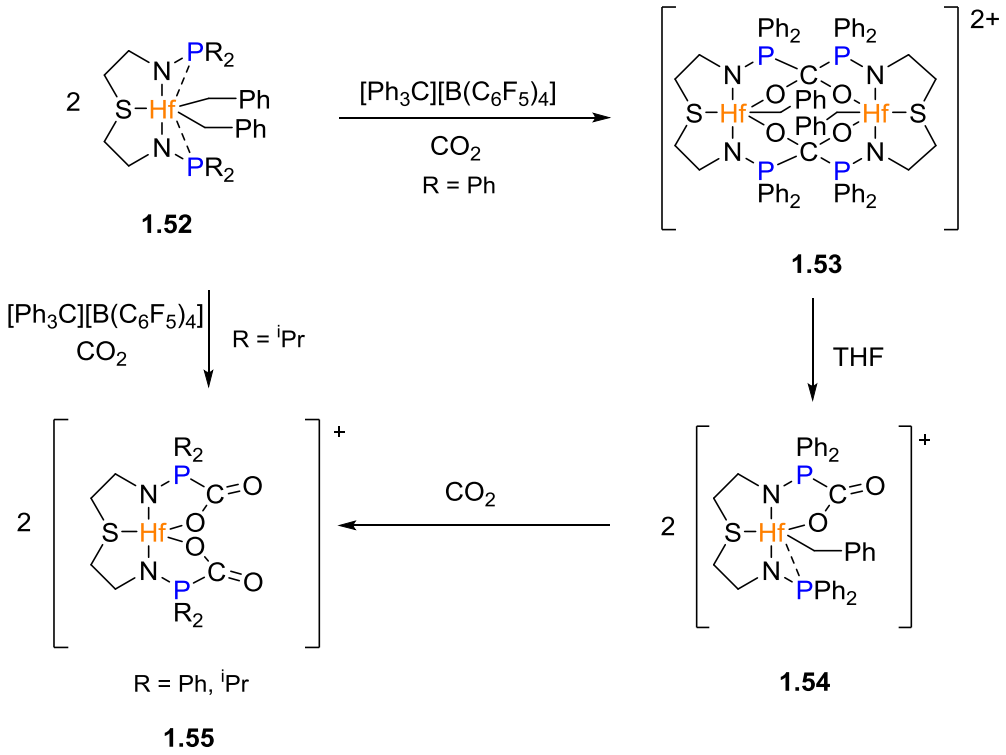

Scheme 1.13: Hafnium FLP **1.52** and its interaction with CO_2. $[B(C_6F_5)_4]^-$ Counterions omitted for clarity.

In recent years, more variety of mid to late transition metals have been reported as active FLP components. It is worth noting here the developments by DuBois and Bullock concerning Fe, Ni, and Mn complexes capable of heterolytic cleavage of H_2.[102–107] These complexes utilise ligands containing pendant amines as an internal base cooperatively activate H_2. Details of this are discussed in Chapter 4.

Berke *et al.* exemplified the use of metal hydrides as the Lewis basic component of FLPs in 2013,[108] and since then the reactivity of metal hydrides with Lewis acids has been reviewed.[109] The rhenium-hydride complexes **1.56** were exposed to CO_2 in the presence

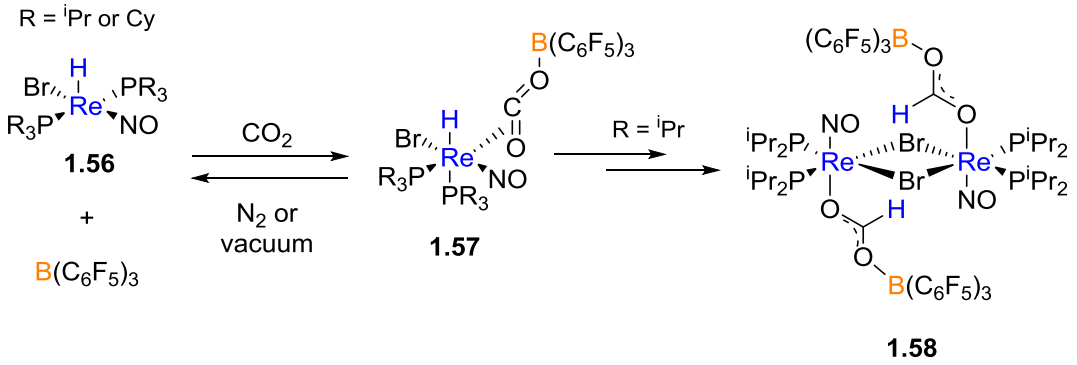

Scheme 1.14: Re-H/B FLP and its interaction with CO_2.

of the Lewis acid $B(C_6F_5)_3$ to yield CO_2 activated complex **1.57** (Scheme 1.14). This complex was unstable when in the absence of a CO_2 atmosphere, and reverted back to starting materials. However, when stored under a CO_2 atmosphere for 4 h at 23 °C, crystals of CO_2-activated complex **1.58** were isolated and characterised.

Stephan *et al*. developed a ruthenium complex **1.59**, bearing a tripodal ligand, which underwent halide and subsequent proton abstraction to form FLP-like species **1.60** (Scheme 1.15).[110] Here, the ruthenium centre acted as a Lewis acid with the phosphine ligand as the Lewis base. This complex was shown to undergo ligand rearrangement upon reaction with CO_2 to form activation species **1.60**. Although this species was shown to be thermally robust up to 80 °C for over 1 week, species **1.61** reacted with HBpin (HBPin = 4,4,5,5-Tetramethyl-1,3,2-dioxaborolane) to reduce CO_2 to MeOBpin and $O(Bpin)_2$. This system was shown to be successful under catalytic conditions for CO_2 reduction. Ru/P FLP was also shown to activate benzaldehyde in a typical FLP manner.

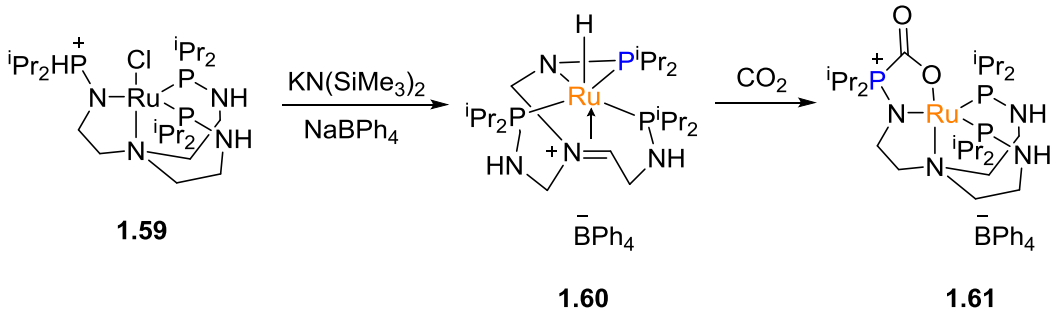

Scheme 1.15: Formation of Ru/P FLP **1.60** and its reaction with CO_2.

Peters *et al*. developed iron, cobalt and nickel complexes which all contain metal-borane bonds (Figure 1.7).[111–113] All of these complexes have demonstrated facile, reversible heterolytic cleavage of H_2 to form species where dihydrogen has inserted into the metal-boron bond. Iron and nickel complexes **1.62** and **1.64** respectively were successful in the

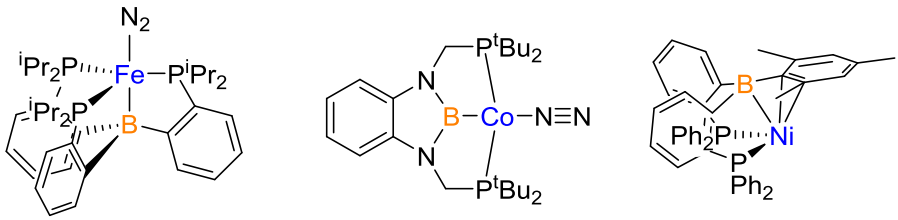

1.62 **1.63** **1.64**

Figure 1.7: Examples of complexes with metal-boron bonds which are capable of reversible H_2 addition.

hydrogenation catalysis of alkenes. Cobalt species **1.63** displayed catalytic activity for hydrogenation of terminal alkenes and dehydrogenation/transfer hydrogenation of amine-boranes. It was rationalised that the enhanced catalytic activity was related to the strong *trans*-influence from the boryl ligand.[114]

In 2017, Simonneau *et al*. described the use of zero-valent group 6 complexes for the activation of dinitrogen in combination with $B(C_6F_5)_3$.[115] The reaction of *trans*-$[M(N_2)_2(dppe)_2]$ (M = Mo or W, dppe = 1,2-bis(diphenylphosphino)ethane) with $B(C_6F_5)_3$ leads to the formation of N_2 activation product $[(dppe)_2M{=}N{=}N\text{-}B(C_6F_5)_3]$. The newly formed B-N linkage displayed further FLP reactivity by activation of B-H and Si-H bonds which provided a stepping stone towards N_2 functionalisation. Further work is being carried out to develop the system for catalytic N_2 reduction.[116]

Perhaps the most versatile example of the use of late transition metals as the Lewis basic component of an FLP was the development of a Pt/B Lewis pair by the Wass and Pringle groups, which is pertinent to this thesis (Scheme 1.16).[117,118] Platinum complex **1.65** bears a bulky diphosphine ligand and a weak interaction was observed with the Lewis acid $B(C_6F_5)_3$. The Pt(0)/$B(C_6F_5)_3$ system was shown to under facile heterolysis of dihydrogen to form ion pair **1.66** and was able to sequester CO_2 to form **1.71**.[117]

Preformation of monoethene complex **1.67** prior to addition of $B(C_6F_5)_3$ led to linear activation of ethene to form **1.68**, analogous to what was reported by Braunschweig *et al*. in 2013 whilst investigating the reactivity between related Pt(0) complex and fluoroboranes.[119] Interestingly, direct reaction of **1.65** and $B(C_6F_5)_3$ with ethene resulted in the formation of **1.69** where ethene has inserted into the Pt-CO bond and activation of the CO ligand is observed. This is an intriguing reaction to investigate as it opens the possibility of C-C bond forming reactions using FLPs. The platinum Lewis base **1.65** also displays ambiphilic behaviour with the reversible coordination of CO to form 18e-

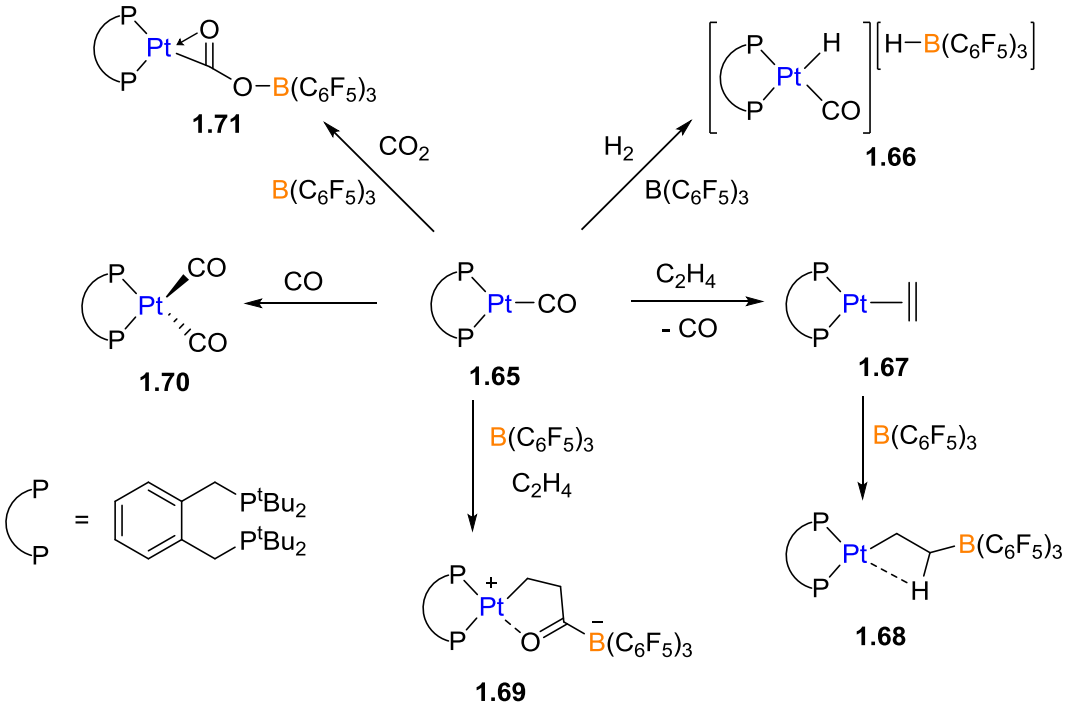

Scheme 1.16: Small molecule activation by Pt/B FLP.

saturated complex **1.70**.[118] The activation of small molecules by the Pt(0)/$B(C_6F_5)_3$ system have only been successful in stoichiometric reactions and have shown no signs of reversibility. Further work on the development of this system is the main focus of Chapter 2 and 3 of this thesis.

Campos has recently reported the first example of a transition metal only FLP in which Au(I) and Pt(0) complexes acted as Lewis acidic and Lewis basic fragments respectively (Scheme 1.17).[120] The FLP pair **1.72/1.73** was subjected to H_2 and, after 5 min, complete consumption of **1.72** was observed. The species in the mixture were identified to be unreacted **1.73**, a novel hydride bridging digold complex and the platinum hydride of **1.73**. This mixture slowly converted to complex **1.74** over 12 h at room temperature. When the FLP pair was exposed to acetylene an instant colour change was observed and the two isomeric products **1.75** and **1.76** were identified in solution in an approximate 4:1 ratio. The composition of the reaction mixture did not change with time and upon heating at 90 °C, which indicated that the two species arise from competitive independent reaction pathways.

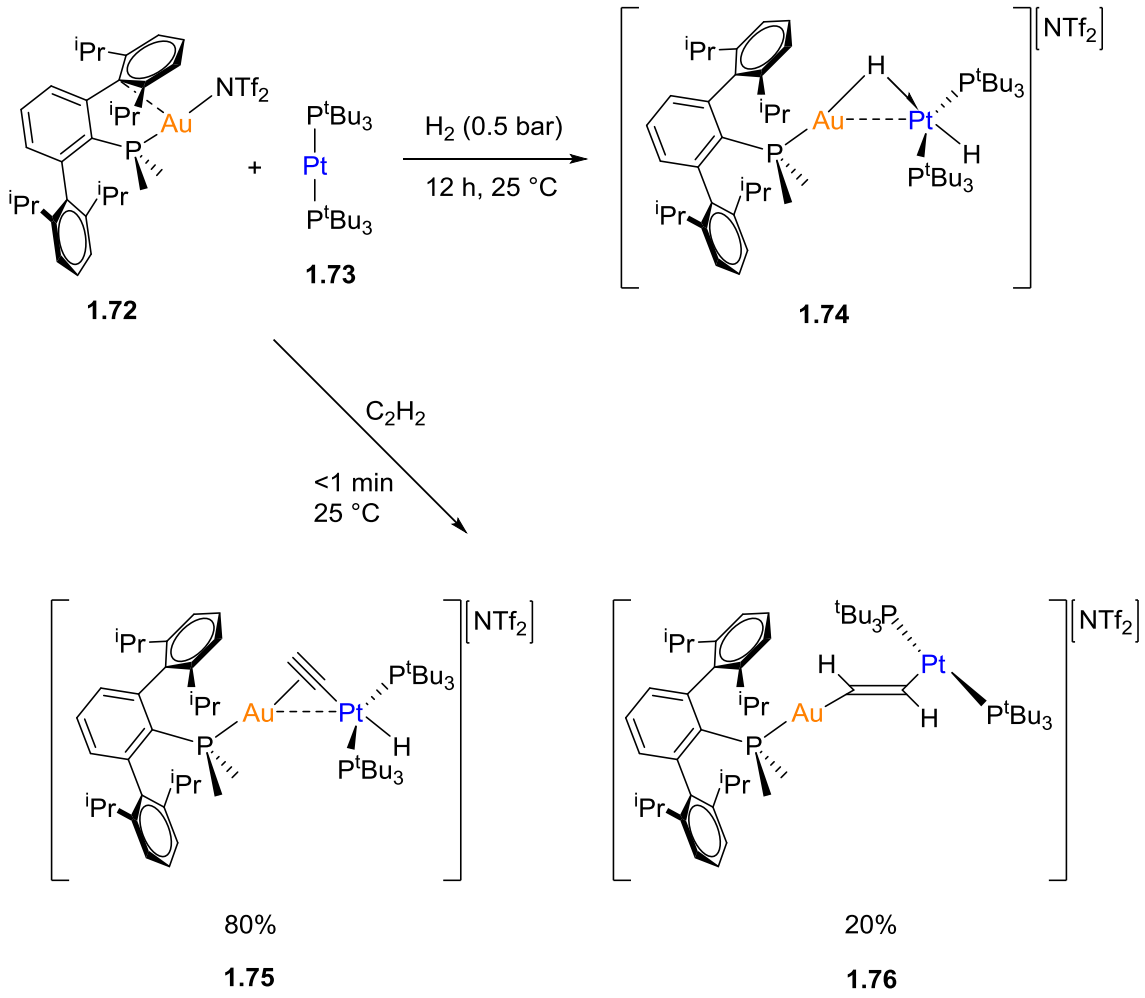

Scheme 1.17: Transition metal only FLP **1.72**/**1.73** and its reactivity with H_2 and acetylene.

1.5 Frustration *vs.* Cooperation

The term 'frustrated Lewis pair' commonly is used to describe systems where the two Lewis components are prevented from forming a classical Lewis adduct and it is this 'unquenched' reactivity which is exploited in small molecule activation. However, there have been many reports of both main group and transition metal systems which are described as 'FLPs' and successfully activate small molecules, but, exhibit an interaction between the Lewis acidic and Lewis basic components. Figure 1.8 shows select examples of FLP systems where an interaction between the Lewis centres has been identified.[20,41,84]

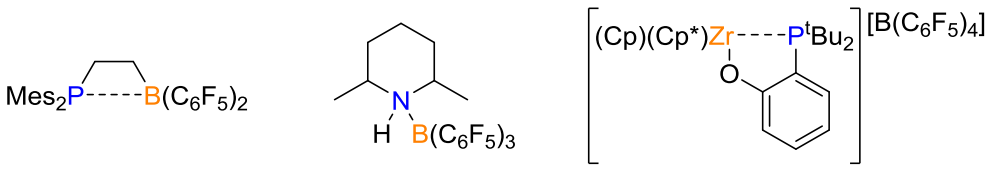

Figure 1.8: Selected examples of FLPs which shown an interaction between the Lewis centres.

Whether or not a Lewis acid-base adduct is capable of FLP reactivity was proposed to be based on the equilibrium between the 'open' and 'closed' states of the system.[12,13,121] Despite the observation of an Lewis pair interaction in these systems, they do exhibit reactivity which follows the FLP paradigm. This calls into question the definition of a frustrated Lewis pair and a more fitting definition of these systems as 'cooperative Lewis pairs' was adopted. The cooperative action of the Lewis pair to activate small molecules was recognised because if either component was absent the reactivity of the system would either cease or the final activation products would differ.

As the field of small molecule activation by Lewis pairs grew to involve transition metals it is important to draw comparisons of these systems to well-established transition metals which fall under the category of cooperative catalysis. These can include systems which contain hybrid ligands, hemilabile ligands and non-innocent ligands.[122,123] It should also be noted that cooperativity in bond activation is prevalent in nature. Dihydrogen activation by [FeFe], [NiFe] and [Fe]-only hydrogenases is facilitated by the cooperation of a pendant thiol ligand with the metal centre to result in heterolytic cleavage of the H-H bond without an overall change in the oxidation state of the metal.[124–126]

One of the seminal examples of metal-ligand cooperation in hydrogenation catalysis comes from the group of Noyori.[127–130] Ketone hydrogenation by **1.77** was shown to proceed *via* a six-member pericycle transition state where the amine proton and the ruthenium-hydride add across a C=O bond in a concerted manner to form an amido complex **1.78** (Figure 1.9). This can then add H_2 to reform the active catalyst. The important feature of the ligand is the presence of either a primary or secondary amine group in the 1st coordination sphere known as the N-H effect.[127,131,132]

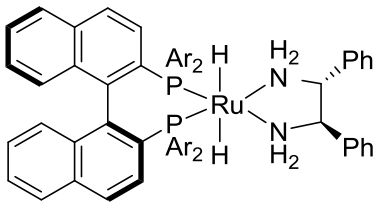

1.77

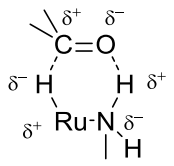

1.78

Figure 1.9: Example of a bifunctional catalyst developed by Noyori for hydrogenation (**1.77**) and the proposed transition state for the hydrogenation of ketones.

Several related ruthenium complexes have been reported which follow this paradigm of metal-ligand cooperation between metal-amine/amido ligands (Figure 1.10).[133–137] These follow the mechanism of addition of H_2 across the M-N amido-bond which then transfers to the substrate or *vice versa* depending on whether the catalyst is being used for hydrogenation or dehydrogenation. Complex **1.81** and **1.82** have also been shown to be active for the coupling of alcohols to higher alcohols which goes *via* a Guerbet mechanism which involves both a dehydrogenation and a hydrogenation of substrates by the same catalyst (known as borrowed hydrogen chemistry).[138]

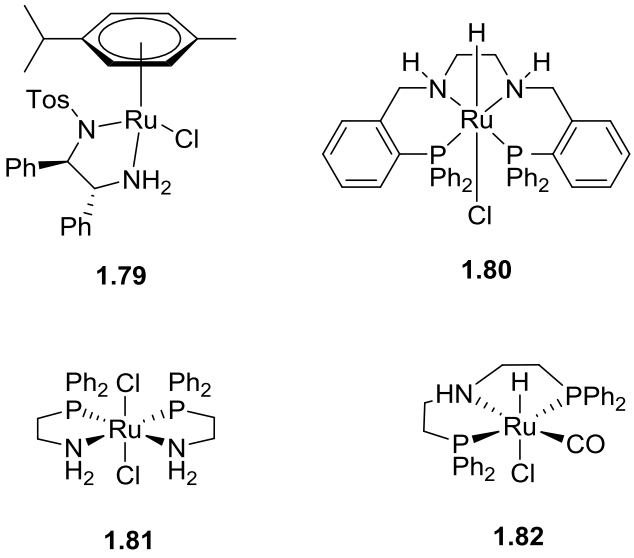

Figure 1.10: Selected pre-catalysts which have been shown to undergo hydrogenation/dehydrogenation pathways by metal-ligand cooperation across the metal amine/amido bond.

As well as dihydrogen, metal-ligand cooperation has been shown to be successful in other small molecule activations. Ruthenium complex **1.83**, which bears a β-diketiminate ligand, displays H_2, ethene and acetylene activation across the Ru centre and the central carbon atom on the ligand.[139] A related aluminium β-diketiminate complex displayed similar reactivity towards ethene.[140]

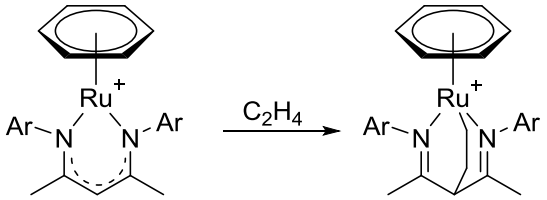

1.83 **1.84**

Scheme 1.18: Example of a β-diketiminate complex capable of activation ethene. $[OTf]^-$ counterion omitted for clarity.

One of the research focuses of the Milstein group centres around the use of tridentate pincer ligand complexes with general structure **1.85** (Scheme 1.19A).[123] The metal-ligand cooperation occurs through dearomatisation of the ligand during the bond activation. These lutidine-based pincer complexes display bond activation of H_2,[141] H_2O,[142] CO_2,[143,144] alcohols,[145] ketones,[146] aldehydes[146] and amines.[147] Many of these Fe, Mn and Ru based catalysts have also been shown to be successful hydrogenation catalysts for a variety of substrates.[148–152]

A

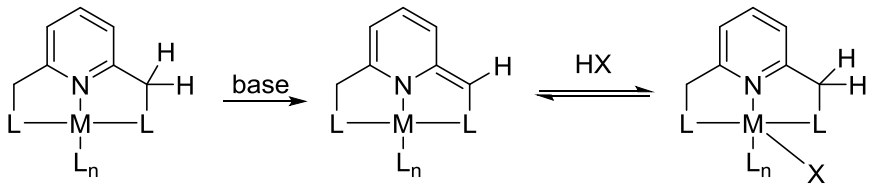

1.85 **1.86** **1.87**

HX = H_2, H_2O, ROH, RNH_2, R_2BH

B

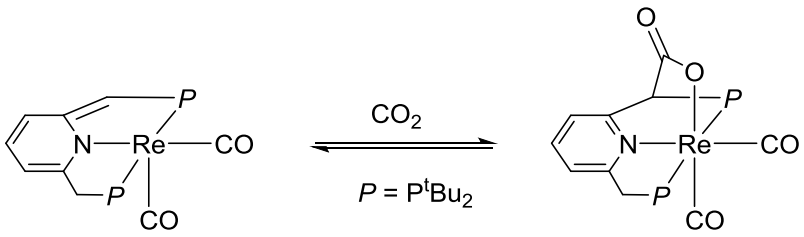

1.88 **1.89**

Scheme 1.19: A) General scheme for bond activation by complexes with lutidine-based pincer ligands. B) Activation of CO_2 by Re complex **1.88**.

The above examples can be likened to the FLP analogy, mainly where the metal centre acts as a Lewis acid in cooperation with an N or C Lewis basic centre on the ligand. It is

important to recognise these complexes undergo cooperative activation of small molecules, although many examples are limited to simple H-X bonds (where X = H, N, O).

As more examples of transition metal FLPs emerge, it should be kept in mind that it may not fit the description of a 'true' FLP. It is more likely that the reaction pathways will involve both 'FLP' reactivity as well as traditional transition metal reactivity. The most significant aspect of these systems is the cooperative action between the Lewis acid and Lewis basic centre, whether that be part of an inter- or intramolecular system, which would not occur if one of the components were absent.

1.6 Thesis Scope

The use of transition metals as part of Lewis pairs which are capable of small molecule activation is a growing field with an increasing number of examples emerging. Unfortunately, many of the main group FLPs and the transition metal FLPs only activate small molecules stoichiometrically and have not been able to be used for catalysis (with the exception of hydrogenation catalysis). There remains scope to expand the substrate library which undergoes small molecule activation with these systems, and to also modify the systems for use in catalysis. The aim of the work presented in this thesis is to expand the understanding of currently known transition metal FLP systems. This will focus on modification of known systems and exploration of new small molecular activation pathways which take into account both traditional transition metal and cooperative activation mechanisms.

1.7 References

1 J. N. Bronsted, *Recl. des Trav. Chim. des Pays-Bas la Belgique*, 1923, **42**, 718–728.

2 T. M. Lowry, *J. Soc. Chem. Ind.*, 1923, **42**, 43–47.

3 G. N. Lewis, *Valence and the Structure of Atoms and Molecules*, The Chemical Catalog Company, inc., New York, 1923.

4 S. G. Shore and R. W. Parry, *J. Am. Chem. Soc.*, 1955, **77**, 6084–6085.

5 H. C. Brown, H. I. Schlesinger and S. Z. Cardon, *J. Am. Chem. Soc.*, 1942, **64**, 325–329.

6 H. C. Brown and B. Kanner, *J. Am. Chem. Soc.*, 1966, **88**, 986–992.

7 G. Wittig and E. Benz, *Chem. Ber.*, 1959, **92**, 1999–2013.

8 W. Tochtermann, *Angew. Chem. Int. Ed.*, 1966, **5**, 351–371.

9 G. C. Welch, R. R. San Juan, J. D. Masuda and D. W. Stephan, *Science*, 2006, **314**, 1124–1126.

10 S. Döring, G. Erker, R. Fröhlich, O. Meyer and K. Bergander, *Organometallics*, 1998, **17**, 2183–2187.

11 J. S. J. McCahill, G. C. Welch and D. W. Stephan, *Angew. Chem. Int. Ed.*, 2007, **46**, 4968–4971.

12 D. W. Stephan and G. Erker, *Angew. Chem. Int. Ed.*, 2010, **49**, 46–76.

13 D. W. Stephan and G. Erker, *Angew. Chem. Int. Ed.*, 2015, **54**, 6400–6441.

14 G. C. Welch and D. W. Stephan, *J. Am. Chem. Soc.*, 2007, **129**, 1880–1881.

15 M. Ullrich, K. S.-H. Seto, A. J. Lough and D. W. Stephan, *Chem. Commun.*, 2009, 2335–2337.

16 M. A. Dureen and D. W. Stephan, *J. Am. Chem. Soc.*, 2009, **131**, 8396–8397.

17 G. C. Welch, J. D. Masuda and D. W. Stephan, *Inorg. Chem.*, 2006, **45**, 478–480.

18 C. M. Mömming, E. Otten, G. Kehr, R. Fröhlich, S. Grimme, D. W. Stephan and

G. Erker, *Angew. Chem. Int. Ed.*, 2009, **48**, 6643–6646.

19 M. Sajid, A. Klose, B. Birkmann, L. Liang, B. Schirmer, T. Wiegand, H. Eckert, A. J. Lough, R. Fröhlich, C. G. Daniliuc, S. Grimme, D. W. Stephan, G. Kehr and G. Erker, *Chem. Sci.*, 2013, **4**, 213–219.

20 P. Spies, G. Erker, G. Kehr, K. Bergander, R. Fröhlich, S. Grimme and D. W. Stephan, *Chem. Commun.*, 2007, 5072–5074.

21 C. M. Mömming, S. Frömel, G. Kehr, R. Fröhlich, S. Grimme and G. Erker, *J. Am. Chem. Soc.*, 2009, **131**, 12280–12289.

22 C. M. Mömming, G. Kehr, B. Wibbeling, R. Fröhlich and G. Erker, *Dalton Trans.*, 2010, **39**, 7556–7564.

23 M. Sajid, G. Kehr, T. Wiegand, H. Eckert, C. Schwickert, R. Pöttgen, A. J. P. Cardenas, T. H. Warren, R. Fröhlich, C. G. Daniliuc and G. Erker, *J. Am. Chem. Soc.*, 2013, **135**, 8882–8895.

24 O. Ekkert, G. G. Miera, T. Wiegand, H. Eckert, B. Schirmer, J. L. Petersen, C. G. Daniliuc, R. Fröhlich, S. Grimme, G. Kehr and G. Erker, *Chem. Sci.*, 2013, **4**, 2657–2664.

25 H. Wang, R. Fröhlich, G. Kehr and G. Erker, *Chem. Commun.* , 2008, 5966–5968.

26 C. Rosorius, G. Kehr, R. Fröhlich, S. Grimme and G. Erker, *Organometallics*, 2011, **30**, 4211–4219.

27 A. Stute, G. Kehr, R. Fröhlich and G. Erker, *Chem. Commun.*, 2011, **47**, 4288–4290.

28 D. Holschumacher, T. Bannenberg, C. G. Hrib, P. G. Jones and M. Tamm, *Angew. Chem. Int. Ed.*, 2008, **47**, 7428–7432.

29 P. A. Chase and D. W. Stephan, *Angew. Chem. Int. Ed.*, 2008, **47**, 7433–7437.

30 C. Appelt, H. Westenberg, F. Bertini, A. W. Ehlers, J. C. Slootweg, K. Lammertsma and W. Uhl, *Angew. Chem. Int. Ed.*, 2011, **50**, 3925–3928.

31 M. Lange, J. C. Tendyck, P. Wegener, A. Hepp, E. U. Würthwein and W. Uhl, *Chem. - A Eur. J.*, 2018, DOI: 10.1002/chem.2017006089.

32 T. E. Stennett, J. Pahl, H. S. Zijlstra, F. W. Seidel and S. Harder, *Organometallics*, 2016, **35**, 207–217.

33 D. Pleschka, M. Layh, F. Rogel and W. Uhl, *Philos. Trans. R. Soc. A Math. Phys. Eng. Sci.*, 2017, **375**, 20170011.

34 G. Ménard and D. W. Stephan, *Angew. Chem. Int. Ed.*, 2011, **50**, 8396–8399.

35 L. J. Hounjet, C. B. Caputo and D. W. Stephan, *Angew. Chem. Int. Ed.*, 2012, **51**, 4714–4717.

36 L. J. Hounjet, C. B. Caputo and D. W. Stephan, *Dalt. Trans.*, 2013, **42**, 2629–2635.

37 M. H. Holthausen, J. M. Bayne, I. Mallov, R. Dobrovetsky and D. W. Stephan, *J. Am. Chem. Soc.*, 2015, **137**, 7298–7301.

38 J. M. Bayne and D. W. Stephan, *Chem. Soc. Rev.*, 2016, **45**, 765–774.

39 V. Sumerin, F. Schulz, M. Nieger, M. Leskel, T. Repo and B. Rieger, *Angew. Chem. Int. Ed.*, 2008, **47**, 6001–6003.

40 V. Sumerin, F. Schulz, M. Atsumi, C. Wang, M. Nieger, M. Leskel, T. Repo, P. Pyykk and B. Rieger, *J. Am. Chem. Soc.*, 2008, **130**, 14117–14119.

41 C. Jiang, O. Blacque, T. Fox and H. Berke, *Organometallics*, 2011, **30**, 2117–2124.

42 F. Schulz, V. Sumerin, S. Heikkinen, B. Pedersen, C. Wang, M. Atsumi, M. Leskelä, T. Repo, P. Pyykkö, W. Petry and B. Rieger, *J. Am. Chem. Soc.*, 2011, **133**, 20245–20257.

43 K. Chernichenko, M. Nieger, M. Leskelä and T. Repo, *Dalt. Trans.*, 2012, **41**, 9029–9032.

44 S. C. Binding, H. Zaher, F. M. Chadwick and D. O'Hare, *Dalt. Trans.*, 2012, **41**, 9061–9066.

45 C. B. Caputo, K. Zhu, V. N. Vukotic, S. J. Loeb and D. W. Stephan, *Angew. Chem. Int. Ed.*, 2013, **52**, 960–963.

46 Z. Lu, Y. Wang, J. Liu, Y. Lin, Z. H. Li and H. Wang, *Organometallics*, 2013, **32**,

6753–6758.

47 A. Karkamkar, K. Parab, D. M. Camaioni, D. Neiner, H. Cho, T. K. Nielsen and T. Autrey, *Dalt. Trans.*, 2013, **42**, 615–619.

48 T. Voss, T. Mahdi, E. Otten, R. Fröhlich, G. Kehr, D. W. Stephan and G. Erker, *Organometallics*, 2012, **31**, 2367–2378.

49 R. Roesler, W. E. Piers and M. Parvez, *J. Organomet. Chem.*, 2003, **680**, 218–222.

50 S. Schwendemann, R. Fröhlich, G. Kehr and G. Erker, *Chem. Sci.*, 2011, **2**, 1842–1849.

51 D. W. Stephan, *Acc. Chem. Res.*, 2015, **48**, 306–316.

52 P. A. Chase, G. C. Welch, T. Jurca and D. W. Stephan, *Angew. Chem. Int. Ed.*, 2007, **46**, 8050–8053.

53 D. J. Scott, M. J. Fuchter and A. E. Ashley, *Chem. Soc. Rev.*, 2017, 46, 5689–5700.

54 P. A. Chase, T. Jurca and D. W. Stephan, *Chem. Commun.*, 2008, 1701–1703.

55 P. Spies, S. Schwendemann, S. Lange, G. Kehr, R. Fröhlich and G. Erker, *Angew. Chem. Int. Ed.*, 2008, **47**, 7543–7546.

56 H. Wang, R. Fröhlich, G. Kehr and G. Erker, *Chem. Commun.*, 2008, 5966–5968.

57 J. Mohr and M. Oestreich, *Angew. Chem. Int. Ed.*, 2014, **53**, 13278–13281.

58 I. Chatterjee and M. Oestreich, *Angew. Chem. Int. Ed.*, 2015, **54**, 1965–1968.

59 J. M. Farrell, Z. M. Heiden and D. W. Stephan, *Organometallics*, 2011, **30**, 4497–4500.

60 L. Greb, P. Oña-Burgos, B. Schirmer, S. Grimme, D. W. Stephan and J. Paradies, *Angew. Chem. Int. Ed.*, 2012, **51**, 10164–10168.

61 L. Greb, C. G. Daniliuc, K. Bergander and J. Paradies, *Angew. Chem. Int. Ed.*, 2013, **52**, 5876–5879.

62 K. Chernichenko, Á. Madarász, I. Pápai, M. Nieger, M. Leskelä and T. Repo, *Nat. Chem.*, 2013, **5**, 718–723.

63 L. E. Longobardi, C. Tang and D. W. Stephan, *Dalt. Trans.*, 2014, **43**, 15723–15726.

64 T. Mahdi and D. W. Stephan, *J. Am. Chem. Soc.*, 2014, **136**, 15809–15812.

65 D. J. Scott, M. J. Fuchter and A. E. Ashley, *J. Am. Chem. Soc.*, 2014, **136**, 15813–15816.

66 T. Mahdi and D. W. Stephan, *Angew. Chem. Int. Ed.*, 2015, **54**, 8511–8514.

67 G. Ghattas, D. Chen, F. Pan and J. Klankermayer, *Dalt. Trans.*, 2012, **41**, 9026–9028.

68 M. Lindqvist, K. Borre, K. Axenov, B. Kótai, M. Nieger, M. Leskelä, I. Pápai and T. Repo, *J. Am. Chem. Soc.*, 2015, **137**, 4038–4041.

69 D. Chen and J. Klankermayer, *Chem. Commun.*, 2008, 2130–2131.

70 X. Wang, G. Kehr, C. G. Daniliuc and G. Erker, *J. Am. Chem. Soc.*, 2014, **136**, 3293–3303.

71 Y. Liu and H. Du, *J. Am. Chem. Soc.*, 2013, **135**, 6810–6813.

72 M. Mewald, R. Fröhlich and M. Oestreich, *Chem. - A Eur. J.*, 2011, **17**, 9406–9414.

73 A. E. Ashley, A. L. Thompson and D. O'Hare, *Angew. Chem. Int. Ed.*, 2009, **48**, 9839–9843.

74 M. A. Courtemanche, M. A. Légaré, L. Maron and F. G. Fontaine, *J. Am. Chem. Soc.*, 2013, **135**, 9326–9329.

75 F. G. Fontaine, M. A. Courtemanche and M. A. Légaré, *Chem. - A Eur. J.*, 2014, **20**, 2990–2996.

76 T. Wang and D. W. Stephan, *Chem. - A Eur. J.*, 2014, **20**, 3036–3039.

77 T. Mahdi and D. W. Stephan, *Angew. Chem. Int. Ed.*, 2013, **52**, 12418–12421.

78 S. R. Flynn and D. F. Wass, *ACS Catal.*, 2013, 3, 2574–2581.

79 T. Keith Hollis, W. Odenkirk, N. P. Robinson, J. Whelan and B. Bosnich, *Tetrahedron*, 1993, **49**, 5415–5430.

80 H. Yamamoto, *Lewis Acids in Organic Synthesis*, Wiley-VCH, New York, 2000.

81 R. C. Neu, E. Otten, A. Lough and D. W. Stephan, *Chem. Sci.*, 2011, **2**, 170–176.

82 A. M. Chapman, M. F. Haddow and D. F. Wass, *J. Am. Chem. Soc.*, 2011, **133**, 8826–8829.

83 A. M. Chapman and D. F. Wass, *Dalton Trans.*, 2012, **41**, 9067–9072.

84 A. M. Chapman, M. F. Haddow and D. F. Wass, *J. Am. Chem. Soc.*, 2011, **133**, 18463–18478.

85 O. J. Metters, S. J. K. Forrest, H. A. Sparkes, I. Manners and D. F. Wass, *J. Am. Chem. Soc.*, 2016, **138**, 1994–2003.

86 S. R. Flynn, O. J. Metters, I. Manners and D. F. Wass, *Organometallics*, 2016, **35**, 847–850.

87 X. Xu, G. Kehr, C. G. Daniliuc and G. Erker, *Angew. Chem. Int. Ed.*, 2013, **52**, 13629–13632.

88 X. Xu, G. Kehr, C. G. Daniliuc and G. Erker, *J. Am. Chem. Soc.*, 2013, **135**, 6465–6476.

89 X. Xu, G. Kehr, C. G. Daniliuc and G. Erker, *J. Am. Chem. Soc.*, 2014, **136**, 12431–12443.

90 X. Xu, G. Kehr, C. G. Daniliuc and G. Erker, *J. Am. Chem. Soc.*, 2015, **137**, 4550–4557.

91 A. T. Normand, C. G. Daniliuc, B. Wibbeling, G. Kehr, P. Le Gendre and G. Erker, *J. Am. Chem. Soc.*, 2015, **137**, 10796–10808.

92 A. T. Normand, C. G. Daniliuc, G. Kehr, P. Le Gendre and G. Erker, *Dalton Trans.*, 2016, **45**, 3711–3714.

93 Z. Jian, C. G. Daniliuc, G. Kehr and G. Erker, *Organometallics*, 2017, **36**, 424–434.

94 G. C. Welch, L. Cabrera, P. A. Chase, E. Hollink, J. D. Masuda, P. Wei and D. W. Stephan, *Dalt. Trans.*, 2007, 3407–3414.

95 Z. Jian, G. Kehr, C. G. Daniliuc, B. Wibbeling, T. Wiegand, M. Siedow, H. Eckert,

M. Bursch, S. Grimme and G. Erker, *J. Am. Chem. Soc.*, 2017, **139**, 6474–6483.

96 Z. Jian, C. G. Daniliuc, G. Kehr and G. Erker, *Chem. Commun.*, 2018, **54**, 5724–5727.

97 A. Berkefeld, W. E. Piers, M. Parvez, L. Castro, L. Maron and O. Eisenstein, *J. Am. Chem. Soc.*, 2012, **134**, 10843–10851.

98 A. Berkefeld, W. E. Piers, M. Parvez, L. Castro, L. Maron and O. Eisenstein, *Chem. Sci.*, 2013, **4**, 2152–2162.

99 K. Chang and X. Xu, *Dalt. Trans.*, 2017, **46**, 4514–4517.

100 P. Xu, Y. Yao and X. Xu, *Chem. - A Eur. J.*, 2017, **23**, 1263–1267.

101 M. J. Sgro and D. W. Stephan, *Chem. Commun.* , 2013, **49**, 2610–2612.

102 T. Liu, Q. Liao, M. O'Hagan, E. B. Hulley, D. L. DuBois and R. M. Bullock, *Organometallics*, 2015, **34**, 2747–2764.

103 D. L. DuBois and R. M. Bullock, *Eur. J. Inorg. Chem.*, 2011, 1017–1027.

104 R. M. Bullock and M. L. Helm, *Acc. Chem. Res.*, 2015, **48**, 2017–2026.

105 C. J. Weiss, A. N. Groves, M. T. Mock, W. G. Dougherty, W. S. Kassel, M. L. Helm, D. L. DuBois and R. M. Bullock, *Dalt. Trans.*, 2012, **41**, 4517–4529.

106 E. B. Hulley, K. D. Welch, A. M. Appel, D. L. DuBois and R. M. Bullock, *J. Am. Chem. Soc.*, 2013, **135**, 11736–11739.

107 J. M. Darmon, S. Raugei, T. Liu, E. B. Hulley, C. J. Weiss, R. M. Bullock and M. L. Helm, *ACS Catal.*, 2014, **4**, 1246–1260.

108 Y. Jiang, O. Blacque, T. Fox and H. Berke, *J. Am. Chem. Soc.*, 2013, **135**, 7751–7760.

109 A. Maity and T. S. Teets, *Chem. Rev.*, , DOI:10.1021/acs.chemrev.6b00034.

110 M. J. Sgro and D. W. Stephan, *Angew. Chem. Int. Ed.*, 2012, **51**, 11343–11345.

111 H. Fong, M. E. Moret, Y. Lee and J. C. Peters, *Organometallics*, 2013, **32**, 3053–3062.

112 T. P. Lin and J. C. Peters, *J. Am. Chem. Soc.*, 2013, **135**, 15310–15313.

113 W. H. Harman and J. C. Peters, *J. Am. Chem. Soc.*, 2012, **134**, 5080–5082.

114 T. P. Lin and J. C. Peters, *J. Am. Chem. Soc.*, 2014, **136**, 13672–13683.

115 A. Simonneau, R. Turrel, L. Vendier and M. Etienne, *Angew. Chem. Int. Ed.*, 2017, **56**, 12268–12272.

116 A. Simonneau and M. Etienne, *Chem. - A Eur. J.*, 2018, DOI: 10.1002/chem.20180040509476539.

117 S. J. K. Forrest, J. Clifton, N. Fey, P. G. Pringle, H. A. Sparkes and D. F. Wass, *Angew. Chem. Int. Ed.*, 2015, **54**, 2223–2227.

118 S. J. K. Forrest, P. G. Pringle, H. A. Sparkes and D. F. Wass, *Dalt. Trans.*, 2014, 8**43**, 16335–16344.

119 J. Bauer, H. Braunschweig, R. D. Dewhurst and K. Radacki, *Chem. - A Eur. J.*, 2013, **19**, 8797–8805.

120 J. Campos, *J. Am. Chem. Soc.*, 2017, **139**, 2944–2947.

121 T. Özgün, K.-Y. Ye, C. G. Daniliuc, B. Wibbeling, L. Liu, S. Grimme, G. Kehr and G. Erker, *Chem. - A Eur. J.*, 2016, **22**, 5988–5995.

122 H. Grützmacher, *Angew. Chem. Int. Ed.*, 2008, **2**, 1814–1818.

123 J. R. Khusnutdinova and D. Milstein, *Angew. Chem. Int. Ed.*, 2015, 54, 12236–12273.

124 M. Frey, *ChemBioChem*, 2002, **3**, 153–160.

125 W. Lubitz, H. Ogata, O. Rüdiger and E. Reijerse, *Chem. Rev.*, 2014, **114**, 4081–54148.

126 D. M. Heinekey, *J. Organomet. Chem.*, 2009, **694**, 2671–2680.

127 J. Takehara, S. Hashiguchi, A. Fujii, S. Inoue, T. Ikariya and R. Noyori, *Chem. Commun.*, 1996, 233–234.

128 R. Noyori and S. Hashiguchi, *Acc. Chem. Res.*, 1997, **30**, 97–102.

129 R. Noyori and T. Ohkuma, *Angew. Chem. Int. Ed.*, 2001, 40, 40–73.

130 C. A. Sandoval, T. Ohkuma, K. Muñiz and R. Noyori, *J. Am. Chem. Soc.*, 2003, **125**, 13490–13503.

131 K. Muñiz, *Angew. Chem. Int. Ed.*, 2005, 44, 6622–6627.

132 S. D. Phillips, J. A. Fuentes and M. L. Clarke, *Chem. - A Eur. J.*, 2010, **16**, 8002–8005.

133 R. Noyori, M. Yamakawa and S. Hashiguchi, *J. Org. Chem.*, 2001, 66, 7931–7944.

134 T. Li, I. Bergner, F. N. Haque, M. Z. De Iuliis, D. Song and R. H. Morris, *Organometallics*, 2007, **26**, 5940–5949.

135 K. Abdur-Rashid, R. Guo, A. Lough, R. Morris and D. Song, *Adv. Synth. Catal.*, 2005, **347**, 571–579.

136 W. Jia, X. Chen, R. Guo, C. Sui-Seng, D. Amoroso, A. J. Lough and K. Abdur-Rashid, *J. Chem. Soc. Dalt. Trans.*, 2009, 8301–8307.

137 S. Gao, W. Tang, M. Zhang, C. Wang and J. Xiao, *Synlett*, 2016, **27**, 1748–1752.

138 K. J. Pellow, R. L. Wingad and D. F. Wass, *Catal. Sci. Technol.*, 2017, **7**, 5128–5134.

139 A. D. Phillips, G. Laurenczy, R. Scopelliti and P. J. Dyson, *Organometallics*, 2007, **26**, 1120–1122.

140 C. E. Radzewich, M. P. Coles and R. F. Jordan, *J. Am. Chem. Soc.*, 1997, **120**, 9384-9385.

141 E. Ben-Ari, G. Leitus, L. J. W. Shimon and D. Milstein, *J. Am. Chem. Soc.*, 2006, **128**, 15390–15391.

142 S. W. Kohl, L. Weiner, L. Schwarstsburd, L. Konstantinovski, L. J. W. Shimon, Y. Ben-David, M. A. Iron and D. Milstein, *Science*, 2009, **324**, 74–77.

143 M. Vogt, M. Gargir, M. A. Iron, Y. Diskin-Posner, Y. Ben-David and D. Milstein, *Chem. - A Eur. J.*, 2012, **18**, 9194–9197.

144 M. Vogt, A. Nerush, Y. Diskin-Posner, Y. Ben-David and D. Milstein, *Chem. Sci.*, 2014, **5**, 2043–2051.

145 M. Montag, J. Zhang and D. Milstein, *J. Am. Chem. Soc.*, 2012, **134**, 10325–10328.

146 C. A. Huff, J. W. Kampf and M. S. Sanford, *Chem. Commun.*, 2013, **49**, 7171–7173.

147 E. Khaskin, M. A. Iron, L. J. W. Shimon, J. Zhang and D. Milstein, *J. Am. Chem. Soc.*, 2010, **132**, 8542–8543.

148 T. Zell and D. Milstein, *Acc. Chem. Res.*, 2015, **48**, 1979–1994.

149 P. Hu, Y. Ben-David and D. Milstein, *Angew. Chem. Int. Ed.*, 2016, **55**, 1061–1064.

150 N. A. Espinosa-Jalapa, A. Nerush, L. J. W. Shimon, G. Leitus, L. Avram, Y. Ben-David and D. Milstein, *Chem. - A Eur. J.*, 2017, **23**, 5934–5938.

151 R. Zeng, M. Feller, Y. Ben-David and D. Milstein, *J. Am. Chem. Soc.*, 2017, **139**, 5720–5723.

152 S. Chakraborty and D. Milstein, *ACS Catal.*, 2017, **7**, 3968–3972.

Chapter 2

Small Molecule Activation by Intermolecular Pt(0)/B Lewis Pairs

2.1 Introduction

Many transition metal complexes can be described as Lewis acids that are coordinated by L-type ligands (neutral ligands which donate two electrons to the metal centre). This concept has driven the use of high valent cationic complexes in frustrated Lewis pair (FLP) chemistry. As described in Chapter 1, the field of FLP chemistry has evolved from main group systems to early transition metal complexes utilised as the Lewis acidic component in both inter- and intramolecular systems. In addition, transition metal complexes have been shown to display Lewis basic behaviour when coordinating to Z-type ligands (ligands which are accept two electrons from the metal centre).[1–3] Some of these Lewis basic complexes have been shown to activate small molecules in an intramolecular FLP-type manner.[4,5]

After the success of using Zr(IV) complexes as Lewis acids, the question arose as to whether a low valent late transition metal complex would be suitable as a Lewis base. Work in the Pringle and Wass groups began by developing a Pt(0) complex for use in an intermolecular FLP.[6–8] The ligand of choice was the electron rich, bulky diphosphine ligand 1,2-bis(di-*tert*-butylphosphino)xylene (dtbpx, **L1**) which has been widely used in platinum chemistry. For example, in 1976, Shaw *et al.* reported the first example of a *cis*-dihydrido Pt(II)-complex of **L1**.[9] Spencer *et al.* utilised **L1** demonstrating that platinum-alkene complexes can react with a Brønsted acid to form some of the first examples of β-agostic C-H-Pt complexes (Figure 2.1).[10,11] **L1** is also used commercially by Lucite in

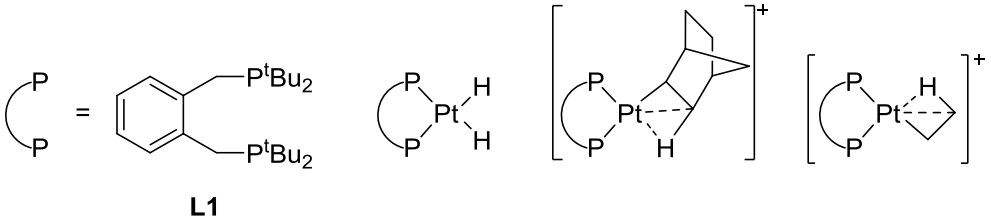

Figure 2.1: Examples of the use of dtbpx in small molecule activation by Pt complexes.

the Pd-catalysed ethene hydromethoxycarbonylation, for the production of methyl propionate as a precursor to methyl methacrylate.[12,13]

Previous work in the Pringle and Wass groups has employed **L1** in the synthesis of a Pt(0) diphosphine monocarbonyl complex which, in combination with $B(C_6F_5)_3$, has displayed cooperative small molecule activation of dihydrogen, ethene and carbon dioxide (see Section 1.4).[6–8]

During the development of this Pt(0) system, Braunschweig *et al.* were investigating the reactivity of Lewis basic Pt(0) complexes with fluoroboranes.[14] [Pt(dcpp)(C_2H_4)] (**2.1**, dcpp = 1,3-bis(dicyclohexylphosphino)propane) was used as a Lewis base for small molecule activation (Scheme 2.1). Addition of $B(C_6F_5)_3$ to **2.1** led to the formation of β-agostic complex, **2.2**, which resembles products from alkene activation by main group FLPs.[15]

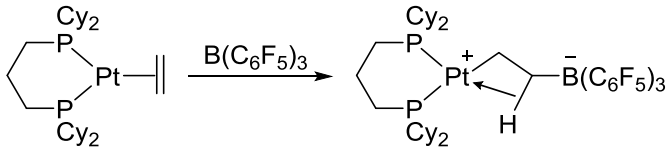

2.1 **2.2**

Scheme 2.1: Reaction of **2.1** with $B(C_6F_5)_3$ to form β-agostic complex **2.2**.

2.1.1 Aims and Objectives

The initial work on the Pt(0)/$B(C_6F_5)_3$ cooperative Lewis pair system by the groups of Wass and Pringle confirmed FLP-like behaviour was displayed by the system, although little was known about the reaction pathway to the activation products. It is of interest to gain insight into how the mixed transition metal/metalloid system activates small molecules and if indeed they proceed by a cooperative Lewis pair mechanism or if more traditional transition metal small molecule activation is at play. The Pt(0)/$B(C_6F_5)_3$ system stoichiometrically activates some small molecules, but the scope of activation chemistry had not been extensively explored. Thus, the aims of this part of the project were as follows:

- To investigate the effect of changing the ligand electronics to the Pt(0) component
- To explore potential pathways to small molecule activation for the Pt(0)/$B(C_6F_5)_3$ Lewis pair
- To expand the scope of molecules which could be activated by the Pt(0)/$B(C_6F_5)_3$ Lewis pair

2.2 Synthesis of 1,2-bis(di-*tert*-butylphosphinooxy)benzene, L2

Changing the ligands in transition metal systems is often a synthetically simple method of changing the stereoelectronic properties of the metal centre. In order to change the electronics of the Pt(0) Lewis base in the cooperative Lewis pair system, the diphosphine backbone was modified by forming the phosphinite analogue of **L1**, 1,2-bis(di-*tert*-butylphosphinooxy)benzene (dtbpob, **L2**). Phosphinites have the general formula $P(OR)R_2$. The π-accepting properties of these ligands are enhanced in comparison to tertiary phosphines due to the electron-withdrawing -OR groups lowering the energy of the π-acceptor orbitals on the phosphorus centre.[16] It was predicted that use of a diphosphinite ligand in place of a diphosphine would reduce the electron density at the metal centre through greater π-back donation to the ligand, therefore creating a less Lewis basic Pt(0) centre.

L2, was synthesised from the reaction of catechol and di-*tert*-butylchlorophosphine (Scheme 2.2). Although there were no literature experimental procedures for this specific phosphinite, the synthesis of the phenyl analogue of **L2** had been reported and requires the addition of triethylamine (as a base) to a mixture of catechol and diphenylchlorophosphine, both on and off-metal.[12,17,18] The synthesis of **L2** was first attempted by employing triethylamine as a base but even upon prolonged heating of the mixture no reaction of the starting chlorophosphine was observed. Deprotonation of the catechol, by sodium hydride, was required before the addition of the chlorophosphine to afford the desired phosphinite ligand **L2** (56% yield). Though the reaction proceeded cleanly, upon workup, minor amounts (< 10%) of hydrolysis product **2.3** from the cleavage of the P-O bond were observed by $^{31}P\{^1H\}$ NMR spectroscopy (Scheme 2.2). Purification attempts removed majority of the hydrolysis product, but it could never be

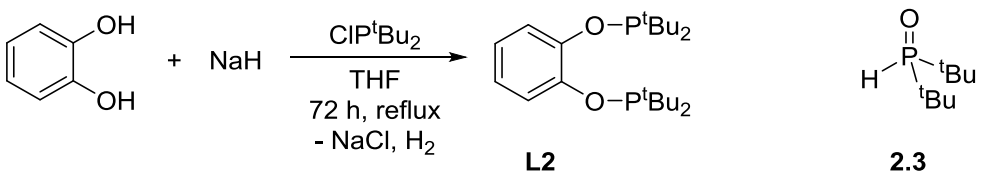

Scheme 2.2: Synthesis of **L2** and the P(V) hydrolysis product **2.3**.

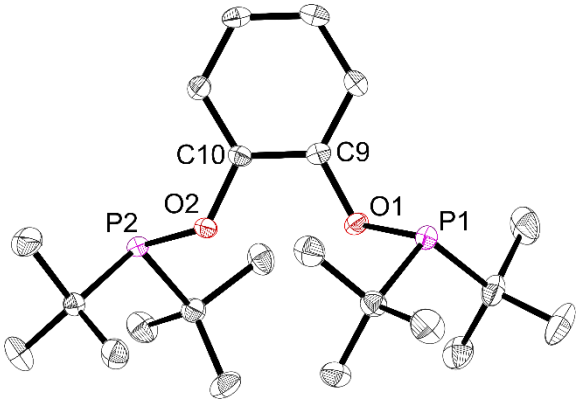

Figure 2.2: Crystal structure of **L2**. Thermal ellipsoids at 50%. Hydrogen atoms omitted for clarity. Selected bond lengths (Å) and angles (°): P1-O1 1.6726(12); O1-C9 1.3824(18); P2-O2 1.6719(12); O2-C10 1.3819(18); P1-O1-C9 120.99(11); P2-O2-C10 121.00(10).

separated completely without a large reduction in product yield. It was possible to carry the mixture of **L2** and **2.3** forward as any further coordination chemistry was not affected by the P(V) species **2.3** and could be removed much more easily away from the metal complex. Crystals of **L2** were grown by slow evaporation of a saturated pentane solution at −40 °C and the molecular structure is shown in Figure 2.2. In the crystal structure of **L1** the phosphines are orientated away from each other to minimise repulsion between the bulky *tert*-butyl groups. For **L2** the P donors are not orientated in the same way as **L1** which is presumably due to the oxygen lone pairs and the structure minimising this repulsion as well as the steric repulsion between the *tert*-butyl groups.

2.2.1 Synthesis of [$PtCl_2$(L2)]

Addition of **L2** to [$PtCl_2$(COD)] (COD = 1,5-cyclooctadiene) yielded the corresponding dichloroplatinum(II) complex [$PtCl_2$(**L2**)] (Scheme 2.3). Slow diffusion of hexane into a saturated solution of complex [$PtCl_2$(**L2**)] in DCM produced crystals suitable for X-ray crystallography (Figure 2.3). The unusual conformation of the 7-membered chelate in [$PtCl_2$(**L2**)] was not expected. The analogous complex [$PtCl_2$(**L1**)] has the conformation that was anticipated for the diphosphinoxylene complexes, where the PtP_2 plane is almost orthogonal to the phenyl ring.[19] Though the xylenyl -CH_2 group has been substituted for

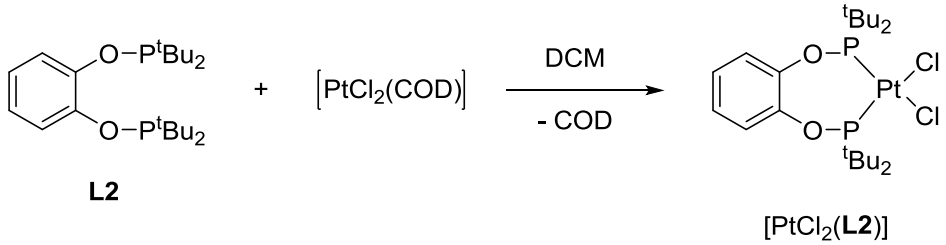

Scheme 2.3: Formation of dichloroplatinum(II) complex [$PtCl_2$(**L2**)].

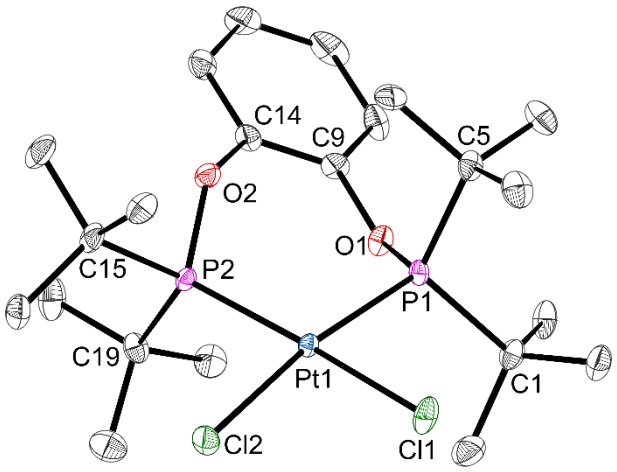

Figure 2.3: Crystal structure of [$PtCl_2$(**L2**)]. Thermal ellipsoids at 50%. Hydrogen atoms omitted for clarity. Selected bond lengths (Å) and angles (°): Pt1-P1 2.2381(10); Pt1-P2 2.2448(11); Pt1-Cl1 2.3531(11); Pt1-Cl2 2.3579(10); P1-O1 1.627(3); P1-C1 1.897(4); P1-C5 1.865(4); P2-O2 1.624(3); P2-C15 1.888(4); P2-C19 1.862(4); P1-Pt1-P2 96.34(4); P1-Pt1-Cl1 89.52(4); P2-Pt1-Cl2 89.93(4); Cl1-Pt1-Cl2 84.54(4).

oxygen in [$PtCl_2$(**L2**)], it was expected to have a similar structure to [$PtCl_2$(**L1**)] due to the R-X-P bend being similar between X = O or CH_2. If the structure observed by X-ray crystallography for [$PtCl_2$(**L2**)] prevailed in solution, the two phosphorus atoms would be magnetically inequivalent and two signals in the $^{31}P\{^1H\}$ NMR spectrum would be seen. Variable temperature NMR spectroscopy studies showed no broadening of the single phosphorus signal observed for this complex leading to the conclusion that the 7-membered chelate ring distortion is a consequence of crystal packing or that it persists in solution but is rapidly fluxional on the NMR timescale even at −85 °C.

2.3 Synthesis of [Pt(CO)(L2)]

The desired monocarbonyl complex [Pt(CO)(**L2**)] was synthesised by reaction of **L2** with [$Pt(nbe)_3$] (nbe = norbornene) to give [Pt(nbe)(**L2**)] followed by treatment of this intermediate with CO (Scheme 2.4). The displacement of nbe by CO was carried out in an analogous manner to the synthesis for [Pt(CO)(**L1**)].[6] The coordinated nbe was displaced by bubbling CO through a toluene solution of the [Pt(diphosphine)(nbe)], and removal of the solvent ensured that the displaced volatile nbe was removed from the

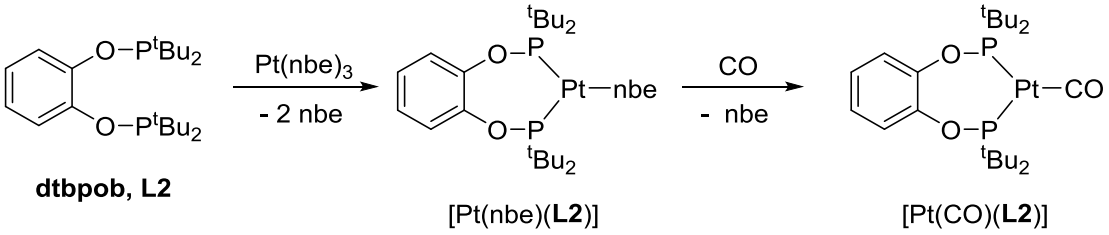

Scheme 2.4: Synthesis of [Pt(CO)(**L2**)] *via* intermediate [Pt(nbe)(**L2**)].

system. This CO/vacuum cycle for [Pt(CO)(**L1**)] needed repeating three times in order to obtain complete displacement of the norbornene ligand. During the synthesis of [Pt(CO)(**L2**)], the effect of changing the electronics of the diphosphine backbone was already apparent, with this complex requiring at least seven CO/vacuum cycles necessary to obtain complete conversion to the desired monocarbonyl complex, indicative of a strongly bound CO ligand.

Crystals suitable for X-ray crystallography of [Pt(CO)(**L1**)] and [Pt(CO)(**L2**)] were grown from saturated solutions in pentane at −40 °C and the molecular structures are shown in Figure 2.4. The two structures are similar and show the expected conformation of the seven membered chelate in contrast to the previous solid state structure of [$PtCl_2$(**L2**)] (see Section 2.2.1). The only significant difference is the more pronounced bend in the seven membered chelate in [Pt(CO)(**L1**)] than in [Pt(CO)(**L2**)] (119.9° vs 130.6°). There was no significant difference in the carbonyl bond length in the solid state but the electronic effect of the ligand backbone can be seen when comparing infra-red (IR) data. The IR stretching frequency for the carbonyl ligand in [Pt(CO)(**L2**)] (ν(CO) = 1933 cm^{-1}) is significantly higher than for [Pt(CO)(**L1**)] (ν(CO) = 1907 cm^{-1}). This is consistent with **L2** reducing the electron density at the metal centre available for back donation to the carbonyl ligand in [Pt(CO)(**L2**)] to a greater extent than **L1** withdraws electron density in [Pt(CO)(**L1**)].

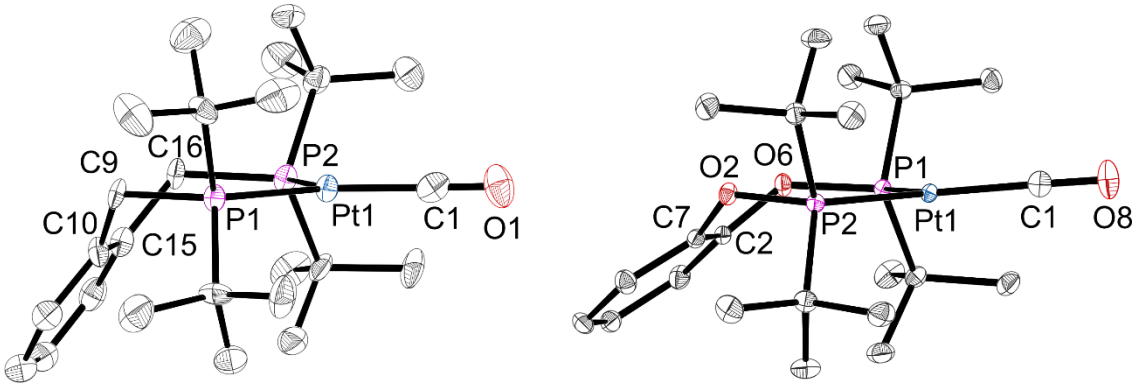

Figure 2.4: Crystal structures of [Pt(CO)(**L1**)] (left) and [Pt(CO)(**L2**)] (right). Thermal ellipsoids at 50%. Hydrogen atoms omitted for clarity. Selected bond lengths (Å) and angles (°) for [Pt(CO)(**L1**)]: Pt1-C1 1.853(12); C1-O1 1.130(14); Pt1-P1 2.312(3); Pt1-P2 2.305(3); Pt1-C1-O1 175.9(10); P1-C9-C10 120.4(7); P2-C16-C15 119.9(7). Selected bond lengths (Å) and angles (°) for [Pt(CO)(**L2**)]: Pt1-C1 1.8773(16); C1-O8 1.148(2); Pt1-P1 2.2745(4); Pt1-P2 2.2796(4); Pt1-C1-O8 176.10(15); P1-O6-C2 130.41(9); P2-O2-C7 130.63(9).

2.3.1 Synthesis of [Pt(^{13}CO)(L2)]

To allow for further studies into the small molecule activation pathways by [Pt(CO)(**L2**)], it was advantageous to synthesise the isotopically labelled complex [Pt(^{13}CO)(**L2**)]. The synthesis of [Pt(^{13}CO)(**L2**)] was achieved by simply subjecting [Pt(CO)(**L2**)] to three ^{13}CO/vacuum cycles, ensuring the majority of the ^{12}CO was displaced by ^{13}CO (Scheme 2.5). The complex [Pt(CO)(**L2**)] displayed analogous amphoteric behaviour to [Pt(CO)(**L1**)] and under an atmosphere of CO formed a tetrahedral Pt(0) dicarbonyl complex. When using ^{13}CO, the formation of the dicarbonyl species was confirmed by low temperature NMR studies (Figure 2.5). In the ^{13}C{^{1}H} NMR spectrum of [Pt(^{13}CO)$_2$(**L2**)], a broad signal at δ_C = 185.1 ppm resolved to a triplet ($^2J_{CP}$ = 15.8 Hz), due to coupling to two identical phosphorus atoms. In the ^{31}P{^{1}H} NMR spectrum, the

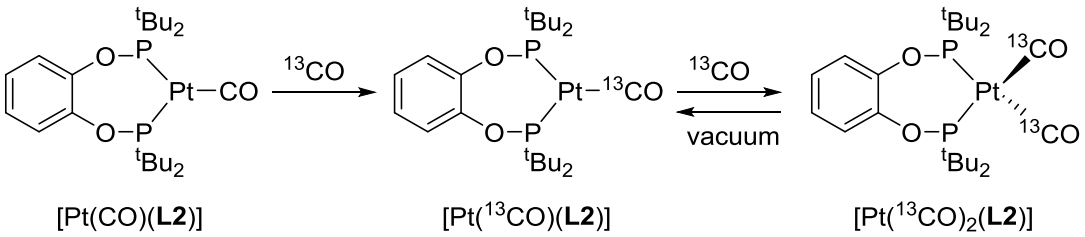

Scheme 2.5: Formation of [Pt(^{13}CO)(**L2**)] and [Pt (^{13}CO)$_2$(**L2**)].

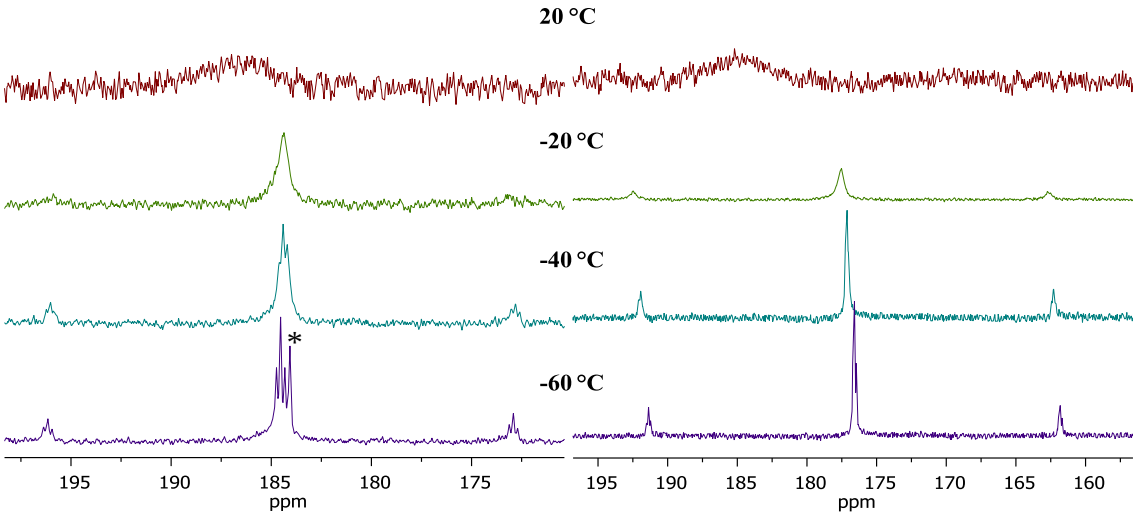

Figure 2.5: *In situ* low temperature ^{13}C{^{1}H} NMR (left) and ^{31}P{^{1}H} (right) NMR spectra of [Pt(^{13}CO)$_2$(**L2**)]. * = free ^{13}CO.

broad signal at δ_P = 176.4 ppm also resolved into a triplet confirming the presence of two equivalent dicarbonyl ligands in a tetrahedral arrangement around the Pt(0).

2.4 Formation of the Cooperative Lewis Pair [Pt(CO)(L2)]/B(C$_6$F$_5$)$_3$

To enable a comparison of FLP character/activation with [Pt(CO)(**L1**)], the Lewis acid tris(pentaflurorophenyl)borane (B(C$_6$F$_5$)$_3$), was used for small molecule activation. B(C$_6$F$_5$)$_3$ was initially chosen due to its known Lewis acidity in organocatalysis as well as its extensive use in FLP chemistry.[15,20–23]

Upon combination of [Pt(CO)(**L2**)] with B(C$_6$F$_5$)$_3$ in chlorobenzene, there was no significant change in chemical shifts in either the $^{11}B\{^1H\}$ NMR or the $^{31}P\{^1H\}$ NMR spectra but line broadening was apparent for the $^{31}P\{^1H\}$ NMR signal ($w_{1/2}$ = 45 Hz). The mixture did not change colour at room temperature but did exhibit thermochromic properties. Upon freezing the solution in liquid nitrogen, the colour of the solution changed from bright orange to a very dark purple. These observations mimic what is seen when [Pt(CO)(**L1**)] and B(C$_6$F$_5$)$_3$ are combined in chlorobenzene (line broadening in the $^{31}P\{^1H\}$ NMR spectrum and a dark green colour in frozen solution).[7,8] It is thought that there is some interaction between the borane and the Pt(0) complex but the exact nature of this is unknown. Previously in the Pringle group, the interaction of [Pt(CO)(**L1**)] and B(C$_6$F$_5$)$_3$ was studied by DFT calculations. It was calculated that an adduct is formed by coordination of B(C$_6$F$_5$)$_3$ to the oxygen of CO, or alternatively, an adduct formed by B(C$_6$F$_5$)$_3$ interacting directly with the Pt centre is possible.[8] Low temperature NMR studies showed sharpening of the $^{31}P\{^1H\}$ NMR signal but no significant change in chemical shift or coupling constant to Pt (J_{PPt}).

Although there appears to be some interaction between the Lewis acid and the Lewis base, the evidence suggests that this interaction is weak, with the complex being dynamic in solution. Since similar interactions in the [Pt(CO)(**L1**)]/B(C$_6$F$_5$)$_3$ system did not inhibit small molecule activation, further studies on the reactivity of [Pt(CO)(**L2**)] were carried out.

2.5 Reaction of Dihydrogen with [Pt(CO)(L2)]/B(C_6F_5)$_3$

All of the dihydrogen activation experiments described in this section were carried out with one equivalent of platinum complex and one equivalent of B(C_6F_5)$_3$ in chlorobenzene at room temperature. This mixture was subjected to 1 bar of H_2 in a Youngs NMR tube. Full experimental details are given in Chapter 5.

The reaction of [Pt(CO)(**L2**)]/B(C_6F_5)$_3$ with dihydrogen resulted in a colour change of the mixture from orange to bright pink in 15 min. The results discussed below will be in reference to when the reaction was repeated with [Pt(^{13}CO)(**L2**)] which unsurprisingly showed no difference in reactivity to the unlabelled complex [Pt(CO)(**L2**)].

The reaction mixture was analysed by *in situ* ^{1}H, ^{11}B{^{1}H}, ^{13}C{^{1}H}, ^{19}F and ^{31}P{^{1}H} NMR spectroscopy. After 15 min, the ^{13}C{^{1}H} NMR spectrum showed the presence of three ^{13}C-enriched products (Figure 2.6A). The signal at δ_C = 249.2 ppm appeared to be a broad 1:1:1:1 quartet with a coupling constant $^1J_{CB}$ = 49.3 Hz, indicating it was directly bonded to boron. This was confirmed in the ^{11}B{^{1}H} NMR spectrum (Figure 2.6B) which showed a doublet at δ_B = −16.7 ppm ($^1J_{BC}$ = 49 Hz). When using [Pt(^{13}CO)(**L2**)], a proton signal at δ_H = 10.80 ppm in the ^{1}H NMR spectrum (Figure 2.6C) then exhibited a ^1J coupling to ^{13}C ($^1J_{HC}$ = 151 Hz). This product was assigned to formyl borate anion **2.7** (Scheme 2.6). This species has been previously reported by Stephan *et al.* whilst investigating the reaction of syngas (50:50 CO/H_2) with the main group FLP P^{t}Bu$_3$/B(C_6F_5)$_3$.[24]

The signal at δ_C = 178.4 ppm in the ^{13}C{^{1}H} NMR spectrum corresponds to the CO ligand in the mononuclear cation **2.4**. The associated signals in the ^{31}P{^{1}H} NMR spectrum occur at δ_P = 174.5 and 163.0 ppm (Figure 2.6D) and the hydride signal in the ^{1}H NMR spectrum at δ_H = −4.15 ppm (Figure 2.6C). When the ligand was **L1**, the analogous cationic species was found to be the product of dihydrogen activation along with the counterion **2.8** (Scheme 2.6) which is seen in the ^{11}B{^{1}H} NMR spectrum (Figure 2.6B).

The final signal in the ^{13}C{^{1}H} NMR spectrum occurs at δ_C = 231.6 ppm and exhibits a 1:8:18:8:1 quintet of binomial quintets and corresponds to species **2.5** (Scheme 2.6). This splitting pattern is indicative of a bridging CO ligand in a binuclear platinum species with two equivalent ^{195}Pt atoms and four equivalent ^{31}P atoms. The signal is a composite of three subspectra occurring from the different isotopic combinations of the platinum

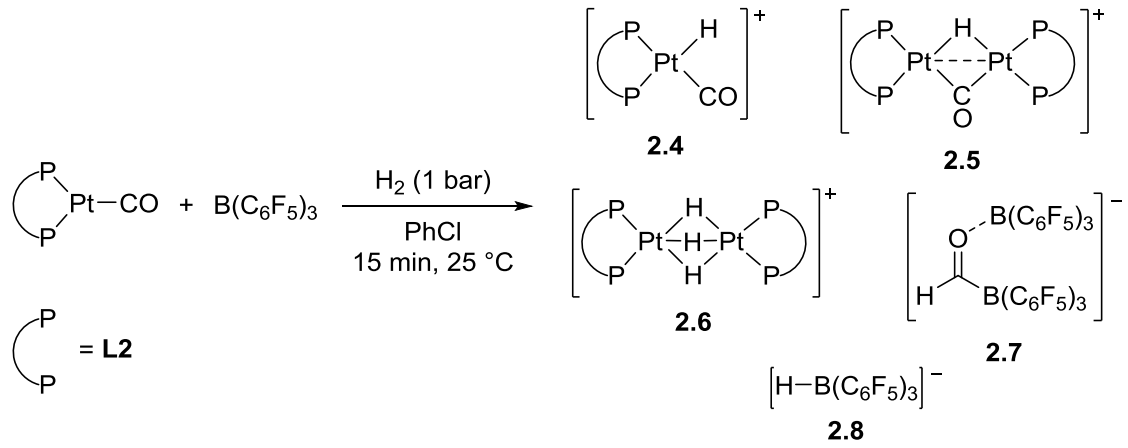

Scheme 2.6: Reaction of [Pt(CO)(**L2**)]/$B(C_6F_5)_3$ with H_2 after 15 min.

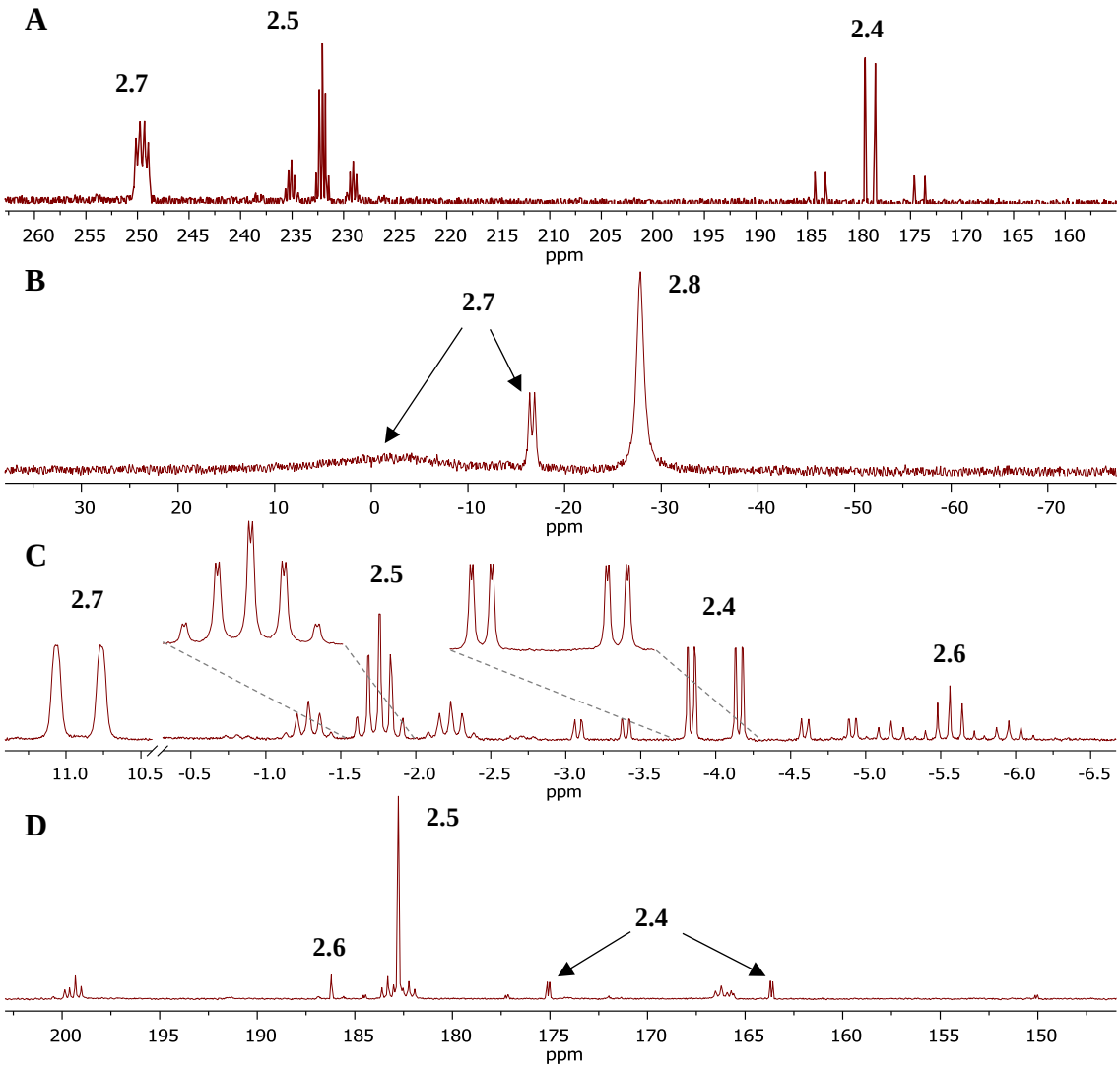

Figure 2.6: *In situ* $^{13}C\{^1H\}$ (A), $^{11}B\{^1H\}$ (B), ^1H (C) and $^{31}P\{^1H\}$ (D)[§] NMR spectra of the reaction between [Pt(^{13}CO)(**L2**)]/$B(C_6F_5)_3$ and H_2 after 15 min. Expansions in C show the ^1H-^{13}C splitting. [§] D shows $^{31}P\{^1H\}$ NMR spectrum of reaction using [Pt(CO)(**L2**)] for clarity.

nuclei. The only isotope of Pt that is NMR active is ^{195}Pt (I = ½) and is 33.8% abundant, therefore there are three possible combinations of two Pt atoms in a binuclear species: ^{195}Pt-^{195}Pt, ^{195}Pt-Pt and Pt-Pt (*ca.* 1:4:4 ratio).[25] The corresponding hydride signal in the

^{1}H NMR spectrum is at δ_H = −1.92 ppm with the same multiplicity indicating the hydride is also bridging. The $^{31}P\{^{1}H\}$ NMR spectrum also has the distinctive multiplicities expected for a binuclear Pt species which has been described by Otsuka in detail for similar binuclear trihydrido species[26] and is also observed for analogues of **2.5**.[27–29]

The final signal in the ^{1}H NMR spectrum at δ_H = −5.72 ppm (Figure 2.6C) corresponds to a signal at δ_P = 185.6 ppm in the $^{31}P\{^{1}H\}$ NMR spectrum (Figure 2.6D) and is attributed to the trihydrido binuclear platinum species **2.6**; this was also confirmed by mass spectrometry. An explanation of the formation of this species is given in Section 2.5.1.

Over time, the composition of this reaction mixture did not change except for the gradual degradation of formyl borate species **2.7** over 4-5 days. None of the degradation products could be identified but it is possible that the fluorophenyl rings undergo intramolecular migration under a dihydrogen atmosphere, analogous to that reported previously by Stephan *et al*. for this species, albeit under different reaction conditions (Figure 2.7).[24]

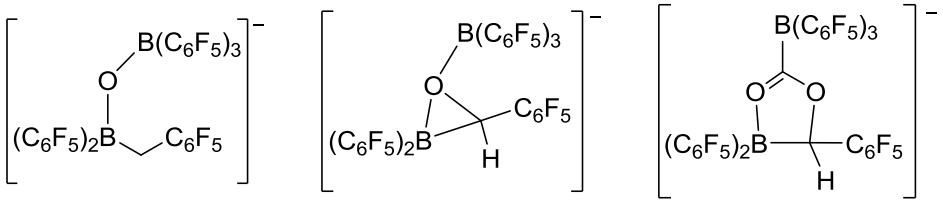

Figure 2.7: Anionic fragments resulting from the migration of pentafluorophenyl groups from anion **2.10** reported by Stephan *et al.*

The concentration of the species in the reaction mixture affected the ratio of products seen as expected: the more concentrated the mixture, the more binuclear species were formed, and the more dilute the mixture, the more mononuclear species were formed.

The activation of dihydrogen was repeated with [Pt(^{13}CO)(**L1**)]/B(C_6F_5)$_3$ to examine if the analogous species from [Pt(^{13}CO)(**L2**)]/B(C_6F_5)$_3$ were formed. The reaction was monitored by NMR spectroscopy and after 15 min, the presence of **2.7**, and analogous species **2.9** and **2.10**, were detected (Scheme 2.7, Figure 2.8A). After 16 h, the NMR spectra revealed that the reaction mixture changed with **2.7** and **2.10** seemingly converting to the two products, **2.8** and **2.9**, which were the originally reported products

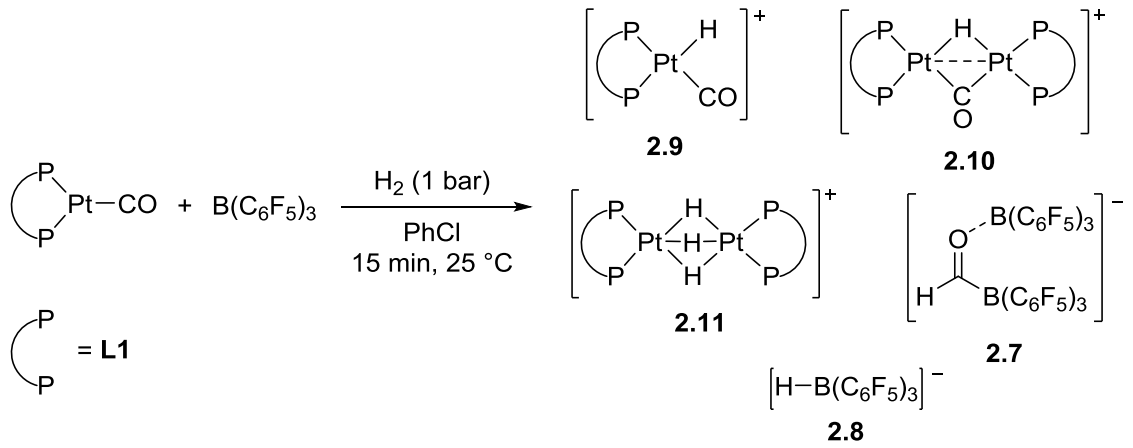

Scheme 2.7: Reaction of [Pt(CO)(**L1**)]/$B(C_6F_5)_3$ with H_2 after 15 min.

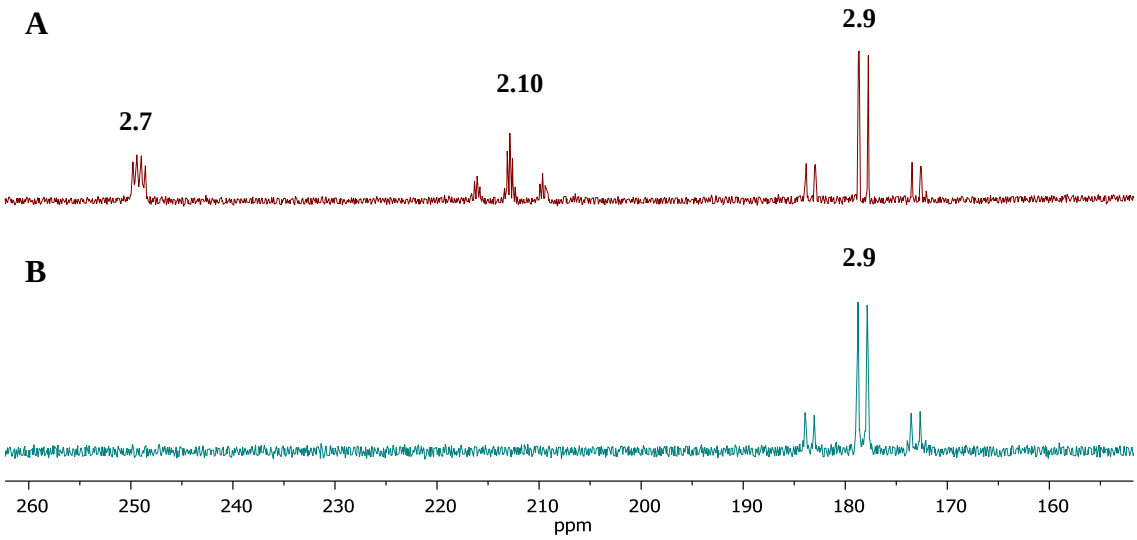

Figure 2.8: *In situ* $^{13}C\{^1H\}$ NMR spectrum of the reaction of [Pt(^{13}CO)(**L1**)]/$B(C_6F_5)_3$ after 15 min (A) and 16 h (B).

for dihydrogen activation by [Pt(CO)(**L1**)]/$B(C_6F_5)_3$.[7,8] There was also a minor amount (< 5%) of **2.11** detected in the ^1H NMR spectrum and this did not change in quantity over time.

Modifying the ligand from a phosphine to a phosphinite donor appears to have had a significant impact on dihydrogen activation. Although the species observed in solution are analogues, the stability of the platinum species are quite different. Cationic species $[Pt_2(\mu\text{-H})(\mu\text{-CO})(\mathbf{L})_2]^+$ is more stable when **L** = **L2** than when **L** = **L1**. This could be explained by the stronger π-accepting properties of **L2** in comparison to **L1** enabling the stabilisation of the lower valent Pt^I centres in $[Pt_2(\mu\text{-H})(\mu\text{-CO})(\mathbf{L})_2]^+$. Studies of the formation of similar complexes suggest that the bridging species could be dynamically switching between states where the ligands are bridging or terminal.[28] For the reactivity of this species, it may be important that the bridging ligands can switch to terminal

positions on the platinum but the phosphinite ligand **L2** appears to stabilise the bridged form of $[Pt_2(H)(CO)(\mathbf{L})_2]^+$.

2.5.1 Proposed Pathway for Dihydrogen Activation by Pt(0)/B(C$_6$F$_5$)$_3$

Previously, two possible reaction pathways were proposed for dihydrogen activation by the Pt(0)/B(C$_6$F$_5$)$_3$ Lewis pair (Scheme 2.8). In pathway (a), classic organometallic oxidative addition of H_2 to the *cis*-dihydride takes place, with loss of CO, which is then followed by hydride abstraction by B(C$_6$F$_5$)$_3$ and reassociation of CO. In pathway (b), the H_2 molecule is bound between the platinum and boron centres in an encounter complex and is then heterolytically cleaved in a concerted process to form the final dihydrogen activation products.[7]

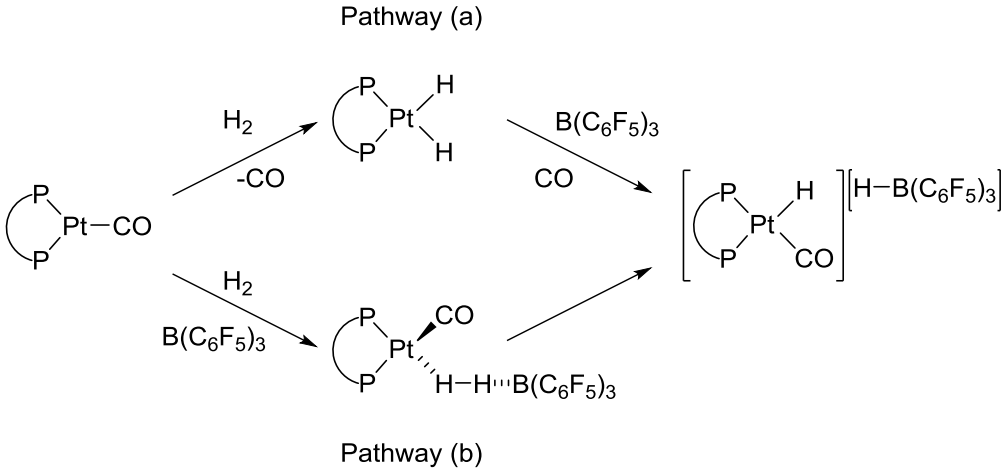

Scheme 2.8: Previously proposed pathways for dihydrogen activation by the Pt(0)/B(C$_6$F$_5$)$_3$ Lewis pair.

Though both of these pathways are possible there is little experimental evidence to support them. The starting complex [Pt(CO)(**L**)] (**L** = **L1** or **L2**) does react with dihydrogen to form *cis*-dihydride $[Pt(H)_2(\mathbf{L})]$, but this is very slow (maximum 40% conversion over 1 week) and the species reverts to the starting complex when the hydrogen atmosphere is removed (Figure 2.9). There is no NMR spectroscopic evidence of the *cis*-dihydride being present in dihydrogen activation for either of the Pt(0)/B(C$_6$F$_5$)$_3$ Lewis pair systems.

From the observations described in Section 2.5, the following pathway is proposed for the activation of dihydrogen by the [Pt(CO)(**L**)]/B(C$_6$F$_5$)$_3$ Lewis pair (Scheme 2.9). It is suggested that two platinum monocarbonyl complexes and two B(C$_6$F$_5$)$_3$ molecules react

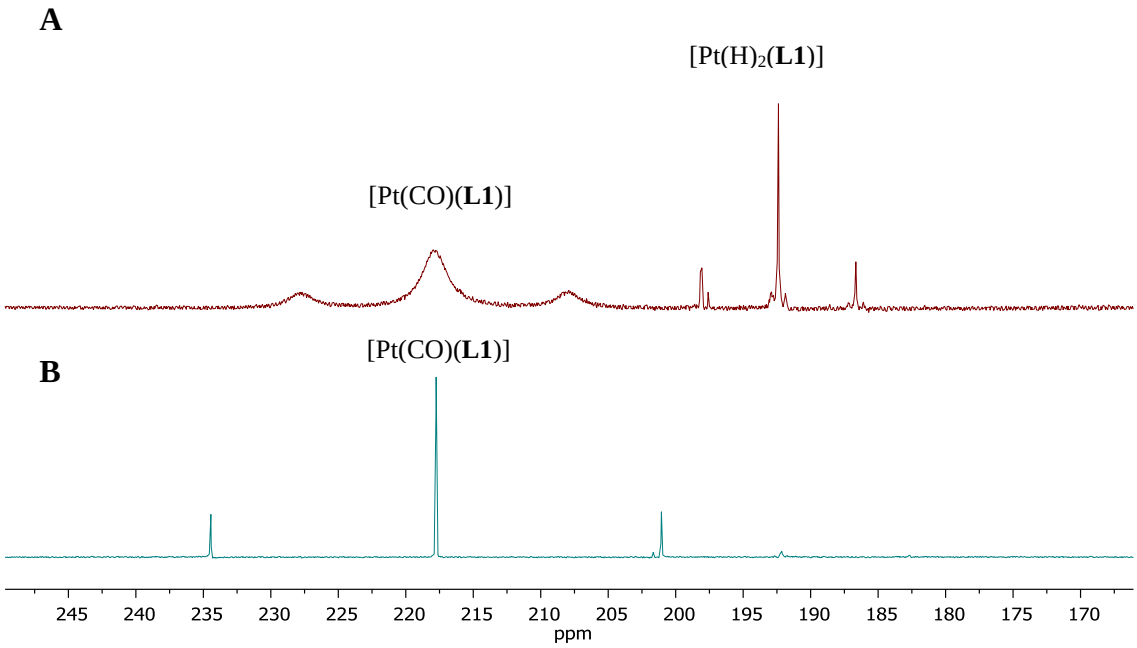

Figure 2.9: $^{31}P\{^{1}H\}$ NMR spectrum of [Pt(CO)(**L1**)] under a dihydrogen atmosphere for 1 week (A) and after the atmosphere of dihydrogen was replaced for nitrogen (B).

with one molecule of dihydrogen to form cation $[Pt_2(\mu\text{-}H)(\mu\text{-}CO)(\mathbf{L})_2]^+$ and counterion **2.7**. These two components then react with a further molecule of dihydrogen to form the final product [Pt(CO)(H)(**L**)][H-B(C_6F_5)$_3$]. When **L** = **L1**, the intermediates were observed within the first 15 min of the reaction, and these species slowly converted to the final products. When **L** = **L2**, full conversion to the final products was never observed. It is thought that the phosphinite ligand stabilises the cationic bridging species $[Pt_2(\mu\text{-}H)(\mu\text{-}CO)(\mathbf{L})_2]^+$ making it unreactive towards the anionic fragment which undergoes independent degradation over time.

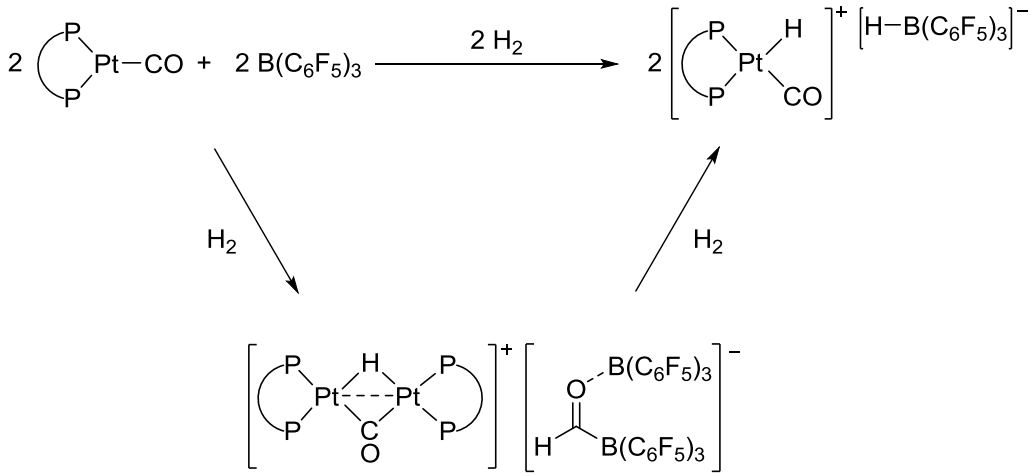

Scheme 2.9: New proposed pathway for the activation of dihydrogen by the Pt(0)/B(C_6F_5)$_3$ Lewis pair.

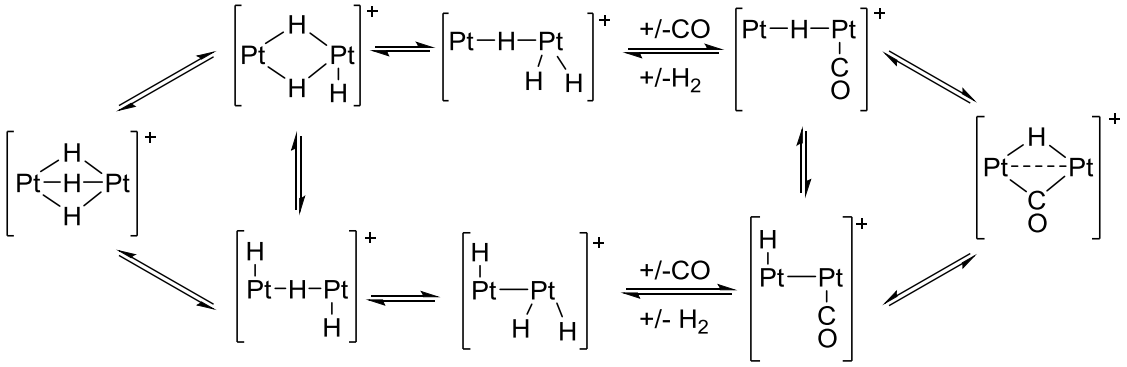

Scheme 2.10: Possible pathway for exchange between $[Pt_2(\mu\text{-}H)_3(\mathbf{L})_2]^+$ and $[Pt_2(\mu\text{-}H)(\mu\text{-}CO)(\mathbf{L})_2]^+$. Ligands omitted from image for clarity. Adapted figure with permission from Minghetti *et al.*, *Inorg. Chem.*, 1983, **22**, 2332-2338. Copyright 1983 American Chemical Society.

It should be noted that the pathway in Scheme 2.9 does not take into account the presence of $[Pt_2(\mu\text{-}H)_3(\mathbf{L})_2]^+$. It is thought that this species is formed from $[Pt_2(\mu\text{-}H)(\mu\text{-}CO)(\mathbf{L})_2]^+$ or is an intermediate in the formation of $[Pt_2(\mu\text{-}H)(\mu\text{-}CO)(\mathbf{L})_2]^+$. Minghetti *et al.* have extensively studied the chemical transformation of $[Pt_2(\mu\text{-}H)_3(\mathbf{L})_2]^+$ to $[Pt_2(\mu\text{-}H)(\mu\text{-}CO)(\mathbf{L})_2]^+$ (**L** = dppe, 1,2-bis(diphenylphosphino)ethane) by the simple addition of CO to a solution of $[Pt_2(\mu\text{-}H)_3(\mathbf{L})_2]^+$.[28] From studies into similar binuclear trihydrido species there is evidence of the structure being dynamic, with hydrido ligand exchange between bridging and terminal sites.[26,27,30,31] Minghetti proposed that a tautomer of the trihydrido species could rearrange to a structure where two terminal hydrido ligands are bonded to one platinum (Scheme 2.10).[28] Traditional organometallic chemistry suggests that it would then be possible for this Pt centre to lose dihydrogen and, in this case, bind to a CO ligand. This can then rearrange to the tautomer observed by NMR spectroscopy in the studies detailed above. Further investigations would need to be made into a possible equilibrium between the two species. If the reverse of the mechanism Minghetti has reported is possible (conversion from $[Pt_2(\mu\text{-}H)(\mu\text{-}CO)(\mathbf{L})_2]^+$ to $[Pt_2(\mu\text{-}H)_3(\mathbf{L})_2]^+$ by addition of H_2 and loss of CO), this could provide an explanation for the presence of the trihydrido species in the dihydrogen activation reaction mixture.

2.6 Reaction of Ethene with Pt(0)/B(C_6F_5)$_3$

All of the ethene activation experiments described in this section were carried out with one equivalent of platinum complex and one equivalent of $B(C_6F_5)_3$ in chlorobenzene at room temperature. This mixture was subjected to 1 bar of ethene in a Youngs NMR tube. Full experimental details are given in Chapter 5.

The reaction of [Pt(CO)(**L2**)]/$B(C_6F_5)_3$ with ethene in chlorobenzene resulted in a colour change from orange to pale pink over 1 h. The reaction mixture was monitored by NMR spectroscopy. Initially the ^{1}H, $^{31}P\{^{1}H\}$, and $^{11}B\{^{1}H\}$ NMR spectra recorded were broad and the species present were not identifiable. After 1 h, the spectra recorded had resolved; the $^{31}P\{^{1}H\}$ NMR spectrum displayed two doublets at δ_P = 173.4 ppm ($^{2}J_{PP}$ = 15 Hz, $^{1}J_{PPt}$ = 2219 Hz) and δ_P = 137.5 ppm ($^{2}J_{PP}$ = 15 Hz, $^{1}J_{PPt}$ = 4662 Hz).[†] Analysis of the $^{11}B\{^{1}H\}$ NMR spectrum showed a single sharp peak at −22 ppm indicating a 4-coordinate boron species and the ^{1}H NMR spectrum displayed two broad signals at δ_H = 2.87 and 1.90 ppm. These proton signals occur in the alkyl region of the spectrum and together with the $^{11}B\{^{1}H\}$ and $^{31}P\{^{1}H\}$ signals, it was determined that the [Pt(CO)(**L2**)]/$B(C_6F_5)_3$ Lewis pair had successfully activated ethene. The exact identity of the activation species was unclear as the two candidate products **2.12** and **2.14** would have very similar NMR spectra (Figure 2.10); **2.12** would result from loss of the CO ligand and linear activation of ethene between the Pt(0) and B centres and **2.13** would result from the activation and coupling of ethene and CO, seen with [Pt(CO)(**L1**)]/$B(C_6F_5)_3$.[7]

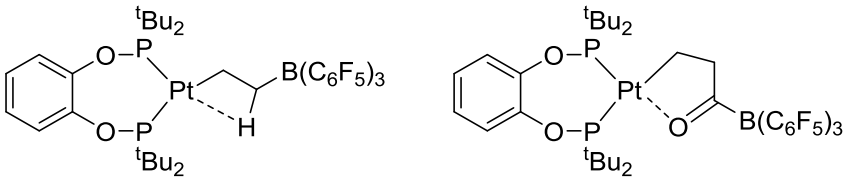

2.12 **2.13**

Figure 2.10: Two possible products from the activation of ethene with [Pt(CO)(**L2**)]/$B(C_6F_5)_3$.

When the reaction was repeated with [Pt(^{13}CO)(**L2**)] a broad quartet was observed in the $^{13}C\{^{1}H\}$ NMR spectrum at δ_C = 278.7 ppm ($^{1}J_{CB}$ = 52 Hz). Attempts to crystallise the product were unsuccessful but the presence of the low field signal in the $^{13}C\{^{1}H\}$ NMR spectrum is strong evidence for the final activation product being **2.13**.

The [Pt(CO)(**L2**)]/$B(C_6F_5)_3$ Lewis pair appears to have activated ethene in a similar manner to [Pt(CO)(**L1**)]/$B(C_6F_5)_3$, except that the rate of reaction is faster, the former only taking 1 h to have resolvable product signals *versus* 16 h for the latter in the $^{31}P\{^{1}H\}$ NMR spectrum. The ethene/CO coupled product **2.13** was also stable when the solvent

[†] Minor amounts of [Pt(H)(CO)(**L2**)] were also seen in the $^{31}P\{^{1}H\}$ NMR spectrum. This is thought to originate from activation of an impurity in the batch of ethene used as this was not seen when a different batch was used. The impurity was not identified.

and ethene atmosphere were removed and the solid product redissolved with only minor amounts of (< 3%) decomposition.

Previous studies into the mechanism have led to the suggestion of initial activation of the ethene in a linear fashion to form a product related to the structure of **2.12** and then further reaction with the CO ligand in the system to form the final product.[7,8] To investigate this the monoethene complex [Pt(C_2H_4)(**L2**)] was formed by subjecting [Pt(CO)(**L2**)] to at least two ethene/vacuum cycles. The formation of [Pt(C_2H_4)(**L2**)] seems favourable as after just one ethene cycle, over 95% of [Pt(CO)(**L2**)] had converted to [Pt(C_2H_4)(**L2**)]. $B(C_6F_5)_3$ was added to a solution of [Pt(C_2H_4)(**L2**)] in chlorobenzene and the mixture instantly turned cloudy. Although it had seemed that the majority of the product had precipitated from solution it was sufficiently soluble to obtain NMR spectroscopic data. The $^{31}P\{^1H\}$ NMR spectrum was significantly broadened but there were two distinctive peaks at δ_P = 184.2 and 167.3 ppm and a sharp peak in the $^{11}B\{^1H\}$ NMR spectrum at δ_B = −14.0 ppm indicating a 4-coordinate boron species. The product was tentatively assigned to be **2.12** (Scheme 2.11). Addition of CO to the reaction mixture resulted in a pale pink solution with almost quantitative conversion to the ethene/CO coupled product **2.13**. This is analogous to what was previously seen with [Pt(CO)(**L1**)]/$B(C_6F_5)_3$.[8]

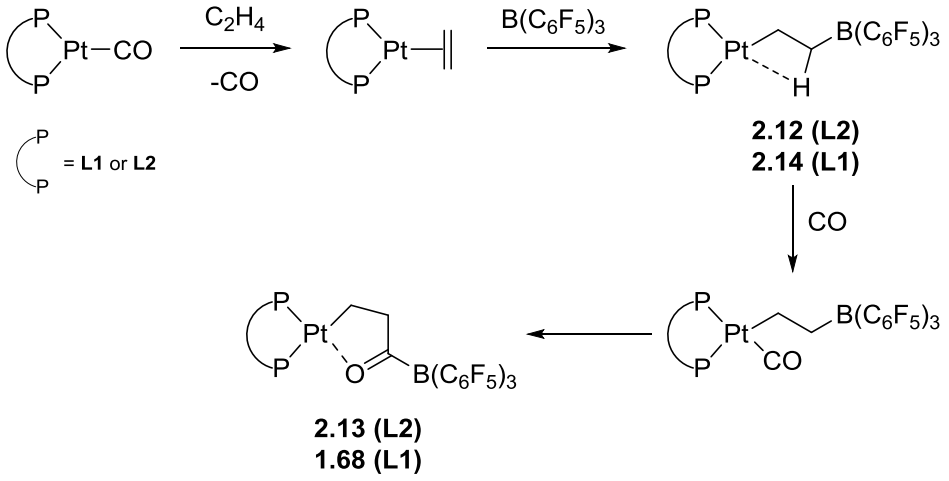

Scheme 2.11: Proposed pathway for the activation of ethene by [Pt(CO)(**L**)]/$B(C_6F_5)_3$ (**L** = **L1** or **L2**).

These observations led to the proposed pathway in which the ethene first displaces the CO to make the monoethene complex (Scheme 2.11). This is then activated by $B(C_6F_5)_3$ to form the linear activation product (**2.12**/**2.14**). Reassociation of the CO ligand to the platinum centre is then followed by migratory insertion/rearrangement to form the final product (**2.13**/**1.68**). Although during the initial period of the reaction all of the NMR

spectra recorded were broad, the presence of a broad resonance at δ_P = 198.0 ppm in the $^{31}P\{^1H\}$ NMR spectrum was always seen for the reaction with [Pt(CO)(**L2**)]/$B(C_6F_5)_3$ which corresponds to the signal for [Pt(C_2H_4)(**L2**)]. Once the final product had been formed, only trace amounts of [Pt(C_2H_4)(**L2**)] could be seen in the $^{31}P\{^1H\}$ NMR spectrum which might have resulted from a slight excess of [Pt(CO)(**L2**)] at the start of the reaction. This shows that the formation of the monoethene species is favourable and supports the proposed pathway detailed in Scheme 2.11

Further reactivity of **1.68** and **2.13** products, with **L** = **L1** and **L2** respectively, was investigated. Repressurising with CO, H_2 and syngas (CO/H_2 1:1) did not have any effect on the system. Attempts to probe the reactivity to the formyl borate fragment were attempted by addition of MeOH and $MeNH_2$. **2.13** was stable to nucleophilic attack and even after heating to 50 °C in the presence of MeOH and $MeNH_2$ no change was seen in the $^{31}P\{^1H\}$ NMR spectrum. On the other hand, **1.68** slowly reacted in the presence of MeOH. Cation [Pt(CO)(H)(**L1**)]$^+$ and [Pt(C_2H_4)(**L1**)] were identified by $^{31}P\{^1H\}$ NMR spectroscopy. It remains unknown how the formation of [Pt(CO)(H)(**L1**)]$^+$ occurs. The $^{11}B\{^1H\}$ NMR spectrum became more complex after heating and two unidentified 4-coordinate species at δ_B = −3.7 and 17.3 ppm were observed. Further investigations need to be carried out to identify these degradation products.

2.7 Reaction of Phenylacetylene with Pt(0)/$B(C_6F_5)_3$

All of the phenylacetylene activation experiments described in this section were carried out with one equivalent of platinum complex and one equivalent of $B(C_6F_5)_3$ in chlorobenzene at room temperature. An excess (*ca*. 30 μl) of phenylacetylene was added under argon in a Youngs NMR tube. Full experimental details are given in Chapter 5.

Activation of terminal alkynes by FLPs is of interest due to the useful synthons it could provide for organic transformations. In general, there are two pathways that terminal alkynes have been found to react with FLPs (Scheme 2.12); the first is deprotonation by the Lewis base and the second is 1,2-addition across the triple bond to typically form an *E*-alkene.[32–34] The selectivity has predominantly been found to depend on the basicity of the phosphine, although a balance of several parameters, such as sterics, is necessary to control the reactivity.

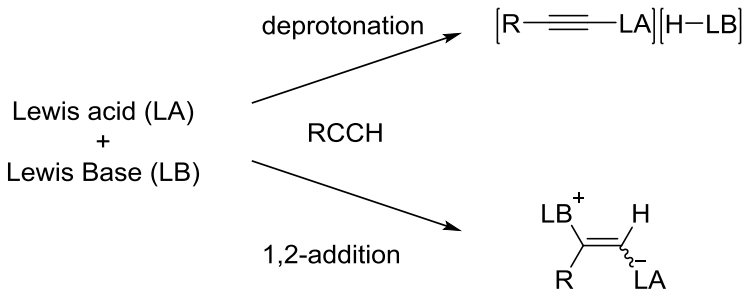

Scheme 2.13: General scheme for the two pathways of reactivity of a Lewis acid and Lewis base with a terminal alkyne.

The Lewis pair [Pt(CO)(**L1**)]/B(C_6F_5)$_3$ was treated with an excess of phenylacetylene and an instant colour change from bright orange to a dark red/brown was observed. After 2 h, analysis of the $^{31}P\{^1H\}$ NMR spectrum showed full conversion of the starting material to the cationic fragment of **2.15** (Scheme 2.13). The anionic fragment has been previously reported in literature so assignment from the $^{11}B\{^1H\}$ NMR and ^{19}F NMR spectra was unambiguous.[35]

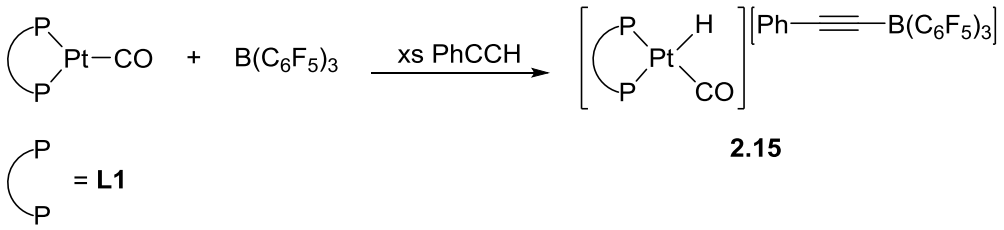

Scheme 2.12: Reaction between [Pt(CO)(**L1**)]/B(C_6F_5)$_3$ and phenylacetylene.

The reaction of [Pt(CO)(**L2**)]/B(C_6F_5)$_3$ did not proceed as cleanly as with the **L1** analogue although the major product remains the result of deprotonation of phenylacetylene. Upon addition of phenylacetylene to [Pt(CO)(**L2**)]/B(C_6F_5)$_3$ in chlorobenzene there was an immediate colour change from bright orange to dark red. Full conversion of the starting material was observed and *ca.* 90% of the product formed was **2.16** (Scheme 2.14). Analysis of the $^{31}P\{^1H\}$ and ^1H NMR spectra revealed a second phosphorus containing species, the binuclear Pt(I) cation **2.5**. There were also three

relatively sharp unassigned signals in the $^{11}B\{^1H\}$ NMR spectrum at δ_B = −6.9, −10.5 and −15.8 ppm indicating formation of 4-coordinate boron species.

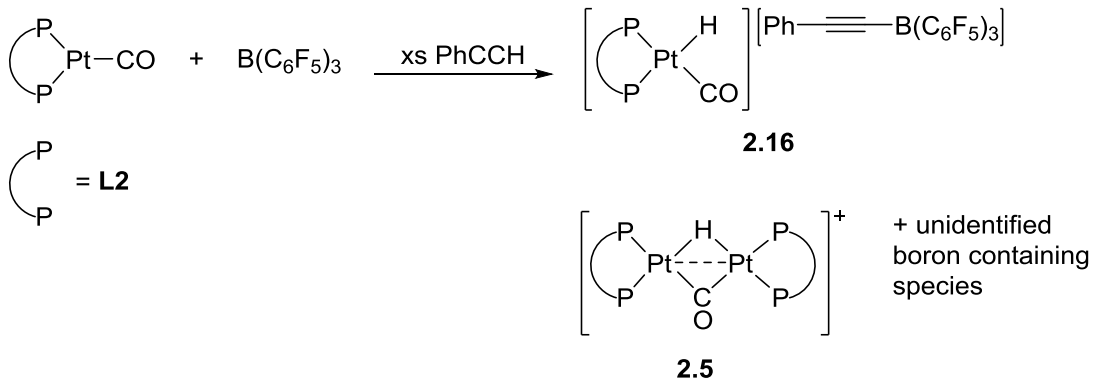

Scheme 2.14: Reaction between [Pt(CO)(**L2**)]/$B(C_6F_5)_3$ and phenylacetylene.

To investigate the mechanism of phenylacetylene activation for both systems, phenylacetylene was added to just the Lewis basic component (Scheme 2.15). When **L** = **L1**, a gradual colour change of the solution of [Pt(^{13}CO)(**L1**)] and PhCCH over 16 h from orange to pale yellow was observed. Two doublets were seen in the $^{31}P\{^1H\}$ NMR spectrum (δ_P = 47.3 and 42.5 ppm, $^2J_{PP}$ = 24 Hz) indicated the formation of a Pt species with inequivalent phosphorus environments (**2.17**, Scheme 2.15). The same was observed for **L** = **L2** (δ_P = 190.5 and 184.9 ppm, $^2J_{PP}$ = 15.9 Hz) although the formation of the species occurred much faster (2 h).

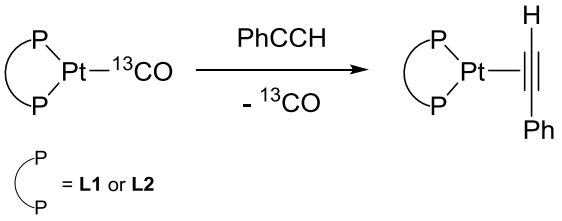

Scheme 2.15: Reaction of [Pt(^{13}CO)(**L**)] with PhCCH.

It is proposed that the phenylacetylene binds to the Pt(0) centre displacing the carbonyl ligand. Low temperature NMR studies gave evidence to support this as there was no change in the $^{31}P\{^1H\}$ NMR spectrum and there was a signal for free ^{13}CO in the $^{13}C\{^1H\}$ NMR spectrum which was not observed at room temperature. The displacement of ^{13}CO from [Pt(^{13}CO)(**L1**)] was also very slow. The low temperature NMR spectroscopic studies of this reaction mixture also showed signals corresponding to [Pt(^{13}CO)(**L1**)] and [Pt(^{13}CO)$_2$(**L1**)] which presumably was formed by coordination of the free ^{13}CO (released in solution) to [Pt(^{13}CO)(**L1**)].

Addition of $B(C_6F_5)_3$ to chlorobenzene solutions of **2.17** only showed *ca*. 60% conversion to the activation products **2.15** and **2.16** (for **L1** and **L2** respectively). Through analysis of the $^{31}P\{^1H\}$ NMR spectrum it was unclear as to what other species had formed in solution, although some of the 4-coordinate ^{11}B species observed in the reaction between [Pt(CO)(**L2**)]/$B(C_6F_5)_3$ and PhCCH were again detected. These observations do not support the pathway of alkyne activation by initial binding by the alkyne before activation by the Pt(0)/$B(C_6F_5)_3$ Lewis pair which would be the analogous reaction seen with alkenes.

Berke *et al.* showed that the reaction of PhCCH with $B(C_6F_5)_3$ results in E/Z-isomers **2.19** *via* vinylidene intermediate **2.18** (Scheme 2.16).[36] In the presence of a Lewis base **2.18** either undergoes an addition reaction or a deprotonation to form **2.20** and **2.21** respectively. A similar deprotonation of the alkyne by [Pt(CO)(**L**)]/$B(C_6F_5)_3$ is most likely occurring based on the experimental evidence collected.

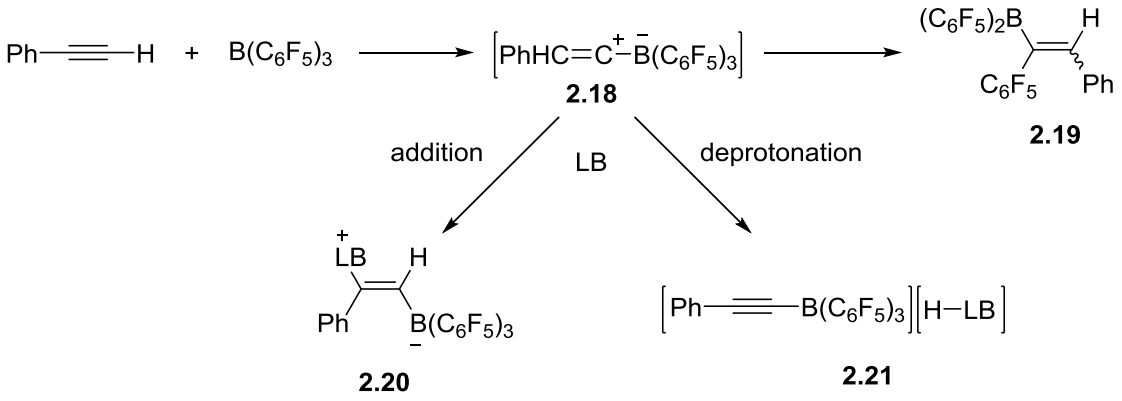

Scheme 2.16: Reaction of PhCCH and $B(C_6F_5)_3$ and the products formed when in the presence of a Lewis base.

2.8 Exploring Other FLP Substrates with Pt(0)/$B(C_6F_5)_3$

The scope of reactivity for the Pt(0)/$B(C_6F_5)_3$ Lewis pair investigated so far is relatively small. In this Section, an initial exploration into activation of other small molecules is described.

2.8.1 Reaction of H_2O with Pt(0)/$B(C_6F_5)_3$

The [Pt(CO)(**L**)]/$B(C_6F_5)_3$ Lewis pair has been successful for the activation of dihydrogen, ethylene and phenylacetylene. So far it has been shown that imparting

reactivity in this system has not required forcing conditions, as all of the results have been achieved at room temperature and only atmospheric pressure of the reagent gas (if applicable).

One of the major issues found with FLP hydrogenation catalysis is the sensitivity of the systems to moisture (as well as other functional groups such as alcohols and amines which are typically the products of hydrogenation catalysis).[37–40] In recent years several groups have focussed their efforts on developing moisture tolerant systems which has typically involved modification/replacement of $B(C_6F_5)_3$,[41–43] as well as the use of chemical scavengers and ethereal solvents to prevent reaction with products formed from catalysis.[44–46] With this in mind, the moisture tolerance of the [Pt(CO)(**L**)]/$B(C_6F_5)_3$ system was investigated.

One equivalent of [Pt(CO)(**L1**)] was combined with one equivalent of $B(C_6F_5)_3$ in chlorobenzene which had not been subjected to any drying processes (and so contains traces of H_2O) but had been deoxygenated prior to use. Immediate reaction was observed according to $^{31}P\{^1H\}$ NMR spectroscopy and any further conversion to products plateaued after 3 h. Two characteristic doublets at δ_P = 43.4 and 34.2 ppm (both with associated platinum satellites) in the $^{31}P\{^1H\}$ NMR spectrum indicated the presence of mononuclear cationic species **2.9** (*ca*. 12%) (Figure 2.11A). This was confirmed by the presence of the hydride signal for **2.9** in the ^1H NMR spectrum. The only other phosphorus-containing species in solution was the starting material [Pt(CO)(**L1**)], which was still broadened by the presence of $B(C_6F_5)_3$. The $^{11}B\{^1H\}$ NMR spectrum contained two significantly broadened signals at δ_B = 59.1 (major species) and −2.0 ppm (minor species), the former corresponding to $B(C_6F_5)_3$. This is reflected in the ^{19}F NMR spectrum (Figure 2.11B). The ^{19}F NMR signals at approx. δ_F = −128, −143 and −160 ppm arise from the *ortho*, *para* and *meta* fluorine atoms on the phenyl rings. The minor ^{19}F NMR signals at approx. δ_F = −133, −158 and −164 ppm corresponds to the broad signal in the $^{11}B\{^1H\}$ NMR spectrum at δ_B = −2.0 ppm but the identity of this intermediate species is still unknown. After leaving the solution for 3 days at room temperature, no further reactivity was observed. It is possible that maximum conversion of the Pt/$B(C_6F_5)_3$ pair was reached as the amount of H_2O in the bench chlorobenzene may be less than one equivalent.

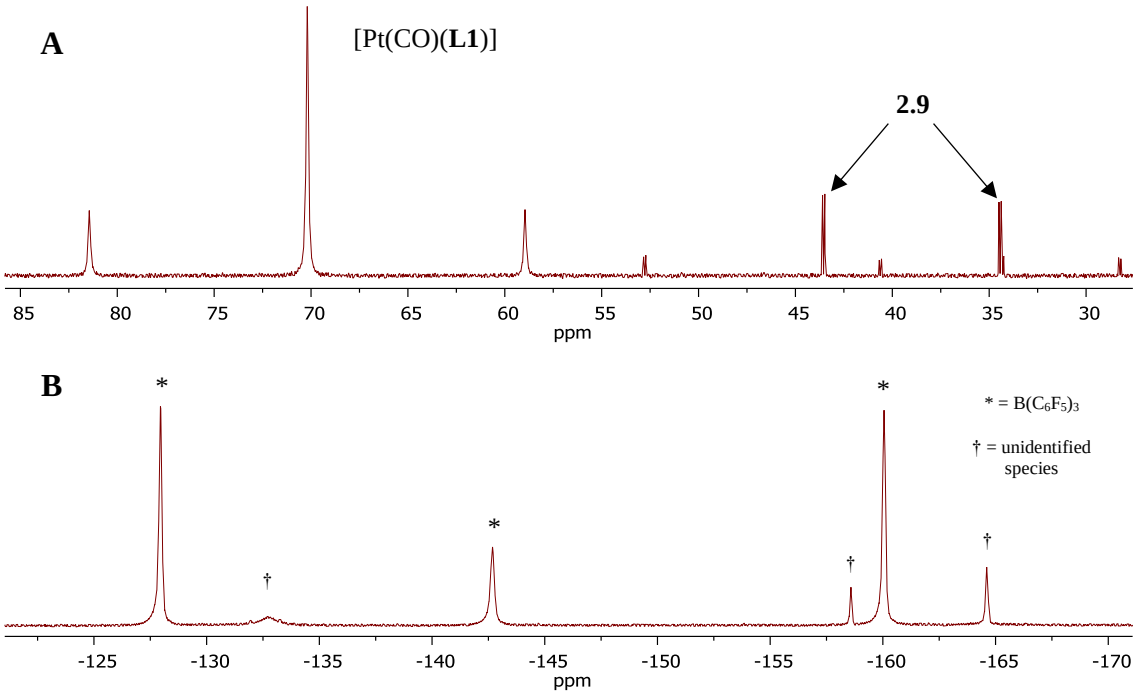

Figure 2.11: $^{31}P\{^{1}H\}$ NMR spectrum (A) and ^{19}F NMR spectrum (B) of [Pt(CO)(**L1**)]/$B(C_6F_5)_3$ in 'wet' PhCl after 3 h at room temperature.

One drop of deoxygenated, deionised H_2O was added to the reaction mixture and immediate conversion to the ion pair **2.22** was seen (Scheme 2.17). The anionic fragment $[HO\text{-}B(C_6F_5)_3]^-$ has been characterised previously.[47] The $^{11}B\{^{1}H\}$ and ^{19}F NMR spectra confirm the presence of only one species whose chemical shifts match well with those reported for $[HO\text{-}B(C_6F_5)_3]^-$. A broad peak at δ_H = 5.09 ppm in the ^{1}H NMR spectrum is tentatively assigned to the OH signal but the integration *versus* the signal for the Pt-H is not consistent with the expected 1:1 ratio (*ca.* 2.3:1 ratio of O-*H* to Pt-*H*). The literature value for the OH proton signal in the ^{1}H NMR spectrum for related anionic fragments are typically found between, 1.5 and 2.0 ppm.[48] Despite this anomaly the boron species in solution was assigned to the anionic fragment $[HO\text{-}B(C_6F_5)_3]^-$. The ion pair remained

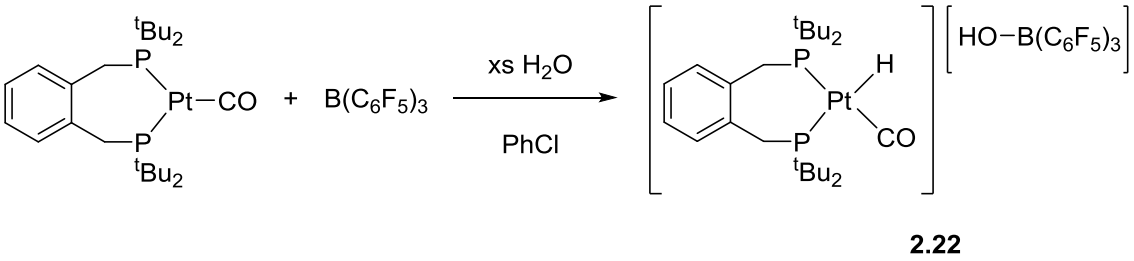

2.22

Scheme 2.17: Reaction of [Pt(CO)(**L1**)]/$B(C_6F_5)_3$ with excess H_2O to form ion pair **2.22**.

stable in solution over 4 days at room temperature. Attempts to crystallise the product for X-ray crystallography were unsuccessful.

The analogous experiments were carried out with [Pt(CO)(**L2**)]/$B(C_6F_5)_3$ which interestingly demonstrated different reactivity. When one equivalent of [Pt(CO)(**L2**)] was combined with $B(C_6F_5)_3$ in undried, deoxygenated chlorobenzene, initial analysis of the $^{31}P\{^1H\}$ NMR spectrum showed the presence of cation **2.4**. Unexpectedly, after 3 h, the only phosphorus-containing species, besides the starting material, was the binuclear cationic species **2.5** (Figure 2.12A). This concurs with the finding that **L2** favours and stabilises binuclear species over the mononuclear species. This is the reverse of that observed for **L1**. It should also be noted that the $^{31}P\{^1H\}$ NMR signal for the starting material is significantly broadened ($w_{1/2}$ = 480 Hz). The signals in the $^{11}B\{^1H\}$ NMR spectrum and the ^{19}F NMR spectrum (Figure 2.12B) are identical to that observed with [Pt(CO)(**L1**)]/$B(C_6F_5)_3$. Again, no further conversion was observed after 3 days.

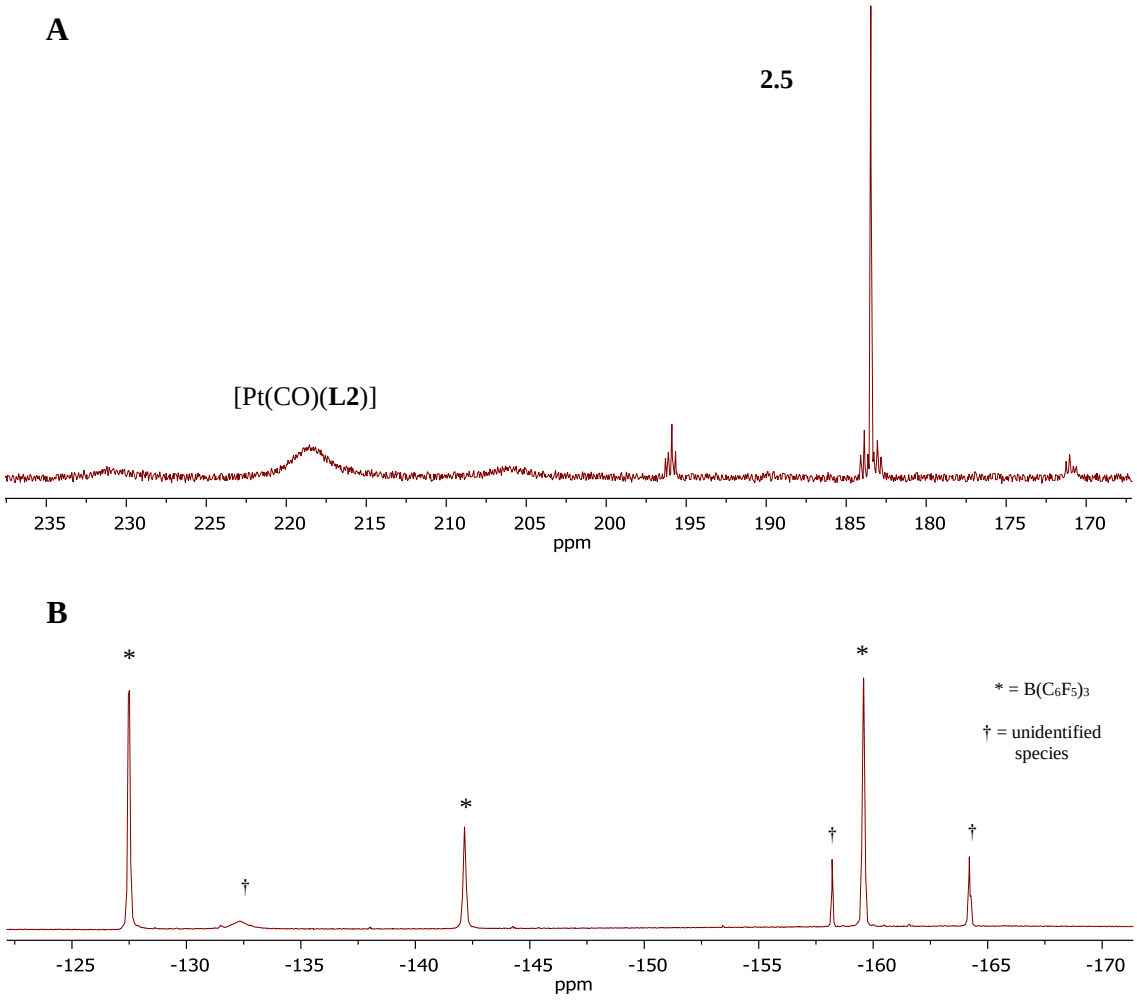

Figure 2.12: $^{31}P\{^1H\}$ NMR spectrum (A) and ^{19}F NMR spectrum of [Pt(CO)(**L1**)]/$B(C_6F_5)_3$ in 'wet' PhCl after 3 h at room temperature.

One drop of degassed H_2O was added to the reaction mixture and immediately full conversion of the starting material was seen by analysis of the $^{31}P\{^1H\}$ NMR spectrum. The major cationic species in solution was now mononuclear platinum species **2.4** (Scheme 2.18). The major species in the $^{11}B\{^1H\}$ NMR spectrum was identified to be anion **2.23** which was confirmed by analysis of the signals in the $^{11}B\{^1H\}$ and ^{19}F NMR spectra. Again, the OH signal in the ^1H NMR spectrum could not be confidently assigned. A second minor (< 3%) four-coordinate boron species was seen at δ_B = 18.6 ppm but the corresponding species has not been identified. Interestingly over time mononuclear species **2.4** slowly converted to binuclear species **2.5**. After 1 week, the binuclear species **2.5** accounted for approx. 60% of the phosphorus containing species in solution. As stated before, this is consistent with the observation found for dihydrogen activation, confirming that the phosphinite ligand **L2** stabilises and favours binuclear platinum bridging species such as **2.5** over mononuclear species.

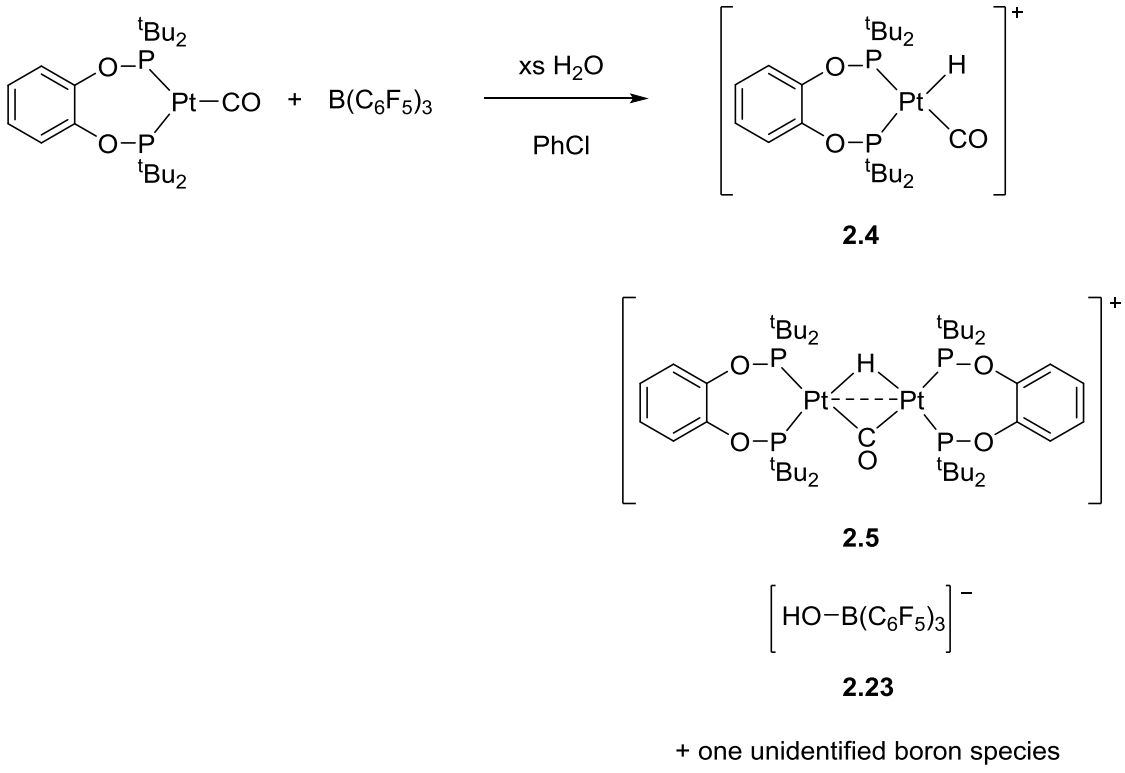

Scheme 2.18: Reaction of [Pt(CO)(**L2**)]/$B(C_6F_5)_3$ with excess H_2O to form species **2.4**, **2.6**, **2.23** and an unidentified boron species.

In both reactions of the different ligand systems there was no evidence for the formation of the trihydride species as observed in dihydrogen activation (see Section 2.5). This provided an opportunity to probe the hypothesis that the two binuclear species (**2.10** and **2.11** for **L1**, **2.5** and **2.6** for **L2**) are interconvertible. Scheme 2.10 in Section 2.5.1 shows

the possible exchange pathways between the two species. In the literature, only the conversion from related trihydride species to the bridging hydride/carbonyl species has been reported.[28]

When the [Pt(CO)(**L2**)]/$B(C_6F_5)_3$/H_2O reaction mixture was subjected to H_2 (1 bar, room temperature) the formation of trihydride species **2.6** was detected immediately in the ^1H NMR spectrum, the concentration of which increased over time. Removing the H_2 atmosphere and replacing it with a carbon monoxide atmosphere did not have a significant effect on the equilibrium. Only a slight increase in the amount of **2.5** was observed under a CO atmosphere implying the equilibrium lies in favour of species **2.6** (Scheme 2.10)

The [Pt(CO)(**L1**)]/$B(C_6F_5)_3$/H_2O reaction mixture was also subjected to H_2 (1 bar, room temperature) and the formation of trihydride species **2.11** was seen immediately in the ^1H NMR spectrum. This was unexpected due to the absence of binuclear species **2.10** and with the only platinum species in solution identified as mononuclear **2.9**. In order for **2.9** to convert to **2.11**, this must go *via* the binuclear species **2.10** as an intermediate, but this species is too reactive to be observed by NMR spectroscopy.

The experiments described above give provide supporting evidence for the equilibria proposed in Scheme 2.10 (Section 2.5.1) for the interconversion between $[Pt_2(\mu\text{-}H)_3(\mathbf{L})_2]^+$ and $[Pt_2(\mu\text{-}H)(\mu\text{-}CO)(\mathbf{L})_2]^+$.

2.8.2 Reaction of THF with Pt(0)/$B(C_6F_5)_3$ Lewis Pair

The ring opening of cyclic ethers by both main group[49–52] and transition metal[33,34] FLPs has been achieved previously, although this reactivity predates the FLP moniker. Over 50 years before the ring opening of THF by FLPs was first reported, Wittig and Rückert described the reaction of THF-BPh_3 with $NaCPh_3$ to form $Na[Ph_3BO(CH_2)_4CPh_3]$.[53] Following this, several Lewis acids, comprising complexes derived from Zr,[54,55] Ti,[56] Sm[57] and U[58] and main group Lewis acids such as alanes[59] and carboranes,[60] coupled with a phosphine or amine base, have displayed similar ether ring-opening reactivity.

An excess of THF was added to a solution of [Pt(CO)(**L**)]/$B(C_6F_5)_3$ (where **L** = **L1** or **L2**) in chlorobenzene at room temperature. No colour change was observed and the $^{11}B\{^1H\}$ NMR spectrum displayed a single peak at 2.0 ppm. This species was identified to be the THF adduct of $B(C_6F_5)_3$ (Scheme 2.19). It is worth noting here that the $^{31}P\{^1H\}$

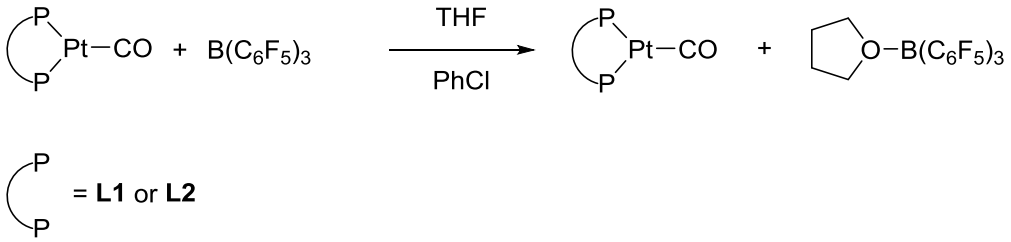

Scheme 2.19: Reaction of [Pt(CO)(**L**)] and $B(C_6F_5)_3$ with THF.

NMR spectrum displayed only the starting [Pt(CO)(**L**)] complex and the line broadening that arose from the [Pt(CO)(**L**)]/$B(C_6F_5)_3$ combination was not observed here (see Section 2.4). It is proposed that $B(C_6F_5)_3$ interacts with [Pt(CO)(**L**)] but this interaction is weak and is disrupted by the more suitably matched 'hard' THF.

The mixture was left at room temperature for 10 days after which no further reactivity was observed. The mixture was also heated to 80 °C for 3 days and yet still no reaction was observed. The proposed mechanism for ring-opening THF by a Lewis pair involves initial binding of the THF to the Lewis acid which then weakens the C-O bond making the α-carbon susceptible to nucleophilic attack by the Lewis base.[55] Evidently, [Pt(CO)(**L**)] is not either electronically or sterically matched to attack the α-carbon of the THF ligand to induce ring-opening.

2.8.3 Reaction of CO_2 with [Pt(CO)(L2)]/$B(C_6F_5)_3$ Lewis Pair

The reaction of CO_2 with [Pt(CO)(**L1**)]/$B(C_6F_5)_3$ has previously been reported by the Wass and Pringle groups.[7,8] Two species were identified in solution but only one was identified by X-ray crystallography and was found to be **1.70** (Scheme 2.20). The formation of this species was confirmed to be a result of cooperative activation of CO_2 (not just binding of CO_2) due to the formation of *ca.* 20% unlabelled product (**1.70**) when using $^{13}CO_2$. This could have only originated from the unlabelled CO ligand in the starting complex. The presence of the Lewis acid is essential for reactivity to occur.

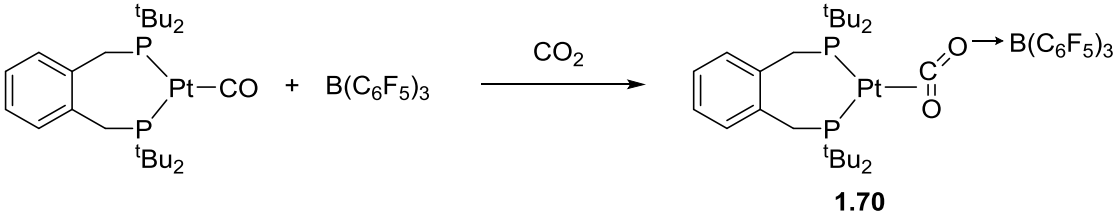

1.70

Scheme 2.20: Reaction of [Pt(CO)(**L1**)] and $B(C_6F_5)_3$ with CO_2.

hen [Pt(CO)(**L2**)]/$B(C_6F_5)_3$ was treated with CO_2 (1 bar) in chlorobenzene at room temperature the bright orange colour of the solution noticeably increased in intensity overnight although there was a distinct colour change. Analysis of the $^{31}P\{^1H\}$ NMR after 16 hours showed the presence of *ca*. 15% starting material as well as several unidentified species with platinum satellites. Attempts to isolate single products were unsuccessful. Although the exact identity of the products remains unknown it can be postulated that the [Pt(CO)(**L2**)]/$B(C_6F_5)_3$ Lewis pair does interact with the CO_2 in a cooperative manner. The evidence supporting this is that the same reactivity is not seen in the absence of $B(C_6F_5)_3$.

2.9 Conclusions and Future Work

This chapter has described the synthesis of a novel Pt(0) Lewis base, [Pt(CO)(**L2**)] and compared its properties and activation chemistry to [Pt(CO)(**L1**)]. Incorporating phosphinite ligand **L2** into the Pt Lewis base significantly reduces the electron density at the metal centre. The impact of this on small molecule activation by the Pt(0)/$B(C_6F_5)_3$ Lewis pair system has been investigated. The formation of the labelled complex [Pt(^{13}CO)(**L2**)] was synthesised in an attempt to identify pathways to activation products.

When [Pt(CO)(**L2**)] and $B(C_6F_5)_3$ were combined in solution, the observations recorded mirrored that observed for [Pt(CO)(**L1**)]/$B(C_6F_5)_3$. The line broadening and thermochromic properties of the solution indicated the presence of a weak interaction between the platinum and borane components. This was supported by the fact that in the presence of THF the Pt(0)/$B(C_6F_5)_3$ interaction was absent due to the THF strongly binding to the borane.

The pathway to dihydrogen activation by [Pt(CO)(**L**)]/$B(C_6F_5)_3$ was proposed to be *via* ion pair **2.10**/**2.7** for **L** = **L1** and **2.5**/**2.7** for **L** = **L2**. These intermediates were not originally observed when using **L1** but the cationic intermediate $[Pt_2(\mu\text{-H})(\mu\text{-CO})(\mathbf{L})_2]^+$ appears to be stable at room temperature when **L** = **L2** which meant full conversion to the final activation products was never achieved. The use of the ^{13}C-labelled starting material [Pt(^{13}CO)(**L1**)] meant the intermediates were observable by $^{13}C\{^1H\}$ NMR spectroscopy in the early stages of the reaction. It is still unknown what the exact mechanism is for the formation of **2.10**/**2.7** and **2.5**/**2.7** and how these species convert to the final products **2.9**/**2.8** and **2.4**/**2.8** respectively. A DFT investigation of possible intermediates and transition states should be carried out.

Binuclear species and $[Pt_2(\mu\text{-}H)(\mu\text{-}CO)(\mathbf{L})_2]^+$ was shown to convert to $[Pt_2(\mu\text{-}H)_3(\mathbf{L})_2]^+$ when subjected to a H_2 atmosphere. This explains the presence of $[Pt_2(\mu\text{-}H)_3(\mathbf{L})_2]^+$ in the dihydrogen activation experiments. Interestingly, incorporation of the phosphinite ligand **L2** into the Pt system stabilised the formation of binuclear Pt species in comparison to using the alkyl phosphine **L1**.

The coupling of ethene and CO was also observed when using **L2** in the $[Pt(CO)(\mathbf{L})]/B(C_6F_5)_3$ system at a much higher rate of formation than for the **L1** system. Again, the activation product appears to be more stable when **L** = **L2** than when **L** = **L1**. Further investigations should be made into the stability of these products to see if it is possible to create a catalytic system for CO/ethene coupling. The basicity of $[Pt(CO)(\mathbf{L})]$ was shown with phenylacetylene activation where the substrate underwent deprotonation rather than 1,2-addition.

It would be of interest to investigate the reactivity with internal alkenes and alkynes to see if similar reactivity is observed or if the steric demands drive the formation of different products. An initial investigation into internal alkyne activation was made using 1-phenyl-1-propyne and the reaction reached full conversion but did not proceed cleanly. There were several species present in the $^{31}P\{^1H\}$ NMR spectrum of the final mixture but there was evidence in the ^1H NMR spectrum of a methyl group coupling to platinum which indicated that there may have been addition to the alkyne triple bond. Further investigation is needed to identify all activation products.

The substrate scope for the $[Pt(CO)(\mathbf{L})]/B(C_6F_5)_3$ system was also explored. Although activation of THF has been shown to be successful with main group systems containing $B(C_6F_5)_3$ as the Lewis acid, the Pt(0) Lewis base did not open the cyclic ether. Cooperative activity was observed whilst exploring the activation of CO_2 by $[Pt(CO)(\mathbf{L2})]/B(C_6F_5)_3$ but the reaction mixture was too complex to deconvolute and identify activation products with confidence. The $[Pt(CO)(\mathbf{L})]/B(C_6F_5)_3$ system was also shown to be intolerant to water and the major products formed were as a result of deprotonation of H_2O.

Further work should include theoretical investigations into the pathways to activation products which have been identified by observable experimental intermediates. There are also several modifications to the system which could be made including modifying the

ligand, the metal centre or the Lewis acid. Initial exploration into these modifications have been made and will be presented in Chapter 3.

2.10 References

1 A. Amgoune and D. Bourissou, *Chem. Commun.*, 2011, **47**, 859–871.

2 G. Bouhadir and D. Bourissou, *The Chemical Bond III*, Springer, 2017, vol. 171.

3 D. F. Shriver, *Acc. Chem. Res.*, 1970, **3**, 231–238.

4 T. P. Lin and J. C. Peters, *J. Am. Chem. Soc.*, 2013, **135**, 15310–15313.

5 W. H. Harman and J. C. Peters, *J. Am. Chem. Soc.*, 2012, **134**, 5080–5082.

6 S. J. K. Forrest, P. G. Pringle, H. A. Sparkes and D. F. Wass, *Dalt. Trans.*, 2014, **43**, 16335–16344.

7 S. J. K. Forrest, J. Clifton, N. Fey, P. G. Pringle, H. A. Sparkes and D. F. Wass, *Angew. Chem. Int. Ed.*, 2015, **54**, 2223–2227.

8 S. J. K. Forrest, PhD Thesis, University of Bristol, 2014.

9 C. J. Moulton and B. L. Shaw, *J. Chem. Soc. Chem. Commun.*, 1976, 365–366.

10 N. Carr, L. Mole, A. G. Orpen and J. L. Spencer, *J. Chem. Soc., Dalt. Trans.*, 1992, 2653–2662.

11 N. Carr, B. J. Dunne, A. G. Orpen and J. L. Spencer, *J. Chem. Soc., Chem. Commun.*, 1988, 926–928.

12 R. P. Tooze, G. R. Eastham, K. Whiston and X. L.Wang, WO9619434 (A1), 1996.

13 R. F. M. J. Parton and M. C. C. Janessen, WO2013030344 (A1), 2013.

14 J. Bauer, H. Braunschweig, R. D. Dewhurst and K. Radacki, *Chem. - A Eur. J.*, 2013, **19**, 8797–8805.

15 D. W. Stephan and G. Erker, *Angew. Chem. Int. Ed.*, 2015, **54**, 6400–6441.

16 P. C. J. Kamer and P. W. N. M. Van Leeuwen, *Phosphorus(III) Ligands in Homogeneous Catalysis: Design and Synthesis*, Wiley, 2012.

17 I. O. Koshevoy, Y. C. Chang, Y. A. Chen, A. J. Karttunen, E. V. Grachova, S. P. Tunik, J. Jänis, T. A. Pakkanen and P. T. Chou, *Organometallics*, 2014, **33**, 2363–2371.

18 P. Bergamini, V. Bertolasi and F. Milani, *Eur. J. Inorg. Chem.*, 2004, **2004**, 1277–1284.

19 T. Fanjul, G. Eastham, J. Floure, S. J. K. Forrest, M. F. Haddow, A. Hamilton, P. G. Pringle, A. G. Orpen and M. Waugh, *Dalton Trans.*, 2013, **42**, 100–115.

20 D. W. Stephan, *Science*, 2016, **354**, 1248.

21 W. E. Piers and T. Chivers, *Chem. Soc. Rev.*, 1997, **26**, 345–354.

22 G. Erker, *Dalt. Trans.*, 2005, **2**, 1883–1890.

23 H. Jacobsen, H. Berke, S. Döring, G. Kehr, G. Erker, R. Fröhlich and O. Meyer, *Organometallics*, 1999, **18**, 1724–1735.

24 R. Dobrovetsky and D. W. Stephan, *J. Am. Chem. Soc.*, 2013, **135**, 4974–4977.

25 C. Brevard and P. Granger, *Handbook of High Resolution Multinuclear NMR*, John Wiley & Sons, Inc., Toronto, 1981.

26 T. Yoshida, T. Yamagata, T. H. Tulip, J. A. Ibers and S. Otsuka, *Inorg. Chem.*, 1979, **18**, 2239–2250.

27 G. A. Minghetti, A. L. Bandini, G. Banditelli and F. Bonati, *J. Organomet. Chem.*, 1979, **179**, C13–C15.

28 G. Minghetti, A. L. Bandini, G. Banditelli, F. Bonati, R. Szostak, C. E. Strouse, C. B. Knobler and H. D. Kaesz, *Inorg. Chem.*, 1983, **22**, 2332–2338.

29 A. L. Bandini, G. Banditelli, M. Grassi and A. Ponti, *Dalt. Trans.*, 2004, 2027–2035.

30 C. B. Knobler, H. D. Kaesz, G. Minghetti, A. L. Bandini, G. Banditelli and F. Bonati, *Inorg. Chem.*, 1983, **22**, 2324–2331.

31 G. Minghetti, G. Banditelli and A. L. Bandini, *J. Organomet. Chem.*, 1977, **139**, C80–C82.

32 M. A. Dureen, C. C. Brown and D. W. Stephan, *Organometallics*, 2010, **29**, 6594–6607.

33 A. M. Chapman, M. F. Haddow and D. F. Wass, *J. Am. Chem. Soc.*, 2011, **133**, 18463–18478.

34 O. J. Metters, S. J. K. Forrest, H. A. Sparkes, I. Manners and D. F. Wass, *J. Am. Chem. Soc.*, 2016, **138**, 1994–2003.

35 M. A. Dureen and D. W. Stephan, *J. Am. Chem. Soc.*, 2009, **131**, 8396–8397.

36 C. Jiang, O. Blacque and H. Berke, *Organometallics*, 2010, **29**, 125–133.

37 D. W. Stephan, S. Greenberg, T. W. Graham, P. Chase, J. J. Hastie, S. J. Geier, J. M. Farrell, C. C. Brown, Z. M. Heiden, G. C. Welch and M. Ullrich, *Inorg. Chem.*, 2011, **50**, 12338–12348.

38 G. Erős, H. Mehdi, I. Pápai, T. A. Rokob, P. Király, G. Tárkányi and T. Soós, *Angew. Chem. Int. Ed.*, 2010, **49**, 6559–6563.

39 L. Greb, C.-G. Daniliuc, K. Bergander and J. Paradies, *Angew. Chem. Int. Ed.*, 2013, **52**, 5876–5879.

40 S. R. Flynn, O. J. Metters, I. Manners and D. F. Wass, *Organometallics*, 2016, **35**, 847–850.

41 Á. Gyömöre, M. Bakos, T. Földes, I. Pápai, A. Domján and T. Soós, *ACS Catal.*, 2015, **5**, 5366–5372.

42 V. Fasano, J. LaFortune, J. Bayne, M. J. Ingleson and D. W. Stephan, *Chem. Commun.*, 2017, **54**, 662–665.

43 V. Fasano and M. J. Ingleson, *Chem. - A Eur. J.*, 2017, **23**, 2217–2224.

44 J. W. Thomson, J. A. Hatnean, J. J. Hastie, A. Pasternak, D. W. Stephan and P. A. Chase, *Org. Process Res. Dev.*, 2013, **17**, 1287–1292.

45 T. Mahdi and D. W. Stephan, *J. Am. Chem. Soc.*, 2014, **136**, 15809–15812.

46 D. J. Scott, T. R. Simmons, E. J. Lawrence, G. G. Wildgoose, M. J. Fuchter and A. E. Ashley, *ACS Catal.*, 2015, **5**, 5540–5544.

47 V. Fasano, J. E. Radcliffe and M. J. Ingleson, *ACS Catal.*, 2016, **6**, 1793–1798.

48 C. Bibal, C. C. Santini, Y. Chauvin, C. Vallée and H. Olivier-Bourbigou, *Dalt. Trans.*, 2008, 2866–2870.

49 B. Birkmann, T. Voss, S. J. Geier, M. Ullrich, G. Kehr, G. Erker and D. W.

Stephan, *Organometallics*, 2010, **29**, 5310–5319.

50 D. Holschumacher, T. Bannenberg, C. G. Hrib, P. G. Jones and M. Tamm, *Angew. Chem. Int. Ed.*, 2008, **47**, 7428–7432.

51 G. C. Welch, J. D. Masuda and D. W. Stephan, *Inorg. Chem.*, 2006, **45**, 478–480.

52 S. J. Geier and D. W. Stephan, *J. Am. Chem. Soc.*, 2009, **131**, 3476–3477.

53 G. Wittig and A. Rückert, *Justus Liebigs Ann. Chem.*, 1950, **566**, 101–113.

54 Z. Y. Guo, P. K. Bradley and R. F. Jordan, *Organometallics*, 1992, **11**, 2690–2693.

55 T. L. Breen and D. W. Stephan, *Inorg. Chem.*, 1992, **31**, 4019–4022.

56 A. Mommertz, R. Leo, W. Massa, K. Harms and K. Dehnicke, *Z. Anorg. Allg. Chem.*, 1998, **624**, 1647–1652.

57 W. J. Evans, J. T. Leman, J. W. Ziller and S. I. Khan, *Inorg. Chem.*, 1996, **35**, 4283–4291.

58 L. R. Avens, D. M. Barnhart, C. J. Burns and S. D. McKee, *Inorg. Chem.*, 1996, **35**, 537–539.

59 J. P. Campbell and W. L. Gladfelter, *Inorg. Chem.*, 1997, **36**, 4094–4098.

60 M. Gómez-Saso, D. F. Mullica, E. Sappenfield and F. G. A. Stone, *Polyhedron*, 1996, **15**, 793–801.

Chapter 3

Modifications to the Pt(0)/B(C_6F_5)$_3$ Lewis Pair System

3.1 Introduction

Chapter 2 described the development of a cooperative Lewis pair: [Pt(CO)(**L**)]/B(C_6F_5)$_3$ where **L** = **L1** or **L2**. There was evidence of an interaction between the platinum(0) Lewis base and the borane Lewis acid, but this interaction was presumed to be weak and reversible. Both systems were effective in the activation of small molecules including dihydrogen, ethene and phenylacetylene. Although there was a significant difference in electronics at the Lewis basic centre when changing from **L1** to **L2** (see Section 2.3), many of the final activation products were analogous.

The more electron-withdrawing ligand **L2** stabilised the formation of binuclear platinum species over mononuclear species which were favoured when using **L1**. This difference allowed the elucidation of previously undetected intermediate in the pathway of dihydrogen activation by [Pt(CO)(**L**)]/B(C_6F_5)$_3$. Further modification to the system could lead to the identification of other intermediates in activation pathways or potentially different activation products.

3.1.1 Aims and Objectives

The mechanism of activation of the substrates described in Chapter 2 were unknown and the scope of the activation chemistry was limited. A simple change of the backbone upon modification from **L1** to **L2** led to the elucidation of a possible activation pathway for dihydrogen. It was of interest to further explore different modifications of the system to deepen the understanding of the route to activation of small molecules. Modification of the system also could lead to the possibility of novel activation products. Thus, the aims of this part of the project were as follows:

- To modify the diphosphine ligand to impart a change in the stereoelectronic properties of the Pt(0) centre

- To explore the use of different Lewis acids in the cooperative Lewis pair
- To investigate the use of different metal complexes as a Lewis base
- To incorporate functionality into the diphosphine backbone

3.2 Modifications to the Diphosphine Ligand

In Chapter 2, the diphosphine ligand was modified from phosphine **L1** to the analogous phosphinite **L2** and the activation chemistry of these two systems was explored and compared. **L2** is electronically different from **L1** but the steric bulk around the metal centre was similar due to the use of the same terminal phosphine substituents. The research described below concerns the synthesis and use of a variety of phosphine ligands in the [Pt(CO)(**L**)]/B(C_6F_5)$_3$ cooperative Lewis pair system.

3.2.1 Synthesis of L3 and Coordination to Pt

Ligand **L3** (Scheme 3.1) was targeted due to the reduced steric bulk of PCy_2 in comparison to P^tBu_2. Phosphinite ligand **L3** was synthesised from the reaction of catechol and NaH with dicyclohexylchlorophosphine (Scheme 3.1). Complete consumption of the $ClPCy_2$ starting material was observed by $^{31}P\{^1H\}$ NMR spectroscopy after only 3 h at room temperature. The much shorter reaction time length and the less harsh (lower temperature) conditions needed to form **L3** compared to **L2** (72 h, reflux in THF) is attributed to the smaller and less electron-donating phosphine substituent on the chlorophosphine electrophile. A small amount of the hydrolysis product $HP(O)Cy_2$ was observed in the crude product but recrystallisation from hexane at −20 °C yielded pure **L3**. Crystals suitable for X-ray crystallography were grown from a saturated solution of **L3** in hexane at −40 °C (Figure 3.1). It can be seen that the phosphorus groups in **L3** are orientated away from each other. This may be a consequence of the repulsion of the lone pairs on the oxygen atom incorporated into the ligand backbone as well as minimising the steric repulsion from the cyclohexyl substituents.

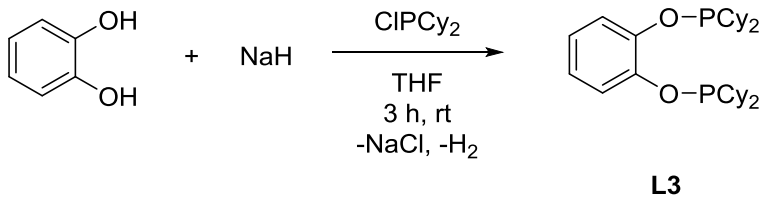

Scheme 3.1: Synthesis of **L3**.

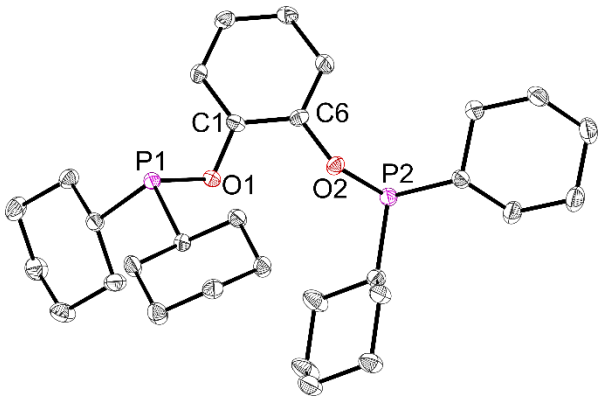

Figure 3.1: Crystal structure of **L3**. Thermal ellipsoids at 50%. Hydrogen atoms omitted for clarity. Selected bond lengths (Å) and angles (°): P1-O1 1.6821(12); O1-C1 1.377(2); P2-O2 1.6764(12); O2-C6 1.3910(19); P1-O1-C1 120.43(11), P2-O2-C6 119.66(10).

Addition of **L3** to [$PtCl_2$(COD)] yielded the corresponding dichloroplatinum complex **3.1** as a white solid in 90% yield (Scheme 3.2). Slow diffusion of hexane into a saturated solution of **3.1** in CH_2Cl_2 produced crystals suitable for X-ray crystallography (Figure 3.2). The 7-membered ring formed has the expected conformation in which the PtP_2 plane is almost orthogonal to the phenyl ring in the backbone of the ligand (See Section 2.2.1).

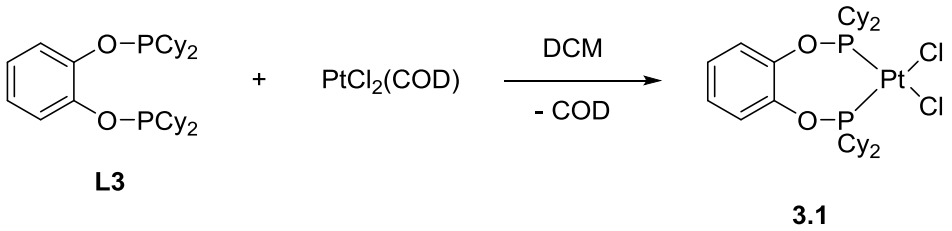

L3 **3.1**

Scheme 3.2: Formation of dichloroplatinum(II) complex **3.1**.

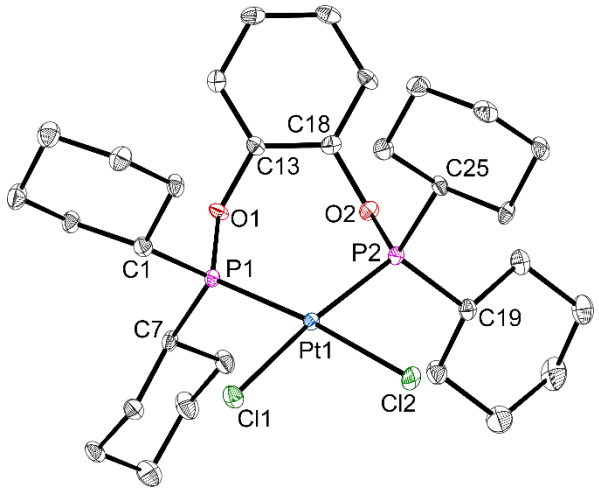

Figure 3.2: Crystal structure of **3.1**. Thermal ellipsoids at 50%. Hydrogen atoms and co-crystallised solvent molecule (CH_2Cl_2) omitted for clarity. Selected bond lengths (Å) and angles (°): Pt1-P1 2.2187(9); Pt1-P2 2.2158(9); Pt1-Cl1 2.3752(8); Pt1-Cl2 2.3457(8); P1-O1 1.623(2); P1-C1 1.825(4); P1-C7 1.720(3); P2-O2 1.632(3); P2-C19 1.818(4); P2-C25 1.842(3); P1-Pt1-P2 99.40(3); P1-Pt1-Cl1 88.12(3); P2-Pt1-Cl2 45.890; Cl1-Pt1-Cl2 46.393.

The first step in the attempted synthesis of [Pt(CO)(**L3**)] was the reaction of [Pt(nbe)$_3$] with **L3.** The reaction mixture was left overnight and analysis by $^{31}P\{^1H\}$ NMR spectroscopy confirmed full complexation of **L3** to form [Pt(nbe)(**L3**)] (δ_P = 181.0 ppm, $^1J_{PPt}$ = 3584 Hz) (Scheme 3.3 and Figure 3.3A). In a Youngs NMR tube, the crude reaction mixture was subjected to a CO atmosphere (1 bar) and an instant colour change from colourless to pale yellow was observed. The $^{31}P\{^1H\}$ NMR spectrum showed full conversion to a new species with a sharp NMR resonance at δ_P = 151.2 ppm ($^1J_{PPt}$ = 3582 Hz). This was unexpected as when the same experiment was carried out using **L1** or **L2**, the complex formed under a CO atmosphere displayed a broad signal in the $^{31}P\{^1H\}$ NMR spectrum at room temperature. It was assumed that the new species formed was the four-coordinate dicarbonyl complex [Pt(CO)$_2$(**L3**)] (Scheme 3.3). To confirm this, the experiment was repeated with ^{13}CO, yielding a complex with an addition NMR spectroscopic handle. Interestingly, at room temperature the expected coupling between the ^{31}P and ^{13}C atoms was not observed and a singlet in the $^{31}P\{^1H\}$ NMR spectrum was observed for [Pt(^{13}CO)$_2$(**L3**)] (Figure 3.3B). At room temperature, a very broad signal in the $^{13}C\{^1H\}$ NMR spectrum was observed at δ_C = 182.4 ppm. Low temperature NMR spectroscopy studies showed the $^{31}P\{^1H\}$ NMR signal to broaden and then resolve to a triplet at −40 °C ($^2J_{PC}$ = 16 Hz, Figure 3.3C). The signal in the $^{13}C\{^1H\}$ NMR spectrum also resolved at low temperature to a triplet confirming the formation of the dicarbonyl species [Pt(^{13}CO)$_2$(**L3**)] when the sample is under an atmosphere of ^{13}CO.

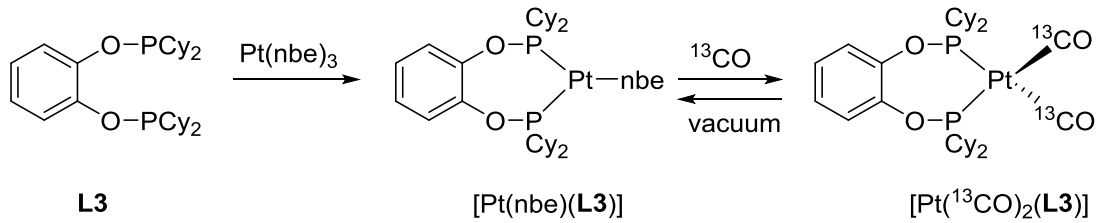

Scheme 3.3: Formation of [Pt(nbe)(**L3**)] and [Pt(^{13}CO)$_2$(**L3**)].

The observation of [Pt(CO)$_2$(**L3**)] under a CO atmosphere is consistent with what was seen when using **L1** and **L2** (See Section 2.3.1). It was hoped that upon removal of the CO atmosphere and the toluene solvent, some of the monocarbonyl complex [Pt(CO)(**L3**)] would be formed in equilibrium with [Pt(nbe)(**L3**)] and, as described before in Section 2.3, and after several CO/vacuum cycles it might be possible to isolate the monocarbonyl complex [Pt(CO)(**L3**)]. However, when this experiment was carried out and the solvent was removed, an off-white solid produced. This was redissolved in

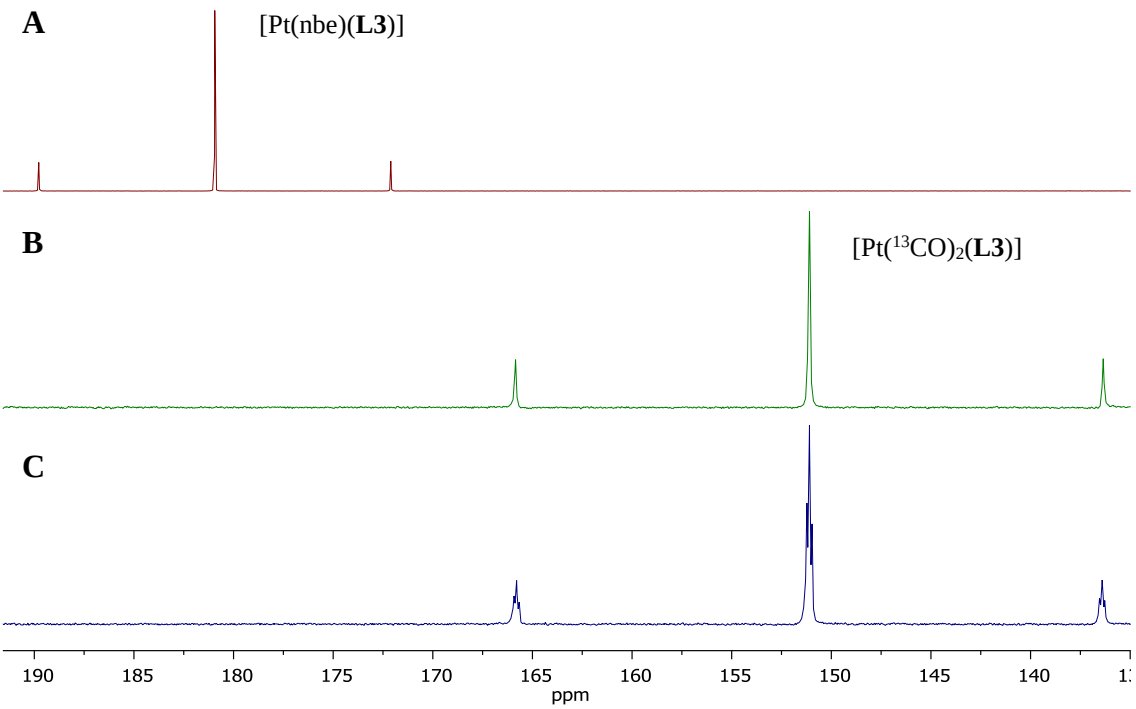

Figure 3.3: $^{31}P\{^{1}H\}$ NMR spectra of (A) [Pt(nbe)(**L3**)] at room temperature, (B) [Pt($^{13}CO)_2$(**L3**)] at room temperature and (C) [Pt($^{13}CO)_2$(**L3**)] at −40 °C.

toluene and analysis of the ^{1}H and $^{31}P\{^{1}H\}$ NMR spectra revealed quantitative conversion back to the mononorbornene complex [Pt(nbe)(**L3**)]. The CO/vacuum cycle was repeated several times but there was no evidence that a monocarbonyl complex had formed, even in a very low conversion.

It appears that **L3** does not have the correct stereoelectronic properties to stabilise either a mono- or dicarbonyl Pt(0) complex in the presence of norbornene, and the absence of a CO atmosphere. The cyclohexyl substituents in **L3** are not as electron-donating nor as bulky as the *tert*-butyl substituents in **L1** or **L2** but it is not clear which one, or if both of these factors led to the relative instability of the [Pt(CO)(**L**)] species. This discussion will be returned to in Section 3.2.2.

3.2.2 Synthesis of L4 and Coordination to Pt

Ligand **L4** was synthesised following a modified literature procedure (Scheme 3.4).[1] In 2007, Wills *et al.* reported the synthesis of **L4** *via* the generation of a diGrignard reagent

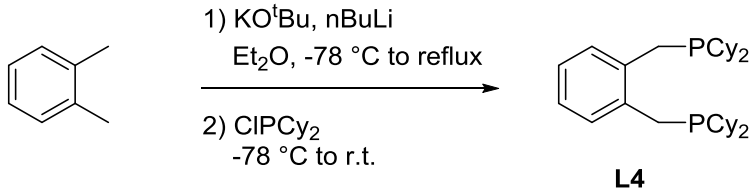

Scheme 3.4: Formation of **L4**.

from α,α'-dichloro-o-xylene followed by reaction with $ClPCy_2$ but obtained low yields (48% after "some experimentation") and no experimental procedure was reported.[2] In our hands, attempts to synthesise **L4** by formation of a diGrignard were unsuccessful. More recently, Beller *et al.* reported the synthesis detailed in Scheme 3.4 but obtained even lower yields (34%) than Wills.[1] Yield would likely have been lost over the several recrystallisations from MeOH needed to obtain pure product. When the route detailed in Scheme 3.4 was attempted by the author, the crude product **L4** was obtained in *ca*. 80% purity. Attempts to recrystallise the crude mixture from MeOH were unsuccessful because the mixture was insoluble, even in refluxing MeOH. **L4** was obtained in sufficient purity (> 98%) by washing the crude mixture several times with hot MeOH (36% yield).

The synthesis of [Pt(CO)(**L4**)] was attempted following the same procedure described in Section 2.3 for [Pt(CO)(**L2**)] with the appropriate ligand. Unfortunately, the monocarbonyl complex was not formed and similar difficulties were encountered with **L4** as with **L3** (Scheme 3.5). Platinum complex [Pt(nbe)(**L4**)] was formed upon addition of **L4** to $Pt(nbe)_3$. Treatment of the solution of [Pt(nbe)(**L4**)] with ^{13}CO led to the formation of dicarbonyl [Pt($^{13}CO)_2$(**L4**)] which reverted back to [Pt(nbe)(**L4**)] upon removal of the solvent. This demonstrates that the dicyclohexyl substituent does not possess the necessary stereoelectronic properties needed to stabilise the formation of [Pt(CO)(**L4**)].

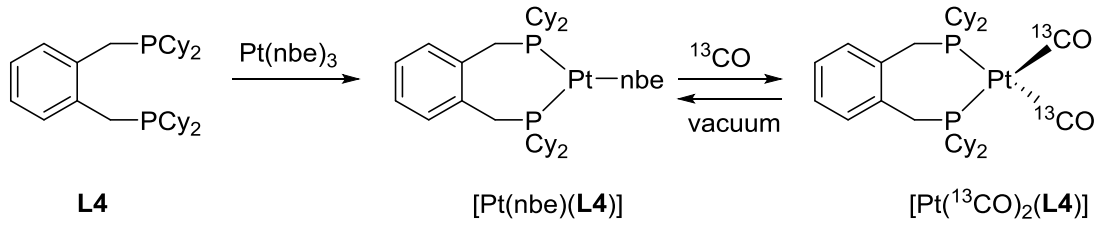

Scheme 3.5: Formation of [Pt(nbe)(**L4**)] and [Pt($^{13}CO)_2$(**L4**)].

3.2.3 Synthesis of L5 and Coordination to Pt

The work presented in this section was started by Gregory Godley, an MSci undergraduate student, under the supervision of the author. The work was repeated by the author and the data presented was collected by the author.

The previous ligands tested in this Pt(0)/B(C_6F_5)$_3$ system have all involved alkyl substituents on the phosphorus atom, so it was of interest to test the suitability of aryl

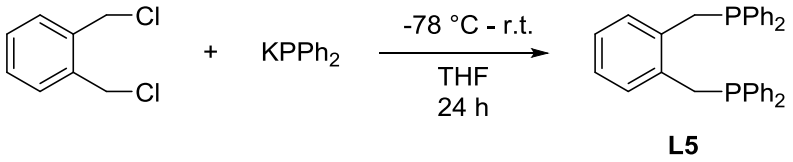

L5

Scheme 3.6: Formation of **L5**.

substituents. Ligand **L5** was synthesised according to previous literature methods (Scheme 3.6).[2]

Ligand **L5** was unexpectedly found to be only partially soluble in common organic solvents (toluene, hexane, dichloromethane) which consequently meant that the coordination to the platinum precursor [Pt(nbe)$_3$] only proceeded in very low conversion. Leaving the reaction mixture for longer (3 d) and refluxing the suspension did not aid the solubility of **L5**. Only a small amount (< 10%) of [Pt(nbe)(**L5**)] was formed in toluene and when this reaction mixture was subjected to CO the decomposition of unreacted [Pt(nbe)$_3$] was apparent due to the formation of Pt(0) metal. A solution phase IR of the reaction mixture after filtration of the metallic platinum particles showed the presence of two carbonyl signals (ν_{CO} = 1997 and 1953 cm^{-1}) indicating the formation of a dicarbonyl species. However, attempts to isolate this species led to further degradation.

Substitution of the phenyl rings in the PPh$_2$ group could possibly lead to better solubility which could aid the initial complexation to the platinum precursor [Pt(nbe)$_3$]. It would also be of interest to investigate substitution at the *ortho* position of the phenyl rings as this would induce more steric hinderance around the metal centre compared to other substitution locations. As discussed previously, steric hinderance may be necessary to stabilise the desired Pt(0)-monocarbonyl complex. Secondary *o*-substituted aryl phosphines are commercially available and would then require an extra step to form the *in situ* KPR$_2$ to follow the analogous synthesis detailed in Scheme 3.6.

Although the desired complex [Pt(CO)(**L5**)] could not be synthesised due to the insolubility of **L5**, it was predicted that it may not have possessed the required stereoelectronic properties needed to stabilise the monocarbonyl complex. This prompted the investigation into the use of **L6** described in the next section.

3.2.4 Synthesis of L6 and Coordination to Pt

The work presented in this section was started by Gregory Godley, an MSci undergraduate student, under the supervision of the author. The work was repeated by the author and the data presented was collected by the author

The tricyclic phosphine 1,3,5,7-tetramethyl-2,4,8-trioxa-6-phospha-adamantane cage (CgPH) is an unusual phosphine synthesised from the reaction of PH_3 with acetylacetone and is formed as a mixture of enantiomers, α-CgPH and β-CgPH (Scheme 3.7).[3] The PCg group is sterically similar to P^tBu_2 but electronically comparable to PPh_2.[3] Ligand **L6** has been previously synthesised by the reaction of diphosphino-*o*-xylene and acetylacetone but in very poor yields (< 6%).[4] A improved synthetic route to **L6** is shown in Scheme 3.7. Lithiation of CgPH.BH_3 at −78 °C followed by addition of α,α'-dichloro-*o*-xylene led to the formation of the borane protected ligand **L6**.BH_3. Deprotection of the phosphine with diethylamine led to the air-stable product **L6** in high yields as 1:2 diastereomeric mixture of *rac* and *meso* isomers (81%). The dichloroplatinum complex [$PtCl_2$(**L6**)] has been previously synthesised and X-ray crystal structure reported by Pugh and Pringle *et al*.[4]

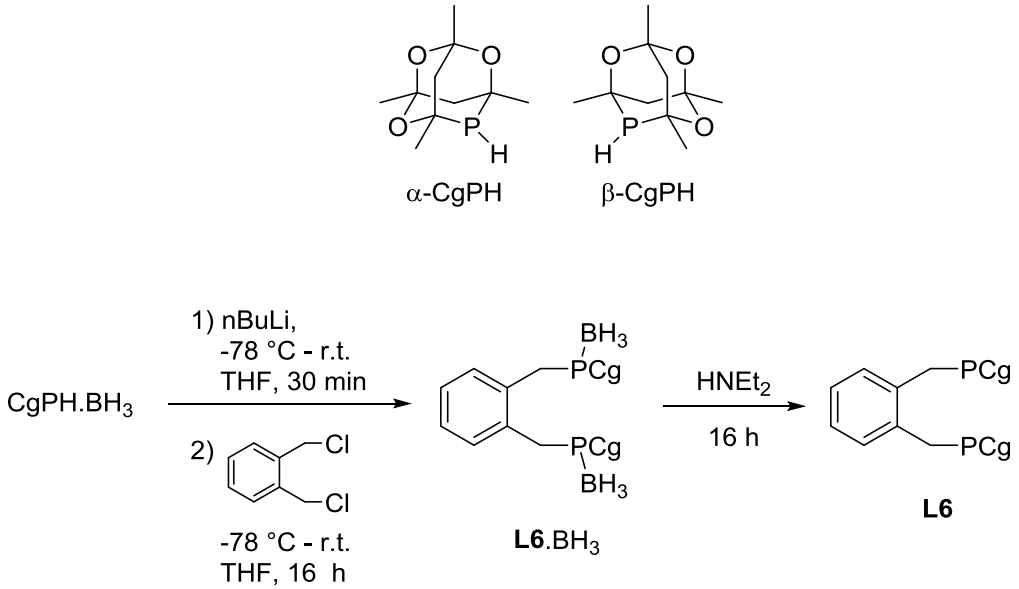

Scheme 3.7: Structure of CgPH enantiomers and the formation of **L6**.

Addition of **L6** to [Pt(nbe)$_3$] led to the formation of mononorbornene complex [Pt(nbe)(**L6**)] (Scheme 3.8). The signal in the $^{31}P\{^1H\}$ NMR spectrum at room temperature was extremely broad (δ_P = 11.4 ppm, $^1J_{PPt}$ = 3489 Hz, $w_{1/2}$ = 832 Hz) (Figure 3.4B). At least two isomers were expected to be observed due to the formation of a

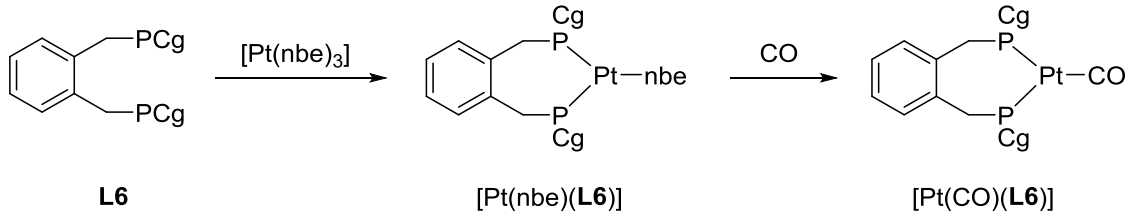

L6 [Pt(nbe)(**L6**)] [Pt(CO)(**L6**)]

Scheme 3.8: Formation of [Pt(CO)(**L6**)] *via* intermediate [Pt(nbe)(**L6**)].

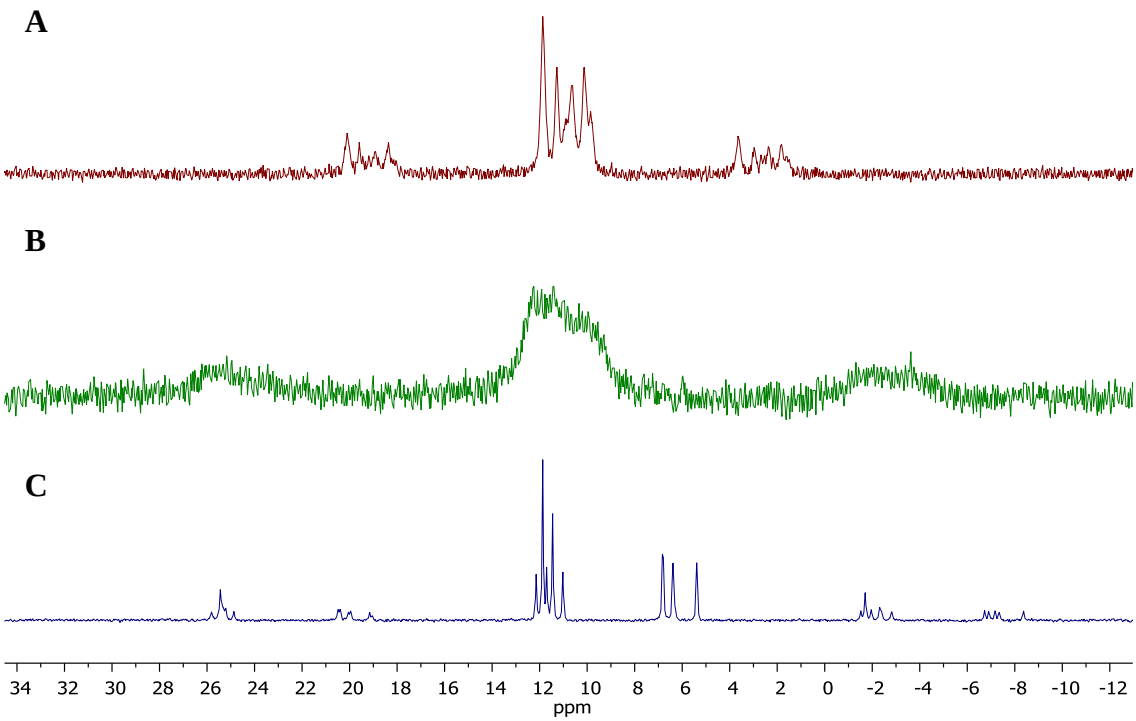

Figure 3.4: $^{31}P\{^{1}H\}$ NMR spectra of [Pt(nbe)(**L6**)] at A) 85 °C, B) room temperature and C) −80 °C.

diastereomeric mixture of *rac*-[Pt(nbe)(**L6**)] and *meso*-[Pt(nbe)(**L6**)]. Both high and low temperature NMR spectroscopy studies were carried out on [Pt(nbe)(**L6**)] (Figure 3.4A and 3.4C respectively).

The resolution of signals in both the high and low temperature NMR spectroscopy studies demonstrate the fluxionality of [Pt(nbe)(**L6**)] on the NMR timescale. Studies on the analogous complex [Pt(nbe)(**L1**)] have already explored the origin of this fluxionality on the NMR timescale.[5,6] In related metal complexes of xylenyl based ligands, the fluxionality has been attributed to inversion of the chelate ring formed with the Pt centre (Figure 3.5A).[7–10] The other origin of fluxionality for a platinum mononorbornene complex is the slow rotation about the Pt-nbe bond which has been observed for similar bulky diphosphines (Figure 3.5B).[5,11]

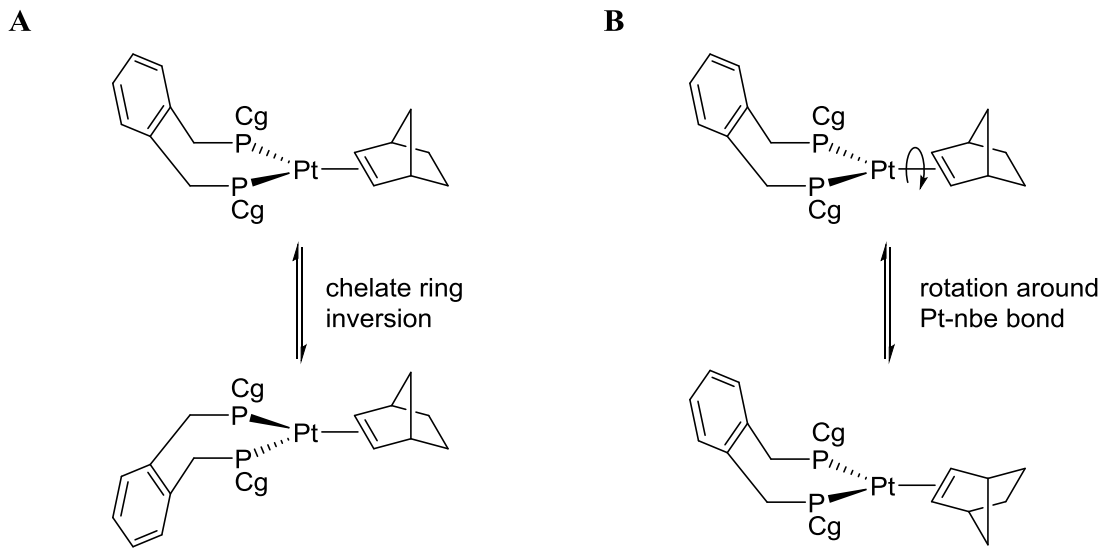

Figure 3.5: Origins of fluxionality in [Pt(nbe)(**L6**)]. A) chelate ring inversion B) rotation about Pt-nbe bond.

With the added complication of having *rac* and *meso* diastereoisomers of [Pt(nbe)(**L6**)] there are several possible conformations in solution. The variable temperature $^{31}P\{^{1}H\}$ NMR spectra obtained display the complexity of the system (Figure 3.4A and 3.4C). Although the low temperature $^{31}P\{^{1}H\}$ NMR spectrum appears to be cleanly resolved, assignment of each signal proved elusive.

The synthesis of [Pt(CO)(**L6**)] was carried out in a Youngs NMR tube and required at least 6 CO/vacuum cycles to convert [Pt(nbe)(**L6**)] to [Pt(CO)(**L6**)]. It was difficult to definitively say that full conversion to the final product was achieved as the NMR spectrum at room temperature of both the starting material and product were broad (Figure 3.4B and Figure 3.6A). [Pt(CO)(**L6**)] gives two broad signals in the $^{31}P\{^{1}H\}$

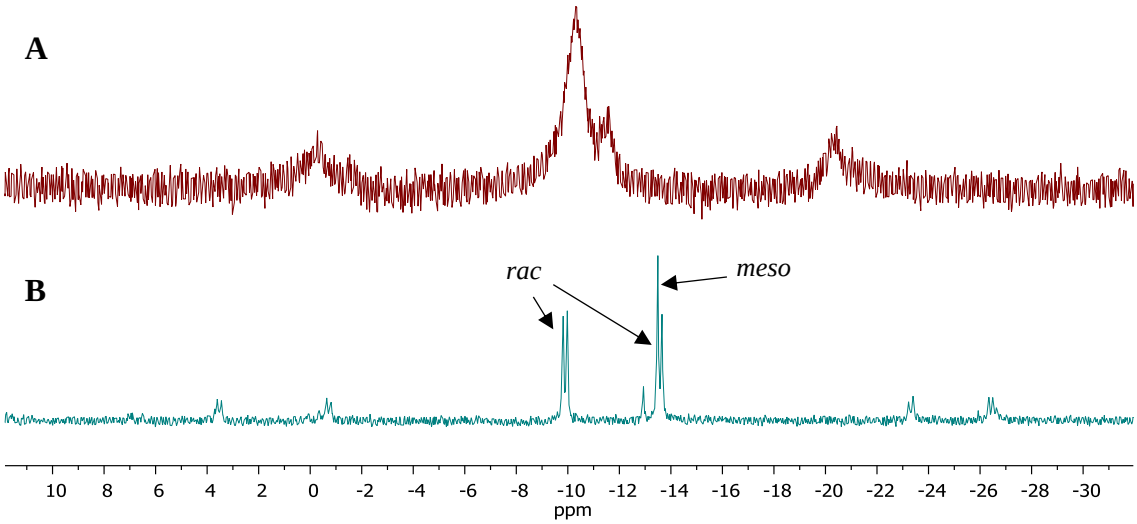

Figure 3.6: $^{31}P\{^{1}H\}$ NMR spectra of [Pt(CO)(**L6**)] at A) room temperature and B) −75 °C.

NMR spectrum at room temperature (δ_P = −10.3 and −11.5 ppm, Figure 3.6A). Low temperature $^{31}P\{^1H\}$ NMR spectroscopy studies showed that the signals resolve into the expected singlet and two doublets for the *meso* and *rac* isomers respectively (Figure 3.6B). It should be noted here that the proportion of the *rac* isomer is much higher than the *meso* isomer of [Pt(CO)(**L6**)]. This originates from the 1:2 diastereomeric mixture of *meso* and *rac* isomers of the ligand **L6** obtained from the ligand synthesis. From this we can also assign the major isomer in the diastereomeric mixture of **L6** to be the *rac* isomer.

3.2.4.1 Reaction of Dihydrogen with [Pt(CO)(L6)]/B(C_6F_5)$_3$

The *in situ* formation of [Pt(CO)(**L6**)] allowed for the study of small molecule activation by the [Pt(CO)(**L6**)]/B(C_6F_5)$_3$ Lewis pair. Addition of 1 equivalent of B(C_6F_5)$_3$ to [Pt(CO)(**L6**)] in d_5-PhCl did not lead to any obvious changes in appearance of the solution or by $^{31}P\{^1H\}$ NMR spectroscopy. When the solution was frozen there were no clear thermochromic effects seen unlike the analogous systems with **L1** and **L2** (see Section 2.4). Upon reaction with H_2 (1 bar, r.t.), an immediate colour change to pale orange (from bright orange) was seen which lightened to a pale yellow over time. After 5 h, the $^{31}P\{^1H\}$ NMR spectrum was very broad with signals observed around δ_P = 12 ppm. Analysis of the hydride region of the ^1H NMR spectrum indicated the formation of a binuclear platinum bridging hydride species at δ_H = −4.86 ppm and potentially the presence of a monohydride platinum complex due to the appearance of a signal resembling a doublet of doublets at δ_H = −3.58 ppm (Figure 3.7). Due to the complexity arising from the diastereoisomers it was difficult to confidently assign the structures of the activation products. The $^{11}B\{^1H\}$ NMR spectrum did show a sharp signal at δ_B = −27.6 ppm which has been previously identified as anion **2.7**. Further analysis of the reaction mixture would be necessary to propose the structures of the activation products and a possible activation pathway.

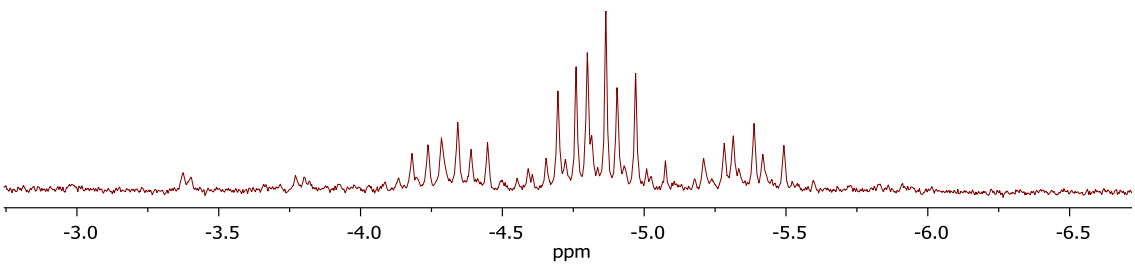

Figure 3.7: Hydride region of the *in situ* ^1H NMR spectrum of the reaction between [Pt(CO)(**L6**)]/B(C_6F_5)$_3$ and H_2 at room temperature after 5 h.

3.2.5 Synthesis of L7 and L8 and Coordination to Pt

The work presented in this section was started by Daniel Feivor, a visiting undergraduate summer student, under the supervision of the author. The work was repeated by the author and the data presented was collected by the author.

Until this point, the mechanisms of the small molecule activation reported in Chapter 2 remained to be elucidated. The use of an unsymmetrical diphosphine ligand was proposed to help identify possible mechanistic intermediates as it would be able to provide information about what is happening at the platinum centre relatively to the individual phosphorus centres. The synthesis of **L7** was attempted using commercially available 3,5-di-*tert*-butylcatechol (Scheme 3.9). It was hoped that the unsymmetrical phosphine formed would have distinct chemical shifts. Unfortunately, the solid isolated from the reaction only contained *ca*. 30% of what was suspected to be product which displayed signals at δ_P = 175.2 and 163.4 ppm in the $^{31}P\{^1H\}$ NMR spectrum. There were two other major peaks in the $^{31}P\{^1H\}$ NMR spectrum: the first at δ_P = 62.9 ppm, which is thought to be the hydrolysis product **2.3** (Section 2.2); the second signal at δ_P = 6.4 ppm was proposed to be the P(V) species **3.2** due to the observation of $^1J_{PH}$ coupling in the ^{31}P proton coupled NMR spectrum (Scheme 3.9). Ligand **L7** was not successfully isolated for use in coordination chemistry.

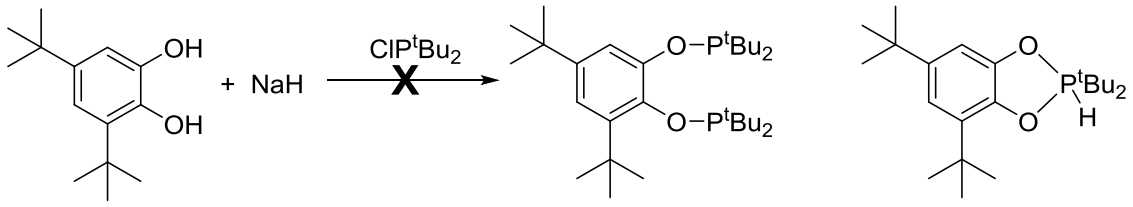

Scheme 3.9: Attempted formation of **L7** and possible by product **3.2**.

The unsymmetrical phosphinite ligand **L8** was synthesised successfully in an analogous reaction to the formation of **L2**; deprotonation of commercially available 4-*tert*-butylcatechol by sodium hydride followed by addition of di-*tert*-butylchlorophosphine (Scheme 3.10).

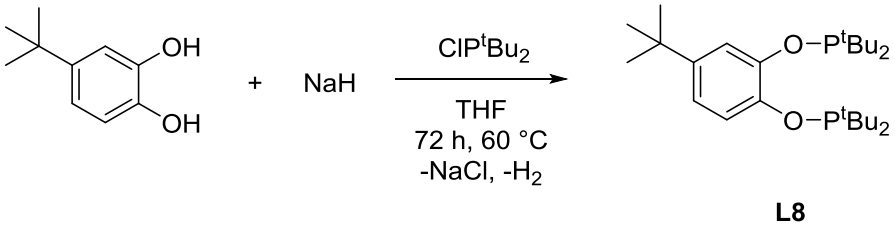

Scheme 3.10: Formation of **L8**.

The $^{31}P\{^{1}H\}$ NMR spectrum of **L8** displayed two signals for the inequivalent phosphines at δ_P = 151.9 and 151.4 ppm. The dichloroplatinum complex [$PtCl_2$(**L8**)] was synthesised by reaction of **L8** with [$PtCl_2$(COD)] and the molecular structure is shown in Figure 3.8. This structure also displays the unusual conformation of the 7-membered ring seen in the molecular structure analogous to [$PtCl_2$(**L2**)] (see Section 2.2.1). Again, variable temperature NMR spectroscopy studies concluded that this conformation does not persist in solution and is most likely an effect of crystal packing.

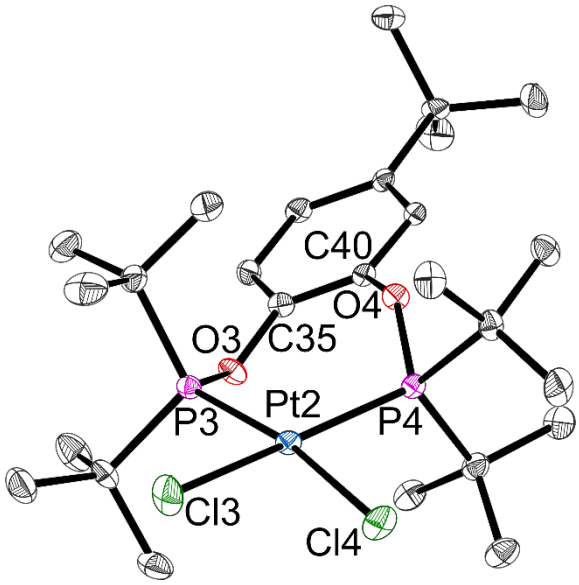

Figure 3.8: Crystal structure of [$PtCl_2$(**L8**)]. Thermal ellipsoids at 50%. Hydrogen atoms and solvent molecules omitted for clarity. Two independent molecules are observed in the asymmetric unit and only differ by the orientation of the Ar-CH_3 and one molecule has been omitted for clarity. Selected bond lengths (Å) and angles (°): Pt2-P3 2.2458(13); Pt2-P4 2.2431(13); Pt2-Cl3 2.3570(14); Pt2-Cl4 (2.3635(13); P3-O3 1.621(3); P4-O4 1.624(4); P3-Pt2-Cl3 89.99(5); P3-Pt2-P4 96.66(5); P4-Pt2-Cl489.99(5); Cl3-Pt2-Cl4 84.09(5); P3-O3-C35 136.8(4); P4-O4-C40 138.9(4).

Figure 3.9 shows the $^{31}P\{^{1}H\}$ NMR spectrum for [$PtCl_2$(**L8**)]. The two signals for the phosphorus atoms are well resolved at δ_P = 135.8 and 135.5 ppm ($^{2}J_{PP}$ = 5.0 Hz and $^{1}J_{PPt}$ = 4145 and 4137 Hz respectively). Although the *tert*-butyl group on the aryl ring is quite remote from the phosphorus centres, it has sufficient influence to produce distinct signals in the $^{31}P\{^{1}H\}$ NMR spectrum for [$PtCl_2$(**L8**)] and the coupling between the two phosphorus centres is well resolved. This makes ligand **L8** an ideal candidate for the formation of the Pt(0) Lewis base in the hope of gaining more information about the mechanism of formation of the activation products. However, time did not permit further exploration of this ligand.

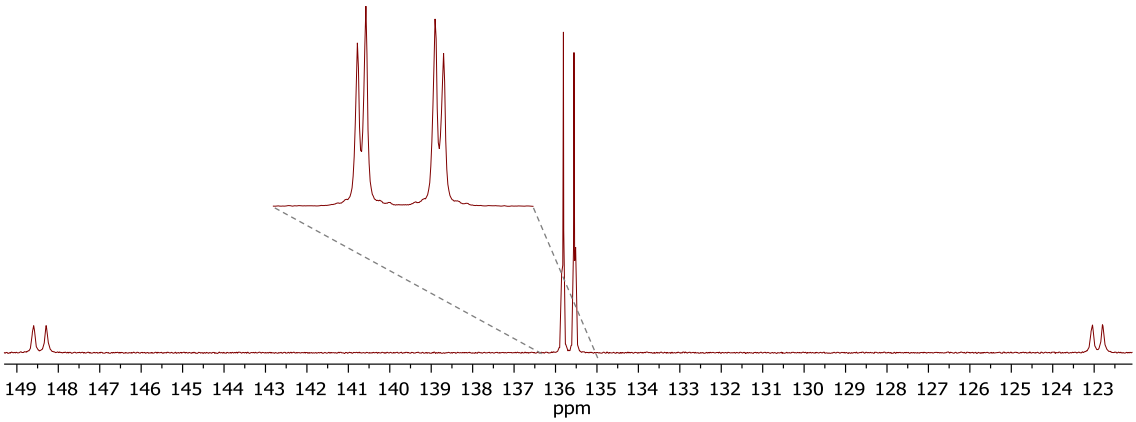

Figure 3.9: $^{31}P\{^{1}H\}$ NMR spectrum of [$PtCl_2$(**L8**)] with an expansion of the main signals to show the observed roofing.

3.3 Variation of the Lewis Acid

All of the activation experiments described in this section were carried out with one equivalent of platinum complex and one equivalent of a Lewis acid in chlorobenzene at room temperature in a Youngs NMR tube unless stated otherwise. Full experimental details are given in Chapter 5.

The work described in Chapter 2 and Chapter 3 so far has only employed B(C_6F_5)$_3$ as the Lewis acid in the cooperative Lewis pair system. Now that it has been shown that both [Pt(CO)(**L1**)] and [Pt(CO)(**L2**)] can be used as a Lewis base in cooperative Lewis pair small molecule activation, it was of interest to explore the scope of Lewis acids which could be used in the system.

3.3.1 Triphenylborane

Substitution of the fluorine substituents on the aromatic rings of B(C_6F_5)$_3$ for hydrogen significantly decreases the Lewis acidity of the borane centre. This was shown by Bristovsek *et al.* who utilised the Gutmann-Beckett measure of Lewis acidity.[12–14]

A 1:1 mixture of [Pt(CO)(**L1**)] and BPh_3 was dissolved in chlorobenzene at room temperature. There was no evidence from analysis of the $^{31}P\{^{1}H\}$ and $^{11}B\{^{1}H\}$ NMR spectra (either a chemical shift difference or broadening of the signals) that there was an interaction between the Lewis acid and Lewis base components. The reaction of the Lewis pair [Pt(CO)(**L1**)]/BPh_3 with H_2 did not result in a significant colour change of the solution. After 1 h, the signals for [Pt(CO)(**L1**)] in the $^{31}P\{^{1}H\}$ NMR spectrum had

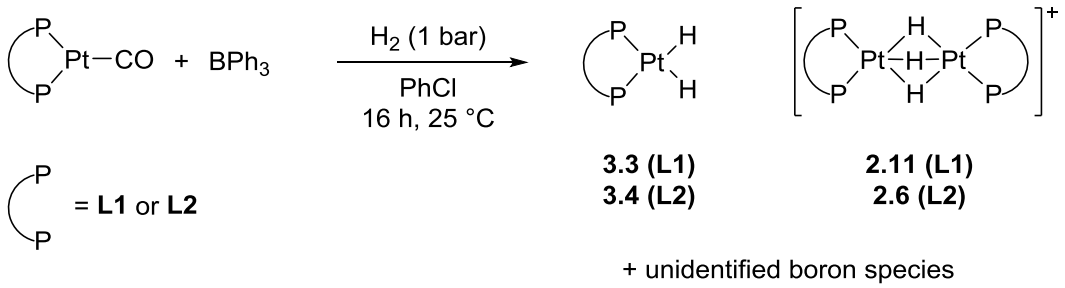

Scheme 3.11: Reaction of [Pt(CO)(**L**)]/BPh_3 with H_2.

significantly broadened ($w_{1/2}$ = 160 Hz) and there was a clear signal for the *cis*-dihydride **3.3** (Scheme 3.11).

After the reaction mixture was left stirring overnight, only *ca*. 20% conversion of [Pt(CO)(**L1**)] was observed by $^{31}P\{^1H\}$ NMR spectroscopy. The two other phosphorus-containing species in solution were **3.3** and trihydride binuclear species **2.11**. This was confirmed by the presence of the corresponding hydride signals in the ^1H NMR spectrum (δ_H = −3.13 (**3.3**) and −7.48 (**2.11**)). The major species in the $^{11}B\{^1H\}$ NMR spectrum was free BPh_3 (δ_B = 64.2 ppm) and there was a second signal at δ_B = 0.7 ppm. The expected anion $[H\text{-}BPh_3]^-$ give a sharp signal in the $^{11}B\{^1H\}$ NMR spectrum at δ_B = −6.9 ppm but this was not seen for the reaction mixture of [Pt(CO)(**L1**)]/BPh_3 with H_2.[15] The only boron containing species observed by ESI-MS in the negative ion spectrum was an anion with *m*/*z* = 273.2 which was deduced to be the methoxy adduct of BPh_3 formed during the acquisition of the mass spectrum which was run in a PhCl/MeOH mixture.

Combination of [Pt(CO)(**L2**)] and BPh_3 in chlorobenzene at room temperature resulted in no change in the NMR spectrum of the individual components. Reaction of [Pt(CO)(**L2**)]/BPh_3 with H_2 occurred in a similar manner to [Pt(CO)(**L1**)]/BPh_3. The main differences observed was that the formation of trihydride species occurred within 1 h (*vs* 16 h for **L1**) and there was much greater broadening of the [Pt(CO)(**L2**)] signal in the $^{31}P\{^1H\}$ NMR spectrum ($w_{1/2}$ = 641 Hz, Figure 3.10A). The origin of the broadening is proposed to be due to association of a dihydrogen molecule with the Pt(0) complex. The stronger π-acceptor **L2**, in comparison to **L1**, may lead to a stronger association with the dihydrogen molecule, which has been shown to be fluxional on the NMR timescale at room temperature. Low temperature NMR spectroscopy studies would need to be

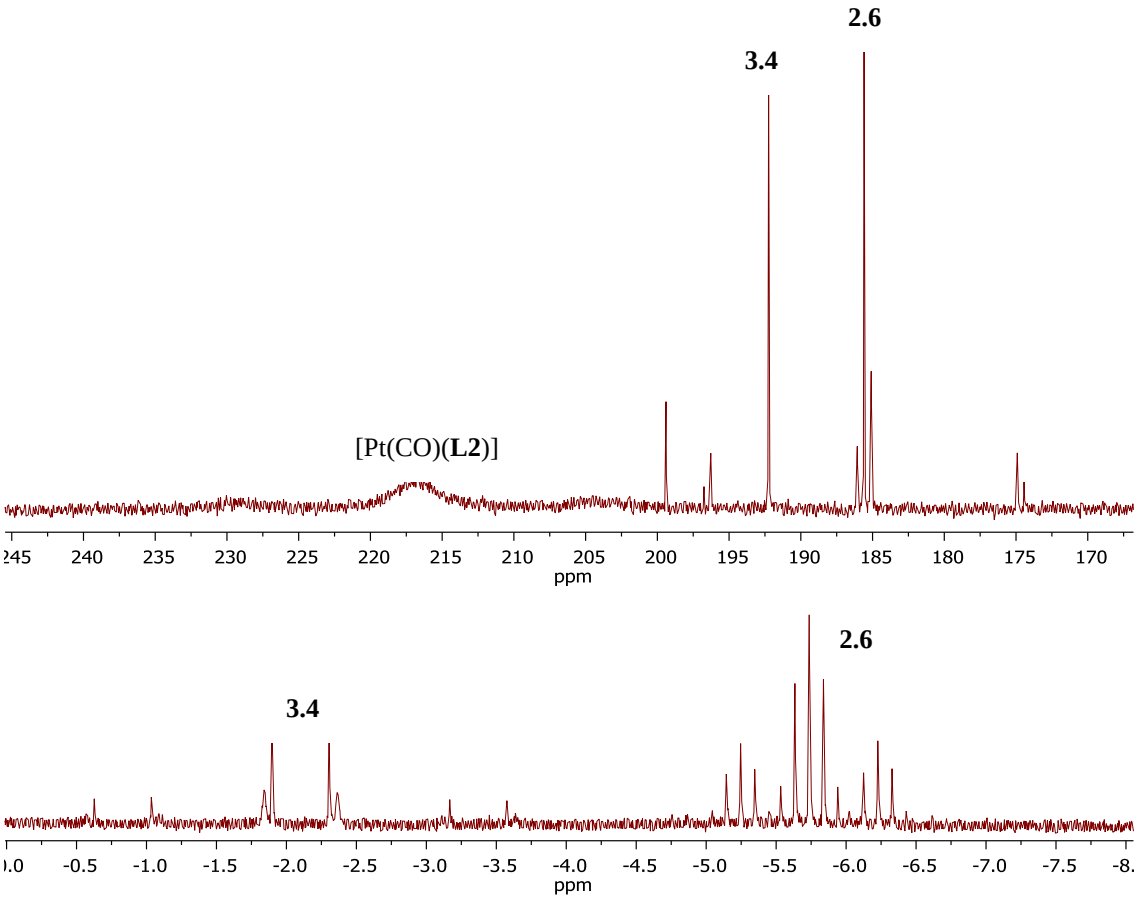

Figure 3.10: A) $^{31}P\{^1H\}$ NMR spectrum and B) hydride region of the ^1H NMR spectrum of the reaction of [Pt(CO)(**L2**)]/BPh_3 with H_2 at room temperature in chlorobenzene after 16 h.

carried out to confirm an interaction between the dihydrogen and the Pt(0) complex. [Pt(CO)(**L2**)] reached a maximum conversion to **3.3** and **2.6** of *ca*. 30% even after 5 d.

Reaction of [Pt(CO)(**L**)]/BPh_3 (**L = L1** or **L2**) with ethene did not lead to any activation products. The only reactivity observed was the quantitative exchange of the CO ligand in [Pt(CO)(**L**)] for ethene to form [Pt(C_2H_4)(**L**)].

3.3.2 Triphenylborate

The incorporation of an oxygen atom between the boron and the carbon substituent of the Lewis acid increases the Lewis acidity of the boron centre. $B(OPh)_3$ is more Lewis acidic than BPh_3 but is less Lewis acidic than $B(C_6F_5)_3$ which makes it a good intermediate candidate for study of the Pt(0)/B Lewis pair system.[12]

Reaction of a combination of [Pt(CO)(**L1**)] and $B(OPh)_3$ in chlorobenzene at room temperature resulted in a bright orange solution which displayed no changes in the NMR spectrum of the individual starting reactants. Reaction of [Pt(CO)(**L1**)]/$B(OPh)_3$ with H_2

at room temperature led to the formation of *cis*-dihydride **3.3** and trihydride species **2.11**, with full conversion of [Pt(CO)(**L1**)] after 16 h (Scheme 3.12). This was confirmed by analysis of the $^{31}P\{^{1}H\}$ and ^{1}H NMR spectra. This is in contrast to when BPh_3 was used as the Lewis acid where only *ca*. 20% conversion of [Pt(CO)(**L1**)] was seen. The $^{11}B\{^{1}H\}$ NMR spectrum still showed the presence of free $B(OPh)_3$ and the only other signal was a sharp singlet at δ_B = 2.4 ppm. The identity of this species was anticipated to be the activation product [H-B(OPh)$_3$], but the coupled ^{11}B NMR spectrum did not exhibit additional splitting. The 4-coordinate species in solution was confirmed by mass spectrometry to be anion **3.5** (Scheme 3.12).[16] This was unexpected and is proposed to form through ligand redistribution of boron species in solution.[17]

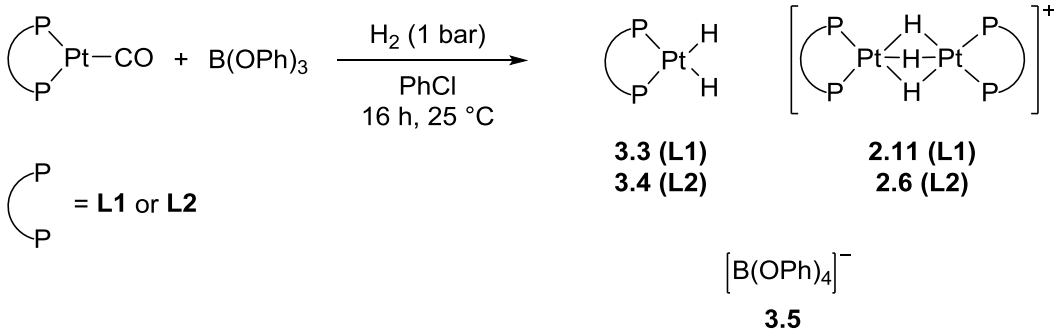

Scheme 3.12: Reaction of [Pt(CO)(**L**)]/B(OPh)$_3$ with H_2.

A slight broadening of the $^{31}P\{^{1}H\}$ NMR signal for [Pt(CO)(**L2**)] ($w_{1/2}$ = 30 Hz) was seen upon combination with $B(OPh)_3$ in chlorobenzene at room temperature. The reactivity was similar to that seen for [Pt(CO)(**L1**)]/B(OPh)$_3$ but occured at a much faster rate where the full conversion of [Pt(CO)(**L2**)] to **2.6** is observed within 3 h. *Cis*-dihydride species **3.4** was observed within the initial stages of the reaction suggesting **3.4** converts to **2.6** (see Section 3.3.6). The only species identifiable in the $^{11}B\{^{1}H\}$ NMR spectrum is free $B(OPh)_3$ and anion **3.5**.

It should be noted that analysis of the $^{31}P\{^{1}H\}$ NMR spectra of the reaction mixtures after 5 d shows the formation of new platinum containing species (Figure 3.11A/B). These signals correspond to a new hydride signal which lies underneath the trihydride signal in the ^{1}H NMR (Figure 3.11C/D). The structures of these species have not been elucidated from the spectroscopic data collected.

Reaction of [Pt(CO)(**L**)]/BPh_3 (**L = L1** or **L2**) with ethene disappointingly did not lead to any activation products. The only reactivity observed was the quantitative exchange of the CO ligand in [Pt(CO)(**L**)] for ethene to form [Pt(C_2H_4)(**L**)] which is the same as

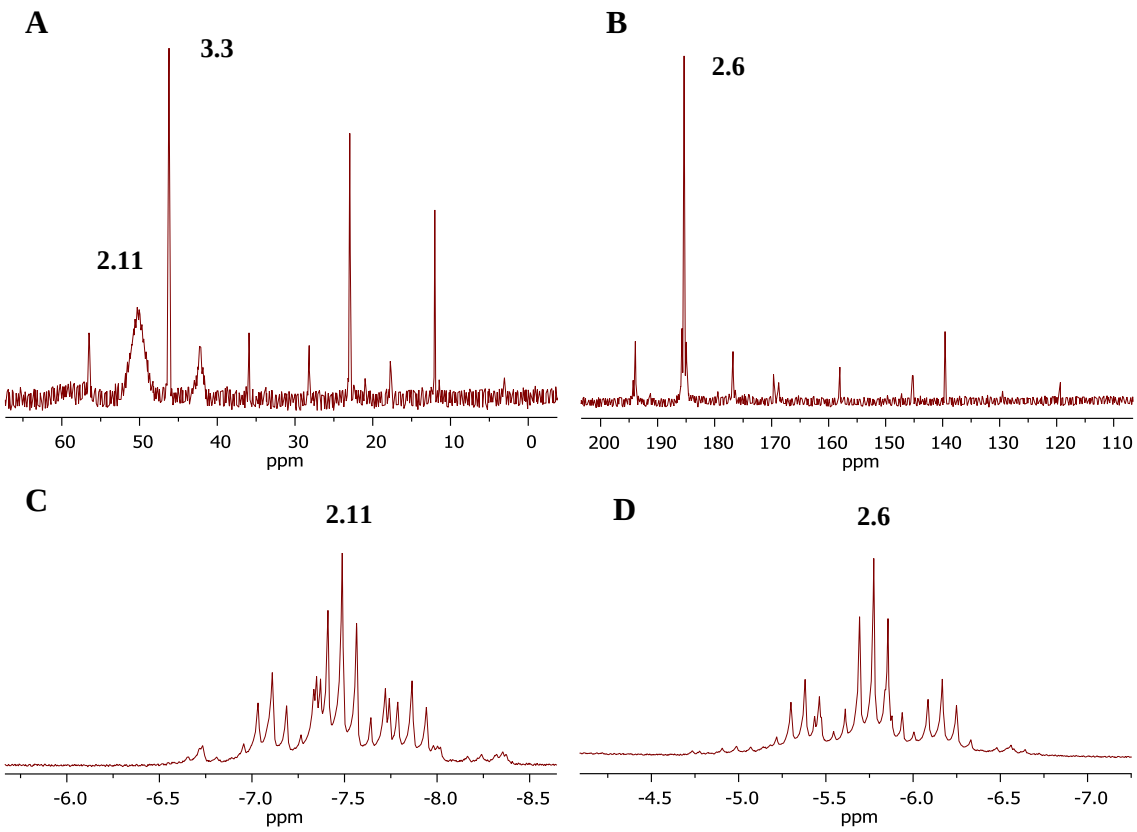

Figure 3.11: NMR spectrum of [Pt(CO)(**L**)]/BPh$_3$ with H$_2$ after 5 d at room temperature. A) ^{31}P{^{1}H} NMR spectrum when **L** = **L1**; B) ^{31}P{^{1}H} NMR spectrum when **L** = **L2**; C) Hydride region of ^{1}H NMR spectrum when **L** = **L1**; D) Hydride region of ^{1}H NMR spectrum when **L** = **L2**.

what was seen with BPh$_3$. Triphenylborate appears to not possess the correct stereoelectronic properties to activate ethene in a similar way to B(C$_6$F$_5$)$_3$.

3.3.3 Tris(3,4,5-trifluorophenyl)borane, B(C$_6$H$_2$F$_3$)$_3$

The use of fluorinated phenyl boranes which are devoid of substitution at the *o*-position have shown some striking reactivity differences in catalytic processes such as the hydroboration of alkenes and imines.[18,19] The successful imine hydroboration with pinacolborane showed the advantages of BAr$^F_3$ over B(C$_6$F$_5$)$_3$. This was rationalised by the reduced steric hinderance around the boron centre in BAr$^F_3$ but similar Lewis acidity to B(C$_6$F$_5$)$_3$.[18,20] B(C$_6$H$_2$F$_3$)$_3$ was also tested for catalytic imine hydroboration and exhibited excellent reactivity with full conversion after just 4 h. This was proposed to proceed *via* initial coordination of B(C$_6$H$_2$F$_3$)$_3$ with the imine to form a Lewis adduct which lowers the LUMO of the imine for attack by pinacolborane. B(C$_6$H$_2$F$_3$)$_3$ has not yet been reported for use in FLP chemistry. It was of interest to investigate whether a lack of substitution at the *ortho* position of the phenyl ring would influence small molecule activation in the Pt(0)/B cooperative Lewis pair system.

[Pt(CO)(**L1**)] and B($C_6H_2F_3$)$_3$ were combined in chlorobenzene at room temperature to produce an orange solution. No change in chemical shift or broadening was observed in the $^{31}P\{^1H\}$ or $^{11}B\{^1H\}$ NMR spectra. When freezing the solution in liquid nitrogen, a colour change from orange to bright red was observed. As seen with B(C_6F_5)$_3$ (see Section 2.4), this thermochromic effect could indicate some interaction between [Pt(CO)(**L1**)] and B($C_6H_2F_3$)$_3$. The same observations, in the $^{31}P\{^1H\}$ and $^{11}B\{^1H\}$ NMR spectra and in frozen solution, were made for the cooperative Lewis pair [Pt(CO)(**L2**)]/B($C_6H_2F_3$)$_3$.

Reaction of [Pt(CO)(**L1**)]/B($C_6H_2F_3$)$_3$ with H_2 in a Youngs NMR tube did not lead to a colour change initially but a gradual change to pale yellow was observed over 16 h. The *in situ* $^{31}P\{^1H\}$ NMR spectrum taken after 10 min showed *ca*. 25% conversion of [Pt(CO)(**L1**)] to **2.9**, **2.11** and a minor amount of **3.3** (Figure 3.12). The corresponding signals in the ^1H NMR spectrum were also seen.

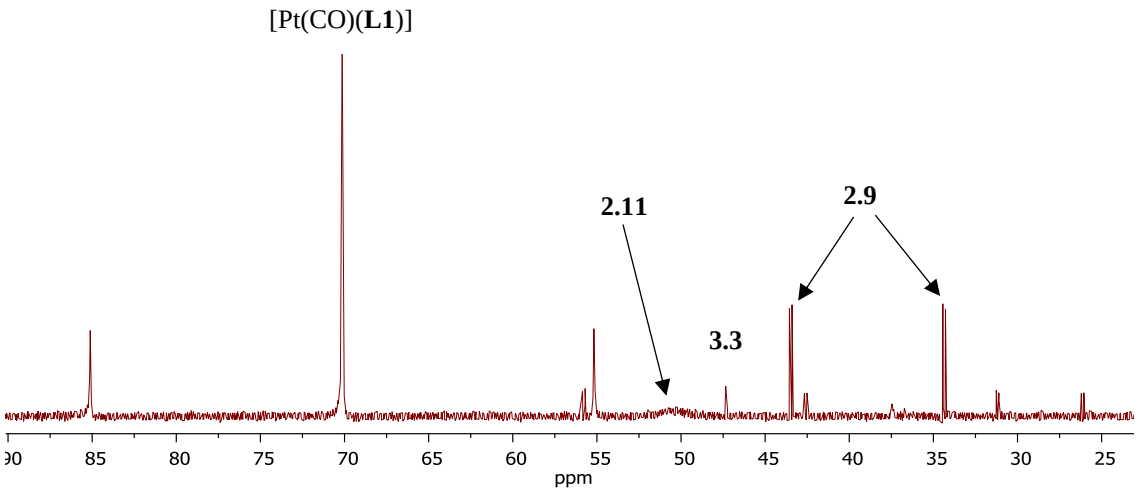

Figure 3.12: $^{31}P\{^1H\}$ NMR spectrum of the reaction of [Pt(CO)(**L1**)]/B(C6H_2F_3)$_3$ with H_2 at room temperature after 10 min.

The $^{11}B\{^1H\}$ NMR spectrum displayed a signal for unreacted B($C_2H_2F_3$)$_3$ (δ_B = 63.1 ppm), one broad signal at δ_B = −0.3 ppm and two minor sharp signals at δ_B = −8.4 and −9.5 ppm. After 8 h, full conversion of the starting material was observed by both $^{31}P\{^1H\}$ and $^{11}B\{^1H\}$ NMR spectroscopy. The only products in the $^{31}P\{^1H\}$ NMR spectrum were now **2.9** and **2.11**, which was confirmed by analysis of the ^1H NMR spectrum and by mass spectrometry. The identity of the boron-containing species in solution was more elusive (Figure 3.13). The major species in the $^{11}B\{^1H\}$ NMR

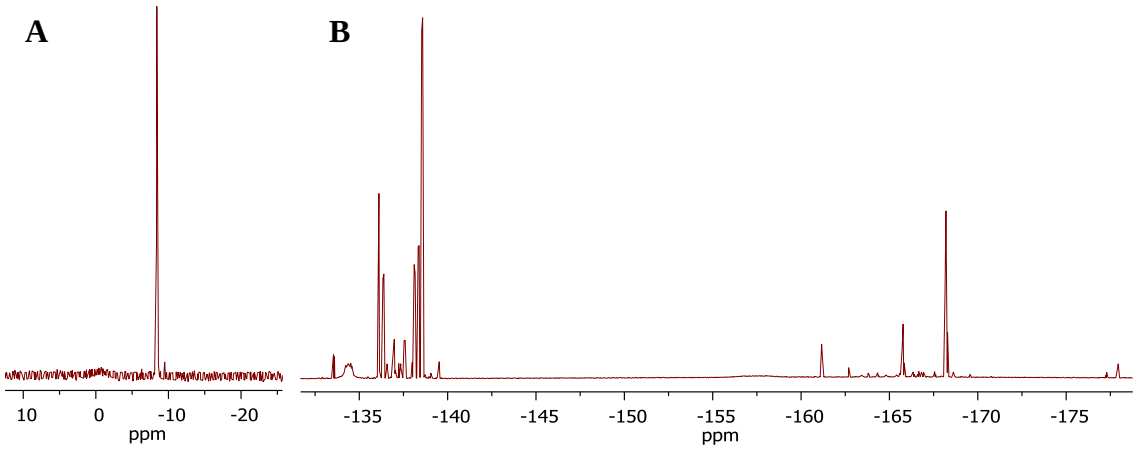

Figure 3.13: $^{11}B\{^1H\}$ NMR (A) and $^{19}F\{^1H\}$ NMR (B) spectra of the reaction of [Pt(CO)(**L1**)]/B($C_6H_2F_3$)$_3$ with H_2 after 8 h.

spectrum was a 4-coordinate species at δ_B = −8.4 ppm (Figure 3.13A). The two other detectable species are a 3-cordinate species at δ_B = –0.3 ppm and a 4-coordinate species at δ_B = −9.5 ppm. The $^{19}F\{^1H\}$ NMR spectrum was complicated with several doublets between δ_F = −133.1 and −140.2 ppm which correspond to *meta*-substituted F and several sets of triplets between δ_F = −160.5 and −178.3 ppm which correspond to *para*-substituted F (Figure 3.13B). No further reactivity was observed after 2 d.

Interestingly, reaction of [Pt(CO)(**L2**)]/B(C_6F_5)$_3$ with H_2 led to almost full conversion to **2.6** as the sole product within 10 min according to the $^{31}P\{^1H\}$ NMR spectrum. After 1 h, full conversion of [Pt(CO)(**L2**)] to **2.6** was observed. The only identifiable species in the $^{11}B\{^1H\}$ NMR spectrum was a 4-coordinate species at δ_B = −8.4 ppm. The ^{19}F NMR spectrum was less ambiguous than for [Pt(CO)(**L1**)]/B($C_6H_2F_3$)$_3$ (Figure 3.14). There are two signals in a 1:3 ratio at δ_F = −136.0 and −138.5 ppm respectively (assigned to *meta*-F) with corresponding signals at δ_F = −165.7 and 168.1 ppm (assigned to *para*-F). There were other minor species apparent in the ^{19}F NMR spectrum and two very broad signals at δ_F = −134.8 and −157.6 ppm which have not been assigned. Curiously, after the reaction was left for 2 d at room temperature, a very small amount of **2.4** could be observed in the ^1H NMR spectrum.

The negative ion ESI mass spectrum (in a PhCl/MeOH mixture) displayed two signals which featured the distinctive isotope pattern for boron. The first at *m*/*z* = 435.1 was assigned to a MeOH adduct of B($C_6H_2F_3$)$_3$ which can be accounted for by a very small amount of unreacted B($C_6H_2F_3$)$_3$ in the reaction mixture. The second at *m*/*z* = 565.1 is

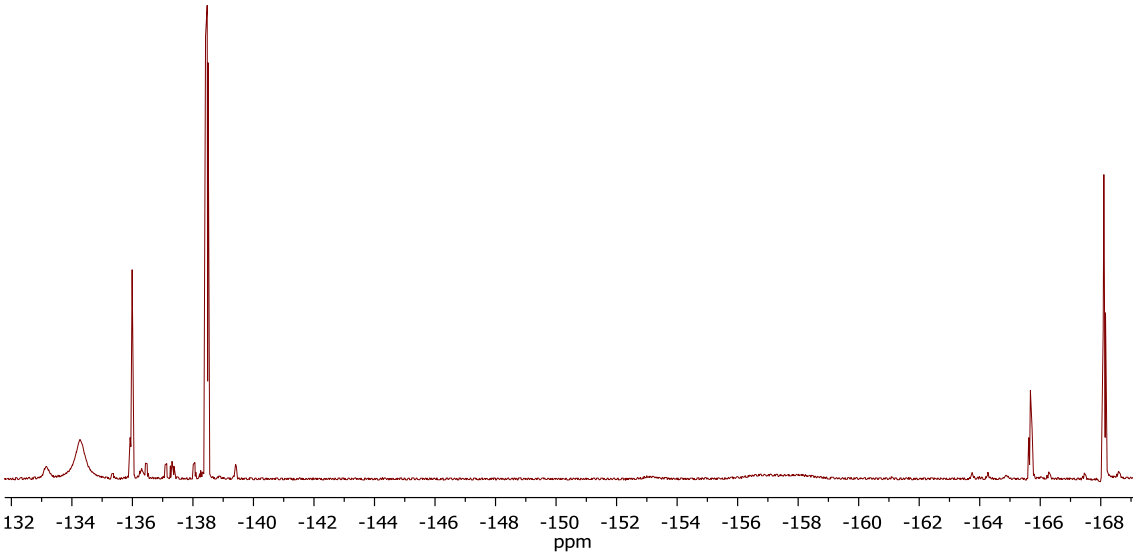

Figure 3.14: ^{19}F NMR spectrum of the reaction between [Pt(CO)(**L2**)]/B($C_6H_2F_3$)$_3$ with H_2 after 1 h.

yet to be identified but does not match any of the expected activation products or species which could occur from ligand redistribution (as seen with other boranes in Section 3.3.2 and 3.3.3). Further analysis needs to be carried out to identify the anion in the reaction of [Pt(CO)(**L2**)]/B($C_6H_2F_3$)$_3$ with H_2.

[Pt(CO)(**L**)]/B($C_6H_2F_3$)$_3$ (**L** = **L1** or **L2**) was subjected to one bar of ethene at room temperature. The orange solution changed to yellow and pale pink for **L1** and **L2** respectively. These colour changes are reminiscent of those seen when forming [Pt(C_2H_4)(**L**)] and the formation of this species was confirmed by ^{31}P{^{1}H} NMR spectroscopy.‡ No further reactivity was seen for either system.

Addition of an excess of phenylacetylene to [Pt(CO)(**L1**)]/B($C_6H_2F_3$)$_3$ in chlorobenzene led to the formation of an intense bright orange solution. After 16 h, signals for **2.9** could be seen in the ^{31}P{^{1}H} NMR spectrum with the corresponding hydride signal in the ^{1}H NMR spectrum. However, [Pt(CO)(**L1**)] was still the major species in solution (> 90%). The ^{11}B{^{1}H} NMR spectrum showed a broad signal attributed to unreacted B($C_6H_2F_3$)$_3$ and a single sharp peak at δ_B = −7.2 ppm which did not display any splitting when the spectrum was coupled to ^{1}H. This product is proposed to be from the reaction of B($C_6H_2F_3$)$_3$ with PhCCH analogous to that seen for B(C_6F_5)$_3$ (see Section 2.6.1).[21]

‡ Minor amounts of [Pt(H)(CO)(**L**)] were also seen in the ^{31}P{^{1}H} NMR spectrum. This is thought to originate from activation of an impurity in the batch of ethylene used as this was not seen when a different batch was used. The impurity was not identified.

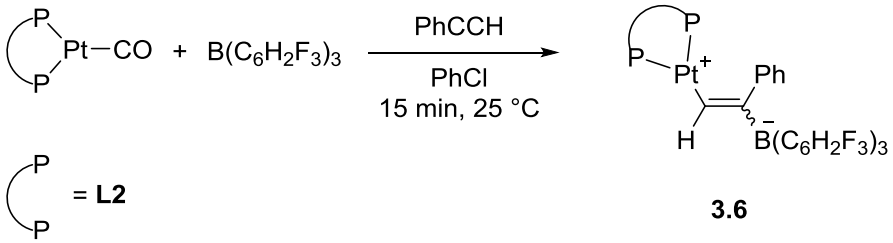

Scheme 3.13: Proposed activation product **3.6** from the reaction of [Pt(CO)(**L2**)]/B(C$_6$H$_2$F$_3$)$_3$ with PhCCH.

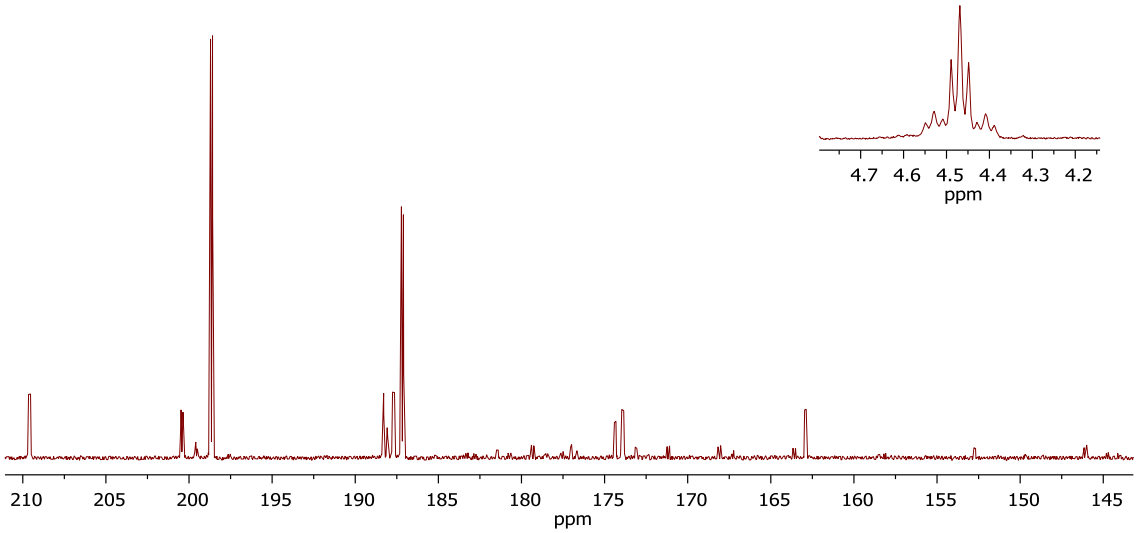

Figure 3.15: $^{31}P\{^1H\}$ NMR spectrum of the reaction of [Pt(CO)(**L2**)]/B(C$_6$H$_2$F$_3$)$_3$ with PhCCH. **Inset:** Alkyl region of ^1H NMR spectrum of the reaction of [Pt(CO)(**L2**)]/B(C$_6$H$_2$F$_3$)$_3$ with PhCCH.

A colour change from orange to deep red was observed upon addition of phenylacetylene to [Pt(CO)(**L2**)]/B(C$_6$H$_2$F$_3$)$_3$. After 10 min, $^{31}P\{^1H\}$ NMR spectroscopy confirmed the full conversion of [Pt(CO)(**L2**)] to several new species (Figure 3.15). The main species displays two doublets at δ_P = 199.1 and 187.6 ppm ($^1J_{PPt}$ = 3550 and 4295 Hz respectively) with a $^2J_{PP}$ of 19 Hz. In the ^1H NMR spectrum, a new signal in the alkyl region is seen at δ_H = 4.33 ppm (Figure 3.15 inset). This signal appears to display platinum satellites and the multiplicity suggests that it could be coupling to two phosphorus atoms. The $^{19}F\{^1H\}$ NMR spectrum is extremely complex and the $^{11}B\{^1H\}$ NMR is broad but two sharp signals can be identified at δ_B = −7.3 and −12.9 ppm. Compiling this NMR evidence together, the major activation product of this reaction is tentatively proposed to be zwitterion **3.6** (Scheme 3.13). This product could result from 1,2-addition of the [Pt(CO)(**L2**)]/B(C$_6$H$_2$F$_3$)$_3$ cooperative Lewis pair to PhCCH. This is one of two activation pathways observed for cooperative Lewis pairs (see Scheme 2.12 in Section 2.7). A small amount of **2.4** can also be identified in the $^{31}P\{^1H\}$ and ^1H NMR spectrum.

3.3.4 [Zr(Cp*)$_2$(OMes)][B(C$_6$F$_5$)$_4$]

Previous research in the Wass group had focused on the development of a zirconocene Lewis acid for use in cooperative Lewis pair small molecule activation and catalysis (see Section 1.4 for a more detailed review of this work).[22–26] The initial work was based on an intramolecular system where the Lewis base was a tethered phosphine. This cooperative Lewis pair was shown to activate a variety of small molecules and was applied in the catalytic dehydrogenation of amine-boranes. Further research led to the development of an intermolecular system which showed a wide range of small molecule activation and was applied to the catalytic dehydrocoupling of amine-boranes. The zirconocene Lewis acid fragment was also shown to catalyse imine hydrogenation *via* an FLP-like mechanism in an analogous manner to B(C$_6$F$_5$)$_3$.

[Zr(Cp*$_2$)(OMes)][B(C$_6$F$_5$)$_4$] (**3.7**) was chosen as the Lewis acid to test in the cooperative Lewis pair system with [Pt(CO)(**L**)] (**L** = **L1** or **L2**, Scheme 3.14). Attempts to isolate **3.7** often led to degradation despite being successfully isolated previously.[24] It is known that the isolated products can be very sensitive and difficult to handle; therefore **3.7** was used *in situ* from the reaction mixture. This meant that the by-product of the first methyl abstraction of [Zr(Cp*)$_2$(Me)$_2$], Ph$_3$CMe, was present in solution but it was thought this would not interfere with the desired small molecule activation. All activation experiments were carried out with the ^{13}C-labelled platinum Lewis base complexes [Pt(^{13}CO)(**L1**)] and [Pt(^{13}CO)(**L2**)] to aid identification of any activation products.

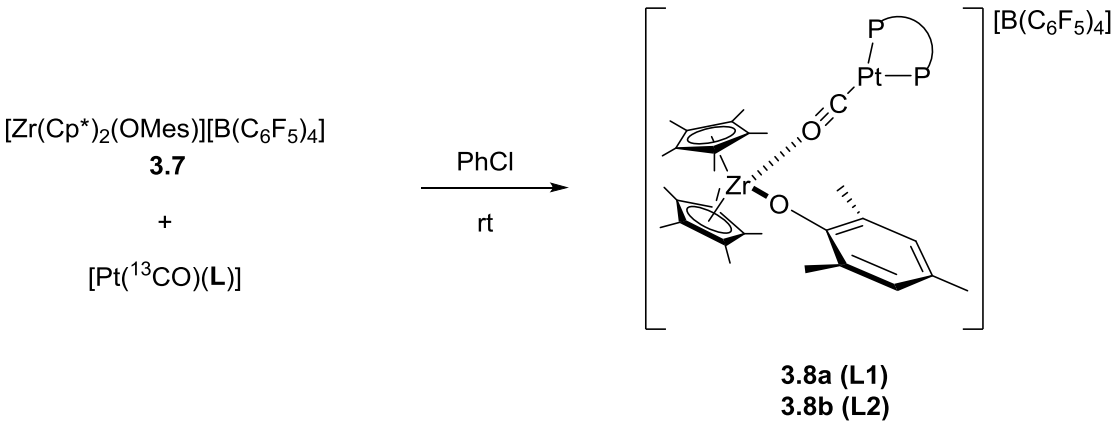

Scheme 3.14: Proposed structure **3.8** of complex formed upon combination of [Pt(CO)(**L**)] and **3.7**.

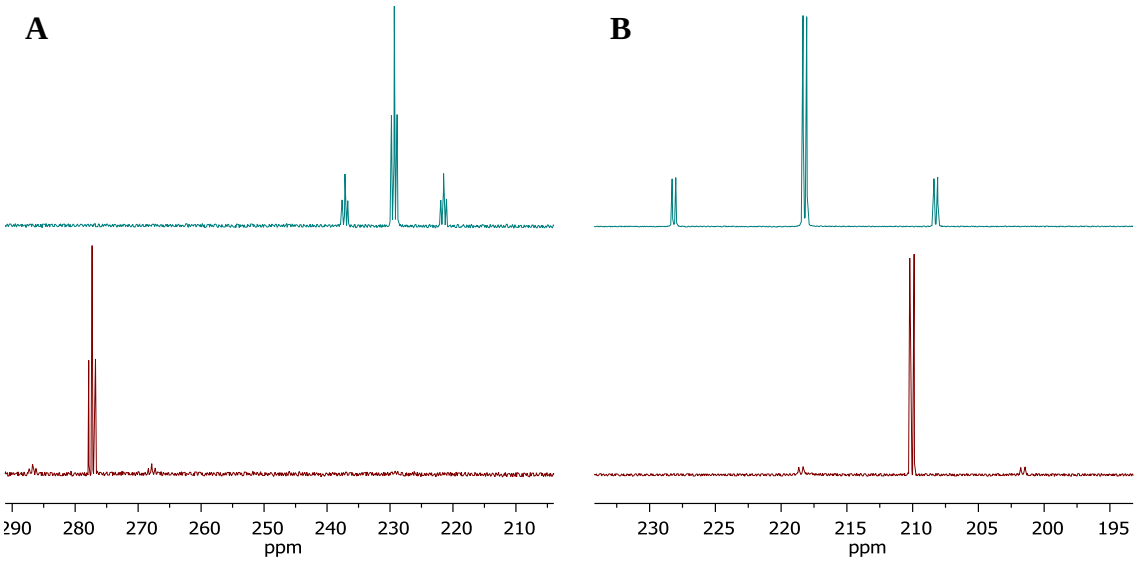

Figure 3.16: A) $^{13}C\{^1H\}$ and B) $^{31}P\{^1H\}$ NMR spectra of [Pt(^{13}CO)(**L2**)] before (top) and after (bottom) combination with **3.7** in chlorobenzene at room temperature.

Upon combination of **3.7** to [Pt(^{13}CO)(**L1**)] in chlorobenzene at room temperature, the intense red colour of **3.7** was quenched to give an orange solution. The $^{31}P\{^1H\}$ NMR signal shifted downfield by 3.7 ppm (70.2 to 66.4 ppm) and the $^1J_{PPt}$ coupling decreased by over 500 Hz (3680 to 3125 Hz). A significant downfield chemical shift difference was seen in the $^{13}C\{^1H\}$ NMR signal for the ^{13}CO ligand (228.7 to 270.8 ppm) and there was increase in $^1J_{CPt}$ (2100 to 2510 Hz). Very similar observations were made when [Pt(^{13}CO)(**L2**)] was combined with *in situ* formed **3.7** in chlorobenzene at room temperature. The $^{13}C\{^1H\}$ and $^{31}P\{^1H\}$ NMR spectra of the signals corresponding to [Pt(^{13}CO)(**L2**)] before and after the combination with **3.7** are shown in Figure 3.16. Due to the oxophilic nature of the zirconium centre, it is proposed that [Pt(^{13}CO)(**L**)] coordinates to the zirconium centre by the oxygen of the CO ligand (Scheme 3.14). Two signals in the ^{1}H NMR for the *o*-methyl groups of the mesityl ligand indicate the zirconocene complex had become unsymmetrical.

[Pt(^{13}CO)(**L1**)]/**3.7** was treated with H_2 (1 bar) at room temperature. After 2 h, the hydride region of the ^{1}H NMR showed the presence of *cis*-dihydride **3.3** and trihydride **2.11**. After 16 h, the only hydride species was **2.11** but the major species in solution was still **3.8a**. No further reactivity was observed after 5 d at room temperature. The analogous reaction with [Pt(^{13}CO)(**L2**)]/**3.7** showed similar results to that observed previously with other Lewis acids such as BPh_3 and $B(OPh)_3$. The ^{1}H NMR spectrum showed the trihydride species **2.6** as the only platinum-hydride species in solution after 2 h. *Cis*-dihydride **3.4** was not detected by NMR spectroscopy but the evidence suggests

that **2.6** is formed from the intermediary **3.4** (see Section 3.3.6). Again, the main phosphorus-containing species in solution was **3.8b** and the composition of the mixture did not change after 5 d at room temperature. It was unclear what the fate of the zirconocene component was. If **3.7** had been protonated, a signal at *ca.* δ_H = 5.60 ppm was expected in the ^{1}H NMR spectrum but no signal was seen around this chemical shift.

[Pt(^{13}CO)(**L**)]/**3.7** did not show any activation chemistry when treated with ethene (1 bar, room temperature) and the only reactivity observed was the formation of [Pt(C_2H_4)(**L**)]. [Pt(^{13}CO)(**L**)]/**3.7** also did not show any reactivity with phenylacetylene. This suggests that when [Pt(^{13}CO)(**L**)] is combined with **3.7**, a strong interaction between the Lewis acidic and Lewis basic components (potentially in the manner shown in proposed structure **3.8**, Scheme 3.14) is preventing further reactivity with small molecules.

3.3.5 Aluminium Lewis Acids

The initial work on small molecule activation by FLPs focussed on P/B systems.[27] The scope was quickly expanded to involve several other main group elements as the Lewis centres including aluminium as the Lewis acid. The intermolecular systems first employed the aluminium analogue of B(C_6F_5)$_3$, Al(C_6F_5)$_3$. This was found to successfully activate alkynes, alkenes and CO_2, although some of the products were more unstable than the boron counterparts.[28–31] It has also been shown that simple aluminium halides are capable of activating ethylene with $PMes_3$ although a second equivalent of AlX_3 was necessary to stabilise the activation product.[28] Aluminium halides have also shown reactivity in the reduction of CO_2 to CO.[31]

The preparation of Al(C_6F_5)$_3$, either solvated[32,33] or unsolvated,[34] has been reported previously. Unfortunately, in our hands attempts at synthesising Al(C_6F_5)$_3$ by the reported method resulted in the formation of an intractable oil. $AlCl_3$ has been reported to have comparable Lewis acidity to B(C_6F_5)$_3$ and has shown success in small molecule activation as part of an FLP.[28,31,35]

Combination of [Pt(CO)(**L1**)] and $AlCl_3$ led to significant broadening in the ^{31}P{^{1}H} NMR spectrum but no difference in chemical shift ($w_{1/2}$ = 189 Hz). Reaction of [Pt(CO)(**L1**)]/$AlCl_3$ with H_2 at room temperature in chlorobenzene led to full conversion of the starting material to **2.9** and **2.11** (*ca.* 4:1 ratio respectively, Scheme 3.15). The ^{27}Al{^{1}H} NMR spectrum showed one sharp signal at δ_{Al} = 97.1 ppm which indicates the

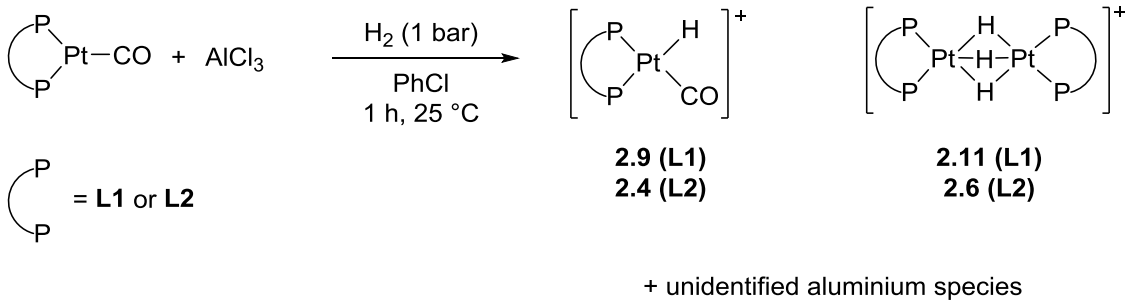

Scheme 3.15: Reaction of [Pt(CO)(**L**)]/$AlCl_3$ with H_2.

formation of a 4-coordinate species. Surprisingly, the coupled ^{27}Al did not show any splitting of the signal and there was no evidence of an aluminium hydride in the ^{1}H NMR spectrum. Similar observations were made for [Pt(CO)(**L2**)] and $AlCl_3$ but the ratio of **2.4** and **2.6** was very different (*ca*. 1:20 respectively, Scheme 3.15). Again, the ^{27}Al{^{1}H} NMR spectrum showed a single sharp signal at δ_{Al} = 97.1 ppm. For both reactions, there was no spectroscopic evidence of the *cis*-dihydride in solution, but this reactivity occurs a lot faster than the previously tested Lewis acids (< 1 h for **L1** and < 10 min for **L2**).

The Lewis pair system [Pt(CO)(**L**)]/$AlCl_3$ did show some reactivity towards ethene but the products were not identified. The presence of [Pt(C_2H_4)(**L**)] could be seen in the ^{31}P{^{1}H} NMR spectrum amongst several other platinum-phosphorus containing species and several sharp signals in the ^{27}Al{^{1}H} NMR indicated the formation of 4-coordinate aluminium species.

3.3.6 Alternate Pathways for Dihydrogen Activation

A pathway to dihydrogen activation was proposed for the cooperative Lewis pair system [Pt(CO)(**L**)]/B(C_6F_5)$_3$ (see Section 2.5.1). Altering the Lewis acid of the system leads to different major activation products which goes against the pathway proposed. Although all of the different Lewis acids tested for dihydrogen activation, described in the Sections above, have their own unique reactivity, many of the platinum-containing activation products remained the same. With this in mind, alternative pathways to the dihydrogen activation products are shown in Scheme 3.16.

Due to the broadening of the ^{31}P{^{1}H} NMR signal for [Pt(CO)(**L**)] in the presence of dihydrogen, it is plausible that this is due to the interaction of H_2 with [Pt(CO)(**L**)] to form a species such as **3.9**. This has been shown to then oxidatively add to the platinum centre to form *cis*-dihydride **3.10**. In the absence of a Lewis acid, this reaction only

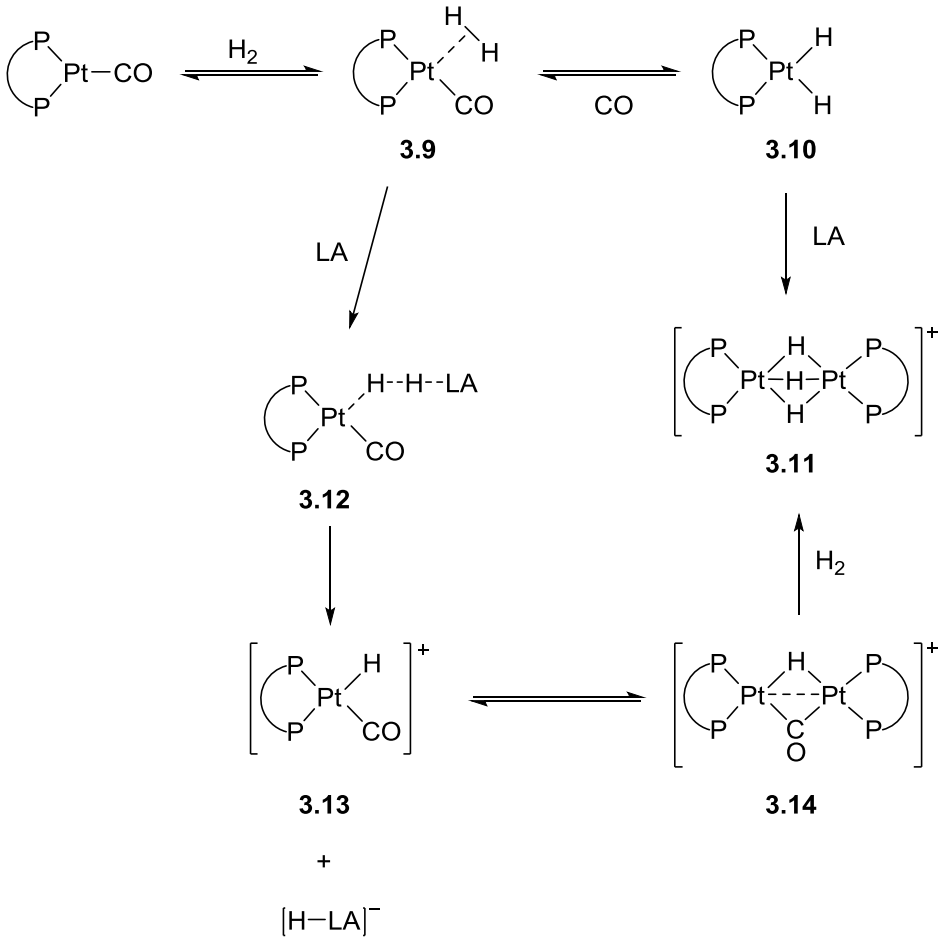

Scheme 3.16: Alternative pathways of dihydrogen activation for the [Pt(CO)(**L**)]/LA cooperative Lewis pair. (LA = Lewis Acid).

proceeds *ca*. 30% and is reversible. In the presence of a Lewis acid this can react further to form trihydride species **3.11**. The fate of the Lewis acid at this stage is unknown and appears to be specific to the Lewis acid being used. The formation of **3.11** is not observed if there is no Lewis acid present.

[Pt(CO)(**L**)]-H_2 **3.9** could react with a Lewis acid to heterolytically cleave H_2 *via* an encounter complex such as **3.12**. This would form cation **3.13** and [H-LA]$^-$. There is some evidence for **3.13** being in equilibrium with Pt(I) species **3.14**. This equilibrium is dependent on the properties of the diphosphine ligand. From the work detailed above, **L2** appears to stabilise the Pt(I) species **3.14** significantly more than **L1**. In the cases where **3.13** is formed with **L2** as the diphosphine, conversion to **3.14** is always seen over time. This is never observed when the diphosphine is **L1**. It was shown in Section 2.5.1 that **3.14** can convert to **3.11** in the presence of hydrogen so it is plausible to suggest that some of **3.11** is being formed by this pathway.

More experimentation and computational studies should be carried out to confirm if these suggested pathways for dihydrogen activation are viable and to explore the mechanisms of how each species is formed.

3.4 Synthesis of a Pd(0) Lewis Base

After the success of using [Pt(CO)(**L**)] as a Lewis base in cooperative Lewis pair small molecule activation, it was of interest to extend this chemistry to palladium with the hope that the chemistry might be transformed into catalytic processes.

The palladium analogue of the platinum Lewis base explored in Chapter 2 and 3, [Pd(CO)(**L1**)] has been reported previously. The palladium monocarbonyl complex was serendipitously isolated when investigating intermediates of the methoxycarbonylation of ethene to form methyl propionate.[36,37] Bellabarba *et* al. showed that the expected carboalkoxide product [PdCl(C(O)OEt)(**L1**)], from the reaction of [$PdCl_2$(**L1**)] with ethanol in the presence of CO and a base, did not form which was surprising in view of palladium carbonyl complexes being known to react with alkoxides.[37,38] It was also reported that the molecular structure of [Pd(CO)(**L1**)] has a planar Pd centre with a similar bend in the **L1** backbone seen for [Pt(CO)(**L1**)] and [Pt(CO)(**L2**)] (see Section 2.3). No detailed experimental procedure was reported for the synthesis of [Pd(CO)(**L1**)] but fortunately NMR spectroscopic data was given. A proposed route to [Pd(CO)(**L1**)] from commercially available starting materials is shown in Scheme 3.17.[36,37,39]

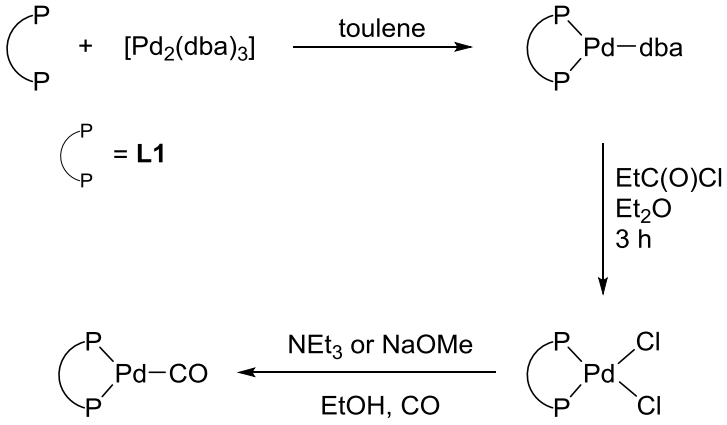

Scheme 3.17: Proposed synthesis of [Pd(CO)(**L1**)] from commercially available [$Pd_2(dba)_3$].

The first step in the proposed synthesis in Scheme 3.17 is combination of diphosphine **L1** with [$Pd_2(dba)_3$] to form [Pd(dba)(**L1**)].[36] This species can then be oxidised to [$PdCl_2$(**L1**)] using propionyl chloride in Et_2O (reported to proceed in good yields).[39]

[$PdCl_2$(**L1**)] can be reduced by EtOH in the presence of a base (NEt_3 or NaOMe) and CO to form the desired complex [Pd(CO)(**L1**)].[37] This proposed synthesis is lengthy and details of experimental procedures for each of these steps are poorly described. After the success of substitution of an alkene ligand to form [Pt(CO)(**L1**)] and [Pt(CO)(**L2**)] (see Section 2.3), attempts to make [Pd(CO)(**L1**)] directly from commercially available [Pd_2(dba)$_3$] (dba = *trans,trans*-dibenzylideneacetone) were made.

[Pd_2(dba)$_3$] and **L1** were combined in toluene but after 16 h very little conversion of **L1** was seen by analysis of the *in situ* $^{31}P\{^1H\}$ NMR spectrum (Figure 3.17A). Heating the reaction mixture to 70 °C for 3 h resulted in the full conversion to [Pd(dba)(**L1**)] (Figure 3.17B). The reaction mixture was treated with CO (1 bar) and resulted in almost quantitative conversion to [Pd(CO)(**L1**)] *in situ* (Figure 3.17C). This was confirmed by comparison to the literature data reported for [Pd(CO)(**L1**)].[37] There was no evidence in the $^{31}P\{^1H\}$ NMR spectrum or the IR spectrum to suggest the formation of a dicarbonyl species (in contrast to the corresponding reaction with Pt, see Section 2.3.1). Removal of the CO atmosphere and solvent, and redissolving in toluene results in a minor amount of

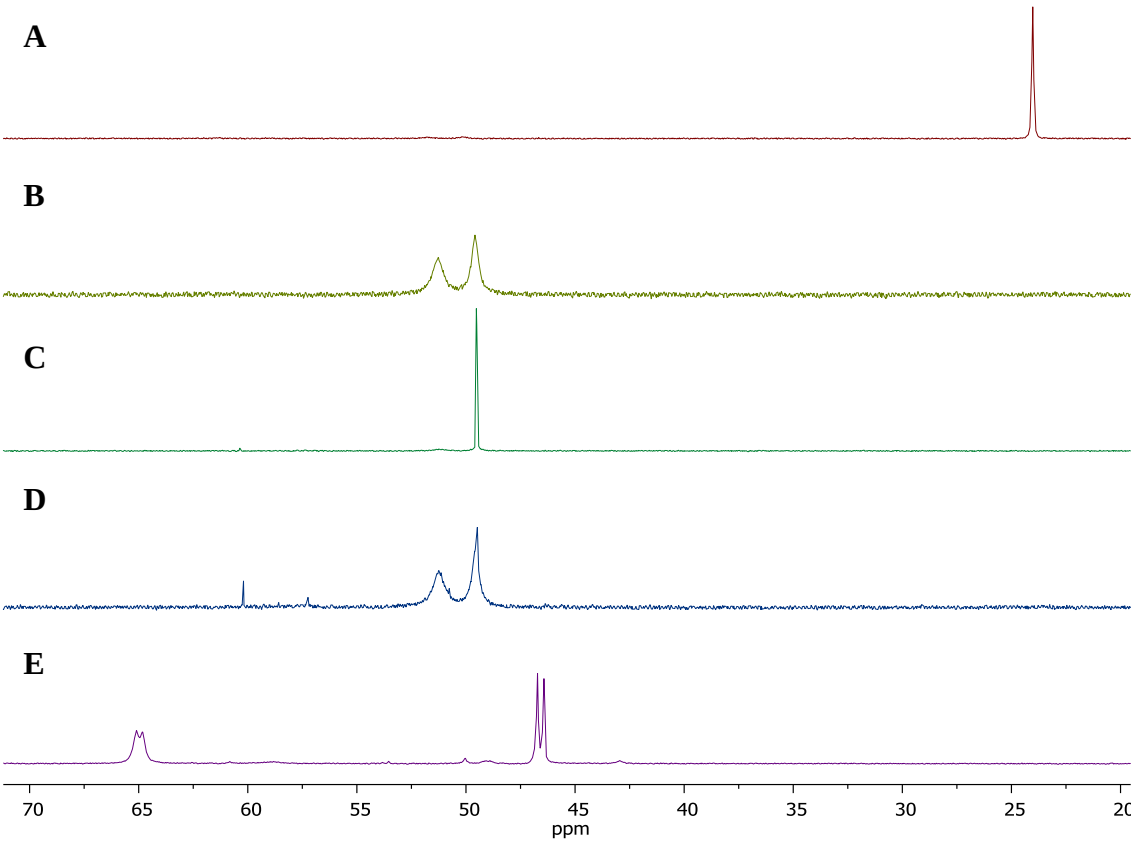

Figure 3.17: *In situ* $^{31}P\{^1H\}$ NMR spectra of A) [Pd_2(dba)$_3$] + **L1** at room temp for 16 h; B) [Pd_2(dba)$_3$] + **L1** at 70 °C for 3 h; C) [Pd(dba)(**L1**)] under a CO atmosphere D) [Pd(dba)(**L1**)] + CO reaction mixture vacced down and redissolved; E) Addition of B(C_6F_5)$_3$ to [Pd(dba)(**L1**)] + CO.

[Pd(CO)(**L1**)] and with [Pd(dba)(**L1**)] as the major species in solution (Figure 3.17D). Several CO/vacuum cycles were repeated but even after 10 cycles, [Pd(dba)(**L1**)] was the major species in solution (> 80%). A possibility was to use the *in situ* formed [Pd(CO)(**L1**)] for combination with B(C_6F_5)$_3$ for small molecule activation. [Pd(dba)(**L1**)] was treated with CO and the *in situ* formation of [Pd(CO)(**L1**)] was confirmed by $^{31}P\{^1H\}$ NMR spectroscopy. One equivalent of B(C_6F_5)$_3$ was added to the reaction mixture and a colour change from orange to dark red was observed. Figure 3.17E shows the resulting $^{31}P\{^1H\}$ NMR spectrum. The two signals at δ_P = 65.0 and 46.6 ppm were confirmed to be from the same species by analysis of a $^{31}P\{^1H\}$ COSY NMR experiment. The $^{11}B\{^1H\}$ NMR spectrum showed complete conversion of B(C_6F_5)$_3$ to a single species at δ_B = −2.4 ppm. It was thought that the product formed is a result of activation of either the alkene double bond or the carbonyl double bond in the residual dba in solution. [Pd(CO)(**L1**)] was eventually isolated (see below) and addition of one equivalent of B(C_6F_5)$_3$ and one equivalent of dba in chlorobenzene led to full conversion to the same species seen in Figure 3.18E. Attempts to remove the dba from *in situ* formed [Pd(CO)(**L1**)] were unsuccessful.

In an attempt to avoid having to oxidise a Pd(0) starting material to then reduce this to gain the final product, the complexation to a Pd(II) starting material was attempted. Ligand **L1** was combined with either [$PdCl_2$(COD)] or [$PdCl_2$($PhCN)_2$] in dichloromethane at room temperature. After 1 h, a bright yellow suspension was formed when using either starting material. This yellow solid was isolated but was insoluble in all of the common organic solvents available (for example DCM, Et_2O, THF, PhCl, PhF, MeCN, benzene and hexane). It is proposed that the resultant diphosphine palladium complex is oligomeric. The material obtained was used in an attempt to form [Pd(CO)(**L1**)] from reaction with EtOH and NEt_3 under a CO atmosphere but this was unsuccessful.

The original synthetic route detailed in Scheme 3.17 was attempted but purification of [Pd(dba)(**L1**)] away from excess dba proved to be problematic. The direct synthesis of [$PdCl_2$(**L1**)] from combination [Pd(dba)$_2$] and **L1** in THF with the addition of HCl has been reported (Scheme 3.18).[40] This synthesis of [$PdCl_2$(**L1**)] worked well and gave the desired product in good yield although required longer reaction times than the 2-step route detailed above (Scheme 3.17).

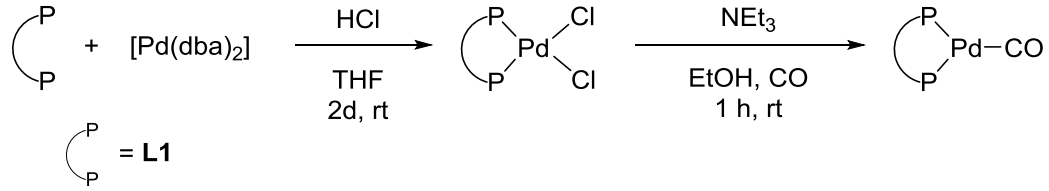

Scheme 3.18: Synthesis of [Pd(CO)(**L1**)].

No detailed experimental procedure was reported for the conversion of [$PdCl_2$(**L1**)] to [Pd(CO)(**L1**)]. Both NEt_3 and NaOMe were tested under the reaction conditions reported by Bellabarba *et al.*[37] but NEt_3 as the base in the reaction gave the best results. [Pd(CO)(**L1**)] precipitated out of the reaction mixture as a yellow solid in pure form but in relatively low yield (*ca*. 50%). Attempts to isolate more product from the resultant filtrate lead to decomposition. [Pd(CO)(**L1**)] was found to be stable as a solid at room temperature when kept under an Ar atmosphere but when in solution [Pd(CO)(**L1**)] would degrade over time unless kept in a CO atmosphere. The analogous procedure for **L2** was tested and proved to be successful in the formation of [Pd(CO)(**L2**)] which displayed a signal in the $^{31}P\{^1H\}$ NMR spectrum at δ_P = 197.2 ppm. Unfortunately, the quantity and purity of material synthesised was insufficient to carry out further analysis/testing for small molecule activation; further work should be carried out on this system.

[Pd(CO)(**L1**)] and B(C_6F_5)$_3$ were combined in chlorobenzene at room temperature to form an orange solution. No significant change in chemical shift was observed in the $^{31}P\{^1H\}$ or $^{11}B\{^1H\}$ NMR spectra but slight broadening of the $^{31}P\{^1H\}$ NMR signal was seen ($w_{1/2}$ = 55 Hz). [Pd(CO)(**L1**)]/B(C_6F_5)$_3$ was treated with H_2 (1 bar) and a colour change from orange to yellow was observed over 6 h. Analysis of the $^{31}P\{^1H\}$ NMR spectrum showed quantitative conversion to a new species at δ_P = 42.0 ppm which appeared as a singlet (Figure 3.18B). This signal corresponds to a quintet observed in the hydride region of the ^1H NMR spectrum (δ_H = −9.96 ppm, $^2J_{HP}$ = 43 Hz, Figure 3.18A). This species is tentatively assigned, from NMR spectroscopic data, as Pd(I) species **3.15** (Scheme 3.19). The presence of **3.15** was seen in positive ion ESI-MS analysis of the reaction mixture. Similar Pd(I) analogues have been synthesised with different diphosphine ligands by the reduction of Pd(II) diphosphine complexes with alcoholic solvents in the presence of a base.[41–45] The $^{11}B\{^1H\}$ NMR spectrum showed a sharp signal at δ_B = −16.2 ppm and a broad signal at δ_B = −2.8 ppm and collectively with the

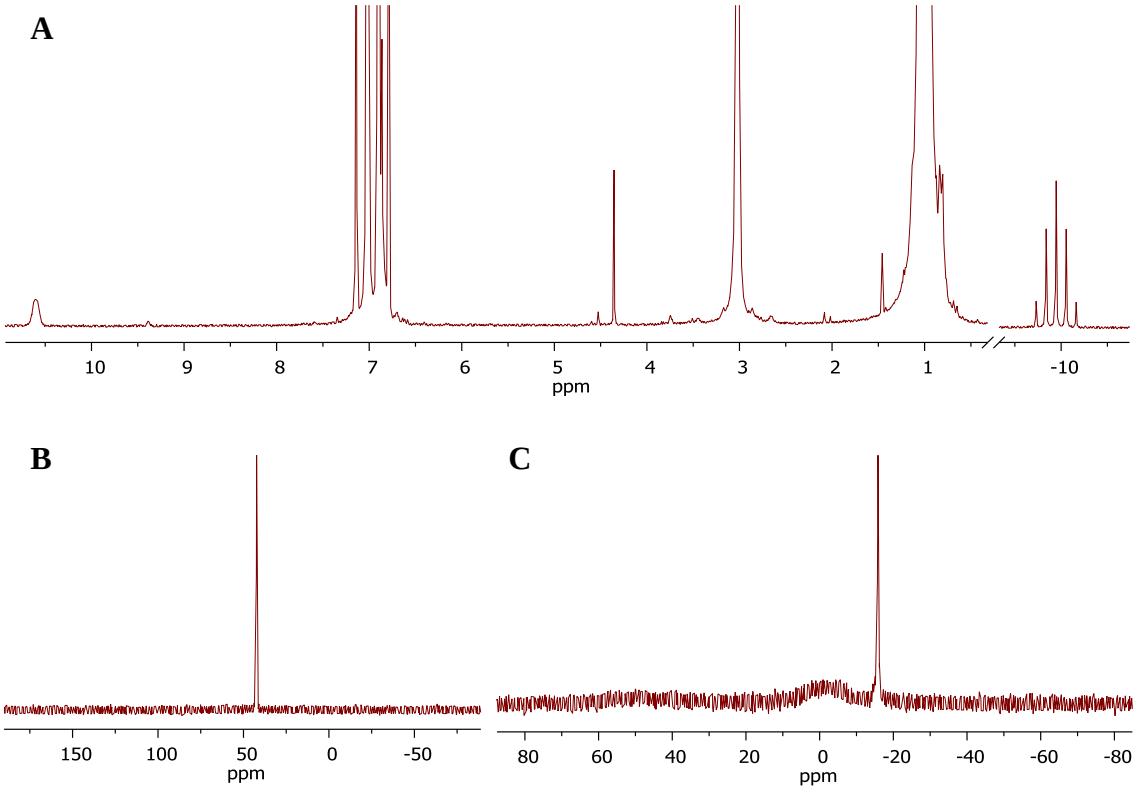

Figure 3.18: A) ^{1}H NMR, B) ^{31}P{^{1}H} NMR and C) ^{11}B{^{1}H} NMR spectra of the *in situ* reaction of [Pd(CO)(L1)]/B(C$_6$F$_5$)$_3$ with H$_2$ at room temperature after 6 h.

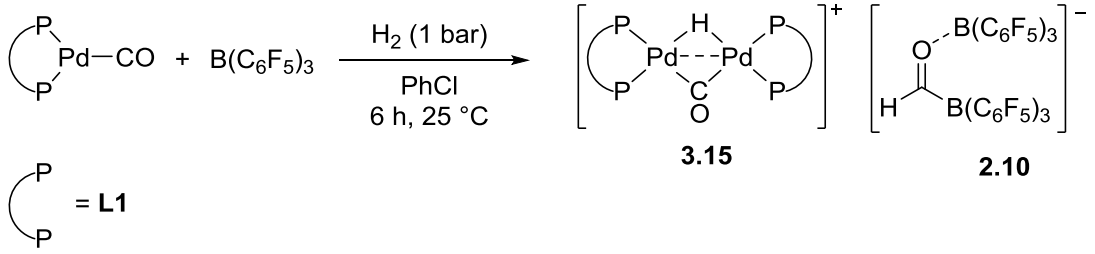

Scheme 3.19: Reaction of [Pd(CO)(**L1**)]/B(C$_6$F$_5$)$_3$ with H$_2$ in chlorobenzene at room temperature.

observation of a broad singlet at δ_H = 10.80 ppm in the ^{1}H NMR spectrum, the anion was confirmed to be **2.10** (Figure 3.18A/C, Scheme 3.19). No further reactivity was observed when leaving the reaction overnight.

[Pd(CO)(**L1**)]/B(C$_6$F$_5$)$_3$ was treated with ethene (1 bar) in chlorobenzene at room temperature which resulted in a colour change from orange to yellow after 16 h. The resulting NMR spectra were broad and it was not clear what the final activation products were but full conversion of both [Pd(CO)(**L1**)] and B(C$_6$F$_5$)$_3$ was observed. This reaction should be further investigated.

3.5 Incorporating Functionality into the Diphosphine Backbone

The work described in Chapter 4 concerns the use of pendant amine ligands for cooperative activation of dihydrogen.[§] The pendant amine and the metal centre are reminiscent of the Lewis base and the Lewis acid of a cooperative Lewis pair. The Pt(0)/B chemistry developed in Chapters 2 and 3 employs the transition metal as the Lewis base in cooperative Pt(0)/B small molecule activation and so incorporation of a pendant amine could lead to competition. The pendant amine could also be envisaged as a potential linker for attachment to a solid support for application in heterogeneous catalysis or synthesis of dendrimeric catalysts analogous to those that have been previously reported.[46–48]

The synthesis of the pendant amine ligand is a one-pot reaction of a secondary phosphine, formaldehyde and a primary amine (see Section 4.2, Scheme 4.2). From the work described in Section 3.2, the optimal phosphine substituent for stabilisation of a platinum monocarbonyl complex is di-*tert*-butyl groups. $P^{tBu}N^{Bn}P^{tBu}$ was obtained in good yields and > 95% purity as a colourless oil by the route shown in Scheme 3.20. This ligand has been previously synthesised *via* the bis-hydroxymethyl phosphonium chloride salt (See Section 4.2, Scheme 4.1).[49]

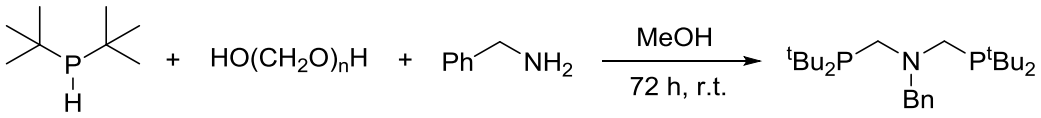

Scheme 3.20: Synthesis of $P^{tBu}N^{Bn}P^{tBu}$.

[Pt(nbe)$_3$] and $P^{tBu}N^{Bn}P^{tBu}$ were combined in toluene at −78 °C and formed a pale yellow solution once the mixture was warmed to room temperature. After 16 h, $^{31}P\{^1H\}$ NMR spectroscopy confirmed quantitative conversion to one Pt species which was assigned to be [Pt(nbe)($P^{tBu}N^{Bn}P^{tBu}$)] (δ_P = 46.1 ppm, $^1J_{PPt}$ = 3169 Hz). In a Youngs NMR tube, the reaction mixture was subjected to CO (1 bar). A slow colour change to pale orange was seen over 48 h. Analysis of the $^{31}P\{^1H\}$ NMR spectrum showed the presence of a broad signal at δ_P = 29.6 ppm ($^1J_{PPt}$ = 3017 Hz, $w_{1/2}$ = 48 Hz, Figure 3.19A) and the sharp signal

[§] See Section 4.1 and 4.2 for an introduction to the use of pendant amine ligands, the common notation used for pendant amine ligands and the optimisation of a synthetic route to a series of pendant amine ligands.

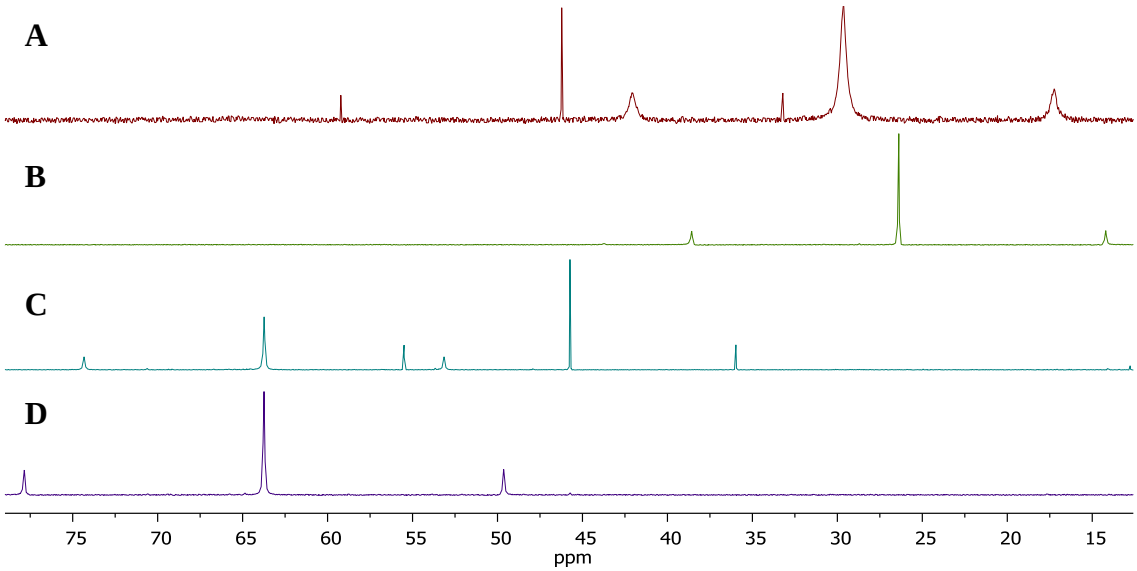

Figure 3.19: $^{31}P\{^1H\}$ NMR spectrum of A) [Pt(nbe)($P^{tBu}N^{Bn}P^{tBu}$)] under a CO atmosphere at room temperature after 48 h; B) [Pt(nbe)($P^{tBu}N^{Bn}P^{tBu}$)] under a CO atmosphere at −80 °C after 48; C) Reaction mixture after 1 CO/vacuum cycle; D) Reaction mixture after 3 CO/vacuum cycles.

for [Pt(nbe)($P^{tBu}N^{Bn}P^{tBu}$)]. The low temperature NMR studies on this sample showed the signal to sharpen at −80 °C to a singlet at δ_P = 26.4 ppm ($^1J_{PPt}$ = 2965 Hz, Figure 3.19B) and was assigned to the dicarbonyl species [Pt(CO)$_2$($P^{tBu}N^{Bn}P^{tBu}$)]. IR studies or repeating the reaction with ^{13}CO would be needed to confirm the identity of this species. Also, at low temperature, it is apparent that the amount of [Pt(nbe)($P^{tBu}N^{Bn}P^{tBu}$)] is negligible so almost full conversion to [Pt(CO)$_2$($P^{tBu}N^{Bn}P^{tBu}$)] is achieved. Removal of the CO atmosphere and the solvent followed by redissolution in toluene led to the partial formation of a new species at δ_P = 63.7 ppm ($^1J_{PPt}$ = 3435 Hz, Figure 3.19C). Two subsequent CO/vacuum cycles led to full conversion to this species which was assigned to the monocarbonyl complex [Pt(CO)($P^{tBu}N^{Bn}P^{tBu}$)] (Figure 3.19D). The product was isolated as an orange solid.

[Pt(CO)($P^{tBu}N^{Bn}P^{tBu}$)]/B(C_6F_5)$_3$ was subjected to H_2 (1 bar) in chlorobenzene at room temperature in a Youngs NMR tube. There was an immediate colour change from bright orange to yellow. Analysis of the ^1H, $^{31}P\{^1H\}$ and $^{11}B\{^1H\}$ NMR spectra and the ESI-mass spectrum confirmed the activation products to be the cationic species **3.16** and **3.17** and anionic species **2.7** and **2.8** (Scheme 3.21).

The composition of the reaction mixture does not change over time. Interestingly, there is no evidence for the formation of the corresponding trihydride species (See Section 2.5.1). The nitrogen of the pendant amine backbone does not appear to play a part in the activation at all with no evidence of protonation at the nitrogen by analysis of the ^1H

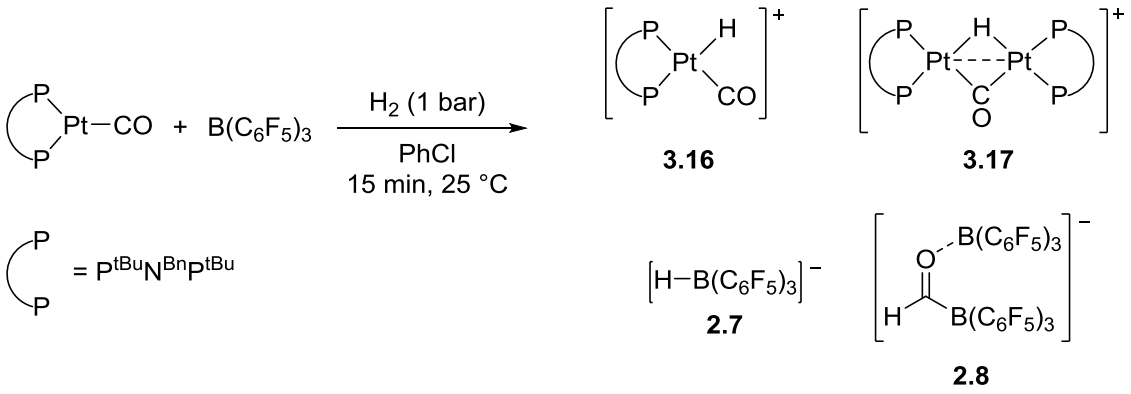

Scheme 3.21: Reaction of [Pt(CO)(P^{tBu}N^{Bn}P^{tBu})]/B(C$_6$F$_5$)$_3$ with H$_2$ after 15 min.

NMR spectrum. A wider scope of activation chemistry is needed to investigate whether the nitrogen can participate in the reactions.

3.6 Conclusions and Future Work

A series of diphosphine ligands have been synthesised based on the xylenyl ligand **L1**. The changes to the ligand altered both the sterics and the electronics at the phosphine donors. **L3** was synthesised by the route developed in Section 2.2 for **L2**, and **L4** and **L5** were successfully prepared from modified literature procedures.[1,2] All three ligands reacted with [Pt(nbe)$_3$] to form the mononorbornene species [Pt(nbe)(**L**)] (where **L** = **L3**, **L4** or **L5**). Under a CO atmosphere the quantitaive formation of [Pt(CO)$_2$(**L**)] was observed by *in situ* NMR spectroscopy. The monocarbonyl complexes [Pt(CO)(**L**)] were never observed due to the quantitative reformation of [Pt(nbe)(**L**)] upon removal of the CO atmosphere and solvent. Even after several CO/vacuum cycles there was no evidence of the production of [Pt(CO)(**L**)]. Ligands **L3**, **L4** and **L5** evidently do not possess the necessary stereoelectronic properties to stabilise the desired platinum monocarbonyl complex [Pt(CO)(**L**)] with respect to [Pt(nbe)(**L**)].

A new, more efficient route to ligand **L6** was described in Section 3.2.4. A complex $^{31}P\{^1H\}$ NMR spectrum was obtained for [Pt(nbe)(**L6**)]. This was attributed to not only *rac* and *meso* diastereoisomers of the complex formed from *rac*/*meso*-**L6** but also the fluxionality caused by chelate ring inversion and rotation around the Pt-nbe bond. This fluxionality was also apparent in the $^{31}P\{^1H\}$ NMR spectrum of [Pt(CO)(**L6**)]. The [Pt(CO)(**L6**)]/B(C$_6$F$_5$)$_3$ cooperative Lewis pair successfully activated dihydrogen in a very similar manner to [Pt(CO)(**L2**)]/B(C$_6$F$_5$)$_3$. Further work on this system should focus on separation of the diastereoisomers of **L6**, ideally isolating the symmetrical *meso* isomer for ease of analysis. This would then reduce the complexity of the NMR spectra

obtained for not only the starting materials but also the activation products. A screen of other small molecule activations should also be carried out.

The steric properties of the PCg group in **L6** are very similar to that of P^{t}Bu$_2$ group. It appears from the results presented in this Chapter that it is necessary to have sufficient steric bulk around the metal centre in order to stabilise the formation of a platinum monocarbonyl complex. The electronics do appear to have an impact on the formation of [Pt(CO)(**L**)], as evidenced by the increase in CO/vacuum cycles needed when using the more electron-withdrawing ligands **L2** and **L6** in comparison to **L1**. Overall, there needs to be a balance of the stereoelectronic properties of the diphosphine ligand to enable efficient synthesis and desired activation chemistry.

Ligand **L8** was synthesised as an unsymmetrical analogue of **L2** in the hope of being able to elucidate the mechanism of activation of the small molecules tested. Distinct signals were observed in the $^{31}P\{^1H\}$ NMR spectrum for the individual phosphorus atoms in the structure of **L8**. In the Pt(II) complex [$PtCl_2$(**L8**)], the coupling between the two phosphorus atoms were well resolved in the $^{31}P\{^1H\}$ NMR spectrum. This desired resolution between the inequivalent phosphorus donors will hopefully be able to give more experimental information about what occurs at the platinum centre during small molecule activation. A preliminary investigation into the formation of [Pt(CO)(**L8**)] was made and the *in situ* formation of the anticipated complex was observed. Work should focus on isolating [Pt(CO)(**L8**)] in order to test it in the cooperative Lewis pair [Pt(CO)(**L8**)]/B(C_6F_5)$_3$ for small molecule activation.

In Section 3.3, the scope of Lewis acids in the cooperative Lewis pair was explored. Triphenylborane, triphenylborate, [Zr(Cp*$_2$)(OMes)][B(C_6F_5)$_4$] and $AlCl_3$ were tested for small molecule activation with [Pt(CO)(**L**)] (**L** = **L1** or **L2**). In all cases the formation of *cis*-dihydride [Pt(H)$_2$(**L**)] was observed and proposed to be an intermediate to the formation of binuclear platinum species [(**L**)Pt(μ-H)$_3$Pt(**L**)]$^+$ (with the exception of $AlCl_3$ where a small amount of [Pt(H)(CO(**L**)] was observed). The counterion to this species varied in each case depending on the Lewis acid used. The formation of [(**L**)Pt(μ-H)$_3$Pt(**L**)]$^+$ is reliant on the presence of the Lewis acid in the system as when [Pt(CO)(**L**)] is subjected to H_2, only [Pt(H)$_2$(**L**)] is observed in less than 40% conversion over 1 week. Although this was not the activation product expected, there is cooperative behaviour

between the Lewis base and the Lewis acid occurring in order to produce [(**L**)Pt(μ-H)$_3$Pt(**L**)]$^+$ as an activation product.

None of the Lewis acids detailed above displayed any activation chemistry of ethene. The only reactivity observed was the quantitative conversion of [Pt(CO)(**L**)] to [Pt(C_2H_4)(**L**)] which did not display any interaction with the Lewis acids.

When using an analogue of B(C_6F_5)$_3$ which is devoid of *ortho*-substitution, the activation chemistry differed to the other Lewis acids used. For the reaction of [Pt(CO)(**L1**)]/B($C_2H_2F_3$)$_3$ with H_2, cationic species **2.9** and **2.11** were both formed after 8 h with no evidence of cation **2.10**. On the other hand, the reaction of [Pt(CO)(**L2**)]/B($C_2H_2F_3$)$_3$ with H_2 led to the immediate formation of **2.6** exclusively. No reaction was seen with ethene for either system. Most interestingly [Pt(CO)(**L1**)]/B($C_2H_2F_3$)$_3$ displayed no reactivity towards phenylacetylene but [Pt(CO)(**L2**)]/B($C_2H_2F_3$)$_3$ appeared to show addition to the alkyne triple bond. Further analysis should be carried out to confirm the identity of the activation product. It would be of interest to test the use of BAr$^F{}_3$ as the Lewis acid as this is also devoid of *ortho*-substitution and its Lewis acidity is comparable to B(C_6F_5)$_3$.[50]

A new proposal for pathways of dihydrogen activation is shown in Scheme 3.16. There are several experiments which could be carried out to test the validity of these pathways. [Pt(H)$_2$(**L**)] should be synthesised independently and then combined with a Lewis acid to investigate if this is an intermediate to the formation of [(**L**)Pt(μ-H)$_3$Pt(**L**)]$^+$. Shaw *et al*. has reported experimental details on the formation of [Pt(H)$_2$(**L1**)],[51] but, unfortunately, isolation of the product proved problematic when this was attempted.

There is some evidence that an equilibrium exists between **3.13** and **3.14**, where **L1** favours **3.13** and **L2** favours **3.14**. Cation **2.9**, can be formed exclusively by reaction of [Pt(CO)(**L1**)] with [H(OEt$_2$)][B(C_6F_5)$_4$].[5,6] When similar chemistry was attempted with [Pt(CO)(**L2**)], the formation of both cationic species **2.4** and **2.5** was observed. This indicates that **3.14** can actually be formed from **3.13** which challenges the pathway of dihydrogen activation for [Pt(CO)(**L**)]/B(C_6F_5)$_3$ proposed in Section 2.5.1. Computational studies on both proposed pathways could help elucidate what was happening in solution.

It appears that in dihydrogen activation there is more than one activation pathway at work. To what extent each pathway is followed apparently relies on a very fine balance of sterics and electronics of both the Lewis acid and the Lewis base centres. There is no clear reactivity pattern for the Lewis acids from the selection tested but there is a fascinating observation for the Lewis bases. The use of the more electron withdrawing diphosphine **L2** promotes the rate of activation chemistry in all cases. This is proposed to be because **L2** creates a more δ^+ charge on the platinum centre in comparison to **L1** which favours the initial binding of the small molecule anticipated to occur before the cooperative Lewis pair activation.

The parallel system with palladium, [Pd(CO)(**L1**)], was synthesised from commercially available [$Pd_2(dba)_3$] in three steps in reasonable yield. The [Pd(CO)(**L1**)]/B(C_6F_5)$_3$ system successfully activated dihydrogen to form cation pair **3.15**/**2.6** exclusively. Initial work on making the phosphinite derivative [Pd(CO)(**L2**)] looks promising. It would be of interest to compare the reactivity of the two systems and how it differs from the original Pt(0) Lewis base.

This system may not be limited to the use of group 10 metals. It can be envisaged that an isoelectronic analogue could be synthesised and tested, for example [Au^{I}(CO)(**L**)] or [Ir^{-1}(CO)(**L**)] which, in theory, should be able to undergo similar 2e$^-$ redox processes that the Pt system has demonstrated to form the activation products.

The use of [Pt(CO)($P^{tBu}N^{Bn}P^{tBu}$)] in a cooperative Lewis pair was successful in dihydrogen activation and the pendant amine did not interfere with the activation chemistry. This provides a plethora of possibilities of having the Lewis base covalently linked to another network. For example, it could be used for attachment to a solid support for use in a heterogenous cooperative Lewis pair system, an area which has recently been reviewed by Qu *et al*.[52]

Overall, the modifications to the original [Pt(CO)(**L**)]/B(C_6F_5)$_3$ cooperative Lewis pair system has provided many possibilities to explore and expand this chemistry and find interesting and new activation products and potentially lead to catalysis.

3.7 References

1 A. Pews-Davtyan, R. Jackstell, A. Spannenberg and M. Beller, *Chem. Commun.*, 2016, **52**, 7568–7571.

2 D. J. Morris, G. Docherty, G. Woodward and M. Wills, *Tetrahedron Lett.*, 2007, **48**, 949–953.

3 R. A. Baber, M. L. Clarke, K. M. Heslop, A. C. Marr, A. G. Orpen, P. G. Pringle, A. Ward and D. E. Zambrano-Williams, *Dalt. Trans.*, 2005, 1079–1085.

4 R. I. Pugh, PhD Thesis, University of Bristol, 2000.

5 S. J. K. Forrest, P. G. Pringle, H. A. Sparkes and D. F. Wass, *Dalt. Trans.*, 2014, **43**, 16335–16344.

6 S. J. K. Forrest, PhD Thesis, University of Bristol, 2014.

7 T. Fanjul, G. Eastham, N. Fey, A. Hamilton, A. G. Orpen, P. G. Pringle and M. Waugh, *Organometallics*, 2010, **29**, 2292–2305.

8 T. Fanjul, G. Eastham, M. F. Haddow, A. Hamilton, P. G. Pringle, A. G. Orpen, T. P. W. Turner and M. Waugh, *Catal. Sci. Technol.*, 2012, **2**, 937–950.

9 V. De La Fuente, M. Waugh, G. R. Eastham, J. A. Iggo, S. Castillón and C. Claver, *Chem. - A Eur. J.*, 2010, **16**, 6919–6932.

10 T. Fanjul, G. Eastham, J. Floure, S. J. K. Forrest, M. F. Haddow, A. Hamilton, P. G. Pringle, A. G. Orpen and M. Waugh, *Dalton Trans.*, 2013, **42**, 100–115.

11 P. G. Edwards, J. C. Knight and P. D. Newman, *Dalt. Trans.*, 2010, **39**, 3851–3860.

12 G. J. P. Britovsek, J. Ugolotti and A. J. P. White, *Organometallics*, 2005, **24**, 1685–1691.

13 M. A. Beckett, G. C. Strickland, J. R. Holland and K. S. Varma, *Polymer*, 1996, **37**, 4629–4631.

14 U. Mayer, V. Gutmann and W. Gerger, *Monatshefte für Chemie*, 1975, **106**, 1235–1257.

15 G. C. Welch and D. W. Stephan, *J. Am. Chem. Soc.*, 2007, **129**, 1880–1881.

16 M. T. Mock, R. G. Potter, D. M. Camaioni, J. Li, W. G. Dougherty, W. S. Kassel, B. Twamley and D. L. DuBois, *J. Am. Chem. Soc.*, 2009, **131**, 14454–14465.

17 S. Hebié, H. P. K. Ngo, J. C. Leprêtre, C. Iojoiu, L. Cointeaux, R. Berthelot and F. Alloin, *ACS Appl. Mater. Interfaces*, 2017, **9**, 28377–28385.

18 Q. Yin, Y. Soltani, R. L. Melen and M. Oestreich, *Organometallics*, 2017, **36**, 2381–2384.

19 Q. Yin, S. Kemper, H. F. T. Klare and M. Oestreich, *Chem. - A Eur. J.*, 2016, **22**, 13840–13844.

20 T. J. Herrington, A. J. W. Thom, A. J. P. White and A. E. Ashley, *Dalt. Trans.*, 2012, **41**, 9019–9022.

21 C. Jiang, O. Blacque and H. Berke, *Organometallics*, 2010, **29**, 125–133.

22 A. M. Chapman, M. F. Haddow and D. F. Wass, *J. Am. Chem. Soc.*, 2011, **133**, 18463–18478.

23 A. M. Chapman, M. F. Haddow and D. F. Wass, *J. Am. Chem. Soc.*, 2011, **133**, 8826–8829.

24 O. J. Metters, S. J. K. Forrest, H. A. Sparkes, I. Manners and D. F. Wass, *J. Am. Chem. Soc.*, 2016, **138**, 1994–2003.

25 O. J. Metters, S. R. Flynn, C. K. Dowds, H. A. Sparkes, I. Manners and D. F. Wass, *ACS Catal.*, 2016, **6**, 6601–6611.

26 S. R. Flynn, O. J. Metters, I. Manners and D. F. Wass, *Organometallics*, 2016, **35**, 847–850.

27 D. W. Stephan and G. Erker, *Angew. Chem. Int. Ed.*, 2010, **49**, 46–76.

28 G. Ménard, L. Tran, J. S. J. McCahill, A. J. Lough and D. W. Stephan, *Organometallics*, 2013, **32**, 6759–6763.

29 M. A. Dureen, C. C. Brown and D. W. Stephan, *Organometallics*, 2010, **29**, 6594–6607.

30 M. A. Dureen and D. W. Stephan, *J. Am. Chem. Soc.*, 2009, **131**, 8396–8397.

31 G. Ménard, T. M. Gilbert, J. A. Hatnean, A. Kraft, I. Krossing and D. W. Stephan, *Organometallics*, 2013, **32**, 4416–4422.

32 G. S. Hair, A. H. Cowley, R. A. Jones, B. G. McBurnett and A. Voigt, *J. Am. Chem. Soc.*, 1999, **121**, 4922–4923.

33 Y. Nakayama, S. Kosaka, K. Yamaguchi, G. Yamazaki, R. Tanaka and T. Shiono, *J. Polym. Sci. Part A Polym. Chem.*, 2017, **55**, 297–303.

34 J. Chen and E. Y.-X. Chen, *Dalt. Trans.*, 2016, **45**, 6105–6110.

35 M. A. Beckett, D. S. Brassington, S. J. Coles and M. B. Hursthouse, *Inorg. Chem. Commun.*, 2000, **3**, 530–533.

36 W. Clegg, M. R. J. Elsegood, G. R. Eastham, R. P. Tooze, X. Lan Wang and K. Whiston, *Chem. Commun.*, 1999, **233**, 1877–1878.

37 R. M. Bellabarba, R. P. Tooze and A. M. Z. Slawin, *Chem. Commun.*, 2003, 1916–1917.

38 M. Hidai, M. Kokura and Y. Uchida, *J. Organomet. Chem.*, 1973, **52**, 431–435.

39 W. Clegg, G. R. Eastham, M. R. J. Elsegood, B. T. Heaton, J. A. Iggo, R. P. Tooze, R. Whyman and S. Zacchini, *Organometallics*, 2002, **21**, 1832–1840.

40 F. Stempfle, D. Quinzler, I. Heckler and S. Mecking, *Macromolecules*, 2011, **44**, 4159–4166.

41 P. Roesle, L. Caporaso, M. Schnitte, V. Goldbach, L. Cavallo and S. Mecking, *J. Am. Chem. Soc.*, 2014, **136**, 16871–16881.

42 M. Portnoy and D. Milstein, *Organometallics*, 1994, **13**, 600–609.

43 M. Portnoy, F. Frolow and D. Milstein, *Organometallics*, 1991, **10**, 3960–3962.

44 Y. Ben-David, M. Gozin, M. Portnoy and D. Milstein, *J. Mol. Catal.*, 1992, **73**, 173–180.

45 C. Ortiz-Cervantes, M. Flores-Alamo and J. J. García, *ACS Catal.*, 2015, **5**, 1424–1431.

46 J. Lemo, K. Heuz, D. Astruc and K. Heuze, *Org. Lett.*, 2005, **7**, 2253–2256.

47 D. Rosario-Amorin, X. Wang, M. Gaboyard, R. Clerac, S. Nlate and K. Heuz, *Chem. - A Eur. J.*, 2009, **15**, 12636–12643.

48 S. Gatard, S. Kahlal, D. Méry, S. Nlate, E. Cloutet, J. Y. Saillard and D. Astruc, *Organometallics*, 2004, **23**, 1313–1324.

49 K. Heuzé, D. Méry, D. Gauss, J. C. Blais and D. Astruc, *Chem. - A Eur. J.*, 2004, **10**, 3936–3944.

50 T. J. Herrington, A. J. W. Thom, A. J. P. White and A. E. Ashley, *Dalt. Trans.*, 2012, **41**, 9019–9022.

51 C. J. Moulton and B. L. Shaw, *J. Chem. Soc. Chem. Commun.*, 1976, 365–366.

52 Y. Ma, S. Zhang, C.-R. Chang, Z.-Q. Huang, J. C. Ho and Y. Qu, *Chem. Soc. Rev.*, 2018, **47**, 5541–5553.

Chapter 4

Pendant Amine Diphosphine Ligands for Intramolecular Cooperativity

4.1 Introduction

The incorporation of transition metals into cooperative Lewis pairs has proven effective in small molecule activation and catalysis. A potential disadvantage of the work described in Chapter 2 and 3 in terms of its technological adoption is that the expensive transition metals platinum and palladium were used. Progression towards the application of cheaper and more earth-abundant transition metals in cooperative Lewis pairs is an exciting prospect.

The global output of electrical energy generated from renewable resources such as solar and wind, has increased drastically but these renewable energy resources are available only intermittently. Finding a means to store and release this energy efficiently and cost-effectively is of great importance. Electrical energy derived from renewable energy resources can be converted into chemical energy stored in the form of reactive chemical bonds. A fuel cell converts chemical energy from fuel into electrical energy by an electrochemical reaction of hydrogen with an oxidising agent, commonly oxygen.[1] Currently, the typical catalysts used in fuel cells are based on platinum, an expensive and low earth-abundant metal.

In nature, iron- and nickel-containing hydrogenase enzymes contain an active site where an amine base is positioned near the metal to assist in the heterolytic cleavage of H_2 (Figure 4.1A).[2–5] Bio-inspired diphosphine ligands containing one or two pendant amines in the backbone have been successfully utilised in the electrocatalytic oxidation of dihydrogen using earth-abundant metals (Figure 4.1B-D).[6–8] Over the past decade, research in the DuBois and Bullock research groups has focussed on the use of the bio-inspired pendant amine ligands coordinated to earth abundant metals, such as Fe, Ni, Co and Mn, for use in electrochemical energy interconversion.[7–21] The ligands with one pendant amine will be referred to as PNP ligands and P_2N_2 ligands if discussing the cyclic

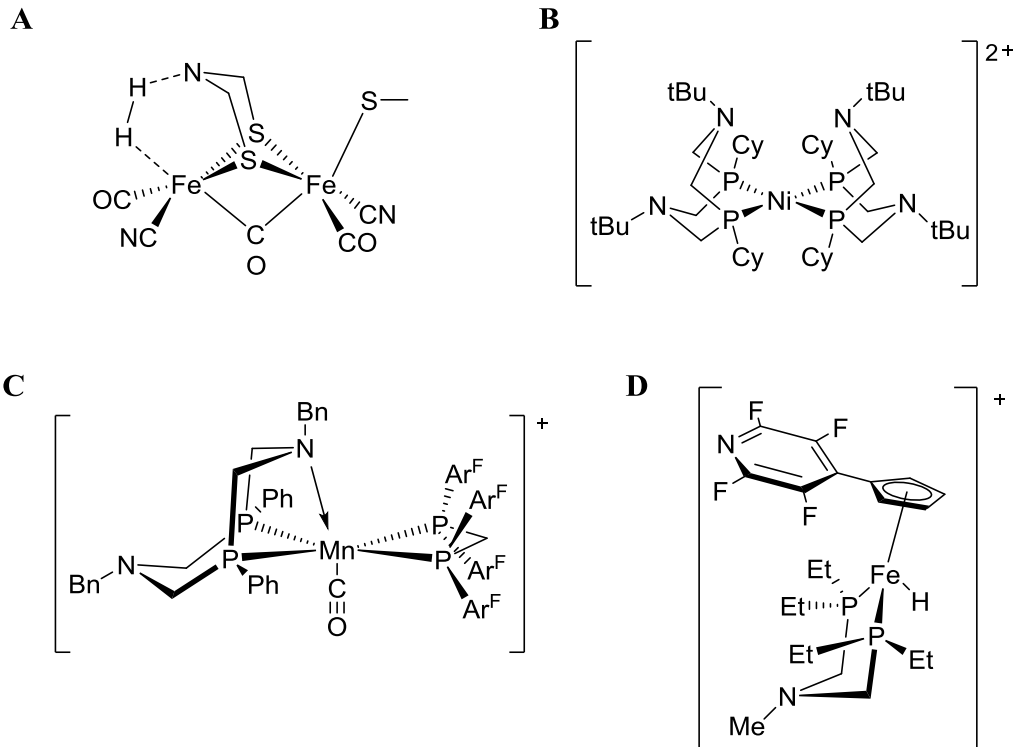

Figure 4.1: (A) Example of the active site of an iron-only hydrogenase enzyme; (B-D) examples of electrocatalysts for hydrogen oxidation.

diphosphine containing two pendant amines. A more detailed outline of the electrocatalytic pathway for the oxidation of H_2 is given in Section 4.7.

These pendant amine complexes often readily bind dihydrogen and many exhibit rapid, reversible heterolytic cleavage of H_2.[22–24] For example, the manganese complex in Figure 4.1C heterolytically cleaves H_2 to form a manganese hydride and a protonated amine. The Mn-H and N-H were shown to exchange *via* an $Mn(\eta^2\text{-}H_2)^+$ complex at an overall exchange rate estimated to be $> 10^7\ s^{-1}$ at 25 °C. This is comparable to rates of H_2 catalysis in [FeFe] hydrogenases[2] and some of the synthetic mimics recorded which replicate this enzyme function.[25]

As metal-based FLP chemistry has developed, the topic is now more broadly linked to the area of metal-ligand cooperation,[26,27] which has been recently reviewed in the context of H_2 heterolytic cleavage by Chambers and Bullock.[28] Metal-ligand cooperation in homogenous catalysis has become more common. Ligands systems, rather than just simply spectating, are involved directly with the bond activation process making a reaction more facile than if it were solely occurring at the metal centre. As mentioned above, this bifunctional catalysis has been known to exist in nature, particularly in

hydrogenase enzymes.[29] Metal-ligand cooperation has been extensively reported and reviewed in the application of hydrogenation reactions and C-H activation.[29–38]

In these PNP-metal complexes the cooperation is between the metal centre and the pendant amine nitrogen. In the context of FLPs the metal centre, in the appropriate oxidation state, would be the Lewis acid and the amine would be the Lewis base. The steric and electronic control at both centres are easily altered by modification of the PNP ligand system itself, as well as other spectator ligands on the metal centre.

4.1.1 Aims and Objectives

The aim of the work presented in this Chapter was to bring together the chemistry described in Chapter 2 and 3, together with the bio-inspired ligand systems described above, for further development. The earth-abundant metal complexes containing pendant amine ligands would be ideal candidates for intramolecular transition metal cooperative Lewis pairs, where the metal centre would act as the Lewis acid and the pendant amine as the Lewis base. The pendant amine diphosphine ligands may also control the stereoelectronic properties of the systems, with the hope of success in catalysis.

Synthetic routes to unusual phosphine ligands derived from PH_3 have been developed in the Pringle group previously. These interesting phosphine groups were investigated in this work in anticipation of this leading to improvements in the systems already developed by Bullock and DuBois *et al*. Thus, the aims of the work presented in this Chapter were as follows:

- Synthesise novel pendant amine ligands containing unusual phosphorus substituents
- Synthesise analogues of manganese complexes previously used for hydrogen oxidation electrocatalysis
- Test these novel complexes for their suitability in electrocatalysis and explore other small molecule activation chemistry

4.2 Synthesis of Novel Pendant Amine Ligands

For the remainder of this chapter the pedant amine ligands will be given the notation $P^{R'}N^{R}P^{R'}$, where R = amine substituent and R' = phosphine substituent and the general formula of the ligand is $(R')PCH_2N(R)CH_2P(R')$.

The stereoelectronic properties of the PNP ligands used in hydrogen electrocatalysis have been studied by Bullock in order to rationally design ligands which will be capable of H_2 cleavage.[13] It was found that more basic centres were more suitable for the oxidation of H_2. More interestingly, the steric bulk of the phosphine substituents influenced the hydride affinity of the metal centre. It was shown that larger substituents on the phosphine resulted in distortion of the geometry at the metal centre, lowering the energy of the LUMO and increasing the hydride acceptor ability.[9]

Bicyclic phosphine 9-phosphabicyclononane (*s*-PhobPH)[39] and tricyclic phosphine 1,3,5,7-tetramethyl-2,4,8-trioxa-6-phospha-adamantane cage (CgPH)[40] are unique in terms of their stereoelectronic properties and their facile synthesis from PH_3 (Figure 4.2). PhobPH is formed from the reaction of PH_3 and 1,5-cyclooctadiene which yields both the symmetric and asymmetric isomers. Methods for their separation have been developed previously in the Pringle group[39] and only *s*-PhobPH was used in the studies detailed in this chapter. CgPH is formed as a racemic mixture (α and β enantiomers shown in Figure 4.2) from the high-yielding reaction of PH_3 with acetylacetone. The use of the racemic mixture of CgPH produces diastereomeric products, a complication that will be discussed in further detail below.

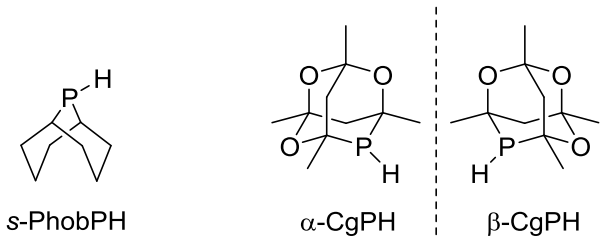

Figure 4.2: Structures of the bicyclic and tricyclic secondary phosphines *s*-PhobPH and CgPH (α/β enantiomers).

The novel PNP ligands explored in this Chapter were initially prepared by the unoptimised reaction shown in Scheme 4.1. The synthesis of the PNP ligands in this manner is *via* the bis(hydroxymethyl)phosphonium chloride salt formed by the reaction of the secondary phosphine and formaldehyde in the presence of HCl (first step of Scheme 4.1). Subsequent reaction of this salt with a primary amine in the presence of

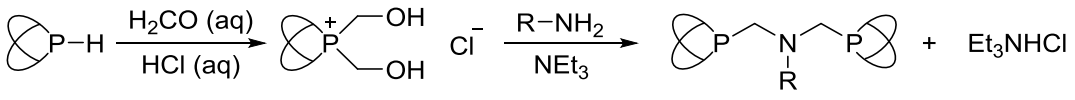

Scheme 4.1: General scheme for the formation of PNP ligands *via* bis(hydroxymethyl)phosphonium chloride salts.

triethylamine yielded the desired PNP ligand. The bis(hydroxymethyl)phosphonium chloride salts of *s*-PhobPH and CgPH have been synthesised previously by Pringle,[41] and others.[42–45] This route has also been employed by Gade *et al.* to form various $P^{iPr}N^{R}P^{iPr}$ ligands for nickel catalysed C-H arylation where the varying stereoelectronic properties of the amine substituent allowed for isolation of catalytic intermediates.[46]

An advantage of the method detailed in Scheme 4.1 is that the intermediate salt is air- and moisture-stable. Both secondary phosphines are moisture-stable but *s*-PhobPH is air-sensitive; therefore, synthesising the PNP ligands *via* the bis-hydroxymethyl phosphonium salt allows for much easier handling of the starting materials to synthesise a library of PNP ligands. A second advantage of the formation of an isolable intermediate compound which can serve as a common intermediate in the preparation of a wide range of PNP ligands, synthesised by derivatisation of this intermediate with a range of primary amines (second step of Scheme 4.1).

The synthesis shown in Scheme 4.1 *via* the bishydroxymethyl phosphonium salt suffered from poor yields (< 30%) and the final desired product required isolation from the triethylammonium salts formed in the second step. It was found that the PNP ligands could be synthesised in high purity and yield by an alternative approach, consisting of a P-based Mannich type reaction of the secondary phosphine, paraformaldehyde and primary amine in MeOH (Scheme 4.2). This route is reported in the literature for analogous compounds.[10,47–51] Advantageously, the pure product was obtained either by spontaneous precipitation from the crude reaction mixture or upon reducing the volume of the solution resulting in product precipitation. Concentration of the resultant filtrate yielded a white solid which was found to comprise product as the major species alongside impurities which could be removed by extraction with ice-cold MeOH. In some cases, ligands with the *s*-PhobP group required recrystallisation from MeOH at −20 °C to obtain the product in sufficient purity (> 98%). Yields and $^{31}P\{^{1}H\}$ NMR chemical shifts of the products are shown in Table 4.1.

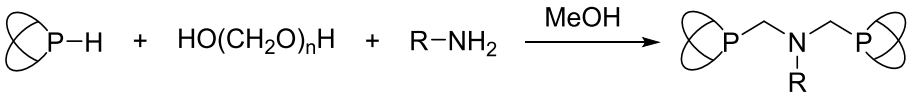

Scheme 4.2: General scheme for the formation of PNP ligands directly from the secondary phosphine.

Table 4.1: Yields and $^{31}P\{^{1}H\}$ NMR chemical shifts for $PN^{R}P$ ligands synthesised.

	**R**	**Yield (%)**	**$^{31}P\{^{1}H\}$ δ (ppm)[a]**
s-PhobP	Me	93	−45.3
	iPr	74	−43.9
	Bn	85	−47.9
CgP	Me	83	−41.8, −42.6
	iPr	71	−40.9, −41.2
	Bn	87	−41.9, −42.2

[a] $^{31}P\{^{1}H\}$ NMR spectrum recorded in $CDCl_3$

For the $P^{Cg}N^{R}P^{Cg}$ (R = Me, iPr and Bn) ligands, two singlets were observed in the $^{31}P\{^{1}H\}$ NMR spectra, consistent with the formation of *rac* and *meso* diastereomers resulting from the use of a racemic mixture of the CgPH phosphine. The diastereoisomers displayed minor differences in solubility in MeOH solvent. Different ratios of the diastereomers were observed between the precipitated product and the product obtained from the filtrate. Previously, this has been exploited to gain pure (> 95%) samples of the *rac* and *meso* isomers of $CgP(CH_2)_3PCg$ by addition of MeOH to a DCM solution of the mixture to precipitate the *rac* isomer.[52] Attempts to apply this purification method were unsuccessful, and only diastereomer purities of *ca*. 70% were obtained. Due to the failed attempts at obtaining pure samples of each diastereoisomer it was decided to carry the ligand forward as a mixture of *rac* and *meso* isomers.

4.2.1 Coordination Studies to Pt(II)

Addition of $P^{Phob}N^{R}P^{Phob}$ (R = Me, iPr, Bn) to $[PtCl_2(COD)]$ yielded the corresponding dichloroplatinum(II) complex **4.1** (Scheme 4.3). Slow diffusion of hexane into a saturated solution of $[PtCl_2(P^{Phob}N^{iPr}P^{Phob})]$ in CH_2Cl_2 gave crystals suitable for X-ray crystallography (Figure 4.3). The $P^{Phob}N^{Me}P^{Phob}$ ligand coordinates in a bidentate fashion through the two phosphines; the nitrogen is non-coordinating. The 6-membered metallacycle sits in the more stable chair conformation, which is expected for this series of ligands[9].

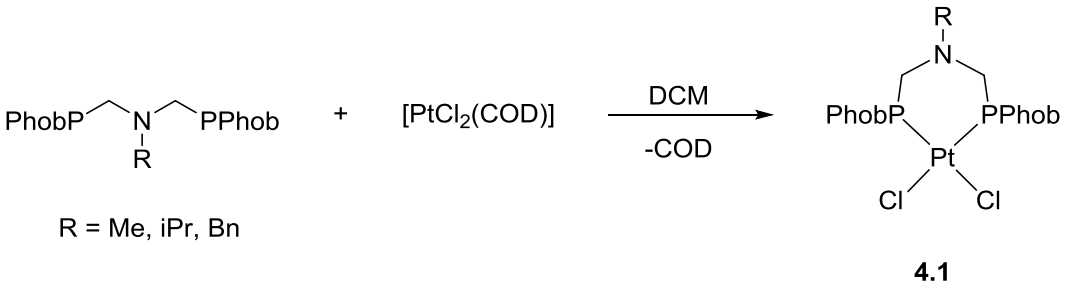

Scheme 4.4: Formation of dichloroplatinum(II) complex **4.1**.

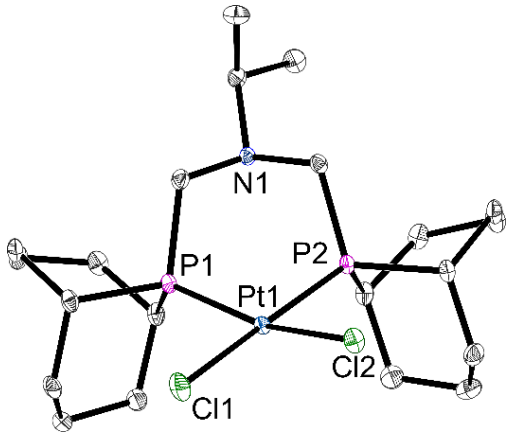

Figure 4.3: Crystal structure of [$PtCl_2(P^{Phob}N^{iPr}P^{Phob})$]. Thermal ellipsoids at 50%. Co-crystallised CH_2Cl_2 and hydrogen atoms omitted for clarity. Selected bond lengths (Å) and angles (°): Pt1-P1 2.2406(7); Pt1-P2 2.2468(6); Pt1-Cl1 2.3584(6); Pt1-Cl2 2.663(6); P1-Pt1-P2 89.16(2); P1-Pt1-Cl1 94.78(2); P2-Pt1-Cl2 91.24(2); Cl1-Pt1-Cl2 84.29(2).

Addition of $P^{Cg}N^{R}P^{Cg}$ to [$PtCl_2$(COD)] led to the formation of the corresponding [$PtCl_2(P^{Cg}N^{R}P^{Cg})$] complexes as sparingly soluble white solids. Alternatively, the more soluble methyl derivatives **4.2** were readily prepared from [$PtMe_2$(COD)] (Scheme 4.4). The *meso* isomer of [$PtMe_2(P^{Cg}N^{iPr}P^{Cg})$] and the *rac* isomers of [$PtMe_2(P^{Cg}N^{Me}P^{Cg})$] and

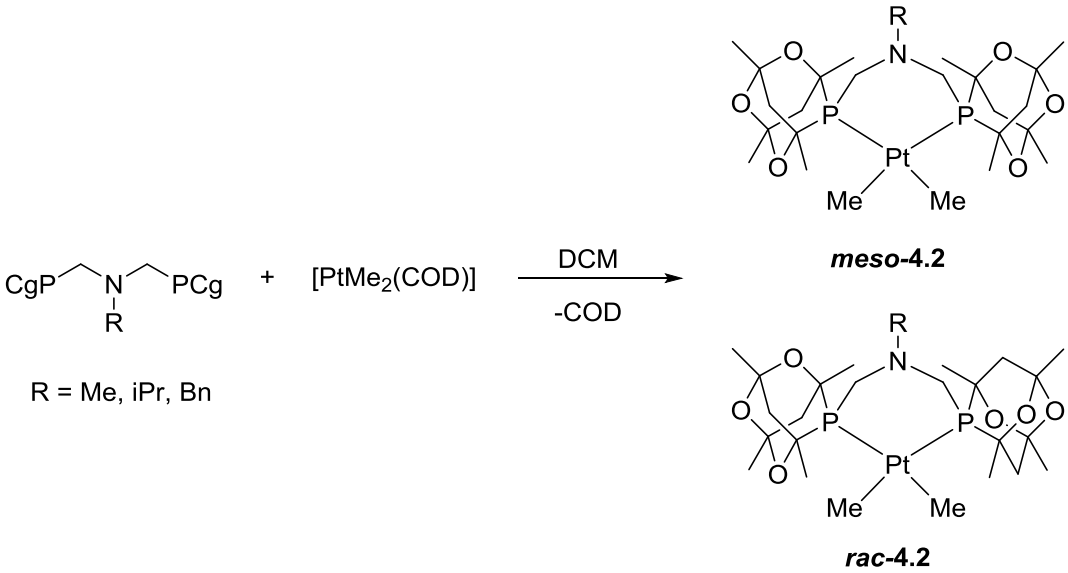

Scheme 4.3: Formation of dichloroplatinum(II) complex **4.2**

[$PtMe_2(P^{Cg}N^{Bn}P^{Cg})$] were crystallised by slow evaporation of a CH_2Cl_2/hexane mixture of the platinum(II) complex (Figure 4.4, 4.5 and 4.6 respectively).

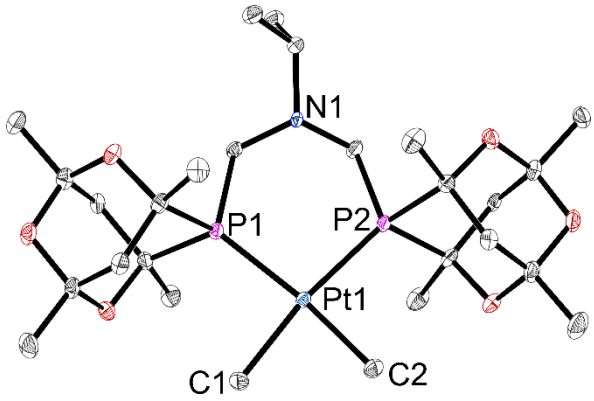

Figure 4.4: Crystal structure of *meso*-[$PtMe_2(P^{Cg}N^{iPr}P^{Cg})$]. Thermal ellipsoids at 50%. Hydrogen atoms omitted for clarity. Selected bond lengths (Å) and angles (°): Pt1-P1 2.2781(6); Pt1-P2 2.2994(5); Pt1-C1 2.098(2); Pt1-C2 2.097(2); P1-Pt1-P2 93.98(2), P1-Pt-C1 91.98(7); P2-Pt1-C2 93.70(7); C1-Pt1-C2 81.24(9).

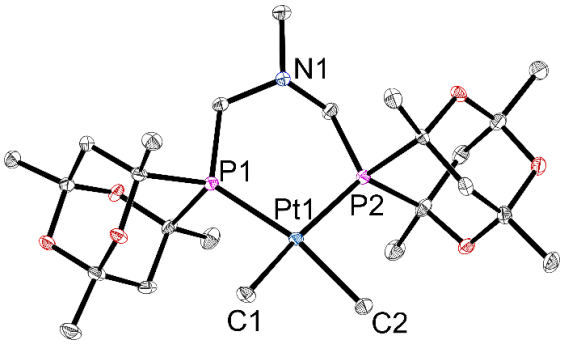

Figure 4.5: Crystal structure of *rac*-[$PtMe_2(P^{Cg}N^{Me}P^{Cg})$]. Thermal ellipsoids at 50%. Hydrogen atoms omitted for clarity. Selected bond lengths (Å) and angles (°): Pt1-P1 2.2854(6); Pt1-P2 2.2691(6); Pt1-C1 2.114(2); Pt1-C2 2.094(2); P1-Pt1-P2 93.10(2), P1-Pt-C1 94.67(6); P2-Pt1-C2 93.32(7); C1-Pt1-C2 80.77(9).

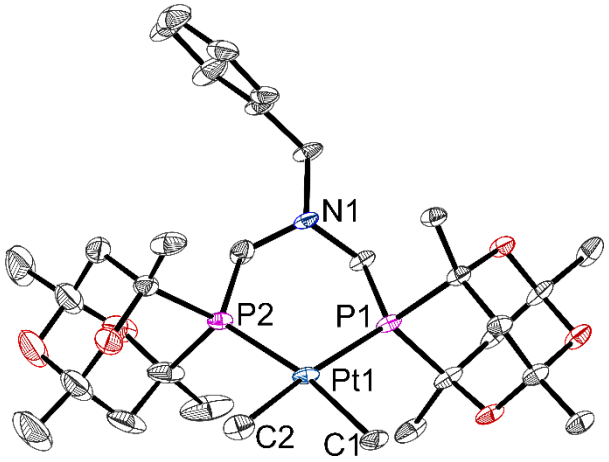

Figure 4.6: Crystal structure of *rac*-[$PtMe_2(P^{Cg}N^{Bn}P^{Cg})$]. Thermal ellipsoids at 50%. Hydrogen atoms omitted for clarity. Selected bond lengths (Å) and angles (°): Pt1-P1 2.2956(6); Pt1-P2 2.2868(6); Pt1-C1 2.112(2); Pt1-C2 2.111(2); P1-Pt1-P2 93.10(2), P1-Pt-C1 93.12(7); P2-Pt1-C2 92.16(7); C1-Pt1-C2 80.25(9).

A difference in the rate of complexation between the *rac* and *meso* isomers was observed for the complexation of $P^{Cg}N^{R}P^{Cg}$ to [$PtMe_2$(COD)]. After 3 h, complete complexation of one isomer was seen with total consumption of [$PtMe_2$(COD)] observed after 16 h. Due to excess ligand being used, this led to an enrichment of either ***rac*-4.2** or ***meso*-4.2**, as determined by $^{31}P\{^{1}H\}$ NMR spectroscopy (Figure 4.7). For [$PtMe_2(P^{Cg}N^{Me}P^{Cg})$] and [$PtMe_2(P^{Cg}N^{Bn}P^{Cg})$], it was not possible to confidently assign $^{31}P\{^{1}H\}$ NMR chemical shifts of the *rac* and *meso* diastereoisomers. Assignment of *rac*-[$PtMe_2(P^{Cg}N^{iPr}P^{Cg})$] and *meso*-[$PtMe_2(P^{Cg}N^{iPr}P^{Cg})$] was possible due to the methyl groups of the *iso*-propyl substituent being diastereotopic for the *rac* isomer of the ligand and appearing as two doublets in the ^{1}H NMR spectrum. In the *meso*-isomer where the methyl groups are equivalent just one doublet is observed in the ^{1}H NMR spectrum. This analysis of the NMR spectra allowed the unambiguous assignment of the major isomer at δ_P = −15.0 ppm to *rac*-[$PtMe_2(P^{Cg}N^{iPr}P^{Cg})$] and the minor isomer at δ_P = −18.0 ppm to *meso*-[$PtMe_2(P^{Cg}N^{iPr}P^{Cg})$].

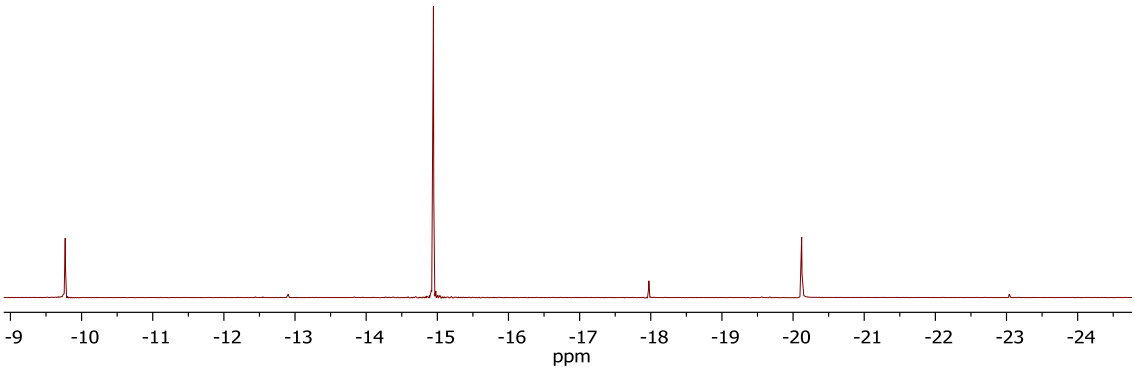

Figure 4.7: $^{31}P\{^{1}H\}$ NMR spectrum of [$PtMe_2(P^{Cg}N^{iPr}P^{Cg})$] as a mixture of *rac* (δ_P = −15.0 ppm) and *meso* (δ_P = −18.0 ppm) isomers.

The difference in rate of complexation to platinum(II) is seen across the series of the $P^{Cg}N^{R}P^{Cg}$ ligands. This could provide a method of separation of the *rac* and *meso* isomers of the ligand if necessary in future work.

4.3 Formation of Pendant Amine Manganese Complexes

Bullock *et al.* have demonstrated the use of manganese complexes, with either PNP or P_2N_2 ligands, for the electrocatalytic oxidation of dihydrogen.[6,53] The most successful manganese complex reported to date bears a P_2N_2 ligand which has the inherent feature of positioning the nitrogen close to the metal centre to impart reactivity (Figure 4.1C).[6,22] Although for both of the six-membered metallocycles the chair conformation is

thermodynamically favourable, this is sterically unfavoured. One ring is forced into a boat conformation which is then positioned next to the metal centre. The exception to this common conformation is when the ligand is protonated after activation of dihydrogen, causing the ligand to sit in an 'exo-pinch' conformation where the two amines are bridged by a proton.[6,54] The cyclic phosphine groups *s*-PhobP and CgP can only be used to form the PNP ligand so the analogue of $[Mn(P^{Ph}N^{Me}P^{Ph})(bppm)(CO)]^+$ (bppm = bis(bis(3,5-bis(trifluoromethyl)phenyl)phosphino)methane) was the target compound for comparison as this has shown rapid cleavage of dihydrogen and is an active electrocatalyst for the oxidation of dihydrogen.[6]

The attempted synthesis of the target Mn(I) complexes followed the general pathway shown in Scheme 4.5. The first step involves complexation of the $P^{R'}N^{R}P^{R'}$ ligand to $[Mn(CO)_5Br]$ by displacement of two carbonyl ligands to generate *fac*-isomer **4.3**. To coordinate the second diphosphine (dppm (= bis(diphenylphosphino)methane) or bppm), it has been shown that UV irradiation is necessary to displace another two carbonyl ligands to generate *trans* complex **4.4**. Abstraction of the bromide ligand with $NaBAr^F_4$ (BAr^F_4 = tetrakis[3,5-bis(trifluoromethyl)phenyl]borate) should lead to the desired cationic complex **4.5**. The bond between the pendant amine nitrogen and the manganese centre is drawn in tentatively, as it is not known that this κ^3 binding in solution will occur, although for analogous complexes there is strong evidence for some interaction between the two centres.[53]

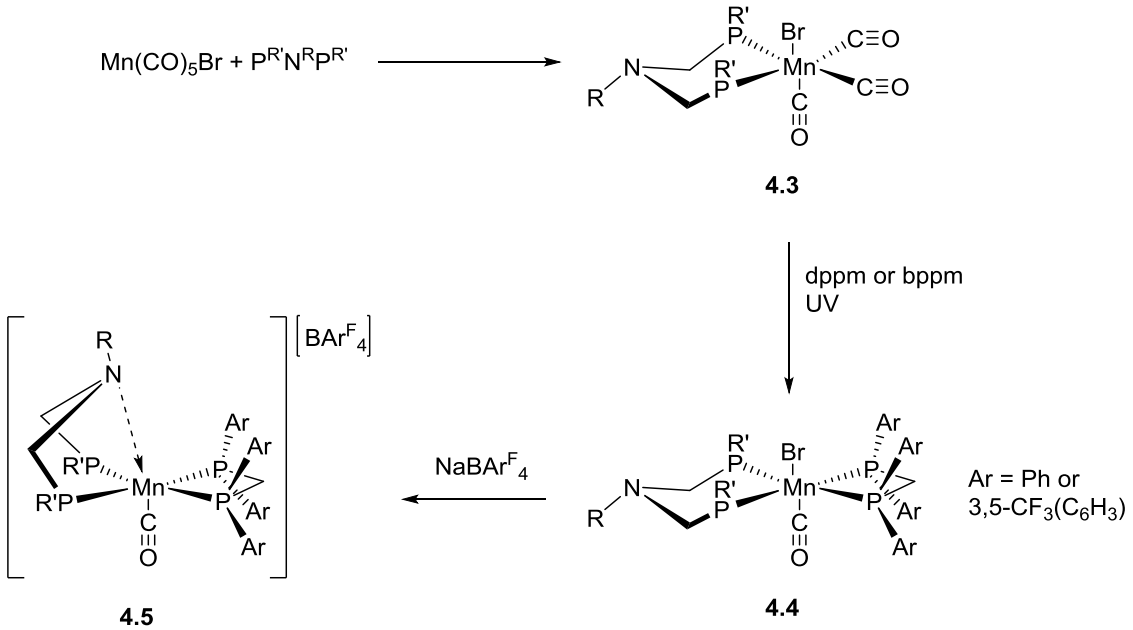

Scheme 4.5: Proposed route to the synthesis of **4.5**.

The series of tricarbonyl bromide complexes [Mn($P^{Phob}N^{R}P^{Phob}$)$(CO)_3$Br] (R = Me, iPr, Bn) were synthesised by heating a suspension of $P^{Phob}N^{R}P^{Phob}$ and [$Mn(CO)_5$Br] in benzene at 50 °C. Analysis of the *in situ* $^{31}P\{^1H\}$ NMR spectrum showed complete complexation after two hours, and [Mn($P^{Phob}N^{R}P^{Phob}$)$(CO)_3$Br] complexes were isolated as yellow solids in good yields. Each of the complexes exhibited a broad singlet ($w_{1/2}$ = *ca.* 72 Hz) in the $^{31}P\{^1H\}$ NMR spectrum indicating the formation of a single isomer (Figure 4.8A). The two possible isomers of [Mn($P^{Phob}N^{R}P^{Phob}$)$(CO)_3$Br] are the *fac* and *mer* isomers with respect to the carbonyl ligands. If the *mer* isomer had formed there would be two signals in the $^{31}P\{^1H\}$ NMR spectrum due to the phosphines being inequivalent. Analysis by IR spectroscopy confirmed the presence of the *fac* isomer in solution for [Mn($P^{Phob}N^{R}P^{Phob}$)$(CO)_3$Br] and the molecular structure of *fac*-[Mn($P^{Phob}N^{iPr}P^{Phob}$)$(CO)_3$Br] is shown in Figure 4.8B. The 6-membered ring formed with the PNP ligand is shown to adopt the thermodynamically favoured chair conformation (Figure 4.8). The line broadening observed in the $^{31}P\{^1H\}$ NMR spectrum is a consequence of the phosphorus atoms being directly coordinated to a ^{55}Mn nucleus which is quadrupolar ($I = {}^5/_2$, 100% abundance).

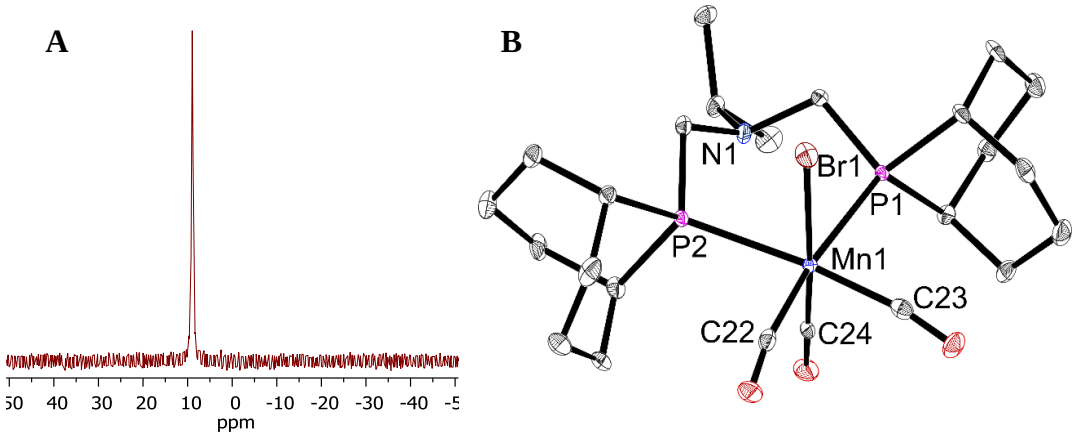

Figure 4.8: A) $^{31}P\{^1H\}$ NMR spectrum of [Mn($P^{Phob}N^{iPr}P^{Phob}$)$(CO)_3$Br]. **B**) Crystal structure of [Mn($P^{Phob}N^{iPr}P^{Phob}$)$(CO)_3$Br]. Thermal ellipsoids at 50%. Hydrogen atoms omitted for clarity. Selected bond lengths (Å) and angles (°): Mn1-P1 2.3707(7), Mn1-P2 2.3619(7); Mn1-C22 1.826(3); Mn1-C23 1.820(3); Mn1-C24 1.785(3); Mn1-Br1 2.5197(5); P1-Mn1-P2 96.32(3); Br1-Mn1-C24 170.15(8).

The series of tricarbonyl bromide complexes [Mn($P^{Cg}N^{R}P^{Cg}$)$(CO)_3$Br] (R = Me, iPr, Bn) were synthesised by heating a suspension of $P^{Cg}N^{R}P^{Cg}$ and [$Mn(CO)_5$Br] in benzene at 50 °C. The complexation of the $P^{Cg}N^{R}P^{Cg}$ ligands to manganese required longer reaction times in comparison to the complexation of the $P^{Phob}N^{R}P^{Phob}$ ligands and were left overnight to reach completion. This was assumed to be due to the increased steric bulk of the CgP group compared to the *s*-PhobP group. The [Mn($P^{Cg}N^{R}P^{Cg}$)$(CO)_3$Br] complexes were isolated as yellow/orange solids in good yield. The molecular structure of *meso*-[Mn($P^{Cg}N^{iPr}P^{Cg}$)$(CO)_3$Br] is shown in Figure 4.9. Again, the molecular structure confirms the formation of the *fac*-isomer and the PNP chelate ring is in a chair conformation. The corresponding $^{31}P\{^{1}H\}$ NMR spectrum of the *rac* and *meso* mixture of [Mn($P^{Cg}N^{iPr}P^{Cg}$)$(CO)_3$Br] is shown in Figure 4.10A and the expected line broadening can be seen. The *rac* and *meso* isomers form in the ratio of the original ligand mixture and no preference is seen for one isomer which contrasts to the observations made when carrying out platinum coordination studies (Section 4.2.1).

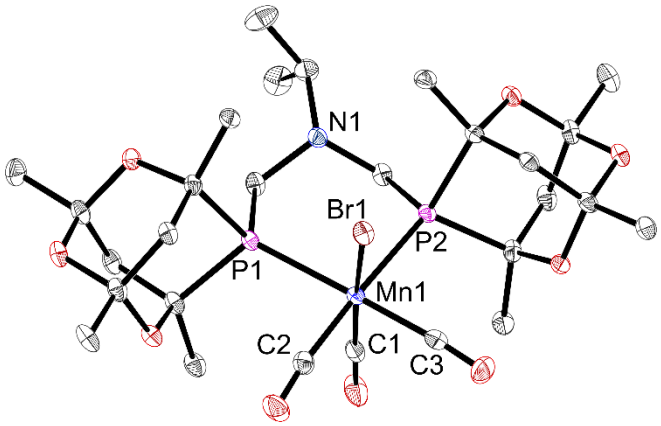

Figure 4.9: Crystal structure of *meso*-[Mn($P^{Cg}N^{iPr}P^{Cg}$)$(CO)_3$Br]. Thermal ellipsoids at 50%. Crystallised C_6H_6 and hydrogen atoms omitted for clarity. Selected bond lengths (Å) and angles (°): Mn1-P1 2.3532(5), Mn1-P2 2.3613(5); Mn1-C2 1.827(2); Mn1-C3 1.836(2); Mn1-Br1 2.5640(3); P1-Mn1-P2 91.961(18); Br1-Mn1-C1 171.34(7).

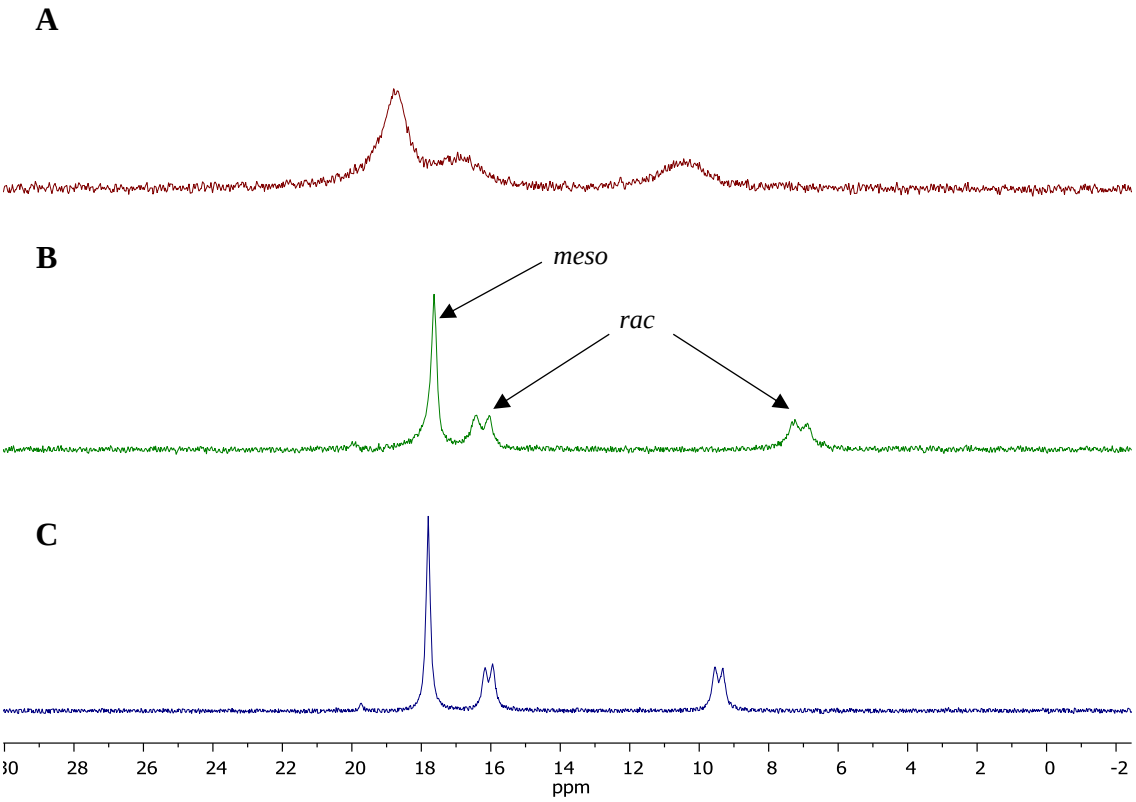

Figure 4.10: $^{31}P\{^{1}H\}$ NMR spectrum of $[(P^{Cg}N^{Me}P^{Cg})Mn(CO)_3Br]$ in d_2-DCM at (A) room temperature, (B) – 60 °C and in (C) TCE at room temperature.

The *meso* isomer of $[Mn(P^{Cg}N^{R}P^{Cg})(CO)_3Br]$ appears as a singlet in the $^{31}P\{^{1}H\}$ NMR spectrum due to the C_s symmetry of that isomer. On the other hand, the *rac*-isomer has C_1 symmetry and as expected, displays two signals in the $^{31}P\{^{1}H\}$ NMR spectrum (Figure 4.10A). Initially, the line broadening was thought to arise from coordination to the quadrupolar manganese nucleus, but the line width measured for the *rac* isomer signals were almost twice that of the *meso* isomer signals ($w_{½}$ = ~130 Hz *vs.* $w_{½}$ = ~70 Hz respectively). Low temperature NMR spectroscopy studies led to the resolution of the coupling between the two phosphines in the *rac* isomer (Figure 4.10B). The signals resolved at −60 °C, −50 °C and −40 °C for R = Me, iPr and Bn respectively. Below these temperatures the signal began to broaden again which is thought to be related to quadrupolar effects from the Mn nucleus. Interestingly, when the solvent of the NMR spectroscopy samples was switched to 1,1,2,2-tetrachloroethane (TCE) from d_2-DCM for high temperature NMR spectroscopy studies the coupling of the two phosphines in the *rac* isomer was resolved at room temperature (Figure 4.10C). The line width also reduces for both the *rac* and *meso* isomers ($w_{½}$ = ~78 Hz and $w_{½}$ = ~31 Hz respectively). These observations indicate that the line broadening is most likely a result of a kinetic process

occurring in relation to the PNP ligand. This process may be attributed to the possible ring flip of the 6-membered metallocycle between the chair and boat conformations. A similar observation was made for the related complex [(κ^3-$P^{Ph}{}_2N^{Bn}{}_2$)Mn(CO)(bppm)][$BAr^F{}_4$] where the dynamic behaviour was attributed to the reversible dissociation of the pendant amine.[22] Although this is for the cationic complex, the same dynamic behaviour could be present in analogues of the starting bromide complex. The bis-diphosphine derivatives [Mn(PNP)(dppm)(CO)(Br)] exhibited very broad signals ($w_{½}$ > 200 Hz) in their $^{31}P\{^1H\}$ NMR spectrum with no discernible coupling.[55] This was attributed to coupling to the Mn nucleus but could be rationalised in a similar manner to the [Mn(PNP)$(CO)_3$Br] described here.

4.4 Attempts at Coordinating a Second Diphosphine

Bullock *et al.* found that it was necessary to have a second diphosphine coordinated to Mn in order to observe reactivity with dihydrogen.[53,55] The second diphosphine exerted electronic control on the system. Initially the use of dppm was not sufficient for the heterolytic cleavage of dihydrogen which is why the electron-withdrawing analogue, bppm was used with success. The electron-withdrawing nature of the ligand ensured that the dihydrogen molecule, when bound to the manganese centre, is acidic enough to allow for deprotonation by the pendant amine or an exogenous base.

The route to coordinate the second diphosphine was the photolysis of [Mn(PNP)$(CO)_3$Br] and either dppm and bppm to form the corresponding *trans*-manganese complex (**4.4**, Scheme 4.5). Following reaction conditions for analogous complexes, the photolysis reaction was attempted with the novel [Mn($P^{R'}N^RP^{R'}$)$(CO)_3$Br] (PR' = *s*-PhobP or CgP, R = Me, iPr, Bn) complexes formed. All combinations of Mn complex and dppm or bppm were tried in both toluene and fluorobenzene and in both pyrex and quartz glassware. Unfortunately, all attempts to form the desired products were unsuccessful. Only partial conversion (< 50%) of starting material was seen by analysis of the $^{31}P\{^1H\}$ NMR spectra. The remaining $^{31}P\{^1H\}$ NMR signals observed did not correspond to signals which would be expected for the desired product. The products could not be not separated and identified.

It was unexpected that the dppm ligand would fail to coordinate, as several analogues had been made by this method in good yields.[55] However, it is known that bppm converts to an unidentified product under photolysis conditions, and this was expected to cause

complications.[53] Bullock *et al.* reported that the addition of a catalytic amount of $NaBAr^F_4$ reversed this transformation and allowed the coordination to Mn under photolysis conditions. With this in mind, the reactions were repeated with the addition of $NaBAr^F_4$ but this made no change to the reaction outcome described above.

Trimethylamine *N*-oxide (TMAO) is a common reagent used in organometallic chemistry to aid the substitution of carbonyl ligands by a decarbonylation mechanism.[56] The $[Mn(P^{R'}N^RP^{R'})(CO)_3Br]$ (PR' = *s*-PhobP or CgP, R = Me, iPr, Bn) were combined with TMAO in dichloromethane but no reaction was seen after 2 days at 40 °C. After this time crystals of TMAO precipitated out from the reaction mixture so longer reaction times could not be investigated.

The chemistry of manganese tricarbonyl cation $[Mn(P^{Ph}N^{Me}P^{Ph})(CO)_3]^+$ has been studied and did not show reactivity with dihydrogen making it unsuitable as a hydrogen oxidation electrocatalyst.[53] It was thought that the novel complexes employing the *s*-PhobP and the CgP phosphorus groups were worth exploring to see how their unusual stereoelectronic properties effects the reactivity of manganese tricarbonyl complex $[Mn(PNP)(CO)_3]^+$ with dihydrogen. The properties of the CgP group, being both sterically bulky and relatively electron withdrawing, would be advantageous and mean that the second electron withdrawing diphosphine may not be necessary.

4.5 Formation of Manganese Cationic Complexes

In order to react with dihydrogen or other small molecules, the bromide ligand needs to be abstracted from $[Mn(P^{R'}N^RP^{R'})(CO)_3Br]$ to form a coordinatively unsaturated species. For the analogues studied previously the bromide was abstracted by treatment of [Mn(PNP)(**L**)Br] (**L** = dppm or bppm) with one equivalent of $NaBAr^F_4$. The attempted formation of cationic complexes from the novel $[Mn(P^{R'}N^RP^{R'})(CO)_3Br]$ complexes and their subsequent reaction with small molecules is described below.

4.5.1 Formation of Cationic Complexes $[Mn(P^{Phob}N^{R}P^{Phob})(CO)_3]^+$

The reaction of $[Mn(P^{Phob}N^{R}P^{Phob})(CO)_3Br]$ (R = Me, iPr, Bn) and one equivalent of $NaBAr^F_4$ in fluorobenzene resulted in the immediate formation of a bright yellow solution and a white precipitate (Scheme 4.6). The reaction mixture showed one singlet in the $^{31}P\{^1H\}$ NMR spectrum which has shifted upfield with respect to the bromide precursor (Table 4.2). This is indicative of the ^{31}P nuclei being in a four-membered ring.[57] This result, along with the precipitation of the NaBr, suggests the quantitative formation of $[Mn(\kappa^3\text{-}P^{Phob}N^{R}P^{Phob})(CO)_3][BAr^F_4]$. The chemical shift differences for these complexes are smaller than for the analogous complex $[Mn(P^{Ph}N^{Me}P^{Ph})(CO)_3]^+$ ($\Delta\delta$ = 24.4 ppm).[53] A more pronounced colour change was also expected (yellow to dark blue or red seen for mixed bis(diphosphine) complexes) but this difference may be due to the absence of a second diphosphine ligand.[53,55]

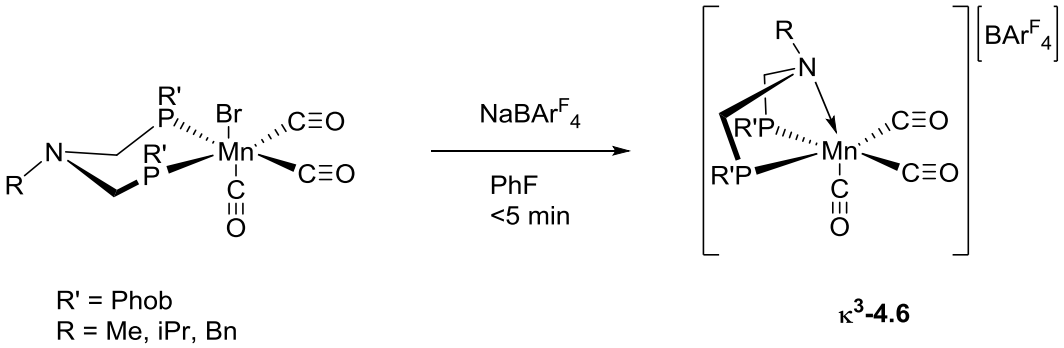

Scheme 4.6: Reaction of $[Mn(P^{Phob}N^{R}P^{Phob})(CO)_3Br]$ and $NaBAr^F_4$ to form tuck-in complex **κ^3-4.6**.

Table 4.2: Differences in $^{31}P\{^1H\}$ NMR chemical shifts between $[Mn(P^{Phob}N^{R}P^{Phob})(CO)_3Br]$ and $[Mn(P^{Phob}N^{R}P^{Phob})(CO)_3][BAr^F_4]$.

R	$^{31}P\{^1H\}$ δ_P (ppm) of $[Mn(P^{Phob}N^{R}P^{Phob})(CO)_3Br]$[a]	$^{31}P\{^1H\}$ δ_P (ppm) of $[Mn(P^{Phob}N^{R}P^{Phob})(CO)_3][BAr^F_4]$[b]	$\Delta\delta_P$ (ppm)
Me	4.4	−7.9	−12.3
iPr	9.5	−6.1	−15.6
Bn	7.6	−5.1	−12.7

[a] $^{31}P\{^1H\}$ NMR spectrum recorded in $CDCl_3$. [b] $^{31}P\{^1H\}$ NMR spectrum recorded in PhF.

The molecular structure of $[Mn(\kappa^3\text{-}P^{Phob}N^{Me}P^{Phob})(CO)_3]^+$ is shown in Figure 4.11 and confirms the formation of the cationic tuck-in complex where the nitrogen is bound to the manganese centre. The structure shows distorted octahedral geometry were the N-Mn-CO bond angle deviates from the expected 180° (163.34(7)°). The Mn-N bond (2.1554(14) Å) is considerably shorter than those reported by Bullock *et al.* (~ 2.30 Å)

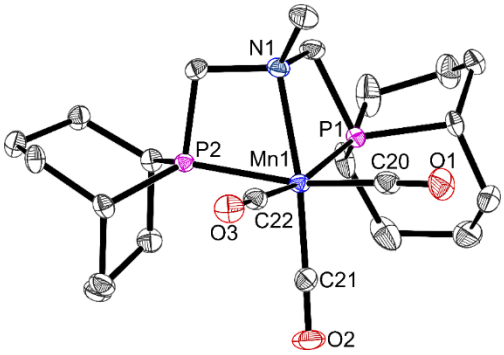

Figure 4.11: Crystal structure of $[Mn(\kappa^3\text{-}P^{Phob}N^{Me}P^{Phob})(CO)_3]^+$. Thermal ellipsoids at 50%. Hydrogen atoms and $[BAr^F{}_4]$ counterion omitted for clarity. Selected bond lengths (Å) and angles (°): Mn1-N1 2.1554(14); Mn1-P1 2.2900(5), Mn1-P2 2.3037(5); Mn1-C20 1.8228(19); Mn1-C21 1.8085(18); Mn1-C22 1.8298(19); P1-Mn1-P2 93.104(18); N1-Mn1-C21 163.34(7).

but is more akin to a typical Mn^I-N(sp^3) bond (2.17 Å).[53] The short length of this bond implies relatively strong binding of the N to the Mn. This may inhibit binding of small molecules if the κ^2-binding mode cannot be accessed (See Section 4.5.1.1 below).

4.5.1.1 Reaction of $[Mn(P^{Phob}N^RP^{Phob})(CO)_3]^+$ with Dihydrogen

The *in situ* formed cationic complexes $[Mn(\kappa^3\text{-}P^{Phob}N^RP^{Phob})(CO)_3]^+$ were subjected to dihydrogen (1 bar). No reaction was seen at room temperature or when heated to reflux in fluorobenzene for 1 week. Abstraction of bromide from $[Mn(P^{Phob}N^RP^{Phob})(CO)_3Br]$ was also carried out under a dihydrogen atmosphere but this gave the same results and the only products were the cationic complexes $[Mn(\kappa^3\text{-}P^{Phob}N^RP^{Phob})(CO)_3]^+$. The cationic complexes $[Mn(\kappa^3\text{-}P^{Phob}N^RP^{Phob})(CO)_3]^+$ were also exposed to ethene, CO_2 and phenylacetylene but showed no reactivity with any of these common FLP substrates.

These observations led to the conclusion that $[Mn(P^{Phob}N^RP^{Phob})(CO)_3]^+$ would not be suitable for small molecule activation or as a dihydrogen oxidation electrocatalyst due to the formation of a stable tuck-in complex. The κ^3-complex appears to be highly stable, and variable temperature NMR studies showed no change in the $^{31}P\{^1H\}$ NMR signal over a wide temperature range (−35 °C – 75 °C).

4.5.2 Attempted Formation of Cationic Complexes $[Mn(P^{Cg}N^RP^{Cg})(CO)_3]^+$

The reaction of $[Mn(P^{Cg}N^RP^{Cg})(CO)_3Br]$ (R = Me, iPr, Bn) and one equivalent of $NaBAr^F{}_4$ in fluorobenzene resulted in the complete dissolution of the sparingly soluble starting material and no precipitation of salt was seen. For all variants, there was no major

shift in the $^{31}P\{^{1}H\}$ NMR resonances for either the *rac* or *meso* isomers but surprisingly the signals became much more resolved (Figure 4.12). The coupling between the two inequivalent phosphorus nuclei in the *rac* isomer was now completely resolved at room temperature (Figure 4.12). A summary of the $^{31}P\{^{1}H\}$ NMR data for the series is presented in Table 4.3.

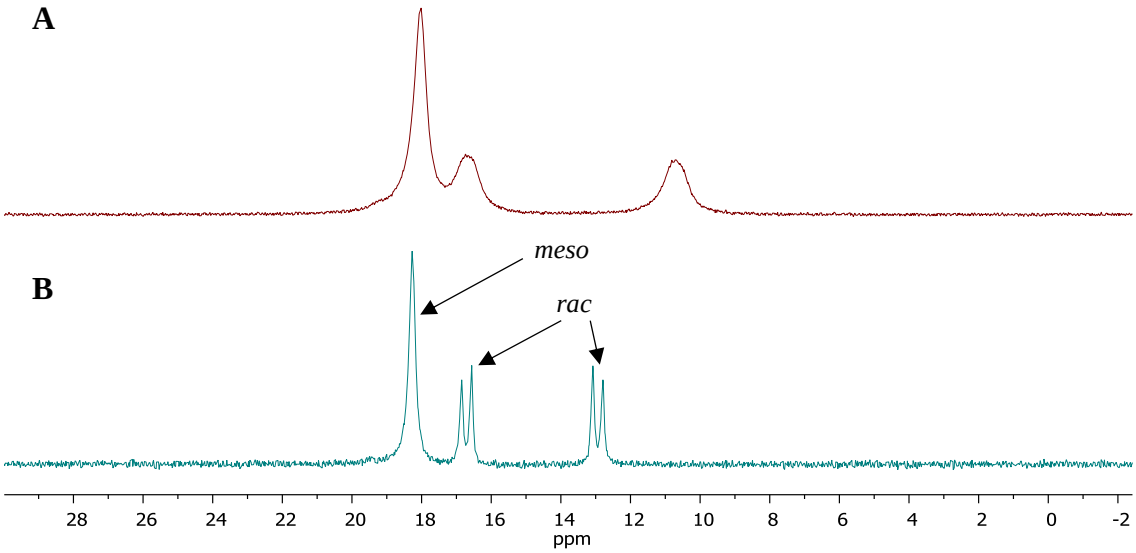

Figure 4.12: $^{31}P\{^{1}H\}$ NMR spectrum of (A) $[Mn(P^{Cg}N^{iPr}P^{Cg})(CO)_3Br]$ and (B) the reaction mixture of $[Mn(P^{Cg}N^{iPr}P^{Cg})(CO)_3Br]$ and $NaBAr^{F}_4$.

Table 4.3: $^{31}P\{^{1}H\}$ NMR data between $[Mn(P^{Cg}N^{R}P^{Cg})(CO)_3Br]$ and the reaction mixture of $[Mn(P^{Cg}N^{R}P^{Cg})(CO)_3Br]$ and $NaBAr^{F}_4$.

R	$^{31}P\{^{1}H\}$ δ_P (ppm) of $[Mn(P^{Cg}N^{R}P^{Cg})(CO)_3Br]$[a]		$^{31}P\{^{1}H\}$ δ_P (ppm) of $[Mn(P^{Cg}N^{R}P^{Cg})(CO)_3][BAr^{F}_4]$[b]		$^{2}J_{PP}$ (Hz)
	meso	*rac*	*meso*	*rac*	
Me	18.9	16.9, 11.3	19.0	17.4, 13.4	45.8
iPr	18.0	16.7, 10.7	17.7	17.6, 13.1	46.7
Bn	18.8	16.2, 11.3	18.6	15.5, 13.3	45.0

[a] $^{31}P\{^{1}H\}$ NMR spectrum recorded in $CDCl_3$. [b] $^{31}P\{^{1}H\}$ NMR spectrum recorded in PhF.

It was noted that the downfield resonance of the *rac* isomer does not shift significantly but the upfield resonance shifts at least 2 ppm downfield. This observed resolution of the $^{31}P\{^{1}H\}$ NMR resonances at room temperature compared to the starting bromide precursor indicates the loss of the dynamic behaviour on the NMR timescale which was proposed to be the reason for the observed broadening of $[Mn(P^{Cg}N^{R}P^{Cg})(CO)_3Br]$. There was no precipitation of NaBr which suggested that the bromide ligand has not been abstracted from the metal centre. The product was crystallised from the reaction mixture and its molecular structure is shown in Figure 4.13.

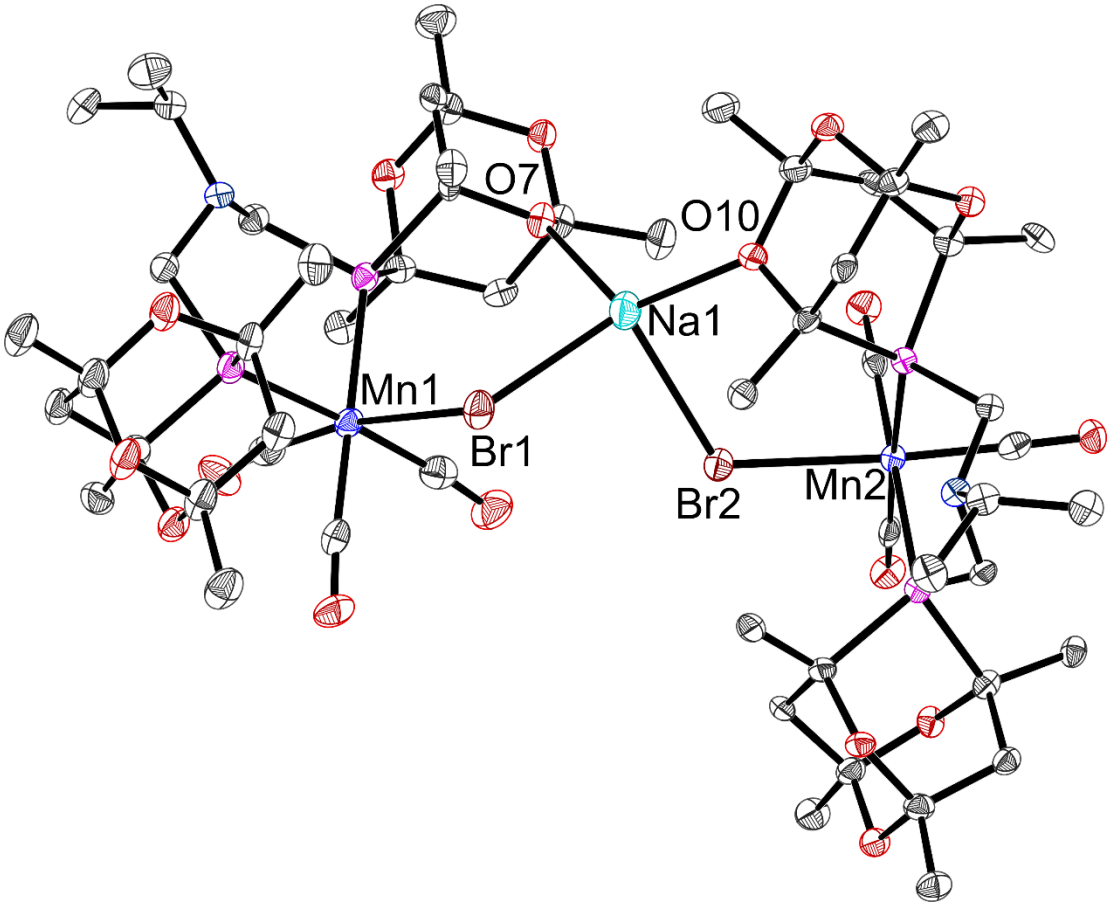

Figure 4.13: Crystal structure obtained from the reaction mixture of [Mn($P^{Cg}N^{iPr}P^{Cg}$)$(CO)_3$Br] and Na BAr^F_4 in fluorobenzene. Thermal ellipsoids at 50%. Hydrogen atoms, $NaBAr^F_4$ counterion, and co-crystallised solvent molecules (PhF and pentane) omitted for clarity. Both Mn complexes are the *rac* isomer. Selected bond lengths (Å) and angles (°): Mn1-Br1 2.5652(7), Mn2-Br2 2.5509(7), Br1-Na1 2.7890(16), Br2-Na1 2.8736(16), Na1-O7 2.359(3), Na1-O10 2.303(3), O7-Na1-Br1 97.59(8), O7-Na1-O10 122.53(11), O10-Na1-Br2 94.04(8), Br1-Na1-Br2 96.18(5).

The two Mn moieties in this crystal structure are *rac*-[Mn($P^{Cg}N^{iPr}P^{Cg}$)$(CO)_3$Br]. The sodium cation appears to be bridging two Mn entities by coordination to oxygens in the CgP structure and the two bromide ligands and the Na has pseudo-tetrahedral geometry. Although it cannot be confirmed whether this species exists in solution, it does provide an explanation for the observations described above. The starting bromide precursor is only sparingly soluble in fluorobenzene, but after 10 minutes the reaction mixture is completely homogenous. The presence of the sodium ion bridging two complexes may be the reason for the dissolution. NaBr did not precipitate from the reaction mixture which is also consistent with this structure. The Mn-Br bond length in the bromide precursor (Figure 4.9) and the structure presented in Figure 4.13 are not significantly different, indicating that although the Na atom is interacting with the bromide ligands the Mn-Br bond has not been significantly weakened (2.5640(3) Å *vs*. 25652(7) and 2.5509(7) Å).

4.6 Reaction of $[Mn(P^{Cg}N^{R}P^{Cg})(CO)_3Br]/NaBAr^{F}_4$ Mixtures with Dihydrogen

All of the dihydrogen activation experiments described in this section were carried out with one equivalent of $[Mn(P^{Cg}N^{R}P^{Cg})(CO)_3Br]$ and one equivalent of $NaBAr^{F}_4$ in either PhF or d_5-PhCl at room temperature unless stated otherwise. It was noted that the starting materials are only partially soluble in d_5-PhCl. This mixture was subjected to 1 bar of H_2 in a Youngs NMR tube. Full experimental details are given in Chapter 5.

Although the exact structure of the species formed in solution upon combination of $[Mn(P^{Cg}N^{R}P^{Cg})(CO)_3Br]$ (R = Me, iPr, Bn) and $NaBAr^{F}_4$ was unknown (See Section 4.5.2), the reaction of this mixture with dihydrogen was investigated. No distinctive colour change was observed when the reaction mixture was subjected to 1 bar of dihydrogen. When the reactions were carried out in fluorobenzene, the homogenous solution slowly became cloudy over time. The appearance of a small amount of precipitate was presumed to be due to the formation of NaBr. This was difficult to observe when the reaction was carried out in d_5-PhCl due to the insolubility of the starting material although it was likely to also have occurred.

When using $[Mn(P^{Cg}N^{Me}P^{Cg})(CO)_3Br]$ as the starting Mn complex, partial reactivity with dihydrogen was seen due to the presence of amine and hydride peaks in the ^{1}H NMR spectrum indicating the formation of **4.7** (Scheme 4.7 and Figure 4.14). The amine signal appeared as a broad singlet at δ_H = 9.70 ppm. The hydride signal occurred at around δ_H = −8.0 ppm which was expected for a manganese hydride of this type. The signal for the *meso* isomer was a triplet at δ_H = −7.93 ppm ($^2J_{HP}$ = 55.6 Hz) and the signal for the *rac* isomer was a doublet of doublets at δ_H = −8.04 ppm ($^2J_{HP}$ = 53.9 and 46.6 Hz). The corresponding signals in the $^{31}P\{^1H\}$ NMR spectrum could also be seen at δ_P = 45.9 ppm for the *meso* isomer and two signals at δ_P = 47.6 and 45.7 ppm ($^2J_{PP}$ = 45.5 Hz) as shown in Figure 4.14. This was confirmed by a ^{1}H-^{31}P HMQC NMR spectroscopy experiment. Curiously, a small peak resembling a doublet of doublets was observed at δ_H = −8.69 ppm which were associated with a set of doublets seen at δ_P = 55.5 and 53.8 ppm ($^2J_{PP}$ = 35.6 Hz). There were also some broad signals seen in the range of δ_P = 27 – 10 ppm which were not identified (Figure 4.14). During an attempt to resolve these signals, low

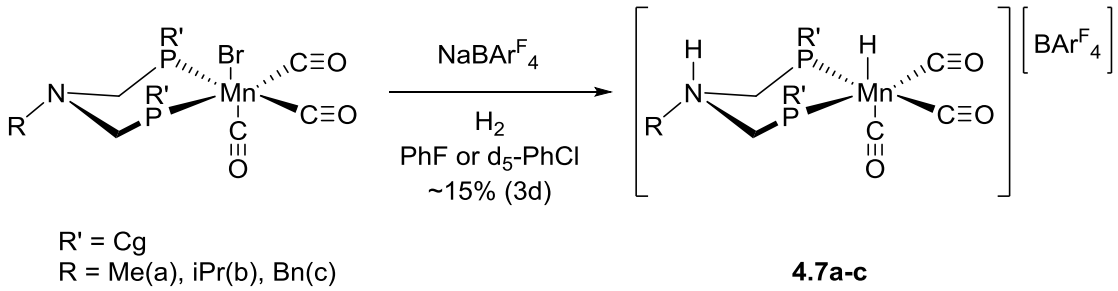

Scheme 4.7: Reaction of [Mn($P^{Cg}N^{R}P^{Cg}$)$(CO)_3$Br]/NaBAr$^F_4$ with H_2.

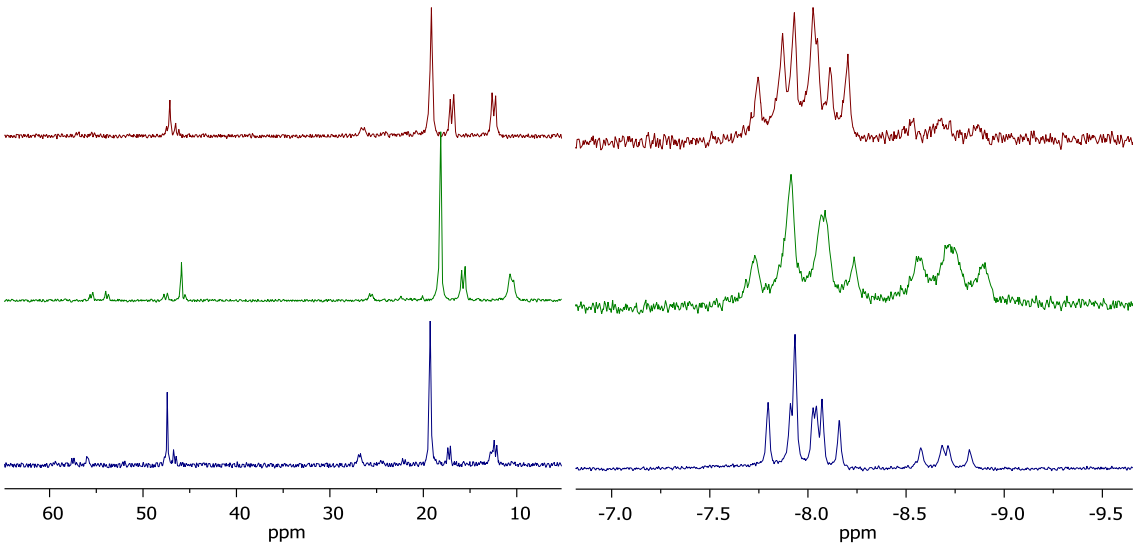

Figure 4.14: $^{31}P\{^1H\}$ NMR (left) and hydride region of ^1H NMR spectrum of [Mn($P^{Cg}N^{Me}P^{Cg}$)$(CO)_3$Br]/NaBAr$^F_4$ reaction with dihydrogen overnight at room temperature (top) −35 °C (middle) and after 3d at room temperature (bottom).

temperature NMR spectroscopy studies revealed an interesting observation. The *rac* hydride species appeared to convert to the unknown hydride species when the solution was cooled to −35 °C (limited due to the freezing point of d_5-PhCl). Also, after the 3d at room temperature the amount of the unknown *rac* hydride species increased (Figure 4.14). It is possible that the protonated nitrogen can invert and result in the formation of *syn* and *anti*-isomers of **4.7a** (Figure 4.15). Bullock *et al.* reported the observation of the

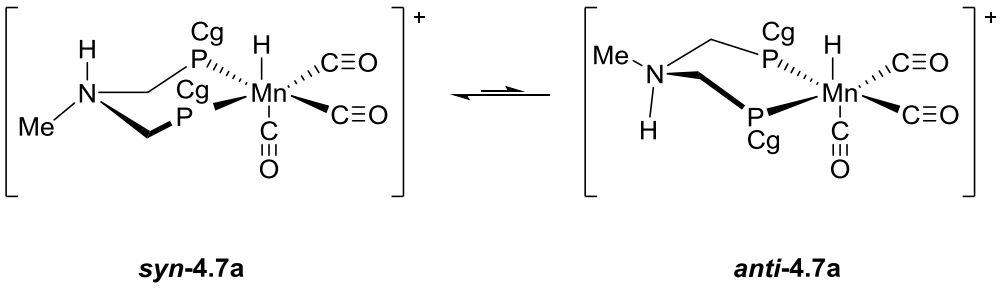

Figure 4.15: Structures and interconversion of the protonation isomers of **4.7a**. *Syn* and *anti* refer to the position of the proton in relation to the hydride.

anti-isomer of $[MnH(P^{Ph}N^{Me}P^{Ph})(H)(bppm)(CO)]^+$ at low temperatures in low abundance but did not report any interconversion at room temperature.[53]

It is curious that only the interconversion of the *rac* isomer is apparently seen. It is possible that the same conversion is happening for the *meso* isomer but at a much lower conversion rate so the hydride and ^{31}P NMR signals were not observed at the temperatures that the NMR spectra were recorded.

Whilst monitoring the reaction, the intensity of a broad peak at $\delta_H = -1.80$ ppm, which was observable after 1 h, and increased over 3 d. This peak was tentatively assigned as the bound dihydrogen complex. One explanation for the increase over time is the slow dissolution into the d_5-PhCl as the dihydrogen molecule binds. After three days there was still some insoluble starting material in the reaction mixture.

Determining the conversion of the starting materials to the dihydrogen heterolysis product was not possible by $^{31}P\{^1H\}$ NMR spectroscopy, but comparison of the $NaBAr^F_4$ signals with the amine proton and the manganese hydride signal in the ^1H NMR spectrum indicated ~15% conversion over 3d. The observation of distinct hydride and protonated amine signals at room temperature point towards the heterolysis of dihydrogen being irreversible. If the process were reversible and rapidly exchanging, it would be expected that a resonance at the average of the chemical shift of the static hydride and protonated amine would be observed. The average of the two observed signals (assuming these are static) would lie underneath the resonances for the $P^{Cg}N^{Me}P^{Cg}$ ligand. From the data available the absence of a reversible process cannot be ruled out.

When using $[Mn(P^{Cg}N^{iPr}P^{Cg})(CO)_3Br]$ as the starting Mn complex, conversion to **4.7b** occurred after 1 hour and increased to 20% conversion over 3 days (Scheme 4.7). Similar observations to those described above for R = Me were seen (Figure 4.16). At room temperature overnight, the protonated amine peak (δ_H = 9.56 ppm) and manganese hydride ($\delta_H = -7.95$ ppm ($^2J_{HP}$ = 55.3 Hz, *meso*), −7.90 ($^2J_{HP}$ = 50.7 and 49.5 Hz, *rac*)) are observed. In the $^{31}P\{^1H\}$ NMR spectrum, a multiplet at δ_P = 45.8 ppm was confirmed to be the corresponding signal for both the *meso* and *rac* isomers by ^1H-^{31}P HMQC. Low temperature NMR studies revealed the formation of a second *rac* hydride species, analogous to before but at an even lower conversion (Figure 4.16). Even after 3 days only a very small amount of this species could be seen at room temperature. Due to the low abundance of *anti*-**4.7b**, a cross peak between the hydride signal at $\delta_H = -8.67$ and a

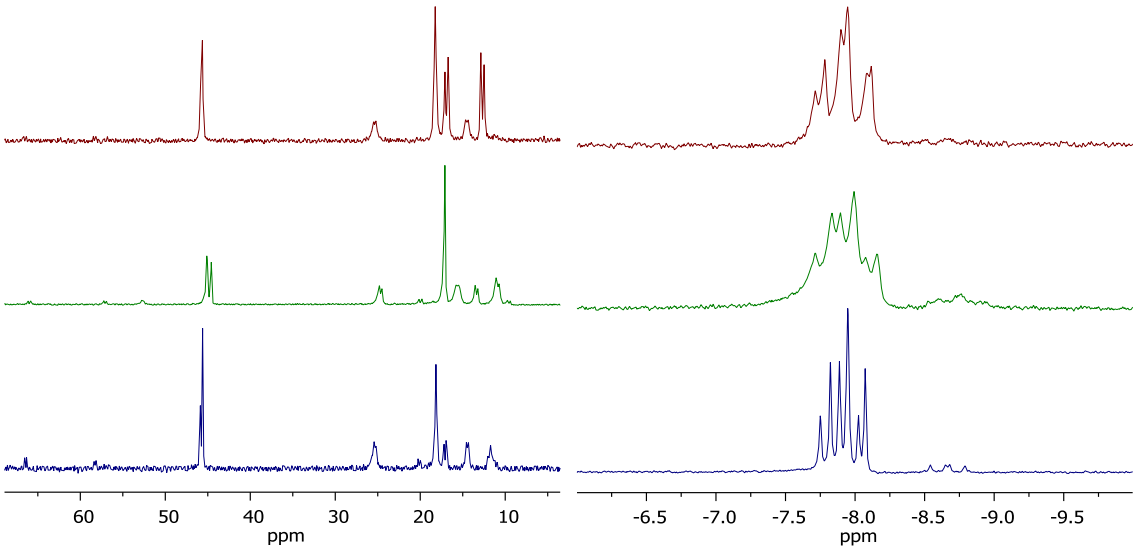

Figure 4.16: $^{31}P\{^{1}H\}$ NMR (left) and hydride region of ^{1}H NMR spectrum of $[Mn(P^{Cg}N^{iPr}P^{Cg})(CO)_3Br]/NaBAr^{F}_4$ reaction with dihydrogen overnight at room temperature (top) −35 °C (middle) and after 3d at room temperature (bottom).

$^{31}P\{^{1}H\}$ NMR signal was not observed but the doublets at δ_P = 66.5 and 58.3 ppm are assumed to be associated with the *anti*-isomer of **4.7b** (Figure 4.16).

Broad signals were observed in the $^{31}P\{^{1}H\}$ NMR spectrum between δ_P = 28 – 10 ppm which are similar to those seen previously when R = Me and remain unassigned (Figure 4.16). A broad singlet in the ^{1}H NMR spectrum at δ_H = −1.82 ppm increases over time and is not observed in the first 24 h of the reaction. This is again assumed to be the bound dihydrogen complex, but this appears to have a slower rate of formation for R = iPr compared to when R = Me.

When using $[Mn(P^{Cg}N^{Bn}P^{Cg})(CO)_3Br]$ as the starting Mn complex, the formation of **4.7c** was seen after 1 hour and reached 30% conversion after 3 days (Scheme 4.7). The protonated amine peak is seen at δ_H = 9.65 ppm and the *meso* and *rac* hydride peaks appear as a multiplet at δ_H = −7.91 ppm. The individual peaks overlap and coupling constants could not be extracted from the data collected. The corresponding $^{31}P\{^{1}H\}$ NMR signals were observed at δ_P = 46.7 ppm for the *meso* isomer and two doublets at δ_P = 46.3 and 45.3 ppm ($^{2}J_{PP}$ = 46.1 Hz) for the *rac* isomer. Interestingly, even at low temperatures and after 3 days, there was no evidence of conversion to the *anti*-isomer of **4.7c** in the ^{1}H NMR or the $^{31}P\{^{1}H\}$ NMR spectra. The hydride signal for the *anti,rac*-isomer (δ_H = −8.63 ppm) was only observed after the reaction mixture was left at room temperature for 6 days, but was still in a very small quantity. There is also a very small peak, only just distinguishable from the baseline, at δ_H = −2.66 ppm in the ^{1}H NMR

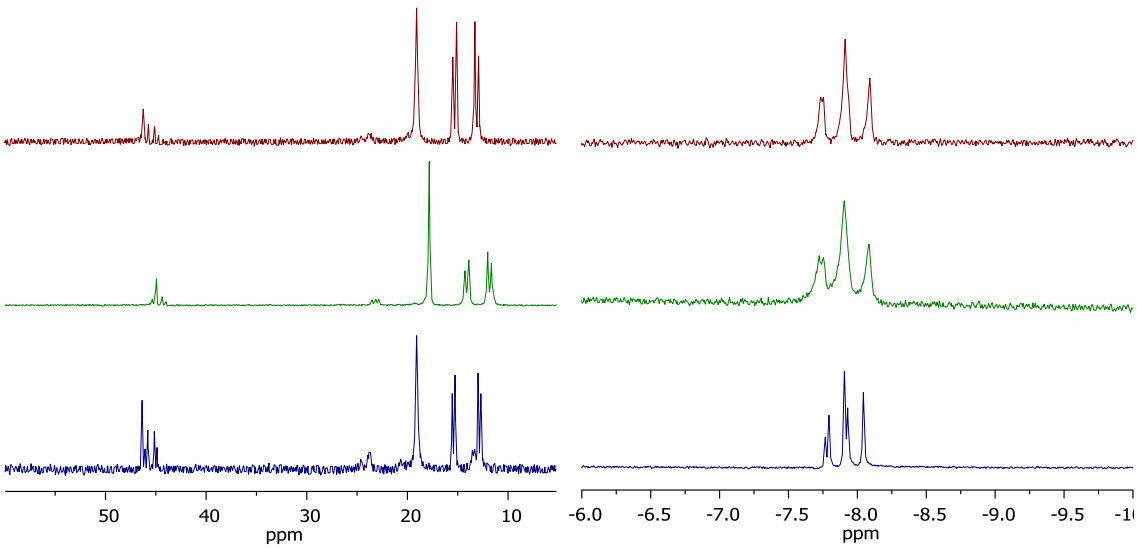

Figure 4.17: $^{31}P\{^{1}H\}$ NMR (left) and hydride region of ^{1}H NMR spectrum of $[Mn(P^{Cg}N^{Bn}P^{Cg})(CO)_3Br]/NaBAr^{F}{}_4$ reaction with dihydrogen overnight at room temperature (top) −35 °C (middle) and after 3d at room temperature (bottom).

spectrum which is tentatively attributed to the bound dihydrogen complex. Broad peaks seen in the $^{31}P\{^{1}H\}$ NMR spectrum between δ_P = 25 – 11 ppm are again unidentified species but could be attributed to the suspected bound dihydrogen complex (Figure 4.17).

The difference in the quantity of ***anti*-4.7** formed at low temperature and over time can be rationalised due to the difference in the sterics of the nitrogen substituent. Benzyl being the largest substituent, does not convert to the *anti*-isomer for at least 6 days whereas when the substituent is a methyl group, the smallest substituent tested, formation of the *anti*-isomer was seen within hours. The conversion between the *syn*- and *anti*-isomer must occur *via* an intramolecular process where the amine is deprotonated (presumably by the starting $[Mn(P^{R'}N^{R}P^{R'})(CO)_3Br]$ complex), the nitrogen centre then inverts and is then reprotonated. This fits with the observation that this conversion is slower with bulky nitrogen substituents as it will be sterically more difficult to deprotonate the amine to allow inversion of the nitrogen centre.

Due to the melting point of d_5-PhCl, lower temperatures could not be reached to investigate if the *anti*-isomer could be observed for **4.7c**. An alternative was to carry out the reaction in d_2-DCM. This proved to be problematic and led to decomposition and only a minute amount of conversion to **4.7**. This correlates with the stability of analogous cationic complexes studied by Bullock *et al*.[53] The tricarbonyl species that were previously investigated were stable in DCM solutions but the bis-diphosphine cations displayed varying levels of decomposition including the isolation of a *trans*-dicarbonyl

species [Mn($P^{Ph}N^{Me}P^{Me}$)$(CO)_2$(bppm)]. The comparable tetracarbonyl species [Mn($P^{Cg}N^{Me}P^{Cg}$)$(CO)_4$] was isolated from a reaction mixture of [Mn($P^{Cg}N^{Me}P^{Cg}$)$(CO)_3$Br]/$NaBAr^F_4$ with H_2 conducted in DCM which displays the instability of the cationic species formed in dihydrogen activation (Figure 4.18).

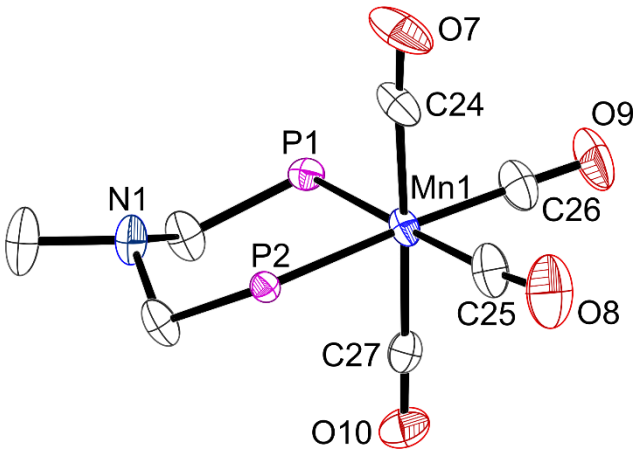

Figure 4.18: Crystal structure obtained from the reaction mixture of [Mn($P^{Cg}N^{Me}P^{Cg}$)$(CO)_3$Br]/$NaBAr^F_4$ with H_2 in DCM. Thermal ellipsoid at 50%. Hydrogen atoms and $NaBAr^F_4$ counterion omitted for clarity. Phosphorus substituents truncated for clarity due to a high level of disorder. Selected bond lengths (Å) and angles (°): Mn-P1 2.3697(8); Mn-P2 2.3665(7); Mn1-C24 1.857(3); Mn1-C25 1.847(3); Mn1-C26 1.838(3); Mn1-C27 1.865(3); C24-Mn1-C27 177.58(14).

4.7 Hydrogen Oxidation Electrocatalysis Testing

Electrochemical experiments detailed in this Section were carried out by the author under the supervision of Dr G. M. Chambers at the Pacific National Northwest Laboratories in collaboration with Professor R. M. Bullock.

Previous work by Bullock and DuBois *et al.* details successful hydrogen oxidation catalysts involving nickel, iron and manganese bearing either PNP or P_2N_2 ligands.[6,13,14,50,58,59] The proposed catalytic cycles for the oxidation of dihydrogen involve alternating chemical (C) and electrochemical steps (E). An example CECE pathway is shown in Figure 4.19 where the electrocatalysis occurs in the presence of an exogenous base, such as 2,6-lutidine, for a $[Mn^I(PNP)]^+$ complex.[6]

Firstly, the PNP ligand interconverts between the κ^3 and κ^2 coordination modes (Step 1) under catalytic conditions to allow for binding of dihydrogen (Step 2). The first chemical step is the heterolysis of H_2 (Step 3) followed by deprotonation by an exogeneous base (Step 4) to form a neutral Mn^I-H. The first electrochemical step is oxidation of this

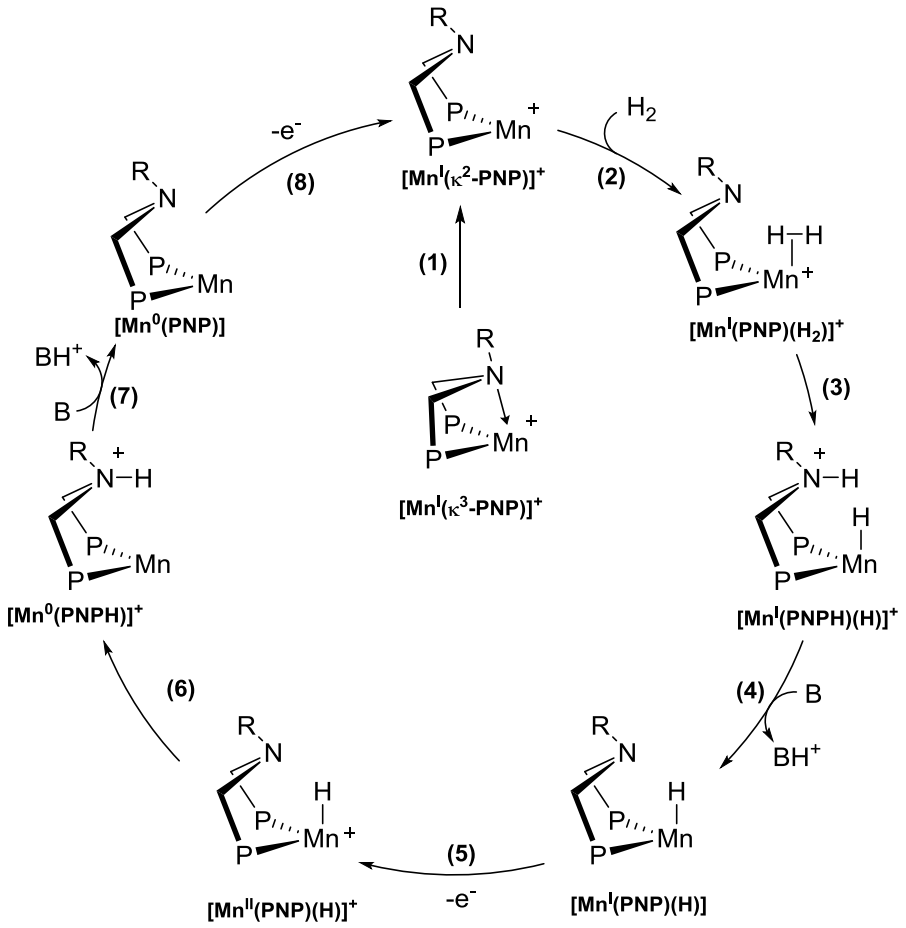

Figure 4.19: Proposed catalytic cycle for the electrocatalytic oxidation of dihydrogen by $[Mn(PNP)(L)_3]^+$ with an exogeneous base. For clarity the phosphine substituents and other Mn bound ligands are omitted.

species (Step 5) to form a Mn^{II}-H. There are now two possible pathways, the first being the intramolecular deprotonation of the Mn^{II}-H (Step 6) with subsequent deprotonation by an exogeneous base (Step 7) and the second being the direct deprotonation of the Mn^{II}-H to form the neutral Mn^0 species. Computational studies on the manganese and iron catalytic cycles showed that although both pathways were endergonic, the second pathway has a much higher activation barrier. This intramolecular deprotonation was proposed to be the rate-determining step for the catalytic cycle. The final step is the oxidation of the Mn^0 species back to the Mn^I species (Step 8) to complete the cycle.

The $[Mn(P^{Phob}N^{R}P^{Phob})(CO)_3]^+$ (R = Me, iPr, Bn) series was thought to be unsuitable for hydrogen oxidation electrocatalysis because no reaction with dihydrogen was observed at room temperature (see Section 4.5.1.1). This was thought to be due to the formation of a strong manganese-nitrogen bond in the κ^3 coordination mode of the PNP ligand which does not interconvert with the κ^2 coordination mode that is needed for the initial binding of H_2. The cyclic voltammogram for $[Mn(P^{Phob}N^{Me}P^{Phob})(CO)_3][BAr^F{}_4]$ in PhF

at 100 mV/s scan rate is shown in Figure 4.20 and is representative of what happened for all of the species in the series. The $Mn^{I/0}$ and $Mn^{0/-}$ redox couples were observable around −1.55 V and −1.94 V respectively vs $Cp_2Fe^{+/0}$ (Cp = η^5-cyclopentadienyl) but they did not appear to be stable as both exhibited irreversible waves, even at faster scan rates (1 V/s). No change was seen when a hydrogen atmosphere and base (either triethylamine or *N*,*N*-diisopropylethylamine) were added, meaning that the $[Mn(P^{Phob}N^{R}P^{Phob})(CO)_3]^+$ series are not electrocatalysts for the oxidation of H_2.

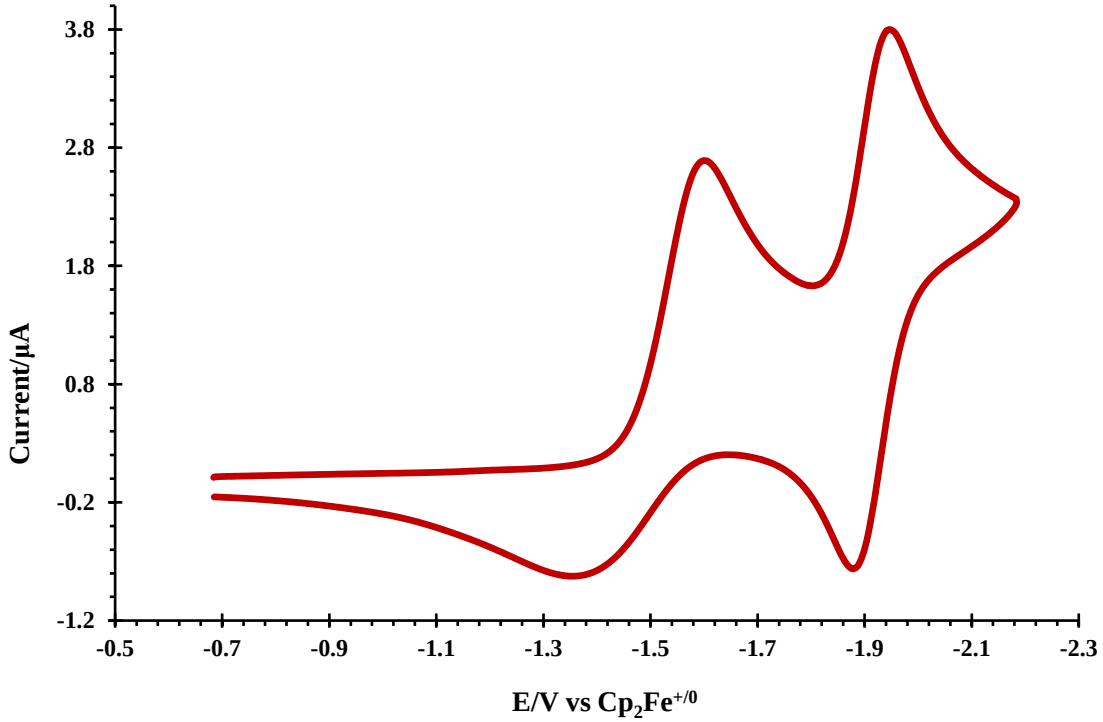

Figure 4.20: Cyclic voltammogram of $[Mn(P^{Phob}N^{iPr}P^{Phob})(CO)_3][BAr^F_4]$ in PhF with 0.1 M $[NBu_4][B(C_6F_5)_4]$ at 100 mV/s referenced to $Cp_2Fe^{+/0}$.

Before any electrochemical event occurs in the catalytic cycle the Mn^IH is formed and previous studies have shown that this species is also a successful catalyst for the electrocatalytic oxidation of H_2. For this reason, the corresponding manganese hydrides **4.9** were formed by reaction of the starting bromide precursor with $LiAlH_4$ (Scheme 4.8). The Mn^IH products displayed the expected triplet resonance in the hydride region of the ^1H NMR spectrum and a downfield shift in the $^{31}P\{^1H\}$ NMR spectrum.

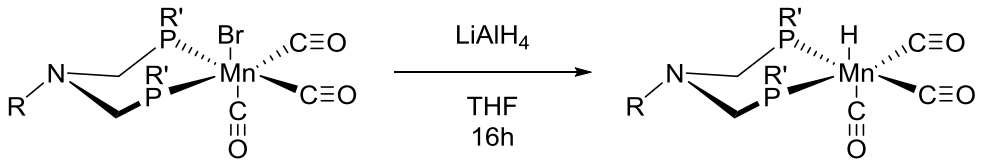

R' = Phob
R = Me, iPr, Bn

4.9

Scheme 4.8: Formation of [Mn($P^{Phob}N^{R}P^{Phob}$)$(CO)_3$(H)] by reaction of [Mn($P^{Phob}N^{R}P^{Phob}$)$(CO)_3$Br] with $LiAlH_4$.

A representative cyclic voltammogram of [Mn($P^{Phob}N^{R}P^{Phob}$)$(CO)_3$(H)] in PhF under the same electrocatalytic conditions described above is shown in Figure 4.21. An irreversible oxidation peak is observed at about 0.38 V vs $Cp_2Fe^{+/0}$. The further decrease in current was due to the beginning of base oxidation as the potential is decreased. This unfortunately convolutes the trace and it cannot be said with certainty that the oxidation is completely irreversible. The data suggests that an irreversible chemical event has occurred resulting in the shutdown of any potential catalysis. It is thought that the $Mn^{I}H$ is oxidised and then deprotonated intramolecularly to form the protonated amine. This species is then deprotonated by the external base and once the nitrogen lone pair is free the immediate formation of the stable, inert κ^3-complex is formed irreversibly which has already been shown to be inactive for hydrogen oxidation electrocatalysis.

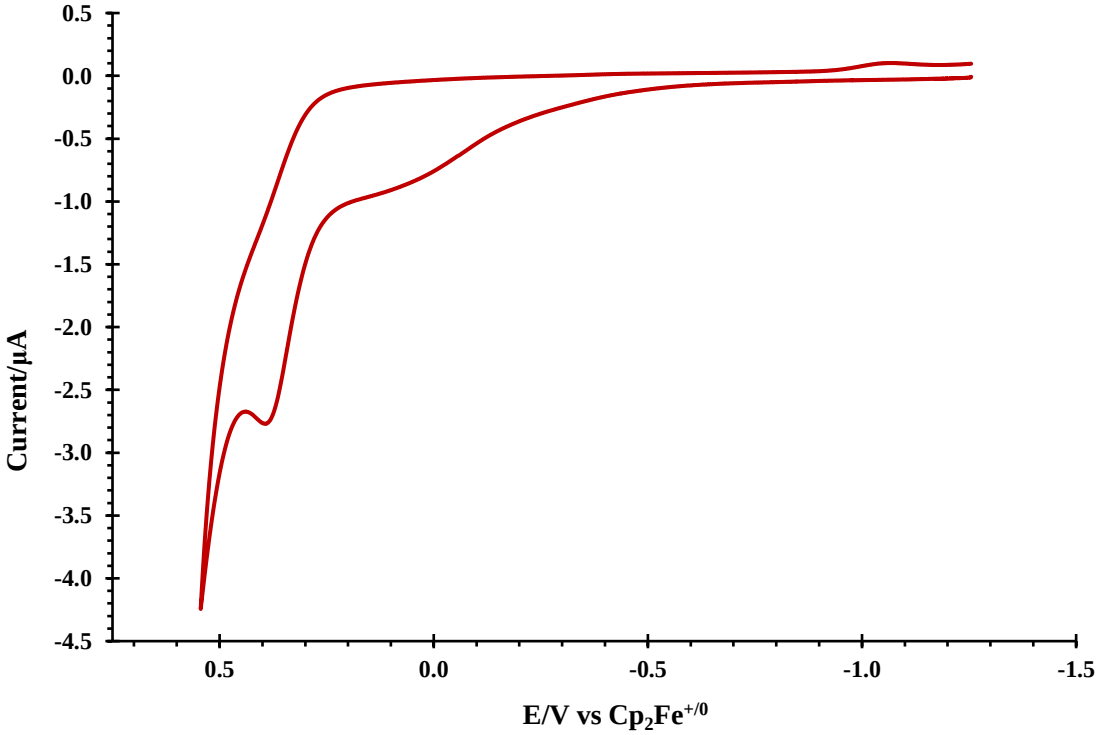

Figure 4.21: Cyclic voltammogram of [Mn($P^{Phob}N^{Me}P^{Phob}$)$(CO)_3$(H)] under 1 atm H_2 with added *N*,*N*-diisopropylethylamine in PhF with 0.1 M [NBu_4][$B(C_6F_5)_4$] at 100 mV/s referenced to $Cp_2Fe^{+/0}$.

The manganese series which employs the $P^{Cg}N^{R}P^{Cg}$ ligands displayed very different electrochemistry to the series with $P^{Phob}N^{R}P^{Phob}$. Although the formation of the cationic species $[Mn(P^{Cg}N^{R}P^{Cg})(CO)_3]^+$ was not successful, the mixture of the starting bromide complex $[Mn(P^{Cg}N^{R}P^{Cg})(CO)_3Br]$ and $NaBAr^{F}_4$ reacted with dihydrogen (Section 4.6). A representative cyclic voltammogram of $[Mn(P^{Cg}N^{R}P^{Cg})(CO)_3Br]/NaBAr^{F}_4$ in PhF under the same electrocatalytic conditions described above is shown in Figure 4.22. An irreversible redox event at about 0.69 V vs $Cp_2Fe^{+/0}$ was attributed to the oxidation of the starting bromide complex. The large quantity of this species in solution meant that any other redox events were not discernible, and no conclusions could be drawn about whether there was any electrocatalysis of oxidation of dihydrogen. The amount of the $[Mn(P^{Cg}N^{R}P^{Cg})(CO)_3Br]$ in the mixture observed by CV corresponds to what was seen when the dihydrogen activation experiments were run on this system, where analysis of the $^{31}P\{^{1}H\}$ NMR spectrum showed the bromide complex to be the major (> 95%) species in solution after 1 h. This series does exhibit H_2 heterolysis, although not with full conversion of the starting material to desired product. It was thought that, as shown previously, that the Mn^{I}-H might serve as a suitable catalyst for the electrocatalytic oxidation of H_2. However, the formation of $[Mn(P^{Cg}N^{R}P^{Cg})(CO)(H)]$ by reaction of

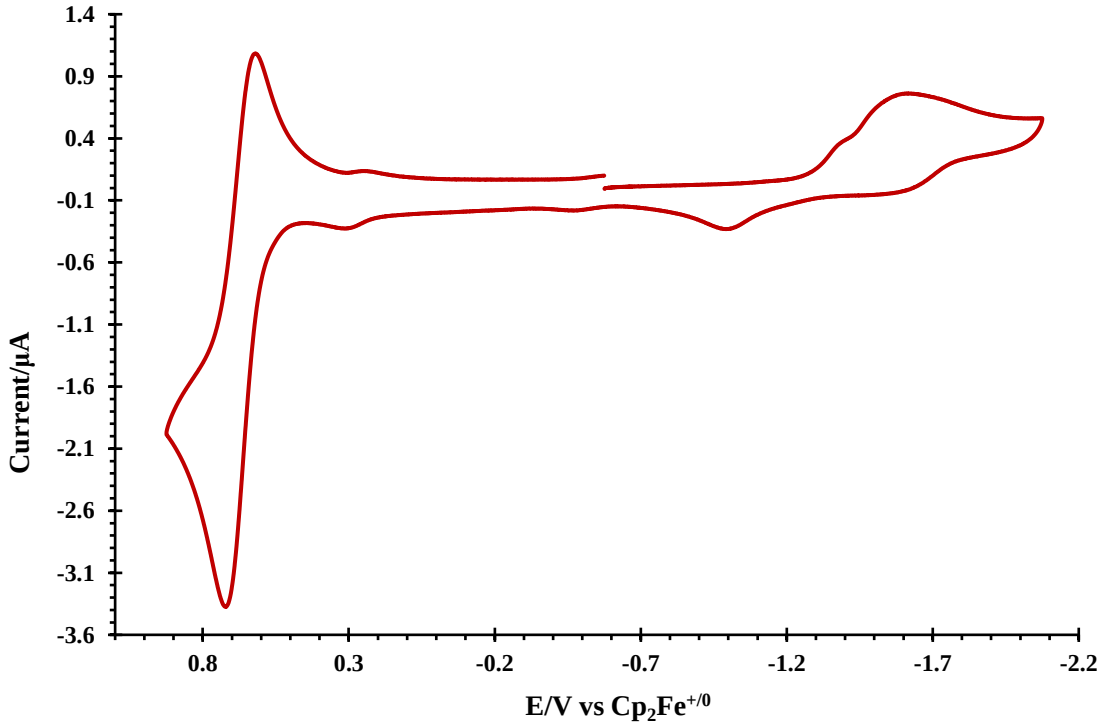

Figure 4.22: Cyclic voltammogram of $[Mn(P^{Cg}N^{Me}P^{Cg})(CO)_3Br]/NaBAr^{F}_4$ under 1 atm H_2 with added *N*,*N*-diisopropylethylamine in PhF with 0.1 M $[NBu_4][B(C_6F_5)_4]$ at 100 mV/s referenced to $Cp_2Fe^{+/0}$.

[Mn($P^{Cg}N^{R}P^{Cg}$)$(CO)_3$Br] with $LiAlH_4$ did not proceed cleanly and the desired product could not be isolated in a sufficient purity for electrochemical studies.

4.8 Conclusions and Future Work

This chapter has described the synthesis of a series of pendant amine diphosphine ligands which contain the unusual phosphine substituents *s*-PhobP and CgP and the nitrogen substituents Me, iPr and Bn. The chirality in the CgP produces a mixture of diastereoisomeric ligands. A suitable route to separation of these isomers was not found although it was noted that the diastereoisomers do exhibit slightly differing solubilities in methanol. An exploration of different alcohols in differing ratios with another solvent such as DCM could lead to the successful separation and isolation of the *rac* and *meso* isomers in the future.

The coordination of the PNP ligands to Pt(II) showed the tendency of the ligands to bind in a κ^2-coordination mode by the two phosphorus atoms leaving the pendant amine in the second coordination sphere. A difference in the rate of coordination of the *rac* and *meso* isomers of the $P^{Cg}N^{R}P^{Cg}$ series of ligands to Pt(II) could serve as a method of separation of the diastereomers.

The novel PNP ligands were successfully coordinated to manganese to form a series of manganese tricarbonyl bromide complexes with the general formula [Mn(PNP)$(CO)_3$Br] which were isolated cleanly as the *fac*-isomers. The inequivalent phosphorus atoms in *rac*-[Mn($P^{Cg}N^{R}P^{Cg}$)$(CO)_3$Br] exhibited broad signals in the $^{31}P\{^1H\}$ NMR spectrum. Variable temperature NMR studies gave evidence to attribute the broadening of these signals at room temperature to the dynamic ring flip of the 6-membered metallacycle formed with the PNP ligand which has not been noted before for related mono-diphosphine manganese complexes.

Attempts to coordinate a second diphosphine to Mn were unsuccessful despite following procedures which are known to aid the substitution of carbonyl ligands in similar complexes. Although a direct comparison could not be made with the bis-diphosphine manganese complexes synthesised previously by Bullock *et al.* the tricarbonyl bromide complexes were tested for small molecule activation and the electrocatalysis of H_2 oxidation.

The cationic complexes $[Mn(P^{Phob}N^{R}P^{Phob})(CO)_3]^+$ were successfully synthesised by abstraction of the bromide of $[Mn(P^{Phob}N^{R}P^{Phob})(CO)_3Br]$ with $NaBAr^F_4$. The PNP ligand in $[Mn(P^{Phob}N^{R}P^{Phob})(CO)_3]^+$ displays the κ^3-coordination mode in the solid state which persists in solution according to the $^{31}P\{^1H\}$ NMR spectra. This Mn-N bond was sustained even in the presence of dihydrogen with no indication of reaction even at elevated temperature and prolonged reaction times. Further work would be needed to explore the incorporation of other ancillary ligands to increase the steric bulk around the Mn centre in order to weaken the Mn-N bond. Previous work by Bullock has shown that the presence of the species in the κ^3-coordination mode does not necessarily inhibit reactivity with dihydrogen but it must be in equilibrium with the κ^2-complex which can then interact with the substrate.[22,53]

Addition of $NaBAr^F_4$ to $[Mn(P^{Cg}N^{R}P^{Cg})(CO)_3Br]$ unexpectedly did not lead to the cationic complexes $[Mn(P^{Cg}N^{R}P^{Cg})(CO)_3]^+$. Evidence from a solid-state structure suggests that a sodium ion bridges two complexes by the oxygens in the CgP groups. Despite the evidence suggesting the Mn-Br bond had not been weakened or broken, this series of manganese complexes showed heterolytic cleavage of H_2. The conversion of starting material to Mn-H/N-H product only reached a maximum of 45% over 7 days at room temperature. Interconversion between the *syn*- and *anti*-protonation isomers of $[Mn(P^{Cg}N^{R}(H)P^{Cg})(CO)_3(H)][BAr^F_4]$ **4.7** was observed for the whole series but was largely dependent on the size of the nitrogen substituent. This series is the first example of heterolytic cleavage of H_2 by a pendant amine manganese complex which did not require the presence of a second diphosphine which previously have been shown to have a significant influence on the electronic properties of the manganese centre.[53]

Electrochemical testing for H_2 oxidation for both series did not yield positive results which was anticipated from the results of their chemical reaction with dihydrogen alone. A wider screen of electrochemical conditions would need to be carried out to conclusively rule out the complexes as electrocatalysts for either H_2 oxidation or production.

Initial testing for small molecule activation of other substrates, such as ethene and phenylacetylene, has been carried out with no evidence of activation products being formed which suggests their unsuitability as a general cooperative Lewis pair. One explanation for this is that because the other substrates are much larger than H_2 there is a

steric mismatch, resulting in the amine and metal centre not being able to act cooperatively for bond activation. A more thorough investigation of substrates and nitrogen substituents should be carried out to explore other possible avenues for reactivity. If it is possible to show that the heterolytic cleavage of dihydrogen is reversible, the application of these pendant amine complexes for borrowed hydrogen processes should be investigated. This could be done by modifying the reaction conditions such as varying the temperature and pressure of the reaction. Previous work in the Wass group has focused in the upgrading of ethanol to various isomers of the more advanced fuel butanol.[60–63] The transformation occurs by cycles of dehydrogenation, followed by aldol condensation and rehydrogenation of the substrates by the transformed catalyst. This borrowed hydrogen process is an example of Guerbet chemistry (Scheme 4.9).[64–66] The complexes explored in this work should be investigated for their catalytic activity in this process.

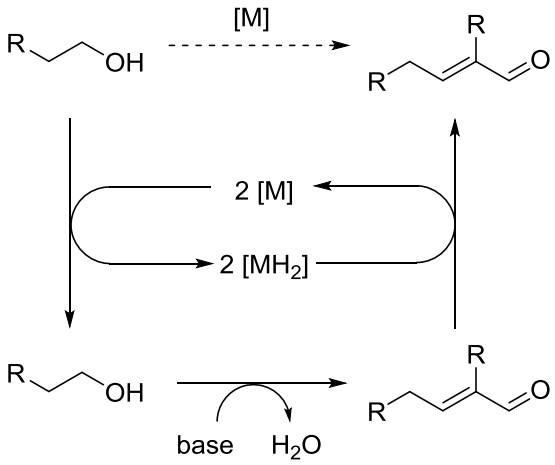

Scheme 4.9: General scheme for the coupling of alcohols *via* the Guerbet reaction.

4.9 References

1 L. Carrette, K. A. Friedrich and U. Stimming, *Fuel Cells*, 2001, **1**, 5–39.

2 M. Frey, *ChemBioChem*, 2002, **3**, 153–160.

3 I. Willner, Y. M. Yan, B. Willner and R. Tel-Vered, *Fuel Cells*, 2009, **9**, 7–24.

4 J. A. Cracknell, K. A. Vincent and F. A. Armstrong, *Chem. Rev.*, 2008, **108**, 2439–2461.

5 W. Lubitz, H. Ogata, O. Rüdiger and E. Reijerse, *Chem. Rev.*, 2014, **114**, 4081–4148.

6 E. B. Hulley, N. Kumar, S. Raugei and R. M. Bullock, *ACS Catal.*, 2015, **5**, 6838–6847.

7 J. M. Darmon, S. Raugei, T. Liu, E. B. Hulley, C. J. Weiss, R. M. Bullock and M. L. Helm, *ACS Catal.*, 2014, **4**, 1246–1260.

8 J. Y. Yang, S. Chen, W. G. Dougherty, W. S. Kassel, R. M. Bullock, D. L. DuBois, S. Raugei, R. Rousseau, M. Dupuis and M. R. DuBois, *Chem. Commun.*, 2010, **46**, 8618.

9 M. Rakowski DuBois and D. L. DuBois, *Chem. Soc. Rev.*, 2009, **38**, 62–72.

10 C. J. Weiss, A. N. Groves, M. T. Mock, W. G. Dougherty, W. S. Kassel, M. L. Helm, D. L. DuBois and R. M. Bullock, *Dalt. Trans.*, 2012, **41**, 4517–4529.

11 R. M. Bullock, A. M. Appel and M. L. Helm, *Chem. Commun.*, 2014, **50**, 3125–3143.

12 R. M. Bullock, *Science*, 2013, **342**, 1054–1055.

13 D. L. DuBois and R. M. Bullock, *Eur. J. Inorg. Chem.*, 2011, 1017–1027.

14 E. S. Wiedner, J. Y. Yang, W. G. Dougherty, W. S. Kassel, R. M. Bullock, M. R. DuBois and D. L. DuBois, *Organometallics*, 2010, **29**, 5390–5401.

15 U. J. Kilgore, M. P. Stewart, M. L. Helm, W. G. Dougherty, W. S. Kassel, M. R. Dubois, D. L. Dubois and R. M. Bullock, *Inorg. Chem.*, 2011, **50**, 10908–10918.

16 R. M. Bullock, A. K. Das and A. M. Appel, *Chem. - A Eur. J.*, 2017, **23**, 7626–

7641.

17 R. M. Henry, R. K. Shoemaker, D. L. DuBois and M. R. DuBois, *J. Am. Chem. Soc.*, 2006, **128**, 3002–3010.

18 S. Zhang, A. M. Appel and R. M. Bullock, *J. Am. Chem. Soc.*, 2017, **139**, 7376–7387.

19 S. Raugei, M. L. Helm, S. Hammes-Schiffer, A. M. Appel, M. O'Hagan, E. S. Wiedner, R. M. Bullock, M. O'Hagan, E. S. Wiedner and R. M. Bullock, *Inorg. Chem.*, 2016, **55**, 445–460.

20 R. M. Bullock and M. L. Helm, *Acc. Chem. Res.*, 2015, **48**, 2017–2026.

21 S. Wiese, U. J. Kilgore, M. H. Ho, S. Raugei, D. L. Dubois, R. M. Bullock and M. L. Helm, *ACS Catal.*, 2013, **3**, 2527–2535.

22 E. B. Hulley, K. D. Welch, A. M. Appel, D. L. DuBois and R. M. Bullock, *J. Am. Chem. Soc.*, 2013, **135**, 11736–11739.

23 T. Liu, S. Chen, M. J. O'Hagan, M. Rakowski DuBois, R. M. Bullock and D. L. DuBois, *J. Am. Chem. Soc.*, 2012, **134**, 6257–6272.

24 C. J. Curtis, A. Miedaner, R. Ciancanelli, W. W. Ellis, B. C. Noll, M. Rakowski DuBois, D. L. DuBois, Calvin J. Curtis, A. Miedaner, R. Ciancanelli, W. W. Ellis, B. C. Noll, A. M. Rakowski DuBois and D. L. DuBois, *Inorg. Chem.*, 2003, **42**, 216–227.

25 M. L. Helm, M. P. Stewart, R. M. Bullock, M. R. DuBois and D. L. DuBois, *Science*, 2011, **333**, 863–866.

26 S. R. Flynn and D. F. Wass, *ACS Catal.*, 2013, **3**, 2574–2581.

27 D. W. Stephan, *Science*, 2016, **354**, 1248.

28 R. M. Bullock and G. M. Chambers, *Philos. Trans. R. Soc. A Math. Phys. Eng. Sci.*, 2017, **375**, 20170002.

29 J. R. Khusnutdinova and D. Milstein, *Angew. Chem. Int. Ed.*, 2015, **54**, 12236–12273.

30 D. Milstein, *Philos. Trans. R. Soc. A Math. Phys. Eng. Sci.*, 2015, **373**, 20140189.

31 C. Effects, *Angew. Chem. Int. Ed.*, 2008, **2**, 1814–1818.

32 R. H. Morris, *Acc. Chem. Res.*, 2015, **48**, 1494–1502.

33 E. Khaskin, M. A. Iron, L. J. W. Shimon, J. Zhang and D. Milstein, *J. Am. Chem. Soc.*, 2010, **132**, 8542–8543.

34 E. Ben-Ari, G. Leitus, L. J. W. Shimon and D. Milstein, *J. Am. Chem. Soc.*, 2006, **128**, 15390–15391.

35 M. Vogt, M. Gargir, M. A. Iron, Y. Diskin-Posner, Y. Ben-David and D. Milstein, *Chem. - A Eur. J.*, 2012, **18**, 9194–9197.

36 C. Gunanathan and D. Milstein, *Acc. Chem. Res.*, 2011, **44**, 588–602.

37 G. A. Filonenko, M. P. Conley, C. Copéret, M. Lutz, E. J. M. Hensen and E. A. Pidko, *ACS Catal.*, 2013, **3**, 2522–2526.

38 A. Kumar, M. Feller, Y. Ben-David, Y. Diskin-Posner and D. Milstein, *Chem. Commun.*, 2018, **54**, 5365–5368.

39 M. Carreira, M. Charernsuk, M. Eberhard, N. Fey, R. Van Ginkel, A. Hamilton, W. P. Mul, A. G. Orpen, H. Phetmung and P. G. Pringle, *J. Am. Chem. Soc.*, 2009, **131**, 3078–3092.

40 R. A. Baber, M. L. Clarke, K. M. Heslop, A. C. Marr, A. G. Orpen, P. G. Pringle, A. Ward and D. E. Zambrano-Williams, *Dalt. Trans.*, 2005, 1079–1085.

41 J. M. Lister, PhD Thesis, University of Bristol, 2013.

42 J. Lloret Fillol, A. Kruckenberg, P. Scherl, H. Wadepohl and L. H. Gade, *Chem. - A Eur. J.*, 2011, **17**, 14047–14062.

43 J. Fawcett, P. A. T. Hoye, R. D. W. Kemmitt, D. J. Law and D. R. Russell, *J. Chem. Soc. Dalt. Trans.*, 1993, 2563–2568.

44 M. Epstein and S. A. Buckler, *J. Am. Chem. Soc.*, 1961, **83**, 3279–3282.

45 A. Phanopoulos, A. J. P. White, N. J. Long and P. W. Miller, *Dalt. Trans.*, 2016, **45**, 5536–5548.

46 A. Kruckenberg, H. Wadepohl and L. H. Gade, *Organometallics*, 2013, **32**, 5153–

5170.

47 K. Moedritzer and R. R. Irani, *J. Org. Chem.*, 1966, **31**, 1603–1607.

48 L. J. Matienzo and S. O. Grim, *Inorganic Syntheses, Vol 16*, McGraw-Hill Book Company, 1976.

49 S. O. Grim and L. J. Matienzo, *Tetrahedron Lett.*, 1973, **14**, 2951–2953.

50 A. D. Wilson, R. H. Newell, M. J. McNevin, J. T. Muckerman, M. Rakowski DuBois and D. L. DuBois, *J. Am. Chem. Soc.*, 2006, **128**, 358–366.

51 V. G. Märkl, G. Y. Jin and C. Schoerner, *Tetrahedron Lett.*, 1980, **21**, 1409–1412.

52 V. Gee, A. G. Orpen, H. Phetmung, P. G. Pringle and R. I. Pugh, *Chem. Commun.*, 1999, 901–902.

53 E. B. Hulley, M. L. Helm and R. M. Bullock, *Chem. Sci.*, 2014, **5**, 4729–4741.

54 J. Y. Yang, S. E. Smith, T. Liu, W. G. Dougherty, W. A. Hoffert, W. S. Kassel, M. R. Dubois, D. L. Dubois and R. M. Bullock, *J. Am. Chem. Soc.*, 2013, **135**, 9700–9712.

55 K. D. Welch, W. G. Dougherty, W. S. Kassel, D. L. DuBois and R. M. Bullock, *Organometallics*, 2010, **29**, 4532–4540.

56 D. B. Snyder, S. J. Schauer, D. P. Eyman, J. L. Moler and J. J. Weers, *J. Am. Chem. Soc.*, 1993, **115**, 6718–6729.

57 P. E. Garrou, *Chem. Rev.*, 1981, **81**, 229–266.

58 T. Liu, D. L. Dubois and R. M. Bullock, *Nat. Chem.*, 2013, **5**, 228–233.

59 T. Liu, Q. Liao, M. O'Hagan, E. B. Hulley, D. L. DuBois and R. M. Bullock, *Organometallics*, 2015, **34**, 2747–2764.

60 G. R. M. Dowson, M. F. Haddow, J. Lee, R. L. Wingad and D. F. Wass, *Angew. Chem. Int. Ed.*, 2013, **52**, 9005–9008.

61 R. L. Wingad, P. J. Gates, S. T. G. Street and D. F. Wass, *ACS Catal.*, 2015, **5**, 5822–5826.

62 H. Aitchison, R. L. Wingad and D. F. Wass, *ACS Catal.*, 2016, **6**, 7125–7132.

63 K. J. Pellow, R. L. Wingad and D. F. Wass, *Catal. Sci. Technol.*, 2017, **7**, 5128–5134.

64 S. Veibel and J. I. Nielsen, *Tetrahedron*, 1967, **23**, 1723–1733.

65 M. Guerbet, *C. R. Hebd. Seances Acad. Sci.*, 1899, **128**, 1002–1004.

66 M. Guerbet, *C. R. Hebd. Seances Acad. Sci.*, 1909, **149**, 129–132.

Chapter 5

Experimental

5.1 General Experimental Considerations

Unless otherwise stated, all reactions were carried out under an inert atmosphere of N_2 or Ar, using standard Schlenk line or glovebox (MBraun O_2 <0.1ppm, H_2O <0.1ppm) techniques. All glassware was dried in an oven (200 °C) for at least 2 hours or flame dried before use. Common laboratory solvents (DCM, diethyl ether, hexane, THF, acetonitrile and toluene) were purified using an anhydrous Grubbs-type solvent system and then degassed by at least three freeze/pump/thaw cycles. Non-standard solvents (pentane, benzene, chlorobenzene and fluorobenzene) were purchased from Sigma-Aldrich, distilled from CaH_2 and degassed by at least three freeze/pump/thaw cycles. Deuterated solvents ($CDCl_3$, CD_2Cl_2, d_5-PhBr, d_5-PhCl, d_6-benzene and d_8-toluene) were obtained from commercial sources, distilled from CaH_2 and degassed by at least three freeze/pump/thaw cycles. Unless otherwise stated, reagents were purchased from commercial sources and used without further purification. Reagent gases (CO_2 and $^{13}CO_2$) were dried prior to use by passing through a −78 °C trap. Catechol was dried by azeotroping with toluene three times before use. $B(OPh)_3$ was purified by sublimation before use (25 °C, 2 x 10^{-2} mBar). Phenylacetylene was purified by distillation before use and stored over 4 Å molecular sieves in an Ar glovebox. $[PtCl_2(COD)]$,[1] $[Pt(norbornene)_3]$,[2] $CgPH.BH_3$,[3] sodium tetrakis[3,5-bis(trifluoromethyl)phenyl]borate ($NaBAr^F_4$)[4] and bis(bis(3,5-bis(trifluoro)phenyl)phosphino)methane (bppm)[5] were synthesised according to literature methods. $B(C_2H_2F_3)_3$ was kindly synthesised and donated by the group of Dr Rebecca Melen (University of Cardiff).

NMR spectra were recorded on Jeol ECS 300, Jeol ECP (Eclipse) 300, Jeol ECS 400, Bruker Nano 400, Varian VNMRS 500 and Bruker Avance III HD 500 Cryo spectrometers in the solvents stated. Chemical shifts are given in parts per million (ppm) and coupling constants (*J*) are given in Hz. For paramagnetic NMR, line widths ($w_{1/2}$) are given in Hz. ^1H and $^{13}C\{^1H\}$ NMR chemical shifts (δ) are reported in parts per million (ppm) and are referenced internally relative to the residual solvent signal. $^{11}B\{^1H\}$, ^{19}F, $^{27}Al\{^1H\}$ and $^{31}P\{^1H\}$ were referenced to $BF_3.OEt_2$, $CFCl_3$, $Al(NO_3)_3$ and 85% H_3PO_4 as

external standards respectively. Data is reported as follows: chemical shift (δ, ppm), integration, multiplicity (s = singlet, d = doublet, t = triplet, q = quartet, qu = quintet, dd = doublet of doublets, dt = doublet of triplets, td = triplet of doublets, ququ = quintet of quintets, m = multiplet, app = apparent, br = broad signal), coupling constants (*J*, Hz) and assignment. Solid-state infrared (IR) absorption spectroscopic data were recorded on a Perkin-Elmer FT-IR instrument in air. Electrospray Ionisation Mass spectra (ESI-MS) were recorded by the mass spectrometry service at the University of Bristol on a Bruker Dalronics microTOF II. Elemental analyses were carried out by the Microanalytical Laboratory in the School of Chemistry, University of Bristol. All X-ray experiments were carried out by Dr. H. A. Sparkes and Dr. N. E. Pridmore who are acknowledged for their input. X-ray diffraction experiments were carried out at 100 K on a Bruker APEX II diffractometer using Mo-Kα radiation (λ = 0.71073 Å). The data collections were performed using a CCD area detector from a single crystal mounted on a glass fibre. Intensities were integrated, and absorption corrections based on equivalent reflections using SADABS were applied. The structures were all solved using Superflip[6] and structures were refined against all F^2 in ShelXL2013[7] using Olex2.[8] All of the non-hydrogen atoms were refined anisotropically. All of the hydrogen atoms were located geometrically and refined using a riding model.

5.2 Chapter 2 Experimental

5.2.1 1,2-bis(di-*tert*-butylphosphinooxy)benzene (dtbpob, L2)

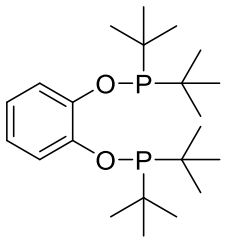

Catechol (596 mg, 5.41 mmol) in THF (10 mL) was added dropwise at room temperature to a suspension of NaH (286 mg, 11.91 mmol) in THF (10 mL). Effervescence of hydrogen gas and the formation of a white suspension was observed. The reaction was left to stir at room temperature until effervescence had subsided (approx. 30 min). Di-*tert*-butylchlorophosphine (2.05 mL, 10.83 mmol) was added dropwise to the reaction mixture and was heated at 60 °C for 72 h. Reaction progress was monitored by $^{31}P\{^{1}H\}$ NMR spectroscopy and upon consumption of the starting chlorophosphine the reaction mixture was filtered through celite under N_2 (extra care was taken to exclude water traces). The solvent was removed *in vacuo* to yield a colourless oily solid. Recrystallisation from hexane at −20 °C yielded a white crystalline solid (1.38 g, 56%). Upon workup, the P−O bond hydrolysis product bond formed. After several unsuccessful attempts to isolate the pure product, the crude product was carried forward to the next step. Crystals suitable for X-ray analysis were obtained by slow evaporation of a pentane solution of **L2** at −40 °C.

^{1}H NMR (400 MHz; C_6D_6) δ_H 7.69 (2H, m, Ar C*H*), 6.82 (2H, m, Ar C*H*), 1.21 (36H, d,^{3} J_{HP} = 11.6 Hz, CH_3); **^{13}C{^{1}H} NMR (100 MHz; C_6D_6)** δ_C 150.2 (dd, *J* = 9.8, 1.7 Hz, Ar *C*), 121.6 (m, Ar *C*H), 118.7 (d, *J* = 22.9 Hz, Ar *C*H), 35.8 (d, *J* = 27.0 Hz, *C*$(CH_3)_3$), 27.6 (d, *J* = 15.9 Hz, C(*C*$H_3)_3$); **^{31}P{^{1}H} NMR (162 MHz; C_6D_6)** δ_P 153.1 (s, *P*^{t}Bu_2); **HR-MS (ESI)** *m/z* calcd. for $C_{22}H_{41}O_2P_2$ $[M+H]^+$ = 399.2576, obs. 399.2568; **Elem. Anal.** (calcd. for $C_{22}H_{40}O_2P_2$) C 66.49 (66.31), H 10.13 (10.12).

5.2.2 [$PtCl_2$(L2)]

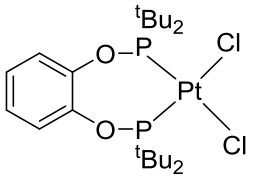

[$PtCl_2$(COD)] (25 mg, 0.07 mmol) and **L2** (32 mg, 0.08 mmol) were dissolved in DCM (0.6 mL) in a Youngs NMR tube. After 30 min, analysis of the $^{31}P\{^1H\}$ NMR spectrum confirmed complete complexation. The complex was precipitated in hexane to yield a white solid, (37 mg, 83%). Crystals suitable for X-ray analysis were obtained by slow diffusion of hexane into a DCM solution of [$PtCl_2$(**L2**)].

^{1}H NMR (400 MHz; CD_2Cl_2) δ_H 7.08 (4H, m, Ar C*H*), 1.55 (36H, d, $^3J_{HP}$ = 15.4 Hz, CH_3); **$^{13}C\{^1H\}$ NMR (100 MHz; CD_2Cl_2)** δ_C 145.2 (m, Ar *C*), 129.1 (s, Ar *C*H), 126.1 (s, Ar *C*H), 45.3 (m, *C*(CH_3)$_3$), 30.0 (C(*C*H_3)$_3$); **$^{31}P\{^1H\}$ NMR (162 MHz; CD_2Cl_2)** δ_P 138.3 (s, $^1J_{PPt}$ = 4130 Hz, *P*^{t}Bu$_2$); **HR-MS (ESI)** *m*/*z* cacld. for $C_{22}H_{40}ClO_2P_2Pt$ $[M-Cl]^+$ = 628.1840, obs. 627.1835; **Elem. Anal.** (calcd. for $C_{22}H_{40}Cl_2O_2P_2Pt$) C 39.82 (39.77), H 6.23 (6.07).

5.2.3 [Pt(CO)(L2)]

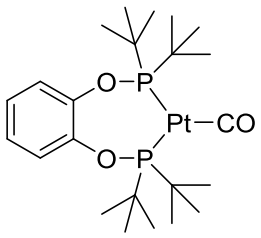

A solution of **L2** (250 mg, 0.5 mmol) in toluene (5 mL) was added dropwise to a solution of Pt(nbe)$_3$ (200 mg, 0.5 mmol) in toluene (5 mL) at −78 °C. After 2 h stirring at −78 °C a yellow suspension formed. The reaction was left to warm to room temperature and stir overnight. CO was bubbled through the suspension for 20 min during which time the reaction mixture changed to a dark orange solution. This solution was filtered to remove any Pt(0) nanoparticles. The solvent was removed *in vacuo* and the solid redissolved in toluene (5 mL). CO was bubbled through for 20 min, solvent removed *in vacuo* and redissolved in toluene (5 mL). This CO/vacuum cycle was repeated five times. The

product was extracted with pentane (3 x 3 mL) and recrystallisation from this solution at −78 °C yielded orange crystals (164 mg, 61%). Crystals suitable for X-ray analysis were obtained from a saturated solution in pentane at −40 °C.

^{1}H NMR (500 MHz; d$_8$-toluene) δ_H 7.03 (2H, m, Ar C*H*), 6.69 (2H, m, Ar C*H*), 1.28 (36H, br d, $^{3}J_{HP}$ = 14.0 Hz, CH_3); **^{13}C{^{1}H} NMR (125 MHz; d$_8$-toluene)** δ_C 147.4 (m, Ar *C*), 128.0 (br s, Ar *C*H), 124.5 (br s, Ar *C*H), 42.4 (app t, J_{CP} = 5.1 Hz, J_{CPt} = 75.3 Hz, *C*CH$_3$), 29.5 (m, C*C*H$_3$); **^{31}P{^{1}H} NMR (202 MHz; d$_8$-toluene)** δ_P 218.2 (s, J_{PPt} = 4062 Hz, *P*^{t}Bu$_2$); **HR-MS (ESI)** *m*/*z* calcd. for $C_{23}H_{41}O_3P_2Pt$ $[M+H]^+$ = 622.2176, obs. 622.2169; **Elem. Anal.** (calcd. for $C_{23}H_{40}O_3P_2Pt$) C 44.81 (44.44), H 6.57 (6.49); **IR νco** 1933 cm^{-1}.

5.2.4 [Pt(^{13}CO)(L2)]

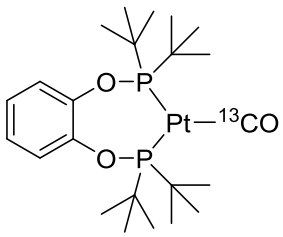

A Youngs NMR tube was charged with a solution of [Pt(CO)(**L2**)] (30.5 mg, 0.049 mmol) in d$_8$-toluene (0.7 mL). The solution was frozen in liquid nitrogen and the tube was evacuated. The solution was thawed and allowed to warm to room temperature. The tube was backfilled with ^{13}CO (1.2 bar). The solution was mixed and left for 5 min before removing the solvent *in vacuo*. The solid was redissolved in d$_8$-toluene. This cycle was repeated three more times to ensure majority of the ^{12}CO had been exchanged for ^{13}CO. This species was confirmed in solution by NMR spectroscopy only.

^{1}H NMR (500 MHz; d$_8$-toluene) δ_H 7.03 (2H, m, Ar C*H*), 6.69 (2H, m, Ar C*H*), 1.29 (36H, br d, $^{3}J_{HP}$ = 14.1 Hz, CH_3); **^{13}C{^{1}H} NMR (125 MHz; d$_8$-toluene)** δ_C 228.8 (t, $^{2}J_{CP}$ = 56.5 Hz, $^{1}J_{CPt}$ = 1964 Hz, Pt^{13}*C*O), 147.4 (m, Ar *C*), 128.0 (br s, Ar *C*H), 124.5 (br s, Ar *C*H), 51.1 (app t, J_{CP} = 5.4 Hz, J_{CPt} = 75.0 Hz, *C*CH$_3$), 38.2 (m, C*C*H$_3$); **^{31}P{^{1}H} NMR (202 MHz; d$_8$-toluene)** δ_P 218.2 (d, $^{2}J_{PC}$ = 56.5 Hz, $^{1}J_{PPt}$ = 4062 Hz, *P*^{t}Bu$_2$).

5.2.5 [Pt(CO)(L1)]

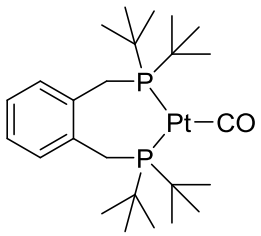

A solution of **L1** (331 mg, 0.84 mmol) in toluene (8 mL) was added dropwise to a solution of $Pt(nbe)_3$ (400 mg, 0.84 mmol) in toluene (8 mL) at −78 °C. After 2 h stirring at −78 °C, the reaction was left to warm to room temperature and stir overnight. CO was bubbled through the solution for 20 min during which time the reaction mixture changed to a dark orange solution. This solution was filtered to remove any Pt(0) nanoparticles. The solvent was removed *in vacuo* and the solid redissolved in toluene (5 mL). CO was bubbled through for 20 min and the solvent was removed *in vacuo* and redissolved in toluene (5 mL). This CO/vacuum cycle was repeated twice more to yield an orange solid. The product was extracted with pentane (3 x 5 mL) and recrystallisation from this solution at −78 °C yielded orange crystals (351 mg, 68%). Crystals suitable for X-ray analysis were obtained from a saturated solution in pentane at −40 °C. NMR data is in agreement with literature.[9]

^{1}H NMR (500 MHz; d$_8$-toluene) δ_H 7.12 (2H, m, Ar C*H*), 6.91 (2H, m, Ar C*H*), 3.50 (2H, br, CH_2), 1.22 (36H, m, CH_3); **^{13}C{^{1}H} NMR (125 MHz; d$_8$-toluene)** δ_C 137.9 (m, Ar *C*), 133.7 (br s, Ar *C*H), 125.5 (br s, Ar *C*H), 37.0 (br, *C*H_2), 32.3 (s, *C*CH_3), 29.8 (s, C*C*H_3); **^{31}P{^{1}H} NMR (202 MHz; d$_8$-toluene)** δ_P 69.7 (s, $^1J_{PPt}$ = 3680 Hz, *P*^{t}Bu$_2$).

5.2.6 [Pt(^{13}CO)(L1)]

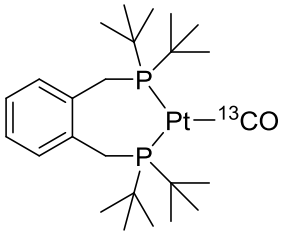

A Youngs NMR tube was charged with a solution of [Pt(CO)(**L1**)] (29.6 mg, 0.048 mmol) in d$_8$-toluene (0.7 mL). The solution was frozen in liquid nitrogen and the tube was evacuated. The solution was thawed and allowed to warm to room temperature. The

tube was backfilled with ^{13}CO (1.2 bar). The solution was mixed and left for 5 min before removing the solvent *in vacuo*. The solid was redissolved in d_8-toluene. This cycle was repeated three more times to ensure most of the ^{12}CO had been exchanged for ^{13}CO. This species was confirmed in solution by NMR spectroscopy only. NMR data is in agreement with literature.[9]

^{1}H NMR (500 MHz; d_8-toluene) δ_H 7.11 (2H, m, Ar C*H*), 6.91 (2H, m, Ar C*H*), 3.49 (2H, br, CH_2), 1.22 (36H, m, CH_3); **^{13}C{^{1}H} NMR (125 MHz; d_8-toluene)** δ_C 224.7 (t, J_{CP} = 44.1 Hz, J_{CPt} = 2095 Hz, Pt-^{13}*C*O), 135.0 (m, Ar *C*), 130.8 (br s, Ar *C*H), 122.7 (br s, Ar *C*H), 33.9 (br, *C*H_2), 29.4 (br s, *C*CH_3), 26.9 (m, C*C*H_3); **^{31}P{^{1}H} NMR (202 MHz; d_8-toluene)** δ_P 69.7 (d, $^2J_{PC}$ = 44.1 Hz, $^1J_{PPt}$ = 3680 Hz, *P*^{t}Bu$_2$).

5.2.7 [Pt(^{13}CO)$_2$(L2)]

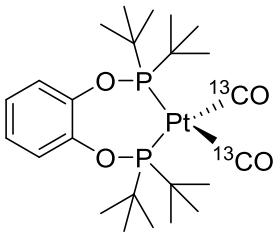

A Youngs NMR tube was charged with a solution of [Pt(CO)(**L2**)] (29.4 mg, 0.048 mmol) in d_8-toluene (0.7 mL). The solution was frozen in liquid nitrogen and the tube was evacuated. The solution was thawed and allowed to warm to room temperature. The tube was backfilled with ^{13}CO (1.2 bar). The solution changed from bright orange to pale yellow. The product was not isolated as it reverts to [Pt(^{13}CO)(**L2**)] upon removal of solvent.

^{13}C{^{1}H} NMR (75 MHz; d_8-toluene; −80 °C) δ_C 185.1 (t, $^2J_{CP}$ = 15.8 Hz, $^1J_{CPt}$ = 1756 Hz, Pt^{13}*C*O); **^{31}P{^{1}H} NMR (122 MHz; d_8-toluene; −80 °C)** δ_P 176.4 (t,$^2J_{PC}$ = 15.9 Hz, $^1J_{PPt}$ = 3578 Hz, *P*^{t}Bu$_2$).

5.2.8 Reaction of [Pt(CO)(L2)]/$B(C_6F_5)_3$ with H_2

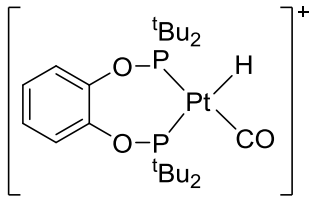

2.4

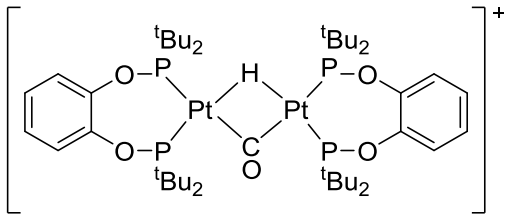

2.5

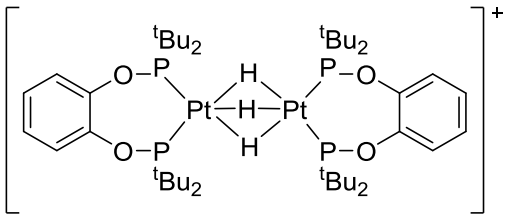

2.6

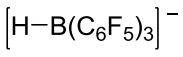

2.7

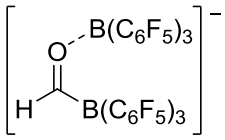

2.8

A Youngs NMR tube was charged with a solution of [Pt(CO)(**L2**)] (31.0 mg, 0.050 mmol) and $B(C_6F_5)_3$ (25.5 mg, 0.050 mmol) in d_5-chlorobenzene (0.7 mL). The orange solution was frozen in liquid nitrogen and the tube was evacuated. The solution was thawed and allowed to warm to room temperature. The tube was backfilled with H_2 (1 bar) and shaken. A colour change from orange to bright pink was observed over 30 min, which intensified over time. Three cationic (**2.4**-**2.6**) and two anionic species (**2.7**-**2.8**) were identified in solution.

2.4: ^{1}H NMR (500 MHz; d_5-PhCl) δ_H 6.99-6.77 (4H, m, Ar C*H*), 1.11-1.02 (36H, m, CC*H*$_3$), −4.15 (1H, dd, $^1J_{HPt}$ = 755 Hz, $^2J_{HP(trans)}$ = 159 Hz, $^2J_{HP(cis)}$ = 24.3 Hz, Pt-*H*); **^{31}P{^{1}H} NMR (202 MHz; d_5-PhCl)** δ_P 174.5 (d, $^1J_{PPt}$ = 3301 Hz, $^2J_{PP}$ = 15.0 Hz, *P*^{t}Bu$_2$), 163.0 (d, $^1J_{PPt}$ = 2294 Hz, $^2J_{PP}$ = 15.0 Hz, *P*^{t}Bu$_2$).

2.5: ^{1}H NMR (500 MHz; d_5-PhCl) δ_H 6.99-6.77 (4H, m, Ar C*H*), 1.27-1.16 (36H, m, CC*H*$_3$), −1.92 (1H, 1:8:18:8:1 ququ, $^1J_{HPt}$ = 475 Hz, $^2J_{HP}$ = 38 Hz, Pt(μ-*H*)Pt); **^{31}P{^{1}H} NMR (202 MHz; d_5-PhCl)** δ_P 182.2 (m, $^1J_{PPt}$ = 4029 Hz, $^2J_{PPt}$ = 131 Hz, $^3J_{PP}$ = 38 Hz, *P*^{t}Bu$_2$).

2.6: ^{1}H NMR (500 MHz; d_5-PhCl) δ_H 6.99-6.77 (4H, m, Ar C*H*), 1.27-1.16 (36H, m, CC*H*$_3$), −5.72 (1H, 1:8:18:8:1 ququ, $^1J_{HPt}$ = 393 Hz, $^2J_{HP}$ = 41.3 Hz, Pt(μ-*H*)$_3$Pt); **^{31}P{^{1}H} NMR (202 MHz; d_5-PhCl)** δ_P 185.6 (m, $^1J_{PPt}$ = 3459 Hz, $^2J_{PPt}$ = 153 Hz, $^3J_{PP}$ = 10.1 Hz,

P^tBu_2).

2.7: ^{1}H NMR (500 MHz; d$_5$-PhCl) δ_H 3.94 (br q, $^1J_{HB}$ = 80.1 Hz, B*H*); **^{11}B{^{1}H} NMR (128 MHz; d$_5$-PhCl)** δ_B −27.7 (br s, *B*H); **^{19}F NMR (471 MHz; d$_5$-PhCl)** δ_F −131.5 (6F, br, *o*-C_6F_5), −163.9 (3F, br, *p*-C_6F_5), −166.2 (6F, br, *m*-C_6F_5).

2.8: ^{1}H NMR (500 MHz; d$_5$-PhCl) δ_H 10.80 (br s, C*H*); **^{11}B{^{1}H} NMR (128 MHz; d$_5$-PhCl)** δ_B −2.4 (br, O*B*), −16.7 (br s, *B*CO); **^{19}F NMR (471 MHz; d$_5$-PhCl)** δ_F −130.3 (6F, br, *o*-C_6F_5), −132.6 (6F, br, *o*-C_6F_5), −157.6 (3F, br, *p*-C_6F_5), −159.2 (3F, br, *p*-C_6F_5), −164.8 (6F, br, *m*-C_6F_5), −165.2 (6F, br, *m*-C_6F_5).

5.2.9 Reaction of [Pt(^{13}CO)(L2)]/B(C$_6$F$_5$)$_3$ with H$_2$

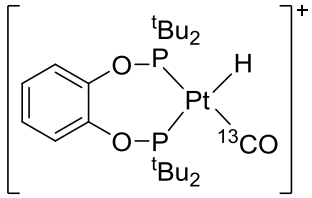

2.4

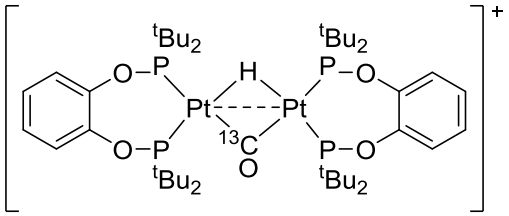

2.5

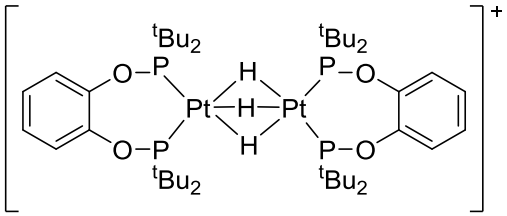

2.6

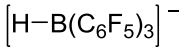

2.7

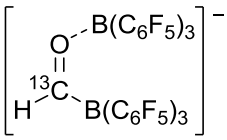

2.8

A Youngs NMR tube was charged with a solution of [Pt(^{13}CO)(**L2**)] (20.0 mg, 0.032 mmol) and B(C$_6$F$_5$)$_3$ (16.4 mg, 0.032 mmol) in d$_5$-chlorobenzene (0.7 mL). The orange solution was frozen in liquid nitrogen and the tube was evacuated. The solution was thawed and allowed to warm to room temperature. The tube was backfilled with H_2 (1 bar) and shaken. A colour change from orange to a bright pink was observed over 30 min which intensified over time. Three cationic (**2.4**-**2.6**) and two anionic species (**2.7**-**2.8**) were identified in solution.

2.4: ^{1}H NMR (500 MHz; d$_5$-PhCl) δ_H 6.99-6.77 (4H, m, Ar C*H*), 1.11-1.02 (36H, m, CC*H*$_3$), −4.15 (1H, ddd, $^1J_{HPt}$ = 755 Hz, $^2J_{HP(trans)}$ = 159 Hz, $^2J_{HP(cis)}$ = 24.3 Hz, $^2J_{HC}$ = 3.5 Hz, Pt*H*); **^{13}C{^{1}H} NMR (125 MHz; d$_5$-PhCl)** δ_C 178.4 (dd, $^1J_{CPt}$ = 1212 Hz, $^2J_{CP}$ = 124 Hz, $^2J_{CP}$ = 6.2 Hz, Pt^{13}*C*O); **^{31}P{^{1}H} NMR (202 MHz; d$_5$-PhCl)** δ_P 174.5 (d, $^1J_{PPt}$ = 3301

Hz, $^2J_{PP}$ = 15.0 Hz, *P*^{t}Bu$_2$), 163.0 (d, $^1J_{PPt}$ = 2294 Hz, $^2J_{PP}$ = 15.0 Hz, *P*^{t}Bu$_2$).

2.5: ^{1}H NMR (500 MHz; d$_5$-PhCl) δ_H 6.99-6.77 (4H, m, Ar C*H*), 1.27-1.16 (36H, m, CC*H*$_3$), −1.92 (1H, 1:8:18:8:1 ququ, $^1J_{HPt}$ = 475 Hz, $^2J_{HP}$ = 38 Hz, $^2J_{H13C}$ = 4.5 Hz, Pt(μ-*H*)Pt); **^{13}C{^{1}H} NMR (125 MHz; d$_5$-PhCl)** δ_C 231.6 (1:8:18:8:1 ququ, $^1J_{CPt}$ = 753 Hz, $^2J_{CP}$ = 38 Hz, Pt(μ-*^{13}C*O)Pt) ; **^{31}P{^{1}H} NMR (202 MHz; d$_5$-PhCl):** δ_P 182.2 (m, $^1J_{PPt}$ = 4029 Hz, $^2J_{PPt}$ = 131 Hz, $^3J_{PP}$ = 38 Hz, *P*^{t}Bu$_2$).

2.6: ^{1}H NMR (500 MHz; d$_5$-PhCl) δ_H 6.99-6.77 (4H, m, Ar C*H*), 1.27-1.16 (36H, m, CC*H*$_3$), −5.72 (1H, 1:8:18:8:1 ququ, $^1J_{HPt}$ = 393 Hz, $^2J_{HP}$ = 41.3 Hz, Pt(μ-*H*)Pt); **^{31}P{^{1}H} NMR (202 MHz; d$_5$-PhCl)** δ_P 185.6 (m, $^1J_{PPt}$ = 3459 Hz, $^2J_{PPt}$ = 153 Hz, $^3J_{PP}$ = 10.1 Hz, *P*^{t}Bu$_2$).

2.7: ^{1}H NMR (500 MHz; d$_5$-PhCl) δ_H 3.94 (br q, $^1J_{HB}$ = 80.1 Hz, B*H*); **^{11}B{^{1}H} NMR (128 MHz; d$_5$-PhCl)** δ_B −27.7 (br s, *B*H); **^{19}F NMR (471 MHz; d$_5$-PhCl)** δ_F −131.5 (6F, br, *o*-C$_6$*F*$_5$), −163.9 (3F, br, *p*-C$_6$*F*$_5$), −166.2 (6F, br, *m*-C$_6$*F*$_5$).

2.8: ^{1}H NMR (500 MHz; d$_5$-PhCl) δ_H 10.80 (br d, $^1J_{HC}$ = 151 Hz, *^{13}C*H**^{11}B{^{1}H}** **NMR (128 MHz; d$_5$-PhCl)** δ_B −2.4 (br, O*B*), −16.7 (br d, $^1J_{BC}$ = 49 Hz, *B*^{13}C);); **^{13}C{^{1}H} NMR (125 MHz; d$_5$-PhCl)** δ_C 249.2 (br q, $^1J_{CB}$ = 53 Hz, B*^{13}C*O); **^{19}F NMR (471 MHz; d$_5$-PhCl)** δ_F −130.3 (6F, br, *o*-C$_6$*F*$_5$), −132.6 (6F, br, *o*-C$_6$*F*$_5$), −157.6 (3F, br, *p*-C$_6$*F*$_5$), −159.2 (3F, br, *p*-C$_6$*F*$_5$), −164.8 (6F, br, *m*-C$_6$*F*$_5$), −165.2 (6F, br, *m*-C$_6$*F*$_5$).

5.2.10 Reaction of [Pt(^{13}CO)(L1)]/B(C$_6$F$_5$)$_3$ with H$_2$

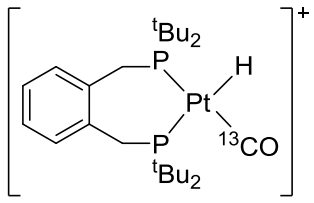

2.9

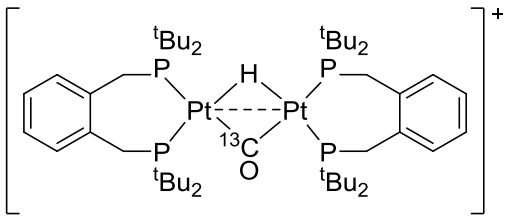

2.10

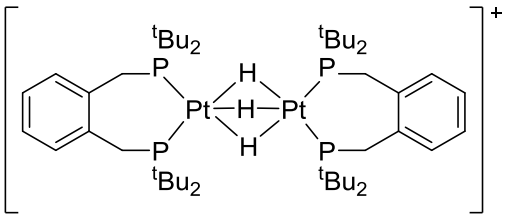

2.11

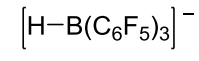

2.7

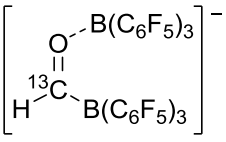

2.8

A Youngs NMR tube was charged with a solution of [Pt(^{13}CO)(**L1**)] (18.4 mg, 0.030 mmol) and B(C_6F_5)$_3$ (15.3 mg, 0.030 mmol) in d_5-chlorobenzene (0.7 mL). The orange solution was frozen in liquid nitrogen and the tube was evacuated. The solution was thawed and allowed to warm to room temperature. The tube was backfilled with H_2 (1 bar) and shaken. A colour change from orange to a pale yellow was observed over 16 h. Three cationic (**2.11**-**2.13**) and two anionic species (**2.7**-**2.8**) were identified in solution after 15 minutes.

2.9: ^{1}H NMR (500 MHz; d_5-PhCl) δ_H 7.20-7.02 (4H, m, ArC*H*), 3.71-3.10 (br, 4H, PCH_2), 1.26-1.09 (36H, m, CCH_3), −4.55 (1H, dd, $^1J_{HPt}$ = 734 Hz, $^2J_{HP(trans)}$ = 145 Hz, $^2J_{HP(cis)}$ = 16 Hz, Pt*H*); **^{13}C{^{1}H} NMR (125 MHz; d_5-PhCl)** δ_C 178.2 (dd, $^1J_{CPt}$ = 1305 Hz, $^2J_{CP}$ = 113 Hz, $^2J_{CP}$ = 8.8 Hz, Pt^{13}*C*O); **^{31}P{^{1}H} NMR (122 MHz; d_5-PhCl)** δ_P 43.4 (d, $^1J_{PPt}$ = 2987 Hz, $^2J_{PP}$ = 19 Hz), 34.2 (d, $^1J_{PPt}$ = 2004 Hz, $^2J_{PP}$ = 19 Hz).

2.10: ^{1}H NMR (500 MHz; d_5-PhCl) δ_H 7.20-7.02 (4H, m, ArC*H*), 3.71-3.10 (br, 4H, PCH_2), 1.08-0.93 (36H, m, CCH_3), −5.75 (1H, 1:8:18:8:1 ququ, $^1J_{HPt}$ = 496 Hz, $^2J_{HP}$ = 35 Hz, Pt(μ-*H*)Pt); **^{13}C{^{1}H} NMR (125 MHz; d_5-PhCl)** δ_C 212.88 (1:8:18:8:1 ququ, $^1J_{CPt}$ = 805 Hz, $^2J_{CP}$ = 33 Hz, Pt(μ-^{13}*C*O)Pt); **^{31}P{^{1}H} NMR (122 MHz; d_5-PhCl)** δ_P 46.4 (m, $^1J_{PPt}$ = 3755 Hz, $^2J_{PPt}$ = 144 Hz, $^3J_{PP}$ = 23 Hz).

2.11: ^{1}H NMR (500 MHz; d_5-PhCl) δ_H 6.99-6.77 (4H, m, ArC*H*), 1.27-1.16 (36H, m, CCH_3), −7.48 (1H, 1:8:18:8:1 ququ, $^1J_{HPt}$ = 393 Hz, $^2J_{HP}$ = 41 Hz, Pt(μ-*H*)$_3$Pt); **^{31}P{^{1}H} NMR (122 MHz; d_5-PhCl)** δ_P 50.8 (br).

2.7: ^{1}H NMR (400 MHz; d_5PhCl) δ_H 3.94 (br q, $^1J_{HB}$ = 80 Hz, B*H*); **^{11}B{^{1}H} NMR (96 MHz; d_5-PhCl)** δ_B −27.7 (br s, *B*H); **^{19}F NMR (376 MHz; d_5-PhCl)** δ_F −131.5 (6F, br, *o*-C$_6F_5$), −163.9 (3F, br, *p*-C$_6F_5$), −166.2 (6F, br, *m*-C$_6F_5$).

2.8: ^{1}H NMR (400 MHz; d_5-PhCl) δ_H 10.80 (br d, $^1J_{HC}$ = 151 Hz, ^{13}C*H*); **^{11}B{^{1}H} NMR (96 MHz; d_5-PhCl)** δ_B −2.4 (br, O*B*), −16.7 (br s, *B*^{13}C); **^{13}C{^{1}H} NMR (125 MHz; d_5-PhCl)** δ_C 249.2 (br q, $^1J_{CB}$ = 51Hz, B^{13}*C*O); **^{19}F NMR (376 MHz; d_5-PhCl)** δ_F −130.3 (6F, br, *o*-C$_6F_5$), −132.6 (6F, br, *o*-C$_6F_5$), −157.6 (3F, br, *p*-C$_6F_5$), −159.2 (3F, br, *p*-C$_6F_5$), −164.8 (6F, br, *m*-C$_6F_5$), −165.2 (6F, br, *m*-C$_6F_5$).

5.2.11 Reaction of [Pt(CO)(L2)]/$B(C_6F_5)_3$ with C_2H_4

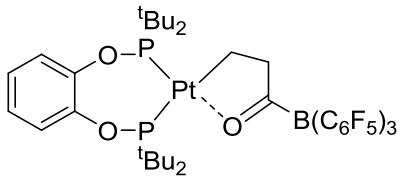

A Youngs NMR tube was charged with a solution of [PtCO(**L2**)] (17.2 mg, 0.028 mmol) and $B(C_6F_5)_3$ (14.2 mg, 0.028 mmol) in d_5-chlorobenzene (0.7 mL). The orange solution was frozen in liquid nitrogen and the tube was evacuated. The solution was thawed and allowed to warm to room temperature. The tube was backfilled with C_2H_4 (1 bar) and shaken. A colour change from orange to pale pink was observed over 1 h and species **2.15** was identified in solution.

^{1}H NMR (400 MHz; d_5-PhCl) δ_H 6.94-6.70 (4H, m, Ar C*H*), 2.87 (2H, br m, BCCH_2), 1.90 (2H, br m, PtCH_2), 1.19-1.08 (36H, m, CCH_3); **^{11}B{^{1}H} NMR (128 MHz; d_5-PhCl)** δ_B −22.0 (br s, C*B*$(C_6F_5)_3$); **^{19}F NMR (376 MHz; d_5-PhCl)** δ_F −137.2 (6F, br, *o*-C_6F_5), −167.1 (3F, br, *p*-C_6F_5), −172.1 (6F, br, *m*-C_6F_5); **^{31}P{^{1}H} NMR (162 MHz; d_5-PhCl)** δ_P 173.4 (d, $^1J_{PPt}$ = 2219 Hz, $^2J_{PP}$ = 15.0 Hz, *P*^{t}Bu$_2$), 137.5 (d, $^1J_{PPt}$ = 4662 Hz, $^2J_{PP}$ = 15.0 Hz, *P*^{t}Bu$_2$).

5.2.12 Reaction of [Pt(^{13}CO)(L2)]/$B(C_6F_5)_3$ with C_2H_4

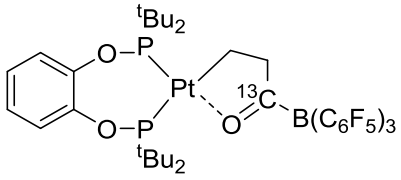

A Youngs NMR tube was charged with a solution of [Pt(^{13}CO)(**L2**)] (15.8 mg, 0.025 mmol) and $B(C_6F_5)_3$ (13.0 mg, 0.025 mmol) in d_5-chlorobenzene (0.7 mL). The orange solution was frozen in liquid nitrogen and the tube was evacuated. The solution was thawed and allowed to warm to room temperature. The tube was backfilled with C_2H_4 (1 bar) and shaken. A colour change from orange to pale pink was observed over 1 h and species **2.15** was identified in solution.

^{1}H NMR (400 MHz; d_5-PhCl) δ_H 6.94-6.70 (4H, m, Ar C*H*), 2.87 (2H, br m, BCCH_2), 1.90 (2H, br m, PtCH_2), 1.19-1.08 (36H, m, CCH_3); **^{11}B{^{1}H} NMR (128 MHz; d_5-PhCl)**

δ_B −22.0 (br d, $^1J_{BC}$ = 52.4 Hz, ^{13}C*B*$(C_6F_5)_3$); **^{13}C{^{1}H} NMR (100 MHz; d$_5$-PhCl)** δ_C 278.7 (br q, $^1J_{CB}$ = 52.4 Hz, B^{13}*C*O); **^{19}F NMR (471 MHz; d$_5$-PhCl)** δ_F −137.2 (6F, br, *o*-C_6F_5), −167.1 (3F, br, *p*-C_6F_5), −172.1 (6F, br, *m*-C_6F_5); **^{31}P{^{1}H} NMR (162 MHz; d$_5$-PhCl)** δ_P 173.4 (d, $^1J_{PPt}$ = 2219 Hz, $^2J_{PP}$ = 15.2 Hz, *P*^{t}Bu$_2$), 137.5 (d, $^1J_{PPt}$ = 4662 Hz, $^2J_{PP}$ = 15.2 Hz, *P*^{t}Bu$_2$).

5.2.13 [Pt(C$_2$H$_4$)(L2)]

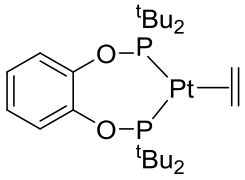

A Youngs NMR tube was charged with a solution of [Pt(CO)(**L2**)] (25.4 mg, 0.041 mmol) in d$_8$-toluene (0.7 mL). The solution was frozen in liquid nitrogen and the tube was evacuated. The solution was thawed and allowed to warm to room temperature. The tube was backfilled with C_2H_4 (1.2 bar). The solution was shaken and left for 5 min before removing the solvent *in vacuo*. The solid was redissolved in d$_8$-toluene. This cycle was repeated twice more. This species was confirmed in solution by NMR spectroscopy only. **^{1}H NMR (400 MHz; d$_8$-toluene)** δ_H 7.06 (2H, m, Ar C*H*), 6.72 (2H, m, Ar C*H*), 2.04 (4H, m, $^1J_{HPt}$ = 55.6 Hz), 1.29 (36H, br d, $^3J_{HP}$ = 14.1 Hz, CH_3); **^{13}C{^{1}H} NMR (100 MHz; d$_8$-toluene)** δ_C 147.7 (m, Ar *C*), 127.3 (s, Ar *C*H), 124.3 (br s, Ar *C*H), 42.4 (m, *C*CH$_3$), 29.5 (m, C*C*H$_3$); **^{31}P{^{1}H} NMR (162 MHz; d$_8$-toluene)** δ_P 198.0 (s, $^1J_{PPt}$ = 3840 Hz, *P*^{t}Bu$_2$).

5.2.14 Reaction of [Pt(CO)(L1)]/B(C$_6$F$_5$)$_3$ with Phenylacetylene, 2.15

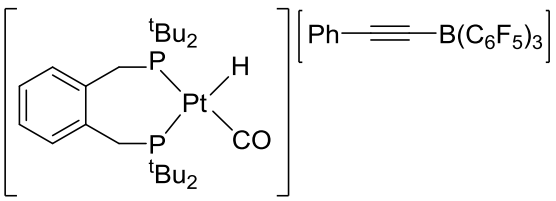

A Youngs NMR tube was charged with a solution of [Pt(CO)(**L1**)] (20.0 mg, 0.032 mmol) and B$(C_6F_5)_3$ (16.6 mg, 0.032 mmol) in d$_5$-chlorobenzene (0.7 mL). Phenylacetylene was added in excess (*ca*. 30 μl) and an instant colour change from bright orange to a dark reddy brown colour was observed. Species **2.15** was identified in solution.

^{1}H NMR (400 MHz; d$_5$-PhCl) δ_H 7.12-6.96 (5H, m *Ph*CC), 7.12-6.96 (4H, m, Ar C*H*), 3.73-2.90 (4H, br, PCH_2), 1.04-0.91 (36H, m, CCH_3), −4.15 (1H, dd, $^{1}J_{HPt}$ = 755 Hz, $^{2}J_{HP(trans)}$ = 159 Hz, $^{2}J_{HP(cis)}$ = 24 Hz, Pt*H*); **^{11}B{^{1}H} NMR (128 MHz; d$_5$-PhCl)** δ_B −21.1 (br s, CC*B*$(C_6F_5)_3$); **^{19}F NMR (376 MHz; d$_5$-PhCl)** δ_F −138.1 (6F, br, *o*-C$_6$*F*$_5$), −170.2 (3F, br, *p*-C$_6$*F*$_5$), −173.5 (6F, br, *m*-C$_6$*F*$_5$); **^{31}P{^{1}H} NMR (162 MHz; d$_5$-PhCl)** δ_P 43.4 (d, $^{1}J_{PPt}$ = 2994 Hz, $^{2}J_{PP}$ = 19 Hz, *P*^{t}Bu$_2$), 34.2 (d, $^{1}J_{PPt}$ = 2018 Hz, $^{2}J_{PP}$ = 19 Hz, *P*^{t}Bu$_2$).

5.2.15 Reaction of [Pt(CO)(L2)]/B(C$_6$F$_5$)$_3$ with Phenylacetylene, 2.16

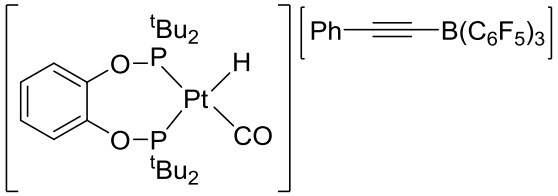

A Youngs NMR tube was charged with a solution of [Pt(CO)(**L2**)] (20.0 mg, 0.032 mmol) and B$(C_6F_5)_3$ (16.5 mg, 0.032 mmol) in d$_5$-chlorobenzene (0.7 mL). Phenylacetylene was added in excess (*ca*. 30 μl) and an instant colour change from bright orange to a dark red colour was observed. Species **2.16** was identified in solution. **^{1}H NMR (400 MHz; d$_5$-PhCl)** δ_H 7.19-6.73 (5H, m *Ph*CC), 6.99-6.77 (4H, m, Ar C*H*), 1.11-1.02 (36H, m, CCH_3), −4.15 (1H, dd, $^{1}J_{HPt}$ = 755 Hz, $^{2}J_{HP(trans)}$ = 159 Hz, $^{2}J_{HP(cis)}$ = 24 Hz, Pt-*H*); **^{11}B{^{1}H} NMR (128 MHz; d$_5$-PhCl)** δ_B −21.1 (br s, CC*B*$(C_6F_5)_3$); **^{19}F NMR (376 MHz; d$_5$-PhCl)** δ_F −138.1 (6F, br, *o*-C$_6$*F*$_5$), −170.2 (3F, br, *p*-C$_6$*F*$_5$), −173.5 (6F, br, *m*-C$_6$*F*$_5$); **^{31}P{^{1}H} NMR (162 MHz; d$_5$-PhCl)** δ_P 174.5 (d, $^{1}J_{PPt}$ = 3301 Hz, $^{2}J_{PP}$ = 15.0 Hz, *P*^{t}Bu$_2$), 163.0 (d, $^{1}J_{PPt}$ = 2294 Hz, $^{2}J_{PP}$ = 15.0 Hz, *P*^{t}Bu$_2$).

5.2.16 Reaction of [Pt(CO)(L1)] and PhCCH

A Youngs NMR tube was charged with a solution of [Pt(CO)(**L1**)] (15.0 mg, 0.024 mmol) in d$_5$-chlorobenzene. Upon addition of excess (*ca*. 15 μl) of PhCCH there was a gradual colour change from orange to pale yellow over 16 h.

^{31}P{^{1}H} NMR (162 MHz; d$_5$-PhCl) δ_P 47.3 (d, $^{2}J_{PP}$ = 23.6 Hz, $^{1}J_{PPt}$ = 3403 Hz, *P*^{t}Bu$_2$), 42.5 (d, $^{2}J_{PP}$ = 23.6 Hz, $^{1}J_{PPt}$ = 3443 Hz, *P*^{t}Bu$_2$).

5.2.17 Reaction of [Pt(CO)(L2)] and PhCCH

A Youngs NMR tube was charged with a solution of [Pt(CO)(**L2**)] (15.2 mg, 0.024 mmol) in d_5-chlorobenzene. Upon addition of excess (*ca*. 15 μl) of PhCCH there was a gradual colour change from orange to pale yellow over 2 h.

$^{31}P\{^1H\}$ NMR (162 MHz; d_5-PhCl) δ_P 190.5 (d, $^2J_{PP}$ = 15.9 Hz, $^1J_{PPt}$ = 3723 Hz, *P*^{t}Bu$_2$), 184.9 (d, $^2J_{PP}$ = 15.9 Hz, $^1J_{PPt}$ = 3672 Hz, *P*^{t}Bu$_2$).

5.2.18 Reaction of [Pt(CO)(L1)]/$B(C_6F_5)_3$ with H_2O

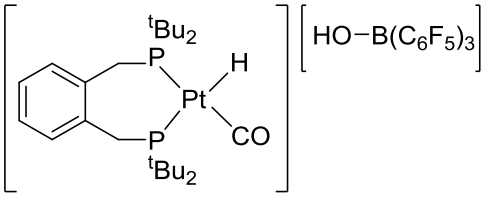

A Youngs NMR tube was charged with [Pt(CO)(**L1**)] (18.5 mg, 0.030 mmol) and $B(C_6F_5)_3$ (15.3 mg, 0.030 mmol) and degassed, undried chlorobenzene was vacuum transferred into the NMR tube to form an orange solution. NMR spectroscopy data was recorded before and after the addition of one drop (*ca*. 5 μl) of degassed, deionised H_2O under N_2.

$^{11}B\{^1H\}$ NMR (128 MHz; PhCl) δ_B −3.43 (s, HO*B*); **^{19}F NMR (376 MHz; PhCl)** δ_F −134.8 (6F, d, *J* = 24.3 Hz, *o*-C_6F_5), −162.8 (3F, t, *J* = 20.5 Hz, *p*-C_6F_5), −16.0 (6F, br t, *J* = 21.8 Hz, *m*-C_6F_5); **$^{31}P\{^1H\}$ NMR (162 MHz; PhCl)** δ_P 43.4 (d, $^1J_{PPt}$ = 2994 Hz, $^2J_{PP}$ = 19 Hz, *P*^{t}Bu$_2$), 34.2 (d, $^1J_{PPt}$ = 2018 Hz, $^2J_{PP}$ = 19 Hz, *P*^{t}Bu$_2$).

5.2.19 Reaction of [Pt(CO)(L2)]/B(C$_6$F$_5$)$_3$ with H$_2$O

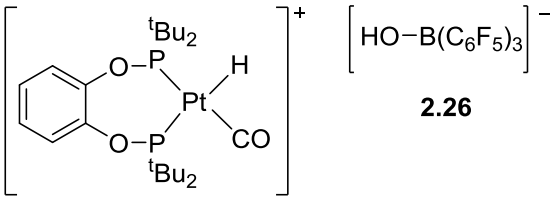

2.6 **2.26**

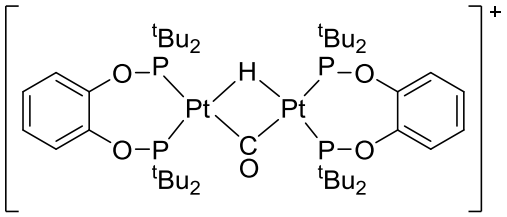

2.7

A Youngs NMR tube was charged with [Pt(CO)(**L2**)] (18.7 mg, 0.030 mmol) and B(C$_6$F$_5$)$_3$ (15.7 mg, 0.030 mmol) and degassed, undried chlorobenzene was vacuum transferred into the NMR tube to form an orange solution. NMR spectroscopy data was recorded before and after the addition of one drop (*ca*. 5 μl) of degassed, deionised H$_2$O under N$_2$.

^{11}B{^{1}H} NMR (128 MHz; PhCl) δ_B 18.6 (s), −3.43 (s, HO-*B*); **^{19}F NMR (376 MHz; PhCl)** δ_F −134.8 (6F, d, *J* = 24.3 Hz, *o*-C$_6$*F*$_5$), −162.8 (3F, t, *J* = 20.5 Hz, *p*-C$_6$*F*$_5$), −16.0 (6F, br t, *J* = 21.8 Hz, *m*-C$_6$*F*$_5$); **^{31}P{^{1}H} NMR (162 MHz; PhCl)** δ_P 182.2 (m, $^1J_{PPt}$ = 4029 Hz, $^2J_{PPt}$ = 131 Hz, $^3J_{PP}$ = 38 Hz, *P*^{t}Bu$_2$ of **2.7**), 174.5 (d, $^1J_{PPt}$ = 3301 Hz, $^2J_{PP}$ = 15.0 Hz, *P*^{t}Bu$_2$ of **2.6**), 163.0 (d, $^1J_{PPt}$ = 2294 Hz, $^2J_{PP}$ = 15.0 Hz, *P*^{t}Bu$_2$ of **2.6**).

5.2.20 Reaction of [Pt(CO)(L1)]/B(C$_6$F$_5$)$_3$ with THF

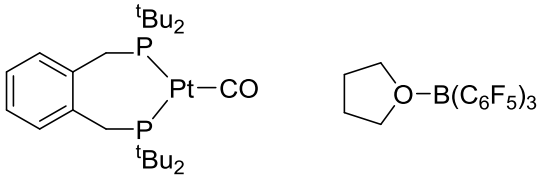

A Youngs NMR tube was charged with a solution of [Pt(CO)(**L1**)] (21.7 mg, 0.035 mmol) and B(C$_6$F$_5$)$_3$ (18.0 mg, 0.035 mmol) in d$_5$-chlorobenzene. An excess (*ca*. 5 μl) of THF was added and no colour change was observed.

^{11}B{^{1}H} NMR (128 MHz; d$_5$-PhCl) δ_B 2.10 (br s, *B*O); **^{31}P{^{1}H} NMR (162 MHz; d$_5$-PhCl)** δ_P 70.2 (s, J_{PPt} = 3645 Hz, *P*^{t}Bu$_2$).

5.2.21 Reaction of [Pt(CO)(L2)]/$B(C_6F_5)_3$ with THF

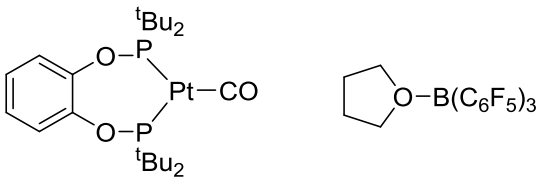

A Youngs NMR tube was charged with a solution of [Pt(CO)(**L2**)] (16.5 mg, 0.027 mmol) and $B(C_6F_5)_3$ (13.6 mg, 0.027 mmol) in d_5-chlorobenzene. An excess (*ca*. 5 µl) of THF was added and no colour change was observed.

$^{11}B\{^1H\}$ NMR (128 MHz; d_5-PhCl) δ_B 2.10 (br s, *B*O); **$^{31}P\{^1H\}$ NMR (162 MHz; d_5-PhCl)** δ_P 218.2 (s, J_{PPt} = 4062 Hz, *P*^{t}Bu$_2$).

5.3 Chapter 3 Experimental

5.3.1 1,2-bis((dicyclohexylphosphanyl)oxy)benzene (L3)

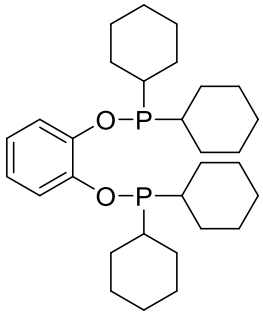

Catechol (125 mg, 1.13 mmol) in THF (5 mL) was added dropwise at room temperature to a suspension of NaH (60 mg, 2.49 mmol) in THF (4 mL). A white suspension and effervescence was seen. Dicyclohexylchlorophosphine (0.5 mL, 2.26 mmol) was added to the reaction mixture dropwise. After stirring for 3 h at room temperature the reaction mixture was filtered through celite under N_2 (extra care was taken to exclude water traces). The solvent was removed *in vacuo* to yield an oily solid. Recrystallisation from hexane at −20 °C yielded white crystals (368 mg, 65%). Crystals suitable for X-ray analysis were obtained from a saturated solution in hexane at −40 °C.

^{1}H NMR (500 MHz; C_6D_6) δ_H 7.50 (2H, m, Ar C*H*), 6.84 (2H, m, Ar C*H*), 2.15-2.01 (4H, m, Cy CH_2/C*H*), 1.88-1.53 (24H, m, Cy CH_2/C*H*), 1.44-1.14 (16H, m, Cy CH_2/C*H*); **^{13}C{^{1}H} NMR (126 MHz; C_6D_6)** δ_C 150.5 (dd, *J* = 8.8, 2.1 Hz, Ar *C*), 122.0 (s, Ar *C*H), 119.4 (d, *J* = 18.7 Hz, Ar *C*H), 38.7 (d, *J* = 19.1 Hz, Cy *C*H), 28.3 (d, *J* = 18.3 Hz, Cy *C*H_2), 27.5-27.2 (m, Cy *C*H_2), 26.8 (d, *J* = 1.0 Hz, Cy *C*H_2); **^{31}P{^{1}H} NMR (202 MHz; C_6D_6)** δ_P 144.9 (s, *P*^{t}Bu$_2$); **HR-MS (ESI)** *m*/*z* calcd. for $C_{30}H_{48}O_2P_2Na$ for $[M+Na]^+$ = 502.3130; obs. = 502.3139; **Elem. Anal.** (calcd. for $C_{30}H_{48}O_2P_2$) C 69.01 (68.77), H 8.24 (8.02).

5.3.2 [$PtCl_2$(L3)] (3.1)

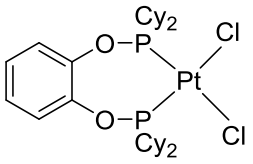

[$PtCl_2$(COD)] (25.0 mg, 0.067 mmol) and **L3** (37 mg, 0.067 mmol) were dissolved in DCM (0.6 mL) in a Youngs NMR tube. After 1 h, $^{31}P\{^1H\}$ NMR confirmed complete complexation. The complex was precipitated in hexane to give a white solid (46 mg, 90%). Crystals suitable for X-ray analysis were obtained by slow diffusion of hexane into a DCM solution of the product.

^{1}H NMR (500 MHz; CD_2Cl_2) δ_H 7.15 (4H, m, Ar *H*), 2.62 (4H, m, Cy C*H*), 2.29 (4H, m, Cy CH_2/C*H*), 1.90-1.65 (20H, m, Cy CH_2/C*H*), 1.40-1.20 (16H, m, Cy CH_2/C*H*); **$^{13}C\{^1H\}$ NMR (126 MHz; CD_2Cl_2)** δ_C 144.5 (dd, J_{CP} = 2.4, 11.5 Hz, Ar *C*), 126.6 (br s, Ar *C*H), 124.3 (br s, Ar *C*H), 40.7 (d, J_{CP} = 39.1 Hz, Cy *C*H), 29.0 (m, Cy *C*H_2), 27.6 (d, J_{CP} = 14.3 Hz, Cy *C*H_2), 26.8 (d, J_{CP} = 12.5 Hz, Cy *C*H_2), 26.5 (s, Cy *C*H_2); **$^{31}P\{^1H\}$ NMR (202 MHz; CD_2Cl_2)** δ_P 123.0 (s, J_{PPt} = 3996 Hz, *P*Cy_2). **HR-MS (ESI):** *m*/*z* calcd. for $C_{30}H_{48}Cl_2O_2P_2Pt$ $[M+Na]^+$ = 791.6327, obs. 791.2015.

5.3.3 [Pt(nbe)(L3)]

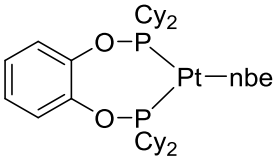

A Youngs NMR tube was charged with a solution of $Pt(nbe)_3$ (13.3 mg, 0.028 mmol) and **L3** (14.0 mg, 0.028 mmol) in d_8-toluene (0.7 mL). The solution was left to react overnight to give a colourless solution. This species was confirmed in solution by NMR spectroscopy only.

^{1}H NMR (400 MHz; d_8-toluene) δ_H 7.01-6.69 (m, Ar C*H*), 2.34 (br m, J_{HPt} = 55.6 Hz), 2.23-0.90 (52H, m, Cy CH_2/C*H* and nbe CH_2/C*H*); **$^{31}P\{^1H\}$ NMR (162 MHz; d_8-toluene)** δ_P 181.0 (s, $^1J_{PPt}$ = 3584 Hz, *P*Cy_2).

5.3.4 [Pt(^{13}CO)$_2$(L3)]

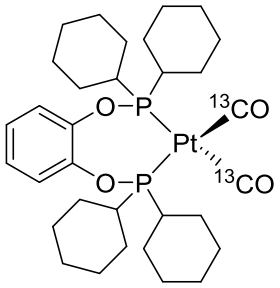

A Youngs NMR tube was charged with a solution of Pt(nbe)$_3$ (13.3 mg, 0.028 mmol) and **L3** (14.0 mg, 0.028 mmol) in d$_8$-toluene (0.7 mL). The solution was frozen in liquid nitrogen and the tube was evacuated. The solution was thawed and allowed to warm to room temperature. The tube was backfilled with ^{13}CO (1.2 bar). The solution changed from colourless to pale yellow. The product was not isolated as it reverts to [Pt(nbe)(**L3**)] upon removal of solvent.

^{13}C{^{1}H} NMR (75 MHz; d$_8$-toluene; −60 °C) δ_C 183.4 (t, $^2J_{CP}$ = 15.7 Hz, $^1J_{CPt}$ = 1743 Hz, Pt^{13}*C*O); **^{31}P{^{1}H} NMR (122 MHz; d$_8$-toluene; −60 °C)** δ_P 151.2 (t,$^2J_{CP}$ = 15.7 Hz, $^1J_{PPt}$ = 3569 Hz, *P*^{t}Bu$_2$).

5.3.5 1,2-bis(dicyclohexylphosphino)xylene (L4)

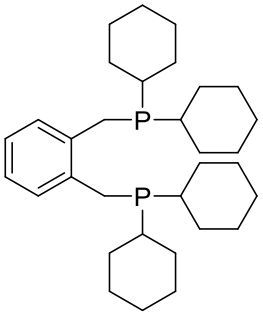

KO^{t}Bu (1.27 g, 11.3 mmol) was added to a solution of *o*-xylene (620 µl, 5.15 mmol) in Et$_2$O (5mL). The white suspension was cooled to −78 °C and *n*-BuLi (~1.6M in hexanes, 7.4 mL, 11.8 mmol) was added dropwise whilst maintaining the temperature. The intense orange coloured solution was allowed to warm to room temperature and then refluxed for 2 h. The reaction mixture was then cooled again to −78 °C and a solution of ClPCy$_2$ (2.5 mL, 11.3 mmol) in Et$_2$O (5 mL) was added dropwise and the temperature was maintained for 1 h. The reaction was warmed to room temperature and degassed H$_2$O

was added slowly. The product was extracted with DCM (4 x 8 mL) and the organic fractions combined and dried over Na_2SO_4. The crude product was washed with hot MeOH to yield **L4** as a white solid (934 mg, 36%). Data is in agreement with literature.[10] **^{1}H NMR (400 MHz; $CDCl_3$)** δ_H 7.14 (2H, m, Ar C*H*), 7.05 (2H, m, Ar C*H*), 3.03 (4H, br s, PCH_2), 1.88-1.63 (20H, m, Cy CH_2/C*H*), 1.57-1.47 (4H, m, Cy CH_2/C*H*), 1.34-1.12 (20H, m, Cy CH_2/C*H*); **^{31}P{^{1}H} NMR (162 MHz; $CDCl_3$)** δ_P −2.86 (s, *P*Cy_2).

5.3.6 [Pt(^{13}CO)$_2$(L4)]

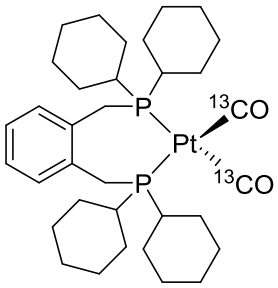

A Youngs NMR tube was charged with a solution of Pt(nbe)$_3$ (26.5 mg, 0.055 mmol) and **L4** (27.7 mg, 0.055 mmol) in d_8-toluene (0.7 mL). The solution was frozen in liquid nitrogen and the tube was evacuated. The solution was thawed and allowed to warm to room temperature. The tube was backfilled with ^{13}CO (1.2 bar). The solution changed from colourless to pale yellow. The product was not isolated as it reverts to [Pt(nbe)(**L4**)] upon removal of solvent.

^{13}C{^{1}H} NMR (75 MHz; d_8-toluene; −60 °C) δ_C 184.1 (t, $^2J_{CP}$ = 11.4 Hz, $^1J_{CPt}$ = 1820 Hz, Pt-*^{13}C*O); **^{31}P{^{1}H} NMR (122 MHz; d_8-toluene; −60 °C)** δ_P 0.37 (t,$^2J_{CP}$ = 11.3 Hz, $^1J_{PPt}$ = 3114 Hz, *P*^{t}Bu$_2$).

5.3.7 1,2-bis(diphenylphosphino)xylene (L5)

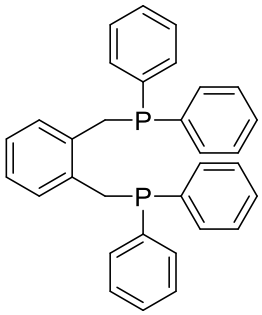

$KPPh_2$ (0.5 M in THF, 5.03 mL, 2.51 mmol) was added dropwise to a solution of α,α'-dichloro-*o*-xylene (200 mg, 1.14 mmol) in THF (10 mL) at −78 °C and the reaction was stirred for 24 h at room temperature. Degassed, deionised H_2O (1 mL) was added to the reaction to quench any remaining $KPPh_2$ and the solution was passed through a silica column, washing with THF (2 x 10 mL). The volatiles were removed *in vacuo* and the product was washed with hexane (3 x 15 mL) to yield a white solid (0.319 g, 59%). Data is in agreement with literature.[11]

^{1}H NMR (400 MHz; $CDCl_3$) δ_H 7.35-7.28 (20H, m, Ph C*H*), 6.90 (2H, m, Ar C*H*), 6.73 (2H, m, Ar C*H*), 3.30 (4H, s, CH_2); **^{13}C{^{1}H} NMR (100 MHz; $CDCl_3$)** δ_C 138.4 (d, $^2J_{CP}$ = 15.1 Hz, Ar *C*), 135.1 , Ar *C*H), 133.2 (d, $^1J_{CP}$ = 19.1 Hz, Ph *C*), 130.7 (s, Ar *C*H), 128.8 (s, Ph-*C*H), 128.5 (s, Ph *C*H), 126.0 (s, Ph *C*H), 33.4 (d, $^1J_{CP}$ = 17.4, *C*H_2); **^{31}P{^{1}H} NMR (162 MHz; $CDCl_3$)** δ_P −13.5 (s, *P*Ph_2).

5.3.8 [Pt(CO)$_2$(L5)]

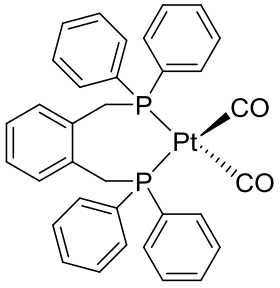

A Youngs NMR tube was charged with a solution of Pt(nbe)$_3$ (28.6 mg, 0.063 mmol) and **L5** (28.4 mg, 0.060 mmol) in d_8-toluene (0.7 mL). The solution was frozen in liquid nitrogen and the tube was evacuated. The solution was thawed and allowed to warm to room temperature. The tube was backfilled with CO (1.2 bar) and the immediate formation of Pt nanoparticles was seen. The solution was filtered to yield a dark red solution. Attempts to isolate the product led to further degradation.

^{1}H NMR (400 MHz; d_8-toluene) δ_H 7.63-7.51 (8H, m, Ph C*H*), 7.15-7.03 (12H, m, Ph C*H*), 6.62 (2H, m, Ar C*H*), 6.10 (2H, m, Ar C*H*), 3.62 (4H, m, CH_2); **^{31}P{^{1}H} NMR (162 MHz; d_8-toluene)** δ_P −9.2 (br s, $^1J_{PPt}$ = 3335 Hz, *P*Ph_2); **ν_{CO} (d_8-toluene)** 1997, 1953 cm^{-1}.

5.3.9 1,2-bis(1,3,5,7-tetramethyl-2,4,8-trioza-6-phospha-adamantane)xylene (L6)

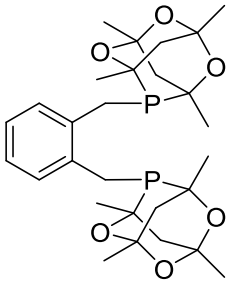

CgPH.BH_3 (500 mg, 2.17 mmol) in THF (15 mL) was cooled to −78 °C and *n*-BuLi (~1.6M in hexanes, 1.63 mL, 2.61 mmol) was added dropwise to form a yellow solution. The reaction mixture was allowed to warm to room temperature and stirred for 30 min. The solution was cooled back to −78 °C and a solution of α,α'-dichloro-*o*-xylene (190 mg, 1.09 mmol) in THF (5 mL) was added dropwise. The reaction mixture was allowed to warm to room temperature and left to stir overnight. $HNEt_2$ (4 mL) was added and the reaction mixture was left to stir for 24 h. The solvent was removed, and the product was extracted with Et_2O (3 x 40 mL) and the solvent was removed *in vacuo* to yield the desired product as a white solid (473 mg, 81%).

^{1}H NMR (400 MHz; $CDCl_3$) δ_H 7.27 (4H, m, Ar C*H*), 7.11 (2H, m, Ar C*H*), 3.41 (2H, dd, *J* = 14.4, 2.1 Hz, PCH_2), 3.23 (2H, br d, *J* = 14.3 Hz, PCH_2), 2.96 (2H, app dt, *J* = 14.3, 2.5 Hz, PCH_2), 2.79 (2H, dd, *J* = 14.4, 2.4 Hz, PCH_2), 2.01-1.77 (12 H, m, Cg CH_2), 1.64 (4H, app dt, *J* = 13.4, 3.8 Hz, Cg CH_2), 1.43 (12H, s, Cg CH_3), 1.36 (12H, s, Cg CH_3), 1.28 (3H, s, Cg CH_3), 1.27 (3H, s, Cg CH_3), 1.25 (3H, s, Cg CH_3), 1.24 (3H, s, Cg CH_3), 1.19 (3H, s, Cg CH_3), 1.16 (3H, s, Cg CH_3), 1.10 (3H, s, Cg CH_3), 1.07 (3H, s, Cg CH_3); **^{13}C NMR (100 MHz; $CDCl_3$)** δ_C 136.5 (m, Ar *C*), 136.2 (Ar *C*), 131.4 (d, *J* = 7.4 Hz, Ar *C*H), 131.2 (d, *J* = 8.8 Hz, Ar *C*H), 126.7 (s, Ar *C*H), 126.6 (s, Ar *C*H), 96.8 (m, Cg *C*), 96.1 (m, Cg *C*), 72.9-72.4 (m, Cg *C*), 45.2 (s, Cg *C*H_2), 45.0 (s, Cg *C*H_2), 37.4 (s, Cg *C*H_2), 37.3 (s, Cg *C*H_2), 28.5-27.8 (m, Cg *C*H_3), 27.6-26.9 (m, Cg *C*H_2 and Cg*C*H_3); **^{31}P NMR (162 MHz; $CDCl_3$)** δ_P 31.2 (s, *P*Cg), 32.3 (s, *P*Cg); **HR-MS (ESI)** *m/z* calcd. for $C_{28}H_{40}NaO_6P_2$ $[M+Na]^+$ = 557.2198; obs. = 557.2200; **Elem. Anal.** (calcd. for $C_{28}H_{40}O_6P_2$) C 63.03 (62.91), H 7.60 (7.54).

5.3.10 [Pt(CO)(L6)]

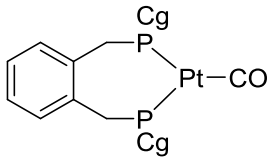

A Youngs NMR tube was charged with a solution of $Pt(nbe)_3$ (40.5 mg, 0.076 mmol) and **L6** (36.2 mg, 0.076 mmol) in d_8-toluene (0.7 mL) and left to react overnight. The solution was frozen in liquid nitrogen and the tube was evacuated. The solution was thawed and backfilled with CO (1 bar) resulting in a colour change to orange. The solvent was removed *in vacuo* and the resulting orange solid was dissolved in toluene. This CO/vacuum cycle was repeated 5 more times to ensure complete displacement of nbe. This species was confirmed by NMR spectroscopy only.

$^{31}P\{^1H\}$ NMR (162 MHz; d_8-toluene, 25 °C) δ_P −10.3 (br, $^1J_{PPt}$ = 3265 Hz, *P*Cg), −11.5 (br, $^1J_{PPt}$ = 3208 Hz, *P*Cg); **$^{31}P\{^1H\}$ NMR (122 MHz; d_8-toluene, −75 °C)** δ_P −9.9 (d, $^2J_{PP}$ = 19.9 Hz, $^1J_{PPt}$ = 3261 Hz, *rac*-*P*Cg), −13.6 (d, $^2J_{PP}$ = 19.9 Hz, $^1J_{PPt}$ = 3261 Hz, *rac*-*P*Cg), −13.5 (s, $^1J_{PPt}$ = 3128 Hz, *meso*-*P*Cg).

5.3.11 4-*tert*-butyl(1,2-bis((di-*tert*-butylphosphanyl)oxy))benzene, L8

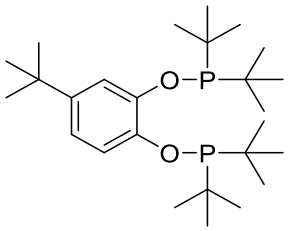

4-*tert*-Butylcatechol (350 mg, 2.11 mmol) in THF (5 mL) was added dropwise at room temperature to a suspension of NaH (101 mg, 4.21 mmol) in THF (4 mL). A white suspension and effervescence was seen. Di-*tert*-butylchlorophosphine (0.8 mL, 4.21 mmol) was added to the reaction mixture dropwise and was heated at 60 °C for 72 h. The reaction mixture was filtered through celite under N_2 (extra care was taken to exclude water traces). The solvent was removed *in vacuo* to yield an oily solid. Recrystallisation from hexane at −20 °C yielded white crystals (598 mg, 62%).

^1H NMR (400 MHz; C_6D_6) δ_H 7.86 (1H, dd, J_{HH} = 5.1, 2.3 Hz, Ar C*H*), 7.65 (1H, dd,

J_{HH} = 8.6, 4.3 Hz, Ar C*H*), 6.89 (1H, dd, J_{HH} = 8.6, 2.3 Hz, Ar C*H*), 1.27 (18H, d, $^3J_{HP}$ = 2.7 Hz, PC(CH_3)$_3$), 1.24 (18H, d, $^3J_{HP}$ = 3.3 Hz, PC(CH_3)$_3$), 1.22 (9H, s, CH_3); **^{13}C{^{1}H} NMR (100 MHz; C_6D_6)** δ_C 149.4 (dd, *J* = 9.0, 1.6 Hz, Ar *C*), 147.9 (dd, *J* = 9.9, 1.6 Hz, Ar *C*), 144.4 (m, Ar *C*), 118.3 (m, Ar *C*H), 118.0 (d, *J* = 22.4 Hz, Ar *C*H), 116.2 (d, *J* = 23.7 Hz, Ar *C*H), 36.0 (d, *J* = 7.0 Hz, P*C*(CH$_3$)$_3$), 35.8 (d, *J* = 7.2 Hz, P*C*(CH$_3$)$_3$), 34.6 (s, *C*(CH$_3$)$_3$), 31.7 (s, C(*C*H$_3$)$_3$), 27.8 (d, *J* = 2.2 Hz, PC(*C*H$_3$)$_3$), 27.6 (d, *J* = 2.3 Hz, PC(*C*H$_3$)$_3$); **^{31}P{^{1}H} NMR (162 MHz; C_6D_6)** δ_P 151.9 (s, *P*^{t}Bu$_2$), 151.4 (s, *P*^{t}Bu$_2$); **HR-MS (ESI)** *m*/*z* calcd. for $C_{26}H_{48}O_2P_2Na$ for $[M+Na]^+$ = 477.3027; obs. = 477.3031; **Elem. Anal.** (calcd. for $C_{26}H_{48}O_2P_2$) C 66.01 (65.39), H 10.68 (10.13).

5.3.12 [PtCl$_2$(L8)]

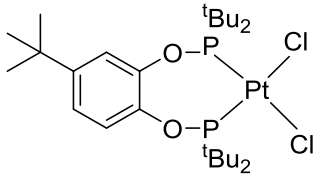

[PtCl$_2$(COD)] (38 mg, 0.10 mmol) and **L8** (51 mg, 0.11 mmol) were dissolved in DCM (0.6 mL) in a Youngs NMR tube. After 12 hours, ^{31}P{^{1}H} NMR spectroscopy confirmed complete complexation. The complex was precipitated in hexane to yield a white solid, (68 mg, 94%). Crystals suitable for X-ray analysis were obtained by slow diffusion of hexane into a DCM solution of the product.

^{1}H NMR (400 MHz; $CDCl_3$) δ_H 7.08 (1H, dd, J_{HH} = 8.6, 2.1 Hz, Ar C*H*), 6.98-6.91 (2H, m, Ar C*H*), 1.58 (18H, d, $^3J_{HP}$ = 1.7 Hz, PC(CH_3)$_3$), 1.54 (18H, d, $^3J_{HP}$ = 1.7 Hz, PC(CH_3)$_3$), 1.28 (9H, s, CH_3); **^{13}C{^{1}H} NMR (100 MHz; $CDCl_3$)** δ_C 149.4 (s, Ar *C*), 144.0 (d, *J* = 15.5 Hz, Ar *C*), 142.2 (d, *J* = 15.5 Hz, Ar *C*), 122.4 (s, Ar *C*H), 121.4 (d, *J* = 2.5 Hz, Ar *C*H), 119.0 (d, *J* = 2.2 Hz, Ar *C*H), 44.9 (m, P*C*(CH$_3$)$_3$), 31.4 (s, *C*(CH$_3$)$_3$), 29.8 (d, *J* = 3.5 Hz, PC(*C*H$_3$)$_3$); **^{31}P{^{1}H} NMR (162 MHz; $CDCl_3$)** δ_P 135.8 (d, $^2J_{PP}$ = 5.0 Hz, $^1J_{PPt}$ = 4145 Hz, *P*^{t}Bu$_2$), 135.5 (d, $^2J_{PP}$ = 5.0 Hz, $^1J_{PPt}$ = 4137 Hz, *P*^{t}Bu$_2$); **HR-MS (ESI)** *m*/*z* calcd. for $C_{26}H_{48}ClO_2P_2Pt$ for $[M-Cl]^+$ = 684.2466; obs. = 684.2462; **Elem. Anal.** (calcd. for $C_{26}H_{48}Cl_2O_2P_2Pt$) C 43.45 (43.34), H 6.89 (6.71).

5.3.13 Reaction of [Pt(CO)(L1)]/BPh$_3$ with H$_2$

A Youngs NMR tube was charged with a solution of [Pt(CO)(**L1**)] (12.1 mg, 0.020 mmol) and BPh$_3$ (4.7 mg, 0.020 mmol) in chlorobenzene (0.6 mL). The orange solution

was frozen in liquid nitrogen and the tube was evacuated. The solution was thawed and allowed to warm to room temperature. The tube was backfilled with H_2 (1 bar) and shaken. The solution lightened to a pale orange colour over time.

^{1}H NMR (400 MHz; PhCl) δ_H −3.13 (m, $^1J_{HPt}$ = 1040 Hz, Pt(*H*)$_2$), −7.48 (1H, 1:8:18:8:1 quqq, $^1J_{HPt}$ = 393 Hz, $^2J_{HP}$ = 41 Hz, Pt(μ-*H*)$_3$Pt); **^{11}B{^{1}H} NMR (128 MHz; PhCl)** δ_B 67.4 (br, *B*Ph$_3$), 0.9 (br s); **^{31}P{^{1}H} NMR (162 MHz; PhCl)** δ_P 70.2 (br, $w_{1/2}$ = 200 Hz, $^2J_{PPt}$ = 3671 Hz, *P*^{t}Bu$_2$ of [Pt(CO)(**L1**)]), 50.8 (br, *P*^{t}Bu$_2$ of [(**L1**)Pt(μ-H)$_3$Pt(**L1**)]), 47.6 (s, $^2J_{PPt}$ = 2077 Hz, *P*^{t}Bu$_2$ of [Pt(H)$_2$(**L1**)]).

5.3.14 Reaction of [Pt(CO)(L2)]/BPh$_3$ with H$_2$

A Youngs NMR tube was charged with a solution of [Pt(CO)(**L2**)] (11.3 mg, 0.018 mmol) and BPh$_3$ (4.4 mg, 0.018 mmol) in chlorobenzene (0.6 mL). The orange solution was frozen in liquid nitrogen and the tube was evacuated. The solution was thawed and allowed to warm to room temperature. The tube was backfilled with H_2 (1 bar) and shaken. The solution lightened to a pale orange colour over time.

^{1}H NMR (400 MHz; PhCl) δ_H −2.12 (m, $^1J_{HPt}$ = 1040 Hz, Pt(*H*)$_2$), −5.72 (1H, 1:8:18:8:1 quqq, $^1J_{HPt}$ = 393 Hz, $^2J_{HP}$ = 41.3 Hz, Pt(μ-*H*)$_3$Pt); **^{11}B{^{1}H} NMR (128 MHz; PhCl)** δ_B 67.4 (br, *B*Ph$_3$), 1.0 (br s); **^{31}P{^{1}H} NMR (162 MHz; PhCl)** δ_P 218.2 (br, $w_{1/2}$ = 200 Hz, $^2J_{PPt}$ = 3940 Hz, *P*^{t}Bu$_2$ of [Pt(CO)(**L2**)]), 192.4 (br, *P*^{t}Bu$_2$ of [(**L2**)Pt(μ-H)$_3$Pt(**L2**)]), 185.6 (m, $^1J_{PPt}$ = 3459 Hz, $^2J_{PPt}$ = 153 Hz, $^3J_{PP}$ = 10.1 Hz, *P*^{t}Bu$_2$ of [Pt(H)$_2$(**L2**)]).

5.3.15 Reaction of [Pt(CO)(L1)]/B(OPh)$_3$ with H$_2$

A Youngs NMR tube was charged with a solution of [Pt(CO)(**L1**)] (15.7 mg, 0.025 mmol) and B(OPh)$_3$ (8.7 mg, 0.025 mmol) in chlorobenzene (0.6 mL). The orange solution was frozen in liquid nitrogen and the tube was evacuated. The solution was thawed and allowed to warm to room temperature. The tube was backfilled with H_2 (1 bar) and shaken. The solution lightened to a pale orange colour over time.

^{1}H NMR (400 MHz; PhCl) δ_H −3.13 (m, $^1J_{HPt}$ = 1040 Hz, Pt(*H*)$_2$), −7.48 (1H, 1:8:18:8:1 quqq, $^1J_{HPt}$ = 393 Hz, $^2J_{HP}$ = 41 Hz, Pt(μ-*H*)$_3$Pt); **^{11}B{^{1}H} NMR (128 MHz; PhCl)** δ_B 14.3 (br, *B*(OPh)$_3$), 0.8 (br s. [*B*(OPh)$_4$]$^-$); **^{31}P{^{1}H} NMR (162 MHz; PhCl)** δ_P 50.8 (br, *P*^{t}Bu$_2$ of [(**L1**)Pt(μ-H)$_3$Pt(**L1**)]), 47.6 (s, $^2J_{PPt}$ = 2077 Hz, *P*^{t}Bu$_2$ of [Pt(H)$_2$(**L1**)]).

5.3.16 Reaction of [Pt(CO)(L2)]/B(OPh)$_3$ with H$_2$

A Youngs NMR tube was charged with a solution of [Pt(CO)(**L2**)] (15.3 mg, 0.025 mmol) and B(OPh)$_3$ (8.4 mg, 0.025 mmol) in chlorobenzene (0.6 mL). The orange solution was frozen in liquid nitrogen and the tube was evacuated. The solution was thawed and allowed to warm to room temperature. The tube was backfilled with H$_2$ (1 bar) and shaken. The solution lightened to a pale orange colour over time.

^{1}H NMR (400 MHz; PhCl) δ_H −5.72 (1H, 1:8:18:8:1 ququ, $^1J_{HPt}$ = 393 Hz, $^2J_{HP}$ = 41.3 Hz, Pt(μ-*H*)$_3$Pt); **^{11}B{^{1}H} NMR (128 MHz; PhCl)** δ_B 14.3 (br, *B*(OPh)$_3$), 0.8 (br s, [*B*(OPh)$_4$]$^-$); **^{31}P{^{1}H} NMR (162 MHz; PhCl)** δ_P 185.6 (m, $^1J_{PPt}$ = 3459 Hz, $^2J_{PPt}$ = 153 Hz, $^3J_{PP}$ = 10.1 Hz, *P*^{t}Bu$_2$ of [(**L2**)Pt(μ-H)$_3$Pt(**L2**)]).

5.3.17 Reaction of [Pt(CO)(L1)]/B(C$_2$H$_2$F$_3$)$_3$ with H$_2$

A Youngs NMR tube was charged with a solution of [Pt(CO)(**L1**)] (25.6 mg, 0.041 mmol) and B(C$_2$H$_2$F$_3$)$_3$ (16.7 mg, 0.041 mmol) in d$_5$-chlorobenzene (0.6 mL). The orange solution was frozen in liquid nitrogen and the tube was evacuated. The solution was thawed and allowed to warm to room temperature. The tube was backfilled with H$_2$ (1 bar) and shaken.

^{1}H NMR (400 MHz; d$_5$-PhCl) δ_H 7.57-6.80 (m, Ar C*H*), 5.86 (br d, *J* = 4.4 Hz), 3.58 (br, C*H*$_2$), 1.41-1.07 (m, C(C*H*$_3$)$_3$), −4.55 (1H, dd, $^1J_{HPt}$ = 734 Hz, $^2J_{HP(trans)}$ = 145 Hz, $^2J_{HP(cis)}$ = 16 Hz, [Pt(*H*)(CO)(**L1**)]), −7.48 (1H, 1:8:18:8:1 ququ, $^1J_{HPt}$ = 393 Hz, $^2J_{HP}$ = 41 Hz, Pt-*H*-Pt); **^{11}B{^{1}H} NMR (128 MHz, d$_5$-PhCl)** δ_B −0.3 (br), −8.4 (s), −9.5 (s); **^{31}P{^{1}H} NMR (162 Hz, d$_5$-PhCl)** δ_P 50.8 (br, *P*^{t}Bu$_2$ of [(**L1**)Pt(μ-H)$_3$Pt(**L1**)]), 43.4 (d, $^1J_{PPt}$ = 2987 Hz, $^2J_{PP}$ = 19 Hz, *P*^{t}Bu$_2$ of [Pt(H)(CO)(**L1**)]), 34.2 (d, $^1J_{PPt}$ = 2004 Hz, $^2J_{PP}$ = 19 Hz, *P*^{t}Bu$_2$ of [Pt(H)(CO)(**L1**)]).

5.3.18 Reaction of [Pt(CO)(L2)]/B(C$_2$H$_2$F$_3$)$_3$ with H$_2$

A Youngs NMR tube was charged with a solution of [Pt(CO)(**L2**)] (25.6 mg, 0.041 mmol) and B(C$_2$H$_2$F$_3$)$_3$ (16.6 mg, 0.041 mmol) in d$_5$-chlorobenzene (0.6 mL). The orange solution was frozen in liquid nitrogen and the tube was evacuated. The solution was thawed and allowed to warm to room temperature. The tube was backfilled with H$_2$ (1 bar) and shaken.

^{1}H NMR (400 MHz; d$_5$-PhCl) δ_H 7.28-6.82 (m, Ar C*H*), 5.87 (br d, *J* = 4.4 Hz), 1.27-1.16 (36H, m, C(C*H*$_3$)$_3$), −5.72 (1H, 1:8:18:8:1 ququ, $^1J_{HPt}$ = 393 Hz, $^2J_{HP}$ = 41.3 Hz,

Pt(μ-*H*)Pt); **^{11}B{^{1}H} NMR (128 MHz, d$_5$-PhCl)** δ_B −8.4 (s); **^{31}P{^{1}H} NMR (162 Hz, d$_5$-PhCl)** δ_P 185.6 (m, $^{1}J_{PPt}$ = 3459 Hz, $^{2}J_{PPt}$ = 153 Hz, $^{3}J_{PP}$ = 10.1 Hz, *P*^{t}Bu$_2$).

5.3.19 Reaction of [Pt(CO)(L1)]/B(C$_2$H$_2$F$_3$)$_3$ with PhCCH

A Youngs NMR tube was charged with a solution of [Pt(CO)(**L1**)] (23.2 mg, 0.038 mmol) and B(C$_2$H$_2$F$_3$)$_3$ (15.2 mg, 0.038 mmol) in d$_5$-chlorobenzene (0.7 mL). Phenylacetylene was added in excess (*ca*. 30 μl).

^{1}H NMR (400 MHz; d$_5$-PhCl) δ_H −4.55 (1H, dd, $^{1}J_{HPt}$ = 734 Hz, $^{2}J_{HP(trans)}$ = 145 Hz, $^{2}J_{HP(cis)}$ = 16 Hz, [Pt(*H*)(CO)(**L1**)]); **^{11}B{^{1}H} NMR (128 MHz, d$_5$-PhCl)** δ_B −7.2 (s); **^{31}P{^{1}H} NMR (162 Hz, d$_5$-PhCl)** δ_P 43.4 (d, $^{1}J_{PPt}$ = 2987 Hz, $^{2}J_{PP}$ = 19 Hz, *P*^{t}Bu$_2$ of [Pt(H)(CO)(**L1**)]), 34.2 (d, $^{1}J_{PPt}$ = 2004 Hz, $^{2}J_{PP}$ = 19 Hz, *P*^{t}Bu$_2$ of [Pt(H)(CO)(**L1**)]).

5.3.20 Reaction of [Pt(CO)(L2)]/B(C$_2$H$_2$F$_3$)$_3$ with PhCCH

A Youngs NMR tube was charged with a solution of [Pt(CO)(**L2**)] (23.5 mg, 0.038 mmol) and B(C$_2$H$_2$F$_3$)$_3$ (15.3 mg, 0.038 mmol) in d$_5$-chlorobenzene (0.7 mL). Phenylacetylene was added in excess (*ca*. 30 μl). A colour change to deep red was observed.

^{1}H NMR (400 MHz; d$_5$-PhCl) δ_H 7.81-6.61 (m, Ar C*H*), 4.33 (t, *J* = 8.3 Hz, $^{1}J_{PPt}$ = 48 Hz), 1.47-0.58 (m, C(C*H*$_3$)$_3$) −4.15 (1H, dd, $^{1}J_{HPt}$ = 755 Hz, $^{2}J_{HP(trans)}$ = 159 Hz, $^{2}J_{HP(cis)}$ = 24.3 Hz, [Pt(*H*)(CO)(**L2**)]); **^{11}B{^{1}H} NMR (128 MHz; d$_5$-PhCl)** δ_B −7.3 (s), −12.9 (s); **^{31}P{^{1}H} NMR (162 MHz; d$_5$-PhCl)** δ_P 199.3 (d, $^{1}J_{PPt}$ = 3550 Hz, $^{2}J_{PP}$ = 19.4 Hz), 187.8 (d, $^{1}J_{PPt}$ = 4301 Hz, $^{2}J_{PP}$ = 19.4 Hz), 174.5 (d, $^{1}J_{PPt}$ = 3301 Hz, $^{2}J_{PP}$ = 15.0 Hz, *P*^{t}Bu$_2$ of [Pt(H)(CO)(**L2**)]), 163.0 (d, $^{1}J_{PPt}$ = 2294 Hz, $^{2}J_{PP}$ = 15.0 Hz, *P*^{t}Bu$_2$ of [Pt(H)(CO)(**L2**)]).

5.3.21 *In situ* formation of [Pt(^{13}CO)(L1)]/[Zr(Cp*)$_2$(OMes)][B(C$_6$F$_5$)$_4$]

In a glovebox, a solution of [CPh$_3$][B(C$_6$F$_5$)$_4$] (20.9 mg, 0.023 mmol) in d$_5$-chlorobenzene (0.2 mL) was added dropwise to a stirred solution of Zr(Cp*)$_2$Me$_2$ (8.9 mg, 0.023 mmol) in d$_5$-chlorobenzene (0.2 mL) to give an orange solution. A solution of MesOH (3.1 mg, 0.023 mmol) in d$_5$-chlorobenzene (0.2 mL) was added dropwise to the reaction mixture and effervescence was observed and a colour change to deep red. After the effervescence ceased (10 min), the reaction mixture was added to [Pt(^{13}CO)(**L1**)] (14.0 mg, 0.023 mmol) in a Youngs NMR tube. A colour change from deep red to orange was observed.

^{1}H NMR (500 MHz; d$_5$-PhCl) δ_H 7.20-6.93 (4H, m, Ar C*H* of [Pt(^{13}CO)(**L1**)]), 6.75(s,

2H, Ar C*H* of **3.6**), 3.57 (4H, br, CH_2), 2.16 (3H, s, *p*-CH_3), 1.93 (3H, s, *o*-CH_3), 1.92 (3H, s, *o*-CH_3), 1.70 (30H, s, Cp* CH_3), 1.23 (36H, br d, J = 7.0 Hz, ^{t}Bu$_2$ CH_3); **^{13}C{^{1}H} NMR (125 MHz; d$_5$-PhCl)** δ_C 270.8 (t, $^2J_{CP}$ = 55.4 Hz, $^1J_{CPt}$ = 2510 Hz, ^{13}*C*O); **^{31}P{^{1}H} NMR (202 MHz; d$_5$-PhCl)** δ_P 66.4 (d, $^2J_{PC}$ = 55.4 Hz, $^1J_{PPt}$ = 3125 Hz, *P*^{t}Bu$_2$).

5.3.22 *In situ* formation of [Pt(^{13}CO)(L2)]/[Zr(Cp*)$_2$(OMes)][B(C$_6$F$_5$)$_4$]

In a glovebox, a solution of [CPh$_3$][B(C$_6$F$_5$)$_4$] (19.3 mg, 0.021 mmol) in d$_5$-chlorobenzene (0.2 mL) was added dropwise to a stirred solution of Zr(Cp*)$_2$Me$_2$ (8.2 mg, 0.021 mmol) in d$_5$-chlorobenzene (0.2 mL) to give an orange solution. A solution of MesOH (2.8 mg, 0.021 mmol) in d$_5$-chlorobenzene (0.2 mL) was added dropwise to the reaction mixture and effervescence was observed and a colour change to deep red. After the effervescence ceased (10 min), the reaction mixture was added to [Pt(^{13}CO)(**L2**)] (13.0 mg, 0.021 mmol) in a Youngs NMR tube. A colour change from deep red to orange was observed. **^{1}H NMR (500 MHz; d$_5$-PhCl)** δ_H 7.03 (2H, m, Ar C*H* of [Pt(^{13}CO)(**L2**)]), 6.89 (2H, m, Ar C*H* of [Pt(^{13}CO)(**L2**)]), 6.78 (s, 2H, Ar C*H* of **3.6**), 2.18 (3H, s, *p*-CH_3), 1.94 (3H, s, *o*-CH_3), 1.93 (3H, s, *o*-CH_3), 1.72 (30H, s, Cp* CH_3), 1.31 (36H, d, J = 14.5 Hz, C(CH_3)$_3$); **^{13}C{^{1}H} NMR (125 MHz; d$_5$-PhCl)** δ_C 277.6 (t, $^2J_{CP}$ = 67.7 Hz, $^1J_{CPt}$ = 2381 Hz, ^{13}*C*O); **^{31}P{^{1}H} NMR (202 MHz; d$_5$-PhCl)** δ_P 210.0 (d, $^2J_{PC}$ = 67.7 Hz, $^1J_{PPt}$ = 3414 Hz, *P*^{t}Bu$_2$).

5.3.23 Reaction of [Pt(^{13}CO)(L1)]/3.7 with H$_2$

An orange solution of [Pt(^{13}CO)(**L1**)]/**3.7** in a Youngs NMR tube was frozen in liquid nitrogen and the tube was evacuated. The solution was thawed and allowed to warm to room temperature. The tube was backfilled with H$_2$ (1 bar) and shaken. The solution lightened to a pale yellow colour over time.

^{1}H NMR (400 MHz; d$_5$-PhCl) δ_H −3.13 (m, $^1J_{HPt}$ = 1040 Hz, Pt(*H*)$_2$), −7.48 (1H, 1:8:18:8:1 quqq, $^1J_{HPt}$ = 393 Hz, $^2J_{HP}$ = 41 Hz, Pt(μ-*H*)$_3$Pt); **^{31}P{^{1}H} NMR (162 MHz; d$_5$-PhCl)** δ_P 66.4 (d, $^2J_{PC}$ = 55.4 Hz, $^1J_{PPt}$ = 3125 Hz, *P*^{t}Bu$_2$), 50.8 (br, *P*^{t}Bu$_2$ of [(**L1**)Pt(μ-H)$_3$Pt(**L1**)]), 47.6 (s, $^2J_{PPt}$ = 2077 Hz, *P*^{t}Bu$_2$ of [Pt(H)$_2$(**L1**)]).

5.3.24 Reaction of [Pt(^{13}CO)(L2)]/3.7 with H$_2$

An orange solution of [Pt(^{13}CO)(**L2**)]/**3.7** in a Youngs NMR tube was frozen in liquid nitrogen and the tube was evacuated. The solution was thawed and allowed to warm to

room temperature. The tube was backfilled with H_2 (1 bar) and shaken. The solution lightened to a pale orange colour over time.

^{1}H NMR (400 MHz; PhCl) δ_H −5.72 (1H, 1:8:18:8:1 ququ, $^1J_{HPt}$ = 393 Hz, $^2J_{HP}$ = 41.3 Hz, Pt(μ-*H*)$_3$Pt); **^{31}P{^{1}H} NMR (162 MHz; PhCl)** δ_P 210.0 (d, $^2J_{PC}$ = 67.7 Hz, $^1J_{PPt}$ = 3414 Hz, *P*^{t}Bu$_2$), 185.6 (m, $^1J_{PPt}$ = 3459 Hz, $^2J_{PPt}$ = 153 Hz, $^3J_{PP}$ = 10.1 Hz, *P*^{t}Bu$_2$ of [(**L2**)Pt(μ-H)$_3$Pt(**L2**)]).

5.3.25 Reaction of [Pt(CO)(L1)]/AlCl$_3$ with H$_2$

A Youngs NMR tube was charged with a solution of [Pt(CO)(**L1**)] (13.5 mg, 0.022 mmol) and $AlCl_3$ (2.9 mg, 0.022 mmol) in d_5-chlorobenzene (0.6 mL). The orange solution was frozen in liquid nitrogen and the tube was evacuated. The solution was thawed and allowed to warm to room temperature. The tube was backfilled with H_2 (1 bar) and shaken.

^{1}H NMR (400 MHz; d$_5$-PhCl) δ_H 7.21-6.95 (m, Ar C*H*), 3.48 (br, C*H*$_2$), 1.27-1.02 (m, C(C*H*$_3$)$_3$), −4.55 (1H, dd, $^1J_{HPt}$ = 734 Hz, $^2J_{HP(trans)}$ = 145 Hz, $^2J_{HP(cis)}$ = 16 Hz, [Pt(*H*)(CO)(**L1**)]), −7.48 (1H, 1:8:18:8:1 q of q, $^1J_{HPt}$ = 393 Hz, $^2J_{HP}$ = 41 Hz, Pt(μ-*H*)$_3$Pt); **^{27}Al{^{1}H} NMR (130 MHz, d$_5$-PhCl)** δ_{Al} 97.1 (s); **^{31}P{^{1}H} NMR (162 Hz, d$_5$-PhCl)** δ_P 50.8 (br, *P*^{t}Bu$_2$ of [(**L1**)Pt(μ-H)$_3$Pt(**L1**)]), 43.4 (d, $^1J_{PPt}$ = 2987 Hz, $^2J_{PP}$ = 19 Hz, *P*^{t}Bu$_2$ of [Pt(H)(CO)(**L1**)]), 34.2 (d, $^1J_{PPt}$ = 2004 Hz, $^2J_{PP}$ = 19 Hz, *P*^{t}Bu$_2$ of [Pt(H)(CO)(**L1**)]).

5.3.26 Reaction of [Pt(CO)(L2)]/AlCl$_3$ with H$_2$

A Youngs NMR tube was charged with a solution of [Pt(CO)(**L2**)] (13.6 mg, 0.023 mmol) and $AlCl_3$ (3.0 mg, 0.023 mmol) in d_5-chlorobenzene (0.6 mL). The orange solution was frozen in liquid nitrogen and the tube was evacuated. The solution was thawed and allowed to warm to room temperature. The tube was backfilled with H_2 (1 bar) and shaken.

^{1}H NMR (400 MHz; d$_5$-PhCl) δ_H 7.22-6.93 (m, Ar C*H*), 1.27 (m, C(C*H*$_3$)$_3$), −4.15 (1H, dd, $^1J_{HPt}$ = 755 Hz, $^2J_{HP(trans)}$ = 159 Hz, $^2J_{HP(cis)}$ = 24.3 Hz, [Pt(*H*)(CO)(**L2**)]), −5.72 (1H, 1:8:18:8:1 ququ, $^1J_{HPt}$ = 393 Hz, $^2J_{HP}$ = 41.3 Hz, Pt(μ-*H*)$_3$Pt); **^{27}Al{^{1}H} NMR (130 MHz, d$_5$-PhCl)** δ_{Al} 97.1 (s); **^{31}P{^{1}H} NMR (162 Hz, d$_5$-PhCl)** δ_P 185.6 (m, $^1J_{PPt}$ = 3459 Hz, $^2J_{PPt}$ = 153 Hz, $^3J_{PP}$ = 10.1 Hz, *P*^{t}Bu$_2$ of [(**L2**)Pt(μ-H)$_3$Pt(**L2**)]), 174.5 (d, $^1J_{PPt}$ = 3301 Hz, $^2J_{PP}$ = 15.0 Hz, *P*^{t}Bu$_2$ of [Pt(H)(CO)(**L2**)]), 163.0 (d, $^1J_{PPt}$ = 2294 Hz, $^2J_{PP}$ = 15.0 Hz, *P*^{t}Bu$_2$ of [Pt(H)(CO)(**L2**)]).

5.3.27 Synthesis of [$PdCl_2$(L1)]

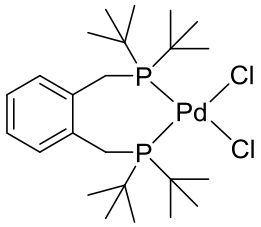

$Pd(dba)_2$ (879 mg, 1.53 mmol) and **L1** (605 mg, 1.53 mmol) were combined and stirred in THF (30 mL) for 2 d at room temperature. The red-orange solution was filtered, and the solvent was removed *in vacuo*. The resulting orange-solid was dissolved in Et_2O (35 mL) and HCl (2.5 mL, 1M in Et_2O) was added. Over 1 h, a dark yellow precipitate had formed. The solid was isolated and washed with Et_2O (3 x 30 mL) and THF (1 x 30 mL). The product was dissolved in DCM and the insoluble material was filtered off. The desired product was then isolated as a yellow solid by precipitation from a DCM solution by slow addition of Et_2O (540 mg, 62%). NMR data is in agreement with literature.[12,13] **^{1}H NMR (400 MHz; CD_2Cl_2)** δ_H 7.38 (2H, m, Ar C*H*), 7.22 (2H, m Ar C*H*), 3.43 (4H, m, CH_2), 1.60 (36 H, d, $^3J_{HP}$ = 14.0 Hz, C(CH_3)$_3$); **^{31}P{^{1}H} NMR (162 MHz; CD_2Cl_2)** δ_P 37.2 (s, P^tBu_2).

5.3.28 Synthesis of [Pd(CO)(L1)]

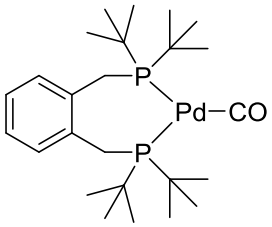

[$PdCl_2$(**L1**)] (100 mg, 0.17 mmol) was dissolved in EtOH (CO saturated) and then the yellow suspension was sparged with CO and kept under a CO atmosphere (CO balloon). NEt_3 (50 µl, 0.35 mmol) was added and then the reaction mixture was sparged with CO. A darkening of the reaction mixture was seen, and a yellow precipitate formed in a dark orange solution. The yellow solid was isolated as the desired product (49 mg, 55%). **^{1}H NMR (400 MHz; d_8-toluene)** δ_H 7.13 (2H, m, Ar C*H*), 6.90 (2H, m, Ar C*H*), 3.10 (4H, m, CH_2), 1.21 (36H, m, C(CH_3)$_3$); **^{31}P{^{1}H} NMR (400 MHz; d_8-toluene)** δ_P 50.0 (s, P^tBu_2).

5.3.29 Synthesis of $^{t}Bu_2PCH_2N(CH_2Ph)CH_2P^{t}Bu_2$ ($P^{tBu}N^{Bn}P^{tBu}$)

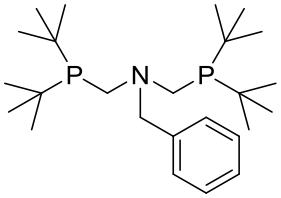

$^{t}Bu_2PH$ (0.25 mL, 1.35 mmol) and paraformaldehyde (41 mg, 1.35 mmol) were combined in degassed MeOH (4 mL) and was left to stir for 30 minutes at room temperature. $BnNH_2$ (75 μL, 0.68 mmol) was added dropwise. The reaction mixture was stirred for 72 h after which the colourless solution was concentrated *in vacuo* to yield the product as a colourless viscous oil (239 mg, 83%) of sufficient purity (> 96%). NMR data is in agreement with literature.[14]

^{1}H NMR (400 MHz; $CDCl_3$) δ_H 7.29-7.12 (5H, m, Ar C*H*), 3.76 (2H, br s, Bn CH_2), 2.70 (4H, br s, PCH_2N), 1.06 (36H, d, $^{3}J_{HP}$ = 10.9 Hz, C(CH_3)$_3$); **^{31}P{^{1}H} NMR (162 MHz; $CDCl_3$)** δ_P 13.7 (s, $P^{t}Bu_2$).

5.3.30 Synthesis of [Pt(CO)($P^{tBu}N^{Bn}P^{tBu}$)]

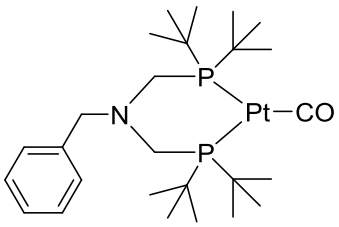

A Youngs NMR tube was charged with a solution of $Pt(nbe)_3$ (34.0 mg, 0.071 mmol) and $P^{tBu}N^{Bn}P^{tBu}$ (30.1 mg, 0.071 mmol) in d_8-toluene (0.7 mL) and left to react overnight. The solution was frozen in liquid nitrogen and the tube was evacuated. The solution was thawed and backfilled with CO (1 bar) resulting in a colour change to orange. The solvent was removed *in vacuo* and the resulting orange solid was dissolved in toluene. This CO/vacuum cycle was repeated 5 more times to ensure complete displacement of nbe. This species was confirmed by NMR spectroscopy only.

^{1}H NMR (400 MHz; d_8-toluene) δ_H 7.17-7.00 (5H, m, Ar C*H*), 3.26 (2H, br s, Bn CH_2), 2.77 (4H, br m, PCH_2N), 1.13 (36H, m, C(CH_3)$_3$); **^{31}P{^{1}H} NMR (162 MHz; $CDCl_3$)** δ_P 63.7 (s, $^{1}J_{PPt}$ = 3429, $P^{t}Bu_2$).

5.3.31 Reaction of [Pt(CO)($P^{tBu}N^{Bn}P^{tBu}$)]/$B(C_6F_5)_3$ with H_2

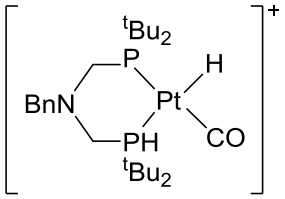

3.16

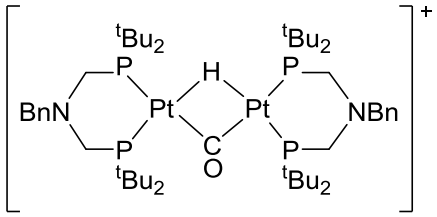

3.17

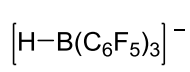

2.7

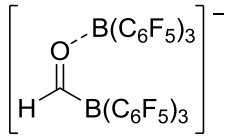

2.8

A Youngs NMR tube was charged with a solution of [Pt(CO)($P^{tBu}N^{Bn}P^{tBu}$)] (24.3 mg, 0.038 mmol) and $B(C_6F_5)_3$ (19.2 mg, 0.038 mmol) in d_5-chlorobenzene (0.7 mL). The orange solution was frozen in liquid nitrogen and the tube was evacuated. The solution was thawed and allowed to warm to room temperature. The tube was backfilled with H_2 (1 bar) and shaken. A colour change from orange to yellow was observed. Two cationic (**3.16** and **3.17**) and two anionic species (**2.7**-**2.8**) were identified in solution.

3.16: ^{1}H NMR (400MHz, PhCl) δ_H 7.08-6.59 (4H, m, Ar C*H*), 3.27 (2H, br s, Bn CH_2), 2.77-2.60 (4H, m, PCH_2N) 0.76 (36H, dd, J = 14.2 and 6.6 Hz, CCH_3), −3.70 (1H, dd, $^1J_{HPt}$ = 809 Hz, $^2J_{HP(trans)}$ = 146 Hz, $^2J_{HP(cis)}$ = 11.7 Hz, Pt-*H*); **^{31}P{^{1}H} NMR (162 MHz; PhCl)** δ_P 38.5 (d, $^1J_{PPt}$ = 2889 Hz, $^2J_{PP}$ = 23.4 Hz, *P*^{t}Bu$_2$), 29.5 (d, $^1J_{PPt}$ = 1845 Hz, $^2J_{PP}$ = 23.4 Hz, *P*^{t}Bu$_2$).

3.17: ^{1}H NMR (400 MHz; PhCl) δ_H 7.08-6.59 (4H, m, Ar C*H*), 3.32 (2H, br s, Bn CH_2), 2.81 (4H, m, PCH_2N) 0.94 (36H, d, J = 13.1 Hz, C(CH_3)$_3$), −2.99 (1H, 1:8:18:8:1 ququ, $^1J_{HPt}$ = 509 Hz, $^2J_{HP}$ = 35 Hz, Pt(μ-*H*)Pt); **^{31}P{^{1}H} NMR (162 MHz; PhCl)** δ_P 36.2 (m, $^1J_{PPt}$ = 3580 Hz, $^2J_{PPt}$ = 152 Hz, $^3J_{PP}$ = 28 Hz, *P*^{t}Bu$_2$).

2.7: ^{1}H NMR (400 MHz; PhCl) δ_H 3.94 (br q, $^1J_{HB}$ = 80.1 Hz, B*H*); **^{11}B{^{1}H} NMR (128 MHz; PhCl)** δ_B −27.7 (br s, *B*H); **^{19}F NMR (376 MHz; PhCl)** δ_F −131.5 (6F, br, *o*-C$_6F_5$), −163.9 (3F, br, *p*-C$_6F_5$), −166.2 (6F, br, *m*-C$_6F_5$).

2.8: ^{1}H NMR (400 MHz; PhCl) δ_H 10.80 (br s, C*H*); **^{11}B{^{1}H} NMR (128 MHz; PhCl)** δ_B −2.4 (br, O*B*), −16.7 (br s, *B*CO); **^{19}F NMR (376 MHz; PhCl)** δ_F −130.3 (6F, br, *o*-

C_6F_5), −132.6 (6F, br, *o*-C_6F_5), −157.6 (3F, br, *p*-C_6F_5), −159.2 (3F, br, *p*-C_6F_5), −164.8 (6F, br, *m*-C_6F_5), −165.2 (6F, br, *m*-C_6F_5).

5.4 Chapter 4 Experimental

5.4.1 Synthesis of *s*-Phob($CH_2OH)_2Cl$

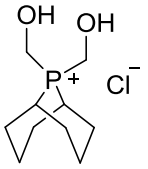

s-PhobPH (250 mg, 1.76 mmol), formaldehyde (37 wt% solution, 0.26 mL, 3.52 mmol) and HCl (37 wt% solution, 0.15 mL, 1.76 mmol) were combined and stirred at room temperature for 90 minutes. The volatiles were removed *in vacuo* to yield a white solid which was triturated with IPA. The desired product was isolated as a white crystalline solid (281 mg, 67%). Data is in agreement with literature.[15]

^{1}H NMR (400 MHz; CD_2Cl_2) δ_H 6.53 (2H, br s, O*H*), 4.74 (4H, br s, PC*H*$_2$OH), 2.60 (2H, br d, $^2J_{HP}$ = 15.1 Hz, PC*H*), 2.35-2.06 (10H, m, *s*-Phob C*H*$_2$), 1.93-1.83 (2H, m, *s*-Phob C*H*$_2$); **^{13}C{^{1}H} NMR (100 MHz; CD_2Cl_2)** δ_C 49.3 (d, $^1J_{CP}$ = 52.1 Hz, P*C*H$_2$OH), 27.5 (d, J_{CP} = 4.4 Hz, *s*-Phob *C*H$_2$), 21.2 (d, J_{CP} = 6.0 Hz, *s*-Phob *C*H$_2$), 19.7 (d, $^1J_{CP}$ = 34.3 Hz, P*C*H); **^{31}P{^{1}H} NMR (162 MHz; CD_2Cl_2)** δ_P 21.5 (s, *s*-Phob*P*); **HR-MS (ESI)** *m/z* calcd. for $C_{10}H_{20}O_2P$ $[M-Cl]^+$ = 203.1195; obs. = 203.1200; **Elem. Anal.** (calcd. for $C_{10}H_{20}ClO_2P$) C 50.56 (50.32), H 8.32 (8.45).

5.4.2 Synthesis of $CgP(CH_2OH)_2Cl$

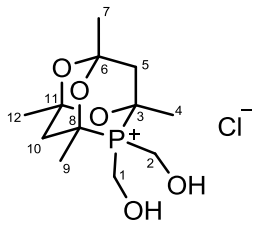

CgPH (500 mg, 2.31 mmol), formaldehyde (37 wt% solution, 0.35 mL, 4.62 mmol) and HCl (37 wt% solution, 0.19 mL, 2.31 mmol) were combined and stirred at room temperature for 90 min. The volatiles were removed *in vacuo* to yield a white solid which was washed with cold acetone (20 mL) and cold Et_2O (20 mL) in air. The desired product was isolated as a white crystalline solid (658 mg, 91%). Data is in agreement with literature.[16]

^{1}H NMR (400 MHz; $CDCl_3$) δ_H 5.28 (2H, d, $^2J_{HP}$ = 14.6 Hz, 1/2 C*H*$_2$OH), 4.62 (2H, dd,

$^{2}J_{HP}$ = 14.6, 1.3 Hz, 1/2 C*H*$_2$OH), 4.00 (2H, br s, O*H*), 2.26 (2H, dd, *J* = 14.4, 2.8 Hz, 5/10 Cg C*H*$_2$), 2.12 (1H, d, *J* = 21.6 Hz, 5/10 Cg C*H*$_2$), 2.07 (1H, d, *J* = 21.6 Hz, 5/10 Cg C*H*$_2$), 1.62 (6H, d, $^{3}J_{HP}$ = 12.5 Hz, 4/9 C*H*$_3$), 1.48 (6H, s, 7/12 C*H*$_3$); **^{13}C{^{1}H} NMR (100 MHz; CDCl$_3$)** δ_C 97.3 (d, $^{3}J_{CP}$ = 1.8 Hz, 6/11 Cg *C*), 71.3 (d, $^{1}J_{CP}$ = 71.2 Hz, 3/8 Cg *C*), 49.3 (d, $^{1}J_{CP}$ = 38.8 Hz, 1/2 *C*H$_2$OH), 40.8 (d, $^{2}J_{CP}$ = 2.4 Hz, 5/10 Cg *C*H$_2$), 27.2 (s, 7/12 Cg *C*H$_3$), 24.5 (s, 4/9 Cg *C*H$_3$); **^{31}P{^{1}H} NMR (162 MHz; CDCl$_3$)** δ_P 2.8 (s, *P*(CH$_2$OH)$_2$); **HR-MS (ESI)** *m/z* calcd. for $C_{12}H_{22}O_5P$ $[M-Cl]^+$ = 277.1199; obs. = 277.1192; **Elem. Anal.** (calcd. for $C_{12}H_{22}ClO_5P$) C 46.13 (46.09), H 7.11 (7.09).

5.4.3 Synthesis of (*s*-Phob)PCH$_2$N(Me)CH$_2$P(*s*-Phob) (P^{Phob}N^{Me}P^{Phob})

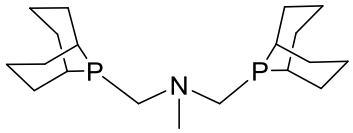

s-PhobPH (581 mg, 4.09 mmol) and paraformaldehyde (123 mg, 4.09 mmol) were combined in degassed MeOH (4 mL) and was left to stir for 30 min at room temperature. A solution of MeNH$_2$ in MeOH (0.4 M, 5.10 mL, 2.04 mmol)) was added dropwise. The reaction mixture was stirred for 72 h after which the colourless solution was concentrated *in vacuo* to yield the product as a colourless viscous oil (643 mg, 93%) of sufficient purity (> 98%).

^{1}H NMR (400 MHz; CDCl$_3$) δ_H 3.02 (4H, br s, PC*H*$_2$N), 2.51 (3H, s, NC*H*$_3$), 2.16-1.92 (16H, m, *s*-Phob C*H*$_2$/C*H*), 1.83-1.56 (12H, m, *s*-Phob C*H*$_2$/C*H*); **^{13}C{^{1}H} NMR (100 MHz; CDCl$_3$)** δ_C 56.4 (dd, J_{CP} = 14.4, 8.9 Hz, P*C*H$_2$N), 46.2 (t, $^{3}J_{CP}$ = 9.0 Hz, N*C*H$_3$), 32.9 (d, J_{CP} = 12.1 Hz, *s*-Phob *C*H$_2$), 25.6 (d, J_{CP} = 12.2 Hz, *s*-Phob *C*H$_2$), 24.8 (d, J_{CP} = 10.8 Hz, *s*-Phob *C*H$_2$), 24.0 (d, J_{CP} = 5.4 Hz, *s*-Phob *C*H), 22.2 (d, J_{CP} = 2.3 Hz, *s*-Phob CH$_2$); **^{31}P{^{1}H} NMR (162 MHz; CDCl$_3$)** δ_P −46.5 (s, *s*-Phob*P*); **HR-MS (ESI)** *m/z* calcd. for (C$_{19}$H$_{36}$NP$_2$) $[M+H]^+$ = 340.2317, obs. = 340.2311; **Elem. Anal.** (calcd. for C$_{21}$H$_{39}$NP$_2$) C 67.56 (67.23), H 10.63 (10.39), N 4.47 (4.13).

5.4.4 Synthesis of (*s*-Phob)PCH$_2$N(iPr)CH$_2$P(*s*-Phob) (P^{Phob}N^{iPr}P^{Phob})

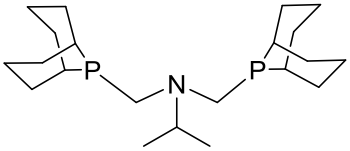

s-PhobPH (851 mg, 5.99 mmol) and paraformaldehyde (179 mg, 5.99 mmol) were combined in degassed MeOH (8 mL) and was left to stir for 30 min at room temperature. Isopropylamine (257 µl, 2.99 mmol) was added dropwise. The reaction mixture was stirred for 72 h after which a white precipitate had formed. The precipitate was isolated by filtration under nitrogen and was found to be the desired product (818 mg, 74%). **^{1}H NMR (400 MHz; CDCl$_3$)** δ_H 3.34 (1H, m, C*H*(CH$_3$)$_2$), 2.97 (4H, s, PC*H*$_2$N), 2.17-1.90 (16H, m, *s*-Phob C*H*$_2$/C*H*), 1.78-1.54 (12H, m, *s*-Phob C*H*$_2$/C*H*), 0.99 (6H, d, $^2J_{HH}$ = 6.6 Hz, CH(C*H*$_3$)$_2$); **^{13}C{^{1}H} NMR (100 MHz; CDCl$_3$)** δ_C 51.9 (t, $^3J_{CP}$ = 8.3 Hz, *C*H(CH$_3$)$_2$), 47.7 (dd, J_{CP} = 11.0, 9.1 Hz, P*C*H$_2$N), 32.5 (d, J_{CP} = 12.2 Hz, *s*-Phob *C*H$_2$), 25.4 (br d, J_{CP} = 3.8 Hz, *s*-Phob *C*H$_2$), 24.2 (d, $^1J_{CP}$ = 10.2 Hz, *s*-Phob *C*H), 23.6 (d, J_{CP} = 5.4 Hz, *s*-Phob *C*H$_2$), 21.8 (d, J_{CP} = 1.8 Hz, *s*-Phob *C*H$_2$), 18.5 (s, CH(*C*H$_3$)$_2$); **^{31}P{^{1}H} NMR (162 MHz; CDCl$_3$)** δ_P −43.5 (s, *s*-PhobP); **HR-MS (ESI)** *m/z* calcd. for (C$_{21}$H$_{40}$NP$_2$) [M+H]$^+$ = 368.2630, obs. = 368.2640; **Elem. Anal.** (calcd. for C$_{21}$H$_{39}$NP$_2$) C 69.05 (68.63), H 10.98 (10.70), N 4.13 (3.81).

5.4.5 Synthesis of (*s*-Phob)PCH$_2$N(Bn)CH$_2$P(*s*-Phob) (P^{Phob}N^{Bn}P^{Phob})

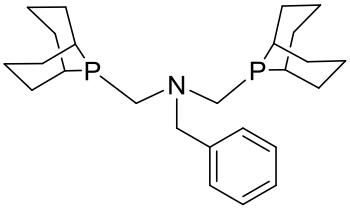

s-PhobPH (665 mg, 4.65 mmol) and paraformaldehyde (140 mg, 4.65 mmol) were combined in degassed MeOH (8 mL) and was left to stir for 30 min at room temperature. Benzylamine (254 µl, 2.33 mmol) was added dropwise. The reaction mixture was stirred for 72 h after which a white precipitate had formed. The precipitate was isolated by

filtration under nitrogen and was found to be the desired product (820 mg, 85%).
^{1}H NMR (400 MHz; $CDCl_3$) δ_H 7.36-7.19 (5H, m, Ar C*H*), 3.89 (2H, s, NCH_2Ph), 3.13 (4H, br s, PCH_2N), 2.18-1.45 (28H, m, *s*-Phob CH_2/C*H*); **^{13}C{^{1}H} NMR (100 MHz; $CDCl_3$)** δ_C 139.8 (s, Ar *C*), 129.4 (s, Ar *C*H), 128.2 (s, Ar *C*H), 127.0 (s, Ar *C*H), 61.2 (t, $^{3}J_{CP}$ = 9.5 Hz, NCH_2Ph), 51.9 (dd, J_{CP} = 14.2 and 8.8 Hz, P*C*H_2N), 32.5 (d, J_{CP} = 12.2 Hz, *s*-Phob *C*H_2), 25.2 (d, J_{CP} = 4.6 Hz, *s*-Phob *C*H_2), 24.3 (d, J_{CP} = 10.3 Hz, *s*-Phob *C*H), 23.5 (d, J_{CP} = 6.6 Hz, *s*-Phob *C*H_2), 21.6 (d, J_{CP} = 2.7 Hz, *s*-Phob CH_2); **^{31}P{^{1}H} NMR (162 MHz; $CDCl_3$)** δ −47.9 (s, *s*-Phob*P*); **HR-MS (ESI)** *m/z* calcd. for ($C_{25}H_{40}NP_2$) $[M+H]^+$ = 416.2630, obs. = 416.2698; **Elem. Anal.** (calcd. for $C_{25}H_{39}NP_2$) C 72.35 (72.26), H 9.65 (9.46), N 3.42 (3.37).

5.4.6 Synthesis of CgPCH$_2$N(Me)CH$_2$PCg ($P^{Cg}N^{Me}P^{Cg}$, *rac*/*meso* mixture)

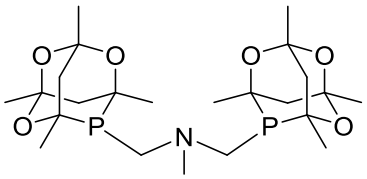

CgPH (500 mg, 2.31 mmol) and paraformaldehyde (69 mg, 2.31 mmol) were combined in degassed MeOH (8 mL) and was left to stir for 30 min at room temperature. A solution of $MeNH_2$ in MeOH (0.4 M, 2.9 mL, 1.16 mmol) was added dropwise. The reaction mixture was stirred for 72 h after which a white precipitate had formed. The precipitate was isolated by filtration under nitrogen and was found to be the desired product with an uneven proportion of the two diastereomers (939 mg, 83%).
^{1}H NMR (400 MHz; $CDCl_3$) δ_H 3.08 (2H, d, $^{1}J_{HH}$ = 13.7 Hz, PCH_2N), 2.88 (2H, d, $^{1}J_{HH}$ = 13.5 Hz, PCH_2N), 2.50 (2H, d, $^{1}J_{HH}$ = 10.2 Hz, PCH_2N), 2.49 (6H, s, NCH_3), 2.35 (2H, d, $^{1}J_{HH}$ = 13.3 Hz, PCH_2N), 1.98-1.91 (4H, m, Cg CH_2), 1.89-1.78 (4H, m, Cg CH_2), 1.69 (2H, d, $^{1}J_{HH}$ = 13.3 Hz, Cg CH_2), 1.63-1.57 (6H, m, Cg CH_2),1.40-1.32 (24H, m, Cg CH_3); **^{13}C{^{1}H} NMR (100 MHz; $CDCl_3$)** δ_C 96.9 (s, Cg *C*), 95.9 (s, Cg *C*), 95.8 (s, Cg *C*), 72.1 (m, Cg *C*), 54.5 (m, P*C*H_2N), 45.7 (m, *C*H_3), 44.8 (d, *J* = 15 Hz, Cg *C*H_2), 37.9 (m, Cg *C*H_2), 28.1 (d, *J* = 22.2 Hz, Cg *C*H_3), 28.0 (d, *J* = 19.1 Hz, Cg *C*H_3), 27.1 (d, *J* = 12.3 Hz, Cg *C*H_3), 27.0 (d, *J* = 12.2 Hz, Cg *C*H_3); **^{31}P{^{1}H} NMR (162 MHz; $CDCl_3$)** δ_P −41.8 (s, *P*Cg), −42.6 (s, *P*Cg); **HR-MS (ESI)** *m/z* calcd. for $C_{25}H_{39}NO_6P_2$ $[M+H]^+$ =

488.2325; obs. = 488.2324; E**lem. Anal.** (calcd. for $C_{23}H_{39}NO_6P_2$) C 57.03 (56.87), H 8.13 (8.06), N 2.60 (2.87).

5.4.7 Synthesis of $CgPCH_2N(iPr)CH_2PCg$ ($P^{Cg}N^{iPr}P^{Cg}$, *rac*/*meso* mixture)

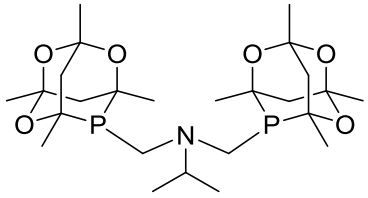

CgPH (1.00 g, 4.62 mmol) and paraformaldehyde (139 mg, 4.62 mmol) were combined in degassed MeOH (10 mL) and was left to stir for 30 min at room temperature. Isopropylamine (199 µl, 2.31 mmol) was added dropwise. The reaction mixture was stirred for 72 h after which a white precipitate had formed. The precipitate was isolated by filtration under nitrogen and was found to be the desired product with an uneven proportion of the two diastereomers (572 mg, 48%). The filtrate was concentrated *in vacuo* to yield a white solid which was washed with MeOH to remove impurities and yield another portion of the desired product with a different ratio of diastereomers (274 mg, 23%).

^{1}H NMR (400 MHz; $CDCl_3$) δ_H 3.60 (2H, m, *rac*/*meso* C*H*$(CH_3)_2$), 3.03 (2H, br d, $^1J_{HH}$ = 13.4 Hz, *rac* PC*H*$_2$N), 2.94 (2H, dd, $^1J_{HH}$ = 13.3 Hz, $^2J_{HP}$ = 3.3 Hz, *meso* PC*H*$_2$N), 2.51 (2H, dd, $^1J_{HH}$ = 13.3 Hz, $^2J_{HP}$ = 2.3 Hz, *meso* PC*H*$_2$N), 2.42 (2H, br d, $^1J_{HH}$ = 13.4 Hz, *meso* PC*H*$_2$N), 1.98-1.91 (4H, m, *rac*/*meso* Cg C*H*$_2$), 1.84 (4H, br d, *rac*/*meso* Cg C*H*$_2$), 1.78 (2H, br d, *J* = 13.3 Hz, *meso* Cg C*H*$_2$), 1.74 (2H, br d, *J* = 13.3 Hz, *rac* Cg C*H*$_2$), 1.64-1.56 (4H,m, *rac*/*meso* Cg C*H*$_2$), 1.41-1.33 (48H, m, *rac*/*meso* Cg C*H*$_3$), 1.03 (3H, d, *J* = 6.6 Hz, *rac* CH(C*H*$_3$)$_2$), 1.01 (6H, d, *J* = 6.6 Hz, *meso* CH(C*H*$_3$)$_2$), 0.96 (3H, d, *J* = 6.6 Hz, *rac* CH(C*H*$_3$)$_2$); **^{13}C{^{1}H} NMR (100 MHz; $CDCl_3$)** δ_C 96.9 (m, Cg *C*), 96.0 (m, Cg *C*), 72.3 (m, Cg *C*), 51.2 (m, *C*H), 46.4 (m, P*C*H$_2$N), 45.0 (m, Cg *C*H$_2$), 37.9 (m, Cg *C*H$_2$), 28.2 (m, Cg *C*H$_3$), 27.0 (m, Cg *C*H$_3$), 17.5 (s, *C*H$_3$), 16.9 (s, *C*H$_3$), 16.6 (s, *C*H$_3$); **^{31}P{^{1}H} NMR (162 MHz; $CDCl_3$)** δ_P −40.6 (s, *rac P*Cg), −40.7 (s, *meso P*Cg); **HR-MS (ESI)** *m/z* calcd. for $C_{25}H_{44}NO_6P_2$ $[M+H]^+$ = 516.2644; obs. = 516.2626; **Elem. Anal.** (calcd. for $C_{25}H_{43}NO_6P_2$) C 59.10 (58.24), H 2.87 (2.72), N 8.51 (8.41).

5.4.8 Synthesis of $CgPCH_2N(Bn)CH_2PCg$ ($P^{Cg}N^{Bn}P^{Cg}$, *rac*/*meso* mixture)

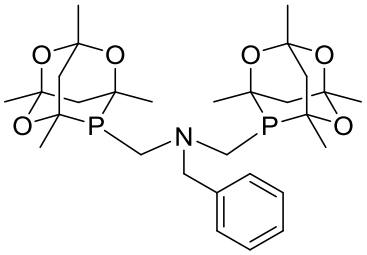

CgPH (1.00 g, 4.62 mmol) and paraformaldehyde (139 mg, 4.62 mmol) were combined in degassed MeOH (8 mL) and was left to stir for 30 min at room temperature. Benzylamine (253 μl, 2.31 mmol) was added dropwise. The reaction mixture was stirred for 72 h after which a white precipitate had formed. The precipitate was isolated by filtration under nitrogen and was found to be the desired product with an uneven proportion of the two diastereomers (1.13 g, 87%).

^{1}H NMR (400 MHz; $CDCl_3$) δ_H 7.29-7.19 (10H, m, Ar C*H*), 3.82 (4H, m, Bn CH_2), 3.01 (2H, dd, *J* = 13.4, 2.3 Hz, PCH_2N), 2.97 (2H, d, *J* = 13.5 Hz, PCH_2N), 2.57 (4H, br d, *J* = 13.5 Hz, PCH_2N), 1.93-1.87 (4H, m, Cg CH_2), 1.82-1.71 (4H, m, Cg CH_2), 1.49-1.19 (64H, m, 8 x Cg CH_2 and 48 x Cg CH_3); **^{13}C{^{1}H} NMR (100 MHz; $CDCl_3$)** δ_C 138.4 (s, Ar *C*), 138.2 (s, Ar *C*), 129.8 (s, Ar *C*H), 129.6 (s, Ar *C*H), 128.5 (s, Ar *C*H), 127.6 (s, Ar *C*H), 127.5 (s, Ar *C*H), 96.8 (s, Cg *C*), 95.8 (d, *J* = 3.2 Hz, Cg *C*), 72.2 (m, Cg *C*), 61.1 (m, Bn *C*H_2), 51.1 (m, P*C*H_2N), 44.9 (dd, *J* = 14.7, 4.0 Hz, Cg *C*H_2), 37.6 (d, *J* = 11.7 Hz, Cg *C*H_2), 28.5, (s, Cg *C*H_3), 28.2, (s, Cg *C*H_3), 28.0 (d, *J* = 9.9 Hz, Cg *C*H_3), 27.2 (dd, *J* = 11.9, 6.1 Hz, Cg *C*H_3); **^{31}P{^{1}H} NMR (162 MHz; $CDCl_3$)** δ_P −42.3 (s, *P*Cg), −42.5 (s, *P*Cg); **HR-MS (ESI)** *m/z* calcd. for $C_{29}H_{43}NO_6P_2$ $[M+H]^+$ = 564.2638; obs. = 564.2637; **Elem. Anal.** (calcd for $C_{29}H_{43}NO_6P_2$) C 61.63 (61.80), H 7.72 (7.69), N 2.57 (2.49).

5.4.9 [$PtCl_2(P^{Phob}N^{Me}P^{Phob})$]

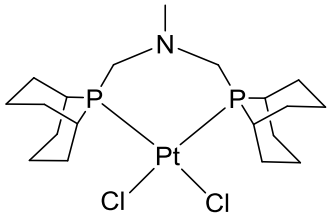

[$PtCl_2$(COD)] (25.3 mg, 0.068 mmol) and $P^{Phob}N^{Me}P^{Phob}$ (23 mg, 0.068 mmol) were dissolved in DCM (0.6 mL) in a Youngs NMR tube. After 1 h, $^{31}P\{^1H\}$ NMR confirmed complete complexation. The complex was precipitated in hexane to give a white solid (38 mg, 93%).

^{1}H NMR (400 MHz; CD_2Cl_2) δ_H 3.70-3.01 (4H, br m, PC*H*$_2$N), 2.89-2.50 (8H, br m, *s*-Phob C*H*$_2$/C*H*), 2.55 (3H, s, NC*H*$_3$), 2.22-1.66 (20H, m, *s*-Phob C*H*$_2$/C*H*); **$^{13}C\{^1H\}$ NMR (100 MHz; CD_2Cl_2)** δ_C 52.8 (m, N*C*H$_3$ and P*C*H$_2$N), 29.6 (s, *s*-Phob *C*H$_2$), 28.2 (br m, *s*-Phob C*H*$_2$), 25.5 (br m, *s*-Phob C*H*), 22.0 (t, *J* = 4.7 Hz, *s*-Phob *C*H$_2$), 20.3 (m, *s*-Phob *C*H$_2$); **$^{31}P\{^1H\}$ NMR (162 MHz; CD_2Cl_2):** δ_P −15.8 (s, $^1J_{PPt}$ = 3245 Hz, *s*-Phob*P*); **HR-MS (ESI)** *m/z* calcd. for $C_{19}H_{35}Cl_2NNaP_2Pt$ $[M+Na]^+$ = 627.1164, obs. = 627.1166.

5.4.10 [$PtCl_2(P^{Phob}N^{iPr}P^{Phob})$]

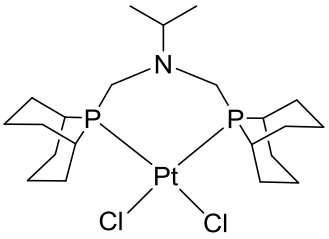

[$PtCl_2$(COD)] (25.0 mg, 0.067 mmol) and $P^{Phob}N^{iPr}P^{Phob}$ (24.6 mg, 0.067 mmol) were dissolved in DCM (0.6 mL) in a Youngs NMR tube. After 1 h, $^{31}P\{^1H\}$ NMR confirmed complete complexation. The complex was precipitated in hexane to give a white solid (40 mg, 95%).

^{1}H NMR (400 MHz; CD_2Cl_2) δ_H 3.94-2.99 (4H, br m, PC*H*$_2$N), 2.99 (1H, sept, *J* = 6.5 Hz, C*H*(CH$_3$)$_2$), 2.92-2.40 (8H, br m, *s*-Phob C*H*$_2$/C*H*), 2.19-1.65 (20H, m, *s*-Phob C*H*$_2$/C*H*), 1.13 (6H, d, *J* = 6.5 Hz, CH(C*H*$_3$)$_2$); **$^{13}C\{^1H\}$ NMR (100 MHz; CD_2Cl_2)** δ_C 61.9 (t, *J* = 10.6 Hz, *C*H(CH$_3$)$_2$), 47.6 (m, P*C*H$_2$N), 29.7 (s, *s*-Phob *C*H$_2$), 29.6-24.3 (br m, *s*-Phob *C*H$_2$/*C*H), 22.0 (t, *J* = 4.4 Hz, *s*-Phob *C*H$_2$), 20.3 (m, *s*-Phob *C*H$_2$), 18.0 (s,

$CH(CH_3)_2$); **$^{31}P\{^1H\}$ NMR (162 MHz; CD_2Cl_2):** δ_P −16.5 (s, $^1J_{PPt}$ = 3248 Hz, *s*-Phob*P*); **HR-MS (ESI)** *m/z* calcd. for $C_{21}H_{39}ClNP_2Pt$ $[M-Cl]^+$ = 597.1891, obs. = 597.1882.

5.4.11 $[PtCl_2(P^{Phob}N^{Bn}P^{Phob})]$

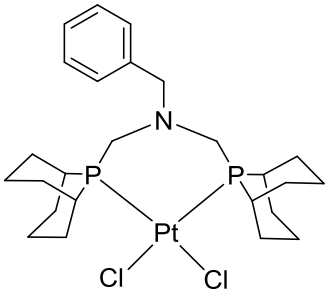

$[PtCl_2(COD)]$ (25.1 mg, 0.067 mmol) and $P^{Phob}N^{Bn}P^{Phob}$ (28.0 mg, 0.067 mmol) were dissolved in DCM (0.6 mL) in a Youngs NMR tube. After 1 h, $^{31}P\{^1H\}$ NMR confirmed complete complexation. The complex was precipitated in hexane to give a white solid (43 mg, 94%).

^1H NMR (400 MHz; CD_2Cl_2) δ_H 7.39-7.27 (5H, m, ArC*H*), 3.84-2.84 (4H, br m, PCH_2N), 3.77 (2H, s, BnCH_2), 2.87-2.17 (8H, br m, *s*-Phob CH_2/C*H*), 2.13-1.36 (20H, m, *s*-Phob CH_2/C*H*); **$^{13}C\{^1H\}$ NMR (100 MHz; CD_2Cl_2)** δ_C 137.2 (s, Ar *C*), 130.7 (s, Ar *C*H); 129.2 (s, Ar *C*H), 129.1 (s, Ar *C*H); 128.8 (s, Ar *C*H); 68.2 (t, *J* = 11.8 Hz, Bn *C*H_2), 50.6 (m, P*C*H_2N), 29.6 (s, *s*-Phob *C*H_2), 27.9 (br m, *s*-Phob *C*H_2), 23.4 (br m, *s*-Phob *C*H), 21.9 (t, *J* = 4.4 Hz, *s*-Phob *C*H_2), 20.2 (m, *s*-Phob *C*H_2), 18.0 (s, $CH(CH_3)_2$); **$^{31}P\{^1H\}$ NMR (162 MHz; CD_2Cl_2)** δ_P −16.4 (s, $^1J_{PPt}$ = 3247 Hz, *s*-Phob*P*); **HR-MS (ESI)** *m/z* calcd. for $C_{25}H_{39}ClNP_2Pt$ $[M-Cl]^+$ = 645.1891, obs. = 645.1886.

5.4.12 $[PtMe_2(P^{Cg}N^{Me}P^{Cg})]$ (*rac*/*meso* mixture)

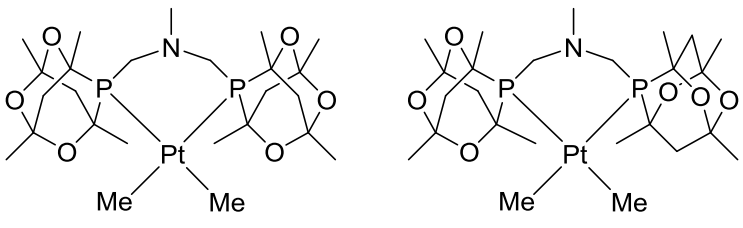

meso ***rac***

$[PtMe_2(COD)]$ (25 mg, 0.075 mmol) and $P^{Cg}N^{Me}P^{Cg}$ (36.6 mg, 0.075 mmol) were dissolved in DCM (0.6 mL) in a Youngs NMR tube. After 16 h, $^{31}P\{^1H\}$ NMR confirmed

complete complexation. The complex was azeotroped twice with toluene to remove any free COD in solution to yield a pale yellow solid (48 mg, 90%). Crystals suitable for X-ray analysis were obtained by slow evaporation of a hexane solution of [$PtMe_2(P^{Cg}N^{Me}P^{Cg})$].

^{1}H NMR (400 MHz; CD_2Cl_2) δ_H 3.12 (2H, m, *rac*/*meso* PC*H*$_2$N), 2.58 (2H, dd, *J* = 13.4, 3.5 Hz, *rac*/*meso* Cg C*H*$_2$), 2.51 (2H, dm, *J* = 14.1 Hz, *rac*/*meso* PC*H*$_2$N), 1.81-1.75 (4H, m, *rac*/*meso* Cg C*H*$_2$), 1.58 (2H, dd, *J* = 20.1, 13.4 Hz, *rac*/*meso* Cg CH$_2$), 1.41-1.30 (29H, m, 2 x *rac*/*meso* Cg C*H*$_2$, 24 x *rac*/*meso* Cg C*H*$_3$, 3 x *rac*/*meso* NC*H*$_3$), 0.72 (6H, appt, *J* = 6.34, $^2J_{HPt}$ = 72.6 Hz, PtC*H*$_3$); **^{13}C{^{1}H} NMR (100 MHz; CD_2Cl_2)** δ_C 99.6 (s, Cg *C*), 97.2 (s, Cg *C*), 96.6 (s, Cg *C*), 73.8 (m, Cg *C*), 73.1 (m, Cg *C*), 53.5 (m, P*C*H$_2$N), 41.2 (m, Cg *C*H$_2$), 40.8 (m, Cg *C*H$_2$), 27.6 (s, *C*H$_3$), 27.15 (s, *C*H$_3$), 26.6 (m, *C*H$_3$), 26.0 (m, *C*H$_3$), 4.21 (dd, *J* = 98.3, 10.2 Hz, $^1J_{CPt}$ = 601 Hz, Pt*C*H$_3$); **^{31}P{^{1}H} NMR (162 MHz; CD_2Cl_2):** δ_P −13.8 (s, $^1J_{PPt}$ = 1664 Hz, *P*Cg (major)), −16.0 (s, $^1J_{PPt}$ = 1640 Hz, *P*Cg (minor)); **HR-MS (ESI)** *m/z* calcd. for $C_{25}H_{45}NNaO_6P_2Pt$ $[M+Na]^+$ = 735.265, obs. = 735.2269.

5.4.13 [$PtMe_2(P^{Cg}N^{iPr}P^{Cg})$] (*rac*/*meso* mixture)

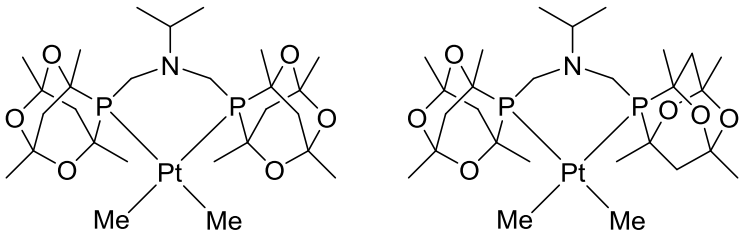

meso ***rac***

[$PtMe_2$(COD)] (25 mg, 0.075 mmol) and $P^{Cg}N^{iPr}P^{Cg}$ (38.7 mg, 0.075 mmol) were dissolved in DCM (0.6 mL) in a Youngs NMR tube. After 16 h, ^{31}P{^{1}H} NMR confirmed complete complexation. The complex was azeotroped twice with toluene to remove any free COD in solution to yield a pale yellow solid (52 mg, 94%). Crystals suitable for X-ray analysis were obtained by slow evaporation of a hexane solution of [$PtMe_2(P^{Cg}N^{iPr}P^{Cg})$].

^{1}H NMR (400 MHz; CD_2Cl_2) δ_H 3.17 (2H, m, *rac*/*meso* PC*H*$_2$N), 2.91 (1H, sept, *J* = 6.6 Hz, C*H*(CH$_3$)$_2$), 2.67-2.57 (4H, m 2 x *rac*/*meso* Cg C*H*$_2$, 2 x *rac*/*meso* PC*H*$_2$N), 1.88-1.74 (4H, m, *rac*/*meso* Cg C*H*$_2$), 1.57 (2H, dd, *J* = 20.1, 14.0 Hz, *rac*/*meso* Cg CH$_2$), 1.43-1.30 (26H, m, 2 x *rac*/*meso* Cg C*H*$_2$, 24 x *rac*/*meso* Cg C*H*$_3$), 1.04 (6H, dd, *J* = 6.6,

2.6 Hz, *rac*/*meso* CH(C*H*$_3$)$_2$), 0.70 (6H, appt, *J* = 6.3 Hz, $^2J_{HPt}$ = 73.0 Hz, Pt-C*H*$_3$); **^{13}C{^{1}H} NMR (100 MHz; CD$_2$Cl$_2$)** δ_C 99.6 (s, Cg *C*), 97.3 (s, Cg *C*), 96.7 (s, Cg *C*), 73.9 (m, Cg *C*), 73.2 (m, Cg *C*), 60.8 (t, *J* = 8.6 Hz, *C*H(CH$_3$)$_2$), 48.8 (m, P*C*H$_2$N), 41.2 (m, Cg *C*H$_2$), 40.9 (m, Cg *C*H$_2$), 28.2 (s, *C*H$_3$), 27.7 (s, *C*H$_3$), 27.2 (m, *C*H$_3$), 26.4 (m, *C*H$_3$), 19.3 (s, CH(*C*H$_3$)$_2$, 17.0 (s, CH(*C*H$_3$)$_2$, 4.21 (dd, *J* = 98.0, 10.1 Hz, $^1J_{CPt}$ = 601 Hz, Pt-*C*H$_3$); **^{31}P{^{1}H} NMR (162 MHz; CD$_2$Cl$_2$):** δ_P −15.0 (s, $^1J_{PPt}$ = 1678 Hz, *P*Cg (major)), −18.0 (s, $^1J_{PPt}$ = 1639 Hz, *P*Cg (minor)); **HR-MS (ESI)** *m/z* calcd. for $C_{27}H_{49}NNaO_6P_2Pt$ $[M+Na]^+$ = 763.2578, obs. = 763.2574.

5.4.14 [PtMe$_2$(P^{Cg}N^{Bn}P^{Cg})] (*rac*/*meso* mixture)

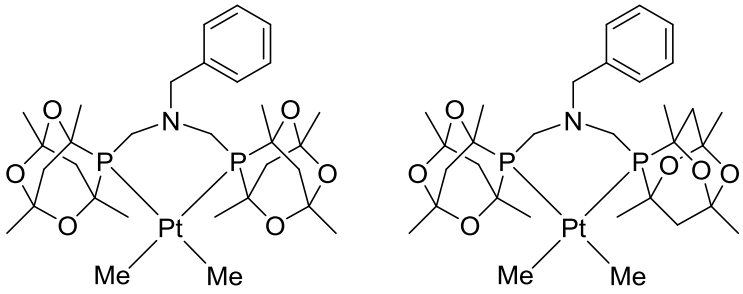

meso ***rac***

[PtMe$_2$(COD)] (25 mg, 0.075 mmol) and P^{Cg}N^{Bn}P^{Cg} (42.3 mg, 0.075mmol) were dissolved in DCM (0.6 mL) in a Youngs NMR tube. After 16 h, ^{31}P{^{1}H} NMR confirmed complete complexation. The complex was azeotroped twice with toluene to remove any free COD in solution to yield a pale yellow solid (58 mg, 98%). Crystals suitable for X-ray analysis were obtained by slow evaporation of a hexane solution of [PtMe$_2$(P^{Cg}N^{Bn}P^{Cg})].

^{1}H NMR (400 MHz; CD$_2$Cl$_2$) δ_H 7.40-7.26 (5H, m, *rac*/*meso* Ar C*H*), 3.85 (1H, br d, *J* = 12.3 Hz, *rac*/*meso* Bn C*H*$_2$), 3.31 (1H, d, *J* = 12.3 Hz, *rac*/*meso* Bn C*H*$_2$), 3.11 (2H, m, *rac*/*meso* PC*H*$_2$N), 2.67 (2H, dm , *J* = 14 Hz, *rac*/*meso* PC*H*$_2$N), 2.57 (2H, dd, *J* = 13.7, 3.3 Hz, *rac*/*meso* Cg C*H*$_2$), 1.64-1.18 (32H, m, 4 x *rac*/*meso* Cg C*H*$_2$), 4 x *rac*/*meso* Cg C*H*$_2$, 24 x *rac*/*meso* Cg C*H*$_3$), 0.70 (6H, appt, *J* = 6.4 Hz, $^2J_{HPt}$ = 73.0 Hz, PtC*H*$_3$); **^{13}C{^{1}H} NMR (100 MHz; CD$_2$Cl$_2$)** δ_C 137.7 (s, Ar *C*), 131.0 (s, Ar *C*H), 129.2 (s, Ar *C*H), 129.1 (s, Ar *C*H), 128.6 (s, Ar *C*H), 99.6 (s, Cg *C*), 97.2 (s, Cg *C*), 96.6 (s, Cg *C*), 73.8 (m, Cg *C*), 73.2 (m, Cg *C*), 68.9 (t, *J* = 9.6 Hz, Bn *C*H$_2$), 52.0 (m, P*C*H$_2$N), 41.1 (m, Cg *C*H$_2$), 40.1 (m, Cg *C*H$_2$), 28.0 (s, *C*H$_3$), 27.8 (s, *C*H$_3$), 27.3 (m, *C*H$_3$), 26.6 (m, *C*H$_3$), 17.0 (s, CH(*C*H$_3$)$_2$, 4.47 (dd, *J* = 98.2, 9.5 Hz, $^1J_{CPt}$ = 500 Hz, Pt*C*H$_3$); **^{31}P{^{1}H} NMR (162 MHz; CD$_2$Cl$_2$):** δ_P −15.7 (s, $^1J_{PPt}$ = 1663 Hz, *P*Cg (major)), −18.1 (s, $^1J_{PPt}$ = 1638 Hz, *P*Cg

(minor)); **HR-MS (ESI)** *m/z* calcd. for $C_{31}H_{49}NNaO_6P_2Pt$ $[M+Na]^+$ = 811.2578, obs. = 811.2570.

5.4.15 [Mn(P^{Phob}N^{Me}P^{Phob})(CO)$_3$Br]

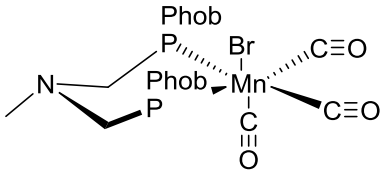

$Mn(CO)_5Br$ (251 mg, 0.91 mmol) and $P^{Phob}N^{Me}P^{Phob}$ (310 mg, 0.91 mmol) were suspended in benzene (5 mL). The reaction mixture was heated at 50 °C for 2 h after which a yellow precipitate had formed. The precipitate was isolated and found to be the desired product (375 mg, 74%).

^{1}H NMR (400 MHz; $CDCl_3$) δ_H 3.64 (2H, m, PC*H*$_2$N), 3.14 (2H, m, PC*H*$_2$N), 2.76 (2H, m, *s*-Phob C*H*$_2$), 2.58 (3H, s, NC*H*$_3$), 2.49-1.71 (m, 4 x *s*-Phob C*H* and 22 x *s*-Phob C*H*$_2$); **^{13}C{^{1}H} NMR (100 MHz; $CDCl_3$)** δ_C 52.7 (m, P*C*H$_2$N), 50.8 (m, N*C*H$_3$), 28.9 (s, *s*-Phob *C*H$_2$), 28.3 (s, *s*-Phob *C*H$_2$), 27.8 (br s, *s*-Phob *C*H$_2$), 27.1 (br s, *s*-Phob *C*H$_2$), 26.6 (t, *J* = 9.2 Hz, *s*-Phob *C*H), 25.0 (t, *J* = 11.1 Hz, s-Phob *C*H), 21.6 (br s, *s*-Phob *C*H$_2$), 20.6 (br s, *s*-Phob *C*H$_2$); **^{31}P{^{1}H} NMR (162 MHz; $CDCl_3$):** δ 4.4 (br s, *s*-Phob*P*); **HR-MS (ESI)** *m/z* calcd. for $C_{22}H_{36}BrMnNO_3P_2$ $[M+H]^+$ = 558.0729, obs. = 558.0722; **Elem. Anal.** (calcd. for $C_{22}H_{35}BrMnNO_3P_2$) C 47.36 (47.33), H 6.38 (6.32), N 2.51 (2.49); **IR ν_{CO}** 1999, 1919, 1886 cm^{-1}.

5.4.16 [Mn(P^{Phob}N^{iPr}P^{Phob})(CO)$_3$Br]

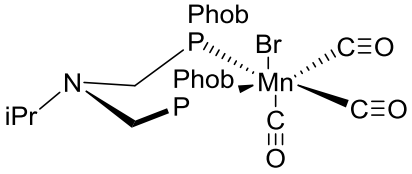

$Mn(CO)_5Br$ (150 mg, 0.55 mmol) and $P^{Phob}N^{iPr}P^{Phob}$ (200 mg, 0.55 mmol) were suspended in benzene (3.5 mL). The reaction mixture was heated at 50 °C for 2 h after which a small amount of precipitate had formed. The filtrate was isolated from the precipitate and concentrated to form a yellow powder which was found to be the desired product (163 mg, 51%). Crystals suitable for X-ray analysis were grown from a saturated solution of the complex in benzene.

^{1}H NMR (400 MHz; $CDCl_3$) δ_H 3.72 (2H, m, PC*H*$_2$N), 2.97-2.69 (5H, m, 1 x C*H*(CH$_3$)$_2$,

2 x PC*H*$_2$N, 2 x *s*-Phob C*H*$_2$), 2.95-1.68 (26H, m, 22 x *s*-Phob C*H*$_2$, 4 x *s*-Phob C*H*), 1.10 (6H, d, $^3J_{HH}$ = 6.6 Hz, CH(C*H*$_3$)$_2$); **^{13}C{^{1}H} NMR (100 MHz; CDCl$_3$)** δ_C 60.1 (t, $^1J_{CP}$ = 8.7 Hz, *C*H(CH$_3$)$_2$), 49.1 (dd, *J* = 16.7, 13.7 Hz, P*C*H$_2$N), 29.1 (s, *s*-Phob *C*H$_2$), 28.1 (t, *J* = 3.4 Hz, *s*-Phob *C*H$_2$), 28.0 (s, *s*-Phob *C*H$_2$), 27.3 (t, *J* = 3.1 Hz, *s*-Phob *C*H$_2$), 25.6 (dd, *J* = 9.1, 8.8 Hz, *s*-Phob *C*H), 24.7 (dd, *J* = 11.4, 10.5 Hz, *s*-Phob *C*H), 21.5 (t, *J* = 2.7 Hz, *s*-Phob *C*H$_2$), 20.7 (t, *J* = 2.2 Hz, *s*-Phob *C*H$_2$), 18.65 (s, CH(*C*H$_3$)$_2$); **^{31}P{^{1}H} NMR (162 MHz; CDCl$_3$)** δ_P 9.5 (br s, *s*-Phob*P*); **HR-MS (ESI)** *m/z* calcd. for $C_{24}H_{39}MnNO_3P_2$ $[M-Br]^+$ = 506.1780, obs. = 506.1784; **Elem. Anal.** (calcd. for $C_{24}H_{39}BrMnNO_3P_2$) C 49.23 (49.16), H 6.89 (6.70), N 2.45 (2.39); **IR ν_{CO}** 2000, 1918, 1897 cm^{-1}.

5.4.17 [Mn(P^{Phob}N^{Bn}P^{Phob})(CO)$_3$Br]

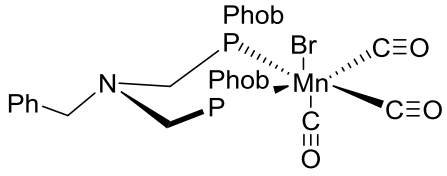

Mn(CO)$_5$Br (263 mg, 0.96 mmol) and P^{Phob}N^{Bn}P^{Phob} (398 mg, 0.96 mmol) created a yellow suspension upon addition of benzene (8 mL). The reaction mixture was heated at 50 °C for 2 h after which a small amount of precipitate had formed. The filtrate was isolated from the precipitate and concentrated to form a yellow powder which was found to be the desired product (474 mg, 78%).

^{1}H NMR (400 MHz; CDCl$_3$) δ_H 7.30-7.19 (5H, m, Ar C*H*), 3.72 (4H, m, 2 x Bn C*H*$_2$ and 2 x PC*H*$_2$N), 2.96 (2H, dm, *J* = 13.5 Hz, PC*H*$_2$N), 2.67 (2H, m, *s*-Phob CH$_2$), 2.37 (4H, m, 2 x *s*-Phob C*H* and 2 x *s*-Phob C*H*$_2$), 2.07-1.41 (22H, m, 2 x *s*-Phob *C*H and 20 x *s*-Phob *C*H$_2$); **^{13}C{^{1}H} NMR (100 MHz; CDCl$_3$)** δ_C 138.4 (s, Ar *C*), 129.5 (s, Ar *C*H), 128.8 (s, Ar *C*H), 128.2 (s, Ar *C*H), 66.9 (t, *J* = 9.1 Hz, Bn *C*H$_2$), 51.9 (dd, *J* = 15.2, 12.4 Hz, P*C*H$_2$N), 28.9 (s, *s*-Phob *C*H$_2$), 28.0 (s, *s*-Phob *C*H$_2$), 27.9 (m, *s*-Phob *C*H$_2$), 26.5 (m, *s*-Phob *C*H$_2$), 36.1 (t, *J* = 9.3 Hz, *s*-Phob *C*H), 24.8 (t, *J* = 11.3 Hz, *s*-Phob *C*H), 21.5 (m, *s*-Phob *C*H$_2$), 20.5 (m, *s*-Phob *C*H$_2$); **^{31}P{^{1}H} NMR (162 MHz; CDCl$_3$)** δ_P 7.6 (br s, *s*-Phob*P*); **HR-MS (ESI)** *m/z* calcd. for $C_{28}H_{40}BrMnNO_3P_2$ $[M+H]^+$ = 634.1042, obs. = 634.1044; **Elem. Anal.** (calcd. for $C_{29}H_{39}BrMnNO_3P_2$) C 53.09 (53.01), H 6.25 (6.20), N 2.23 (2.21); **IR ν_{CO}:** 2005, 1926, 1898 cm^{-1}.

5.4.18 [Mn($P^{Cg}N^{Me}P^{Cg}$)$(CO)_3$Br] (*rac*/*meso* mixture)

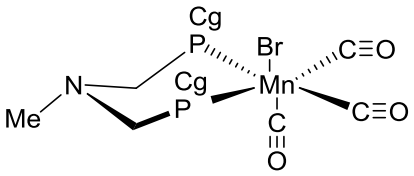

$Mn(CO)_5Br$ (150 mg, 0.55 mmol) and $P^{Cg}N^{Me}P^{Cg}$ (292 mg, 0.60 mmol) were suspended in benzene (4 mL). The reaction was heated at 50 °C overnight after which a bright orange solution formed. The solution was concentrated *in vacuo* and the resulting solid was washed with hexane (3 x 2.5 mL) to remove residual ligand to give the product as a yellow powder (305 mg, 79%).

^{1}H NMR (400 MHz; $CDCl_3$) δ_H 3.67 (1H, dd, $^1J_{HH}$ = 14.0 Hz, $^2J_{HP}$ = 3.5 Hz, *rac* PC*H*$_2$N), 3.60 (2H, m, *meso* PC*H*$_2$N), 3.16 (1H, dd, $^1J_{HH}$ = 14.1 Hz, $^2J_{HP}$ = 2.7 Hz, *rac* PC*H*$_2$N), 3.08 (1H, br d, $^1J_{HH}$ = 14.1 Hz, *rac* PC*H*$_2$N), 2.94 (2H, br d, $^3J_{HP}$ = 14.0 Hz, Cg C*H*$_2$), 2.87 (1H, dd, $^1J_{HH}$ = 14.0 Hz, $^2J_{HP}$ = 4.1 Hz, Cg C*H*$_2$), 2.72 (1H, dd, $^1J_{HH}$ = 13.8 Hz, $^2J_{HP}$ = 2.2 Hz, *rac* PC*H*$_2$N), 2.59 (3H, s, NC*H*$_3$), 2.59 (1H, obscured by NCH_3 signal, Cg C*H*$_2$), 2.54 (3H, s, NC*H*$_3$), 2.34 (2H, m, *meso* PC*H*$_2$N), 1.99-1.88 (3H, m, Cg C*H*$_2$), 1.87-1.71 (12H, m, Cg C*H*$_2$/C*H*$_3$), 1.61-1.39 (45H, m, Cg C*H*$_2$/C*H*$_3$); **^{13}C{^{1}H} NMR (100 MHz; $CDCl_3$)** δ_C 96.8 (s, Cg *C*), 96.7 (s, Cg *C*), 96.3 (s, Cg *C*), 95.8 (s, Cg *C*), 95.6 (s, Cg *C*), 95.5 (s, Cg *C*), 72.3 (m, Cg *C*), 76.5 (s, Cg *C*), 76.1 (m, Cg *C*), 53.6 (d, *J* = 25 Hz, P*C*H$_2$N), 52.9 (d, *J* = 25, P*C*H$_2$N), 52.0 (m, P*C*H$_2$N and N*C*H$_3$), 41.7 (m, Cg *C*H$_2$), 40.9 (m, Cg *C*H$_2$), 30.7 (d, *J* = 5.8 Hz, Cg *C*H$_3$), 29.7 (d, *J* = 6.4 Hz, Cg *C*H$_3$), 29.1 (m, Cg *C*H$_3$), 27.6 (m, Cg *C*H$_3$); **^{31}P{^{1}H} NMR (162 MHz; $CDCl_3$)** δ_P 18.9 (br s, *meso P*Cg), 16.9 (br s, *rac P*Cg), 11.3 (br s, *rac P*Cg); **HR-MS (ESI)** *m/z* calcd. for $C_{26}H_{39}BrNMnO_9P_2Na$ $[M+H]^+$ = 706.0737, obs. = 706.0734; **Elem. Anal.** (calcd. for $C_{26}H_{39}BrMnNO_9P_2$) C 44.36 (44.21), H 5.63 (5.57), N 2.03 (1.98); **IR ν_{CO}** 2026, 1969, 1907 cm^{-1}.

5.4.19 [Mn($P^{Cg}N^{iPr}P^{Cg}$)$(CO)_3$Br] (*rac*/*meso* mixture)

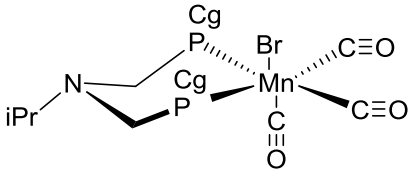

$Mn(CO)_5Br$ (100 mg, 0.36 mmol) and $P^{Cg}N^{iPr}P^{Cg}$ (206 mg, 0.40 mmol) were suspended in benzene (2.5 mL) and the reaction was heated at 50 °C overnight after which a bright orange solution formed. The solution was concentrated *in vacuo* and the resulting solid was washed with hexane (3 x 2 mL) to remove residual ligand to give the product as a yellow powder (217 mg, 81%). Crystals suitable for X-ray analysis were obtained from a saturated solution of the complex in benzene.

^{1}H NMR (400 MHz; $CDCl_3$) δ_H 3.73-3.62 (3H, m, 2 x *meso* PC*H*$_2$N and 1 x *rac* NC*H*$_2$P), 3.22 (1H, d, $^1J_{HH}$ = 14.0 Hz, *rac* PC*H*$_2$N), 3.14-3.01 (2H, m, 1 x *rac* PC*H*$_2$N and 1 x *meso* C*H*(CH$_3$)$_2$), 2.98-2.85 (4H, m, 1 x *rac* C*H*(CH$_3$)$_2$, 2 x *meso* Cg C*H*$_2$, 1 x *rac* Cg C*H*$_2$), 2.71 (1H, d, $^1J_{HH}$ = 14.0 Hz, *rac* PC*H*$_2$N), 2.59 (1H, dd, $^1J_{HH}$ = 13.4 Hz, J_{HP} = 3.6 Hz, 1 x *rac* Cg C*H*$_2$) 2.32 (2H, m, 2 x *meso* PC*H*$_2$N), 2.04-1.36 (60H, m, 30 x *rac* Cg C*H*$_2$/C*H*$_3$ and 30 x *meso* Cg C*H*$_2$/C*H*$_3$), 1.16 (3H, d, $^3J_{HH}$ = 6.6 Hz, *rac* NCH(C*H*$_3$)$_2$), 1.10 (6H, d, $^3J_{HH}$ = 6.5 Hz, *meso* NCH(C*H*$_3$)$_2$), 1.05 (3H, d, $^3J_{HH}$ = 6.6 Hz, *rac* NCH(C*H*$_3$)$_2$); **^{13}C{^{1}H} NMR (100 MHz; $CDCl_3$)** δ_C 96.8 (s, Cg *C*), 96.7 (s, Cg *C*), 96.3 (s, Cg *C*), 95.8 (s, Cg *C*), 95.6 (s, Cg *C*), 95.5 (s, Cg *C*), 77.3 (m, Cg *C*), 76.5 (s, Cg *C*), 76.3 (m, Cg *C*), 74.7 (m, Cg *C*), 61.5 (m, *C*H), 49.6 (d, *J* = 25 Hz, P*C*H$_2$N), 47.4 (d, *J* = 12 Hz, P*C*H$_2$N), 47.3 (d, *J* = 12 Hz, P*C*H$_2$N), 46.7 (d, *J* = 25 Hz, P*C*H$_2$N), 41.9 (m, Cg *C*H$_2$), 41.0 (s, Cg *C*H$_2$), 40.8 (s, Cg *C*H$_2$), 30.1 (dd, *J* = 82, 5 Hz, Cg *C*H$_3$), 29.1 (m, Cg *C*H$_3$), 28.9 (m, Cg *C*H$_3$), 28.0-27.4 (m, Cg *C*H$_3$), 19.7 (s, CH(*C*H$_3$)$_2$), 17.7 (s, CH(*C*H$_3$)$_2$), 16.3 (s, CH(*C*H$_3$)$_2$); **^{31}P{^{1}H} NMR (162 MHz; $CDCl_3$)** δ_P 18.0 (br s, *meso P*Cg), 16.7 (br s, *rac P*Cg), 10.7 (br s, *rac P*Cg); **HR-MS (ESI)** *m/z* calcd. for $C_{28}H_{43}BrNMnO_9P_2Na$ $[M+Na]^+$ = 758.0849, obs. = 758.0855; **Elem. Anal.** (calcd. for $C_{28}H_{43}BrMnNO_9P_2$) C 46.01 (45.79), H 5.96 (5.90), N 1.94 (1.91); **IR ν_{CO}** 2027, 1966, 1906 cm^{-1}.

5.4.20 [Mn(P^{Cg}N^{Bn}P^{Cg})(CO)$_3$Br] (*rac*/*meso* mixture)

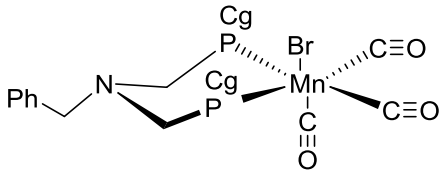

$Mn(CO)_5Br$ (136 mg, 0.49 mmol) and $P^{Cg}N^{Bn}P^{Cg}$ (306 mg, 0.54 mmol) were suspended in benzene (3.5 mL). The reaction was heated at 50 °C overnight after which a bright orange solution formed. The solution was concentrated *in vacuo* and the resulting solid was washed with hexane (3 x 2.5 mL) to remove residual ligand to give the product as a yellow powder (318 mg, 83%).

^{1}H NMR (400 MHz; $CDCl_3$) δ_H 7.34-7.14 (10H, m, Ar-C*H*), 3.78 (1H, br d, $^{1}J_{HH}$ = 12.1 Hz, *meso* PCH_2N), 3.67 (5H, m, 4 x Bn CH_2 and 1 x *rac* PCH_2N), 3.57 (^{1}H, dd, $^{1}J_{HH}$ = 13.7 Hz, $^{3}J_{HP}$ = 3.9 Hz, *rac* PCH_2N), 3.34 (1H, br d, $^{1}J_{HH}$ = 12.0 Hz, *meso* PCH_2N), 3.18 (1H, dd, $^{1}J_{HH}$ = 14.0 Hz, $^{3}J_{HP}$ = 3.7 Hz, *meso* PCH_2N), 2.98 (1H, br d, $^{1}J_{HH}$ = 14.0 Hz, *meso* PCH_2N), 2.83-2.69 (4H, m, 1 x *rac* PCH_2N, 2 x *meso* Cg CH_2 and 1 x *rac* Cg CH_2), 2.44 (1H, dd, $^{1}J_{HH}$ = 13.8 Hz, $^{2}J_{HP}$ = 3.8 Hz, Cg CH_2), 2.13 (1H, br m, *rac* PCH_2N), 1.82-1.07 (28H, 2 x *rac* Cg CH_2, 2 x *meso* Cg CH_2, 12 x *rac* Cg CH_3 and 12 x *meso* Cg CH_3); **^{13}C{^{1}H} NMR (100 MHz; $CDCl_3$)** δ_C 136.4 (s, Ar *C*), 135.3 (s, Ar *C*), 131.2 (s, Ar *C*H), 130.7 (s, Ar *C*H), 129.1 (s, Ar *C*H), 128.9 (s, Ar *C*H), 128.7 (s, Ar *C*H), 128.54 (s, Ar *C*H), 128.47 (s, Ar *C*H), 96.8 (s, Cg *C*), 96.6 (s, Cg *C*), 96.2 (s, Cg *C*), 95.7 (s, Cg *C*), 95.6 (s, Cg *C*), 95.5 (s, Cg *C*), 77.3 (m, obscured by $CDCl_3$ signal, Cg *C*), 74.8 (m, Cg *C*), 68.6 (m P*C*H_2N and Bn *C*H_2), 50.9 (d, *J* = 23.8 Hz, P*C*H_2N), 50.2 (d, *J* = 22.6 Hz, P*C*H_2N), 49.6 (m, P*C*H_2N), 41.8 (m, Cg *C*H_2), 40.7 (s, Cg *C*H_2), 40.6 (s, Cg *C*H_2), 40.2 (s, Cg *C*H_2), 30.7 (d, *J* = 5.8 Hz, Cg *C*H_3), 29.7 (d, *J* = 6.4 Hz, Cg *C*H_3), 29.1 (m, Cg *C*H_3), 27.9-27.4 (m, Cg *C*H_3); **^{31}P{^{1}H} NMR (162 MHz; $CDCl_3$)** δ_P 18.8 (br s, *meso P*Cg), 16.2 (br s, *rac P*Cg), 11.3 (br s, *rac P*Cg); **HR-MS (ESI)** *m/z* calcd. for $C_{39}H_{43}BrNMnO_9P_2Na$ $[M+H]^+$ = 782.1050, obs. = 782.1057; **Elem. Anal.** (calcd. for $C_{32}H_{43}BrMnNO_9P_2$) C 49.21 (49.12), H 5.55 (5.54), N 1.88 (1.79); **IR ν_{CO}** 2024, 1960, 1906 cm^{-1}.

5.4.21 *In situ* formation of [Mn(P^{Phob}N^{Me}P^{Phob})(CO)$_3$][BAr$^{F}_4$]

A Youngs NMR tube was charged with [Mn(P^{Phob}N^{Me}P^{Phob})(CO)$_3$Br] (24.7 mg, 0.044 mmol) and NaBAr$^{F}_4$ (39.2 mg, 0.044 mmol) in a glovebox. Upon the addition of fluorobenzene solvent (~0.6 mL) a bright yellow solution and a white precipitate formed. **^{31}P{^{1}H} NMR (122 MHz; C_6H_5F)** δ_P −7.9 (s, *P*Phob).

5.4.22 *In situ* formation of [Mn(P^{Phob}N^{iPr}P^{Phob})(CO)$_3$][BAr$^{F}_4$]

A Youngs NMR tube was charged with [Mn(P^{Phob}N^{iPr}P^{Phob})(CO)$_3$Br] (34.7 mg, 0.059 mmol) and NaBAr$^{F}_4$ (52.4 mg, 0.059 mmol) in a glovebox. Upon the addition of fluorobenzene solvent (~0.6 mL) a bright yellow solution and a white precipitate formed. **^{31}P{^{1}H} NMR (122 MHz; C_6H_5F)** δ_P −6.1 (s, *P*Phob).

5.4.23 *In situ* formation of [Mn($P^{Phob}N^{Bn}P^{Phob}$)$(CO)_3$][BAr^F_4]

A Youngs NMR tube was charged with [Mn($P^{Phob}N^{Bn}P^{Phob}$)$(CO)_3$Br] (27.3 mg, 0.043 mmol) and $NaBAr^F_4$ (38.1 mg, 0.043 mmol) in a glovebox. Upon the addition of fluorobenzene solvent (~0.6 mL) a bright yellow solution and a white precipitate formed.

$^{31}P\{^1H\}$ NMR (122 MHz; C_6H_5F) δ_P −5.1 (s, *P*Phob).

5.4.24 *In situ* reaction of [Mn($P^{Cg}N^{Me}P^{Cg}$)$(CO)_3$Br] and $NaBAr^F_4$

A Youngs NMR tube was charged with [Mn($P^{Cg}N^{Me}P^{Cg}$)$(CO)_3$Br] (19.2 mg, 0.027 mmol) and $NaBAr^F_4$ (24.1 mg, 0.027 mmol) in a glovebox. Upon the addition of fluorobenzene solvent (~0.6 mL) a bright yellow solution formed.

$^{31}P\{^1H\}$ NMR (122 MHz; C_6H_5F) δ_P 19.0 (s, *meso P*Cg), 17.4 (d, $^2J_{PP}$ = 45.8 Hz, *rac P*Cg), 13.4 (d, $^2J_{PP}$ = 45.8 Hz, *rac P*Cg).

5.4.25 *In situ* reaction of [Mn($P^{Cg}N^{iPr}P^{Cg}$)$(CO)_3$Br] and $NaBAr^F_4$

A Youngs NMR tube was charged with [Mn($P^{Cg}N^{iPr}P^{Cg}$)$(CO)_3$Br] (19.4 mg, 0.026 mmol) and $NaBAr^F_4$ (23.4 mg, 0.024 mmol) in a glovebox. Upon the addition of fluorobenzene solvent (~0.6 mL) a bright yellow solution formed.

$^{31}P\{^1H\}$ NMR (122 MHz; C_6H_5F) δ_P 17.7 (s, *meso P*Cg), 17.6 (d, $^2J_{PP}$ = 46.7 Hz, *rac P*Cg), 13.1 (d, $^2J_{PP}$ = 46.7 Hz, *rac P*Cg).

5.4.26 *In situ* reaction of [Mn($P^{Cg}N^{Bn}P^{Cg}$)$(CO)_3$Br] and $NaBAr^F_4$

A Youngs NMR tube was charged with [Mn($P^{Cg}N^{Bn}P^{Cg}$)$(CO)_3$Br] (21.9 mg, 0.028 mmol) and $NaBAr^F_4$ (24.8 mg, 0.028 mmol) in a glovebox. Upon the addition of fluorobenzene solvent (~0.6 mL) a bright yellow solution formed.

$^{31}P\{^1H\}$ NMR (122 MHz; C_6H_5F) δ_P 18.6 (s, *meso P*Cg), 15.5 (d, $^2J_{PP}$ = 45.0 Hz, *rac P*Cg), 13.3 (d, $^2J_{PP}$ = 45.0 Hz, *rac P*Cg).

5.4.27 *In situ* reaction of [Mn(P^{Cg}N^{Me}P^{Cg})(CO)$_3$Br/NaBAr$^F_4$ with H$_2$

A Youngs NMR tube was charged with [Mn(P^{Cg}N^{Me}P^{Cg})(CO)$_3$Br] (28.0 mg, 0.040 mmol) and NaBAr$^F_4$ (35.1 mg, 0.040 mmol) in a glovebox and d$_5$-PhCl (~0.6 mL) was added to form a yellow/orange suspension. The suspension was frozen in liquid nitrogen and the tube was evacuated. The solution was thawed and allowed to warm to room temperature. The tube was backfilled with H_2 (1 bar) and shaken.

^{1}H NMR (400 MHz; d$_5$-PhCl) δ_H 9.70 (1H, br s, N*H*), 8.22 (8H, br s, *o*-Ar C*H* of BAr$^F_4$), 7.61 (4H, br s, *p*-Ar C*H* of BAr$^F_4$), 3.92 – 1.16 (39 H, m, 4 x PC*H*$_2$N, 8 x Cg C*H*$_2$, 24 x Cg C*H*$_3$, 3 x NC*H*$_3$), −7.93 (1H, t, $^2J_{HP}$ = 55.6 Hz, *meso* Mn*H*), −8.04 (1H, dd, $^2J_{HP}$ = 53.9, 46.6 Hz, *syn,rac* Mn*H*), -8.69 (1H, dd, $^2J_{HP}$ = 56.0, 43.7 Hz, *anti,rac* Mn*H*); **^{31}P{^{1}H} NMR (162 MHz; d$_5$-PhCl)** δ_P 55.5 (d, $^2J_{PP}$ = 35.6 Hz, *anti,rac P*Cg), 53.8 (d, $^2J_{PP}$ = 35.6 Hz, *anti,rac P*Cg), 47.6 (d, $^2J_{PP}$ = 45.5 Hz, *syn,rac P*Cg), 45.9 (s, *meso P*Cg), 45.7 (d, ^2J = 45.5 Hz, *syn,rac P*Cg).

5.4.28 *In situ* reaction of [Mn(P^{Cg}N^{iPr}P^{Cg})(CO)$_3$Br/NaBAr$^F_4$ with H$_2$

A Youngs NMR tube was charged with [Mn(P^{Cg}N^{iPr}P^{Cg})(CO)$_3$Br] (34.6 mg, 0.047 mmol) and NaBAr$^F_4$ (41.7 mg, 0.047 mmol) in a glovebox and d$_5$-PhCl (~0.6 mL) was added to form a yellow/orange suspension. The suspension was frozen in liquid nitrogen and the tube was evacuated. The solution was thawed and allowed to warm to room temperature. The tube was backfilled with H_2 (1 bar) and shaken.

^{1}H NMR (400 MHz; d$_5$-PhCl) δ_H 9.56 (1H, br s, N*H*), 8.15 (8H, br s, *o*-Ar C*H* of BAr$^F_4$), 7.55 (4H, br s, *p*-Ar C*H* of BAr$^F_4$), 3.93 – 0.62 (43 H, m, 1 x NC*H*(CH$_3$)$_2$, 4 x PC*H*$_2$N, 8 x Cg C*H*$_2$, 24 x Cg C*H*$_3$, NCH(C*H*$_3$)$_2$), −7.90 (1H, dd, $^2J_{HP}$ = 50.7, 49.5 Hz, *syn,rac* Mn*H*), −7.95 (1H, t, $^2J_{HP}$ = 55.3 Hz, *meso* Mn*H*), −8.67 (1H, dd, $^2J_{HP}$ = 55.6, 43.2 Hz, *anti,rac* Mn*H*); **^{31}P{^{1}H} NMR (162 MHz; d$_5$-PhCl)** δ_P 66.5 (d, $^2J_{PP}$ = 36.1 Hz, *anti,rac P*Cg), 58.3 (d, $^2J_{PP}$ = 36.1 Hz, *anti,rac P*Cg), 45.8 (m, *syn,rac P*Cg, *meso P*Cg).

5.4.29 *In situ* reaction of [Mn(P^{Cg}N^{Bn}P^{Cg})(CO)$_3$Br/NaBAr$^F_4$ with H$_2$

A Youngs NMR tube was charged with [Mn(P^{Cg}N^{Bn}P^{Cg})(CO)$_3$Br] (31.6 mg, 0.040 mmol) and NaBAr$^F_4$ (35.9 mg, 0.040 mmol) in a glovebox and d$_5$-chlorobenzene (~0.6 mL) was

added to form a yellow/orange suspension. The suspension was frozen in liquid nitrogen and the tube was evacuated. The solution was thawed and allowed to warm to room temperature. The tube was backfilled with H_2 (1 bar) and shaken.

^{1}H NMR (400 MHz; d$_5$-PhCl) δ_H 9.65 (1H, br s, N*H*), 8.24 (8H, br s, *o*-Ar C*H* of BAr^F_4), 7.61 (4H, br s, *p*-Ar C*H* of BAr^F_4), 7.30-7.08 (5H, m, Ar C*H*), 4.28 – 0.51 (38 H, m, 2x Bn CH_2), 4 x PCH_2N, 8 x Cg CH_2, 24 x Cg CH_3), −8.06 (2H, m, 1 x *meso* Mn*H*, 1 x *syn,rac* Mn*H*), −8.63 (1H, m, *anti,rac* Mn*H*); **^{31}P{^{1}H} NMR (162 MHz; d$_5$-PhCl)** δ_P 58.6 (br, *anti,rac P*Cg), 52.0 (br, *anti,rac P*Cg), 46.7 (s, *meso P*Cg), 46.3 (d, $^2J_{PP}$ = 46.1 Hz, *syn,rac P*Cg), 45.3 (d, ^2J = 46.1 Hz, *syn,rac P*Cg).

5.5 Electrochemical Experimental Details

Cyclic voltammograms were recorded under Ar in a glovebox in 0.1 M $[Bu_4N][B(C_6F_5)_4]$ electrolyte solutions in PhF at ambient temperature, 20-22 °C. Cyclic voltammetry experiments, using a standard three-electrode configuration, were conducted using a CHI 660C potentiostat interfaced with a computer using CHI 700D software. Cyclic voltammetric scans were recorded using a glassy carbon working electrode with 1 mm disc diameter, a silver wire pseudoreference electrode, and a platinum wire counter electrode. All potentials were referenced to the $[Cp_2Fe]^{0/+}$ couple.

5.6 Crystallographic Data

Table 5.1: Crystal data and structure refinement for **L2**

Identification code	**L2**
Empirical formula	$C_{22}H_{40}O_2P_2$
Formula weight	398.48
Temperature/K	100(2)
Crystal system	triclinic
Space group	P-1
a/Å	8.7382(2)
b/Å	11.1445(3)
c/Å	13.4535(4)
α/°	104.296(2)
β/°	95.231(2)
γ/°	103.828(2)
Volume/Å^3	1216.97(6)
Z	2
ρ_{calc}g/cm^3	1.087
μ/mm^{-1}	0.191
F(000)	436.0
Crystal size/mm^3	0.367 × 0.269 × 0.232
Radiation	MoKα (λ = 0.71073)
2Θ range for data collection/°	3.918 to 55.968
Index ranges	$-11 \leq h \leq 11$, $-14 \leq k \leq 14$, $-17 \leq l \leq 9$
Reflections collected	21452
Independent reflections	5869 [R_{int} = 0.0423, R_{sigma} = 0.0414]
Data/restraints/parameters	5869/0/247
Goodness-of-fit on F^2	1.034
Final R indexes [I>=2σ (I)]	R_1 = 0.0409, wR_2 = 0.0925
Final R indexes [all data]	R_1 = 0.0630, wR_2 = 0.1035
Largest diff. peak/hole / e Å^{-3}	0.64/-0.43

Table 5.2: Crystal data and structure refinement for [$PtCl_2$(**L2**)]

Identification code	[$PtCl_2$(**L2**)]
Empirical formula	$C_{23}H_{42}Cl_4O_2P_2Pt$
Formula weight	749.39
Temperature/K	100(2)
Crystal system	monoclinic
Space group	$P2_1/c$
a/Å	15.3027(6)
b/Å	11.8212(4)
c/Å	17.6415(6)
α/°	90

β/°	111.981(2)
γ/°	90
Volume/Å^3	2959.30(19)
Z	4
ρ_{calc}g/cm^3	1.682
μ/mm^{-1}	5.229
F(000)	1488.0
Crystal size/mm^3	0.352 × 0.204 × 0.19
Radiation	MoKα (λ = 0.71073)
2Θ range for data collection/°	4.252 to 55.974
Index ranges	$-20 \leq h \leq 18$, $0 \leq k \leq 15$, $0 \leq l \leq 23$
Reflections collected	7113
Independent reflections	7113 [R_{int} = N/A, R_{sigma} = 0.0369]
Data/restraints/parameters	7113/12/302
Goodness-of-fit on F^2	1.045
Final R indexes [I>=2σ (I)]	R_1 = 0.0289, wR_2 = 0.0642
Final R indexes [all data]	R_1 = 0.0369, wR_2 = 0.0673
Largest diff. peak/hole / e Å^{-3}	2.47/-1.28

Table 5.3: Crystal data and structure refinement for [Pt(CO)(**L1**)]

Identification code	[Pt(CO)(**L1**)]
Empirical formula	$C_{25}H_{44}OP_2Pt$
Formula weight	617.63
Temperature/K	100(2)
Crystal system	monoclinic
Space group	$P2_1/n$
a/Å	11.6873(4)
b/Å	15.8581(6)
c/Å	14.5212(5)
α/°	90
β/°	94.052(2)
γ/°	90
Volume/Å^3	2684.61(17)
Z	4
ρ_{calc}g/cm^3	1.528
μ/mm^{-1}	5.359
F(000)	1240.0
Crystal size/mm^3	0.25 × 0.2 × 0.19
Radiation	MoKα (λ = 0.71073)
2Θ range for data collection/°	3.808 to 55.762
Index ranges	$-15 \leq h \leq 15$, $0 \leq k \leq 20$, $0 \leq l \leq 19$
Reflections collected	8036
Independent reflections	8036 [R_{int} = N/A, R_{sigma} = 0.0934]
Data/restraints/parameters	8036/0/275

Goodness-of-fit on F^2	1.038
Final R indexes [I>=2σ (I)]	R_1 = 0.0587, wR_2 = 0.1283
Final R indexes [all data]	R_1 = 0.0869, wR_2 = 0.1406
Largest diff. peak/hole / e $Å^{-3}$	2.83/-2.23

Table 5.4: Crystal data and structure refinement for [Pt(CO)(**L2**)]

Identification code	[Pt(CO)(**L2**)]
Empirical formula	$C_{23}H_{40}O_3P_2Pt$
Formula weight	621.58
Temperature/K	100
Crystal system	triclinic
Space group	P-1
a/Å	10.3806(6)
b/Å	11.5388(7)
c/Å	12.1554(7)
α/°	65.148(2)
β/°	81.680(3)
γ/°	75.180(2)
Volume/$Å^3$	1276.04(13)
Z	2
$\rho_{calc}g/cm^3$	1.618
μ/mm^{-1}	5.644
F(000)	620.0
Crystal size/mm^3	0.453 × 0.233 × 0.196
Radiation	MoKα (λ = 0.71073)
2Θ range for data collection/°	3.986 to 61.114
Index ranges	$-14 \leq h \leq 14$, $-16 \leq k \leq 16$, $-17 \leq l \leq 17$
Reflections collected	30064
Independent reflections	7805 [R_{int} = 0.0215, R_{sigma} = 0.0193]
Data/restraints/parameters	7805/0/274
Goodness-of-fit on F^2	1.037
Final R indexes [I>=2σ (I)]	R_1 = 0.0139, wR_2 = 0.0308
Final R indexes [all data]	R_1 = 0.0148, wR_2 = 0.0310
Largest diff. peak/hole / e $Å^{-3}$	0.57/-0.69

Table 5.5: Crystal data and structure refinement for **L3**

Identification code	**L3**
Empirical formula	$C_{30}H_{48}O_2P_2$
Formula weight	502.62
Temperature/K	100.03
Crystal system	monoclinic
Space group	$P2_1/c$
a/Å	9.5684(3)

b/Å	24.5414(8)
c/Å	11.9780(4)
α/°	90
β/°	94.2236(19)
γ/°	90
Volume/Å^3	2805.06(16)
Z	4
ρ_{calc}g/cm^3	1.190
μ/mm^{-1}	0.180
F(000)	1096.0
Crystal size/mm^3	0.235 × 0.212 × 0.095
Radiation	MoKα (λ = 0.71073)
2Θ range for data collection/°	3.32 to 55.928
Index ranges	$-12 \leq h \leq 9$, $-32 \leq k \leq 32$, $-15 \leq l \leq 15$
Reflections collected	38237
Independent reflections	6730 [R_{int} = 0.0823, R_{sigma} = 0.0599]
Data/restraints/parameters	6730/0/307
Goodness-of-fit on F^2	1.016
Final R indexes [I>=2σ (I)]	R_1 = 0.0427, wR_2 = 0.0874
Final R indexes [all data]	R_1 = 0.0728, wR_2 = 0.0990
Largest diff. peak/hole / e Å^{-3}	0.30/-0.28

Table 5.6: Crystal data and structure refinement for **3.1**.CH_2Cl_2

Identification code	**3.1**.CH_2Cl_2
Empirical formula	$C_{31}H_{50}Cl_4O_2P_2Pt$
Formula weight	853.54
Temperature/K	100(2)
Crystal system	monoclinic
Space group	$P2_1/n$
a/Å	12.1548(3)
b/Å	21.7169(6)
c/Å	13.4481(4)
α/°	90
β/°	102.4443(17)
γ/°	90
Volume/Å^3	3466.42(17)
Z	4
ρ_{calc}g/cm^3	1.635
μ/mm^{-1}	4.475
F(000)	1712.0
Crystal size/mm^3	0.33 × 0.28 × 0.12
Radiation	MoKα (λ = 0.71073)
2Θ range for data collection/°	3.624 to 55.904
Index ranges	$-15 \leq h \leq 15$, $-28 \leq k \leq 27$, $-17 \leq l \leq 17$

Reflections collected	31000
Independent reflections	8284 [R_{int} = 0.0460, R_{sigma} = 0.0432]
Data/restraints/parameters	8284/0/361
Goodness-of-fit on F^2	0.999
Final R indexes [I>=2σ (I)]	R_1 = 0.0302, wR_2 = 0.0664
Final R indexes [all data]	R_1 = 0.0408, wR_2 = 0.0702
Largest diff. peak/hole / e Å^{-3}	2.49/-1.21

Table 5.7: Crystal data and structure refinement for $[PtCl_2(P^{Phob}N^{iPr}P^{Phob})].CH_2Cl_2$

Identification code	$[PtCl_2(P^{Phob}N^{iPr}P^{Phob})].CH_2Cl_2$
Empirical formula	$C_{22}H_{41}Cl_4NP_2Pt$
Formula weight	718.39
Temperature/K	100(2)
Crystal system	monoclinic
Space group	$P2_1/c$
a/Å	14.0845(4)
b/Å	12.9761(3)
c/Å	14.3493(3)
α/°	90
β/°	91.0190(14)
γ/°	90
Volume/Å^3	2622.09(11)
Z	4
ρ_{calc}g/cm^3	1.820
μ/mm^{-1}	5.893
F(000)	1424.0
Crystal size/mm^3	0.408 × 0.245 × 0.171
Radiation	MoKα (λ = 0.71073)
2Θ range for data collection/°	2.892 to 55.902
Index ranges	-17 ≤ h ≤ 18, -16 ≤ k ≤ 17, -18 ≤ l ≤ 18
Reflections collected	23831
Independent reflections	6303 [R_{int} = 0.0322, R_{sigma} = 0.0317]
Data/restraints/parameters	6303/0/273
Goodness-of-fit on F^2	1.016
Final R indexes [I>=2σ (I)]	R_1 = 0.0209, wR_2 = 0.0429
Final R indexes [all data]	R_1 = 0.0256, wR_2 = 0.0442
Largest diff. peak/hole / e Å^{-3}	1.42/-0.69

Table 5.8: Crystal data and structure refinement for $[PtCl_2(P^{Cg}N^{Me}P^{Cg})]$

Identification code	$[PtMe_2(P^{Cg}N^{Me}P^{Cg})]$
Empirical formula	$C_{25}H_{45}NO_6P_2Pt$
Formula weight	712.65
Temperature/K	100(2)

Crystal system	monoclinic
Space group	$P2_1/c$
a/Å	12.6070(7)
b/Å	13.5183(8)
c/Å	16.3130(10)
α/°	90
β/°	95.759(4)
γ/°	90
Volume/Å^3	2766.1(3)
Z	4
ρ_{calc}g/cm^3	1.711
μ/mm^{-1}	5.228
F(000)	1432.0
Crystal size/mm^3	0.542 × 0.417 × 0.352
Radiation	MoKα (λ = 0.71073)
2Θ range for data collection/°	3.922 to 56.144
Index ranges	$-16 \leq h \leq 16$, $-17 \leq k \leq 17$, $-21 \leq l \leq 20$
Reflections collected	25135
Independent reflections	6682 [R_{int} = 0.0242, R_{sigma} = 0.0222]
Data/restraints/parameters	6682/0/327
Goodness-of-fit on F^2	1.023
Final R indexes [I>=2σ (I)]	R_1 = 0.0180, wR_2 = 0.0402
Final R indexes [all data]	R_1 = 0.0215, wR_2 = 0.0412
Largest diff. peak/hole / e Å^{-3}	1.14/-0.81

Table 5.9: Crystal data and structure refinement for [$PtMe_2(P^{Cg}N^{iPr}P^{Cg})$]

Identification code	[$PtMe_2(P^{Cg}N^{iPr}P^{Cg})$]
Empirical formula	$C_{27}H_{49}NO_6P_2Pt$
Formula weight	740.70
Temperature/K	100(2)
Crystal system	monoclinic
Space group	$P2_1/c$
a/Å	12.4146(3)
b/Å	16.8178(5)
c/Å	14.6775(4)
α/°	90
β/°	98.409(2)
γ/°	90
Volume/Å^3	3031.51(14)
Z	4
ρ_{calc}g/cm^3	1.623
μ/mm^{-1}	4.773
F(000)	1496.0
Crystal size/mm^3	0.316 × 0.258 × 0.186

Radiation	MoKα (λ = 0.71073)
2Θ range for data collection/°	3.316 to 55.898
Index ranges	$-16 \leq h \leq 16$, $-22 \leq k \leq 22$, $-18 \leq l \leq 19$
Reflections collected	27231
Independent reflections	7265 [R_{int} = 0.0278, R_{sigma} = 0.0265]
Data/restraints/parameters	7265/0/346
Goodness-of-fit on F^2	1.028
Final R indexes [I>=2σ (I)]	R_1 = 0.0189, wR_2 = 0.0367
Final R indexes [all data]	R_1 = 0.0229, wR_2 = 0.0375
Largest diff. peak/hole / e $Å^{-3}$	0.57/-0.43

Table 5.10: Crystal data and structure refinement for $[PtMe_2(P^{Cg}N^{Bn}P^{Cg})]$

Identification code	$[PtMe_2(P^{Cg}N^{Bn}P^{Cg})]$
Empirical formula	$C_{31}H_{49}NO_6P_2Pt$
Formula weight	788.74
Temperature/K	100(2)
Crystal system	triclinic
Space group	P-1
a/Å	8.85060(10)
b/Å	13.7294(2)
c/Å	15.7434(2)
α/°	72.4960(10)
β/°	79.0820(10)
γ/°	87.4030(10)
Volume/$Å^3$	1791.29(4)
Z	2
ρ_{calc}g/cm^3	1.462
μ/mm^{-1}	4.044
F(000)	796.0
Crystal size/mm^3	0.374 × 0.312 × 0.138
Radiation	MoKα (λ = 0.71073)
2Θ range for data collection/°	2.76 to 55.972
Index ranges	$-11 \leq h \leq 11$, $-18 \leq k \leq 18$, $-20 \leq l \leq 20$
Reflections collected	32909
Independent reflections	8595 [R_{int} = 0.0254, R_{sigma} = 0.0234]
Data/restraints/parameters	8595/60/396
Goodness-of-fit on F^2	1.023
Final R indexes [I>=2σ (I)]	R_1 = 0.0189, wR_2 = 0.0427
Final R indexes [all data]	R_1 = 0.0214, wR_2 = 0.0434
Largest diff. peak/hole / e $Å^{-3}$	1.22/-0.46

Table 5.11: Crystal structure and data refinement for $[Mn(P^{Phob}N^{iPr}P^{Phob})(CO)_3Br]$

Identification code	$[Mn(P^{Phob}N^{iPr}P^{Phob})(CO)_3Br]$

Empirical formula	$C_{24}H_{39}BrMnNO_3P_2$
Formula weight	586.35
Temperature/K	100(2)
Crystal system	monoclinic
Space group	$P2_1/n$
a/Å	9.21980(10)
b/Å	15.7075(3)
c/Å	17.8248(3)
α/°	90
β/°	90.6360(10)
γ/°	90
Volume/Å^3	2581.23(7)
Z	4
ρ_{calc}g/cm^3	1.509
μ/mm^{-1}	2.209
F(000)	1216.0
Crystal size/mm^3	0.499 × 0.306 × 0.245
Radiation	MoKα (λ = 0.71073)
2Θ range for data collection/°	4.952 to 55.896
Index ranges	$-12 \leq h \leq 12$, $-20 \leq k \leq 20$, $-22 \leq l \leq 23$
Reflections collected	23450
Independent reflections	6190 [R_{int} = 0.0429, R_{sigma} = 0.0407]
Data/restraints/parameters	6190/0/291
Goodness-of-fit on F^2	1.039
Final R indexes [I>=2σ (I)]	R_1 = 0.0349, wR_2 = 0.0892
Final R indexes [all data]	R_1 = 0.0467, wR_2 = 0.0945
Largest diff. peak/hole / e Å^{-3}	0.54/-0.92

Table 5.12: Crystal structure and data refinement for $[Mn(P^{Cg}N^{iPr}P^{Cg})(CO)_3Br].C_6H_6$

Identification code	$[Mn(P^{Cg}N^{iPr}P^{Cg})(CO)_3Br].C_6H_6$
Empirical formula	$C_{34}H_{49}BrMnNO_9P_2$
Formula weight	812.53
Temperature/K	99.99
Crystal system	orthorhombic
Space group	Pbca
a/Å	20.2109(7)
b/Å	17.9696(6)
c/Å	20.4065(7)
α/°	90
β/°	90
γ/°	90
Volume/Å^3	7411.3(4)
Z	8
ρ_{calc}g/cm^3	1.456

μ/mm^{-1}	1.573
F(000)	3376.0
Crystal size/mm^3	0.401 × 0.347 × 0.206
Radiation	MoKα (λ = 0.71073)
2Θ range for data collection/°	3.63 to 55.92
Index ranges	$-26 \leq h \leq 26$, $-23 \leq k \leq 23$, $-26 \leq l \leq 26$
Reflections collected	130814
Independent reflections	8908 [R_{int} = 0.0801, R_{sigma} = 0.0363]
Data/restraints/parameters	8908/180/474
Goodness-of-fit on F^2	1.006
Final R indexes [I>=2σ (I)]	R_1 = 0.0283, wR_2 = 0.0582
Final R indexes [all data]	R_1 = 0.0457, wR_2 = 0.0642
Largest diff. peak/hole / e $Å^{-3}$	

Table 5.13: Crystal structure and data refinement for $[Mn(P^{Phob}N^{Me}P^{Phob})(CO)_3][BAr^F_4]$

Identification code	$[Mn(P^{Phob}N^{Me}P^{Phob})(CO)_3][BAr^F_4]$
Empirical formula	$C_{54}H_{47}BF_{24}MnNO_3P_2$
Formula weight	1341.61
Temperature/K	100(2)
Crystal system	monoclinic
Space group	$P2_1/n$
a/Å	19.6524(4)
b/Å	14.5535(4)
c/Å	21.3986(5)
α/°	90
β/°	113.0170(10)
γ/°	90
Volume/$Å^3$	5633.0(2)
Z	4
$\rho_{calc}g/cm^3$	1.582
μ/mm^{-1}	0.415
F(000)	2712.0
Crystal size/mm^3	0.427 × 0.239 × 0.233
Radiation	MoKα (λ = 0.71073)
2Θ range for data collection/°	2.388 to 55.874
Index ranges	$-25 \leq h \leq 25$, $-18 \leq k \leq 19$, $-27 \leq l \leq 28$
Reflections collected	38204
Independent reflections	13386 [R_{int} = 0.0337, R_{sigma} = 0.0404]
Data/restraints/parameters	13386/108/830
Goodness-of-fit on F^2	1.022
Final R indexes [I>=2σ (I)]	R_1 = 0.0369, wR_2 = 0.0786
Final R indexes [all data]	R_1 = 0.0545, wR_2 = 0.0860
Largest diff. peak/hole / e $Å^{-3}$	0.49/-0.41

Table 5.14: Crystal structure and refinement data for $[(Mn(P^{Cg}N^{iPr}P^{Cg})(CO)_3Br)_2Na][BAr^F{}_4].C_5H_{12}.½C_6H_5F$

Identification code	$[(Mn(P^{Cg}N^{iPr}P^{Cg})(CO)_3Br)_2Na][BAr^F{}_4].C_5H_{12}.½C_6H_5F$
Empirical formula	$C_{96}H_{112.5}BBr_2F_{24.5}Mn_2N_2NaO_{18}P_4$
Formula weight	2475.25
Temperature/K	100
Crystal system	triclinic
Space group	P-1
a/Å	13.4405(4)
b/Å	19.9309(7)
c/Å	23.9066(8)
α/°	69.526(2)
β/°	88.416(2)
γ/°	74.164(2)
Volume/Å^3	5755.5(3)
Z	2
ρ_{calc}g/cm^3	1.428
μ/mm^{-1}	1.072
F(000)	2526.0
Crystal size/mm^3	0.422 × 0.149 × 0.07
Radiation	MoKα (λ = 0.71073)
2Θ range for data collection/°	3.158 to 50.7
Index ranges	$-15 \leq h \leq 16$, $-23 \leq k \leq 24$, $-28 \leq l \leq 28$
Reflections collected	87939
Independent reflections	21081 [R_{int} = 0.0866, R_{sigma} = 0.0767]
Data/restraints/parameters	21081/555/1532
Goodness-of-fit on F^2	1.021
Final R indexes [I>=2σ (I)]	R_1 = 0.0481, wR_2 = 0.1057
Final R indexes [all data]	R_1 = 0.0849, wR_2 = 0.1197
Largest diff. peak/hole / e Å^{-3}	0.94/-0.94

5.7 References

1 T. A. Antkowiak and H. Shechter, *J. Am. Chem. Soc.*, 1972, **94**, 5361–5366.

2 R. J. Angelici, Ed., *Inorganic Syntheses*, John Wiley & Sons, Inc., Hoboken, NJ, USA, 1990, vol. 28.

3 J. H. Downing, J. Roure, K. Heslop, M. F. Haddow, J. Hopewell, M. Lusi, H. Phetmung, A. G. Orpen, P. G. Pringle, R. I. Pugh and D. Zambrano-Williams, *Organometallics*, 2008, **27**, 3216–3224.

4 D. L. Reger, T. D. Wright, C. A. Little, J. J. S. Lamba and M. D. Smith, *Inorg. Chem.*, 2001, **40**, 3810–3814.

5 E. B. Hulley, K. D. Welch, A. M. Appel, D. L. DuBois and R. M. Bullock, *J. Am. Chem. Soc.*, 2013, **135**, 11736–11739.

6 L. Palatinus and G. Chapuis, *J. Appl. Crystallogr.*, 2007, **40**, 786–790.

7 G. M. Sheldrick, *Acta Crystallogr. Sect. A Found. Crystallogr.*, 2008, **64**, 112–122.

8 O. V. Dolomanov, L. J. Bourhis, R. J. Gildea, J. A. K. Howard and H. Puschmann, *J. Appl. Crystallogr.*, 2009, **42**, 339–341.

9 S. J. K. Forrest, P. G. Pringle, H. A. Sparkes and D. F. Wass, *Dalt. Trans.*, 2014, **43**, 16335–16344.

10 A. Pews-Davtyan, R. Jackstell, A. Spannenberg and M. Beller, *Chem. Commun.*, 2016, **52**, 7568–7571.

11 D. J. Morris, G. Docherty, G. Woodward and M. Wills, *Tetrahedron Lett.*, 2007, **48**, 949–953.

12 W. Clegg, G. R. Eastham, M. R. J. Elsegood, B. T. Heaton, J. A. Iggo, R. P. Tooze, R. Whyman and S. Zacchini, *Organometallics*, 2002, **21**, 1832–1840.

13 F. Stempfle, D. Quinzler, I. Heckler and S. Mecking, *Macromolecules*, 2011, **44**, 4159–4166.

14 K. Heuzé, D. Méry, D. Gauss, J. C. Blais and D. Astruc, *Chem. - A Eur. J.*, 2004, **10**, 3936–3944.

15 M. Carreira, M. Charernsuk, M. Eberhard, N. Fey, R. Van Ginkel, A. Hamilton, W. P. Mul, A. G. Orpen, H. Phetmung and P. G. Pringle, *J. Am. Chem. Soc.*, 2009, **131**, 3078–3092.

16 M. Epstein and S. A. Buckler, *J. Am. Chem. Soc.*, 1961, **83**, 3279–3282.